MINISTERE DE L'ENSEIGNEMENT SUPERIEUR ET DE LA RECHERCHE SCIENTIFIQUE

UNIVERSITE MOULOUD MAMMERI, TIZI-OUZOU

FACULTE DES SCIENCES

DEPARTEMENT DE PHYSIQUE

THESE DE DOCTORAT

SPECIALITE: PHYSIQUE

OPTION: PHYSIQUE THEORIQUE

Présentée par:

AIT-EL-DJOUDI AMEL

Sujet:

ETUDE DES EFFETS DE VOLUME DE LA TRANSITION DE DECONFINEMENT VERS UN QGP SANS COULEUR

devant le jury d'examen composé de:

. Lamrous Omar;	Professeur;	Université de Tizi-Ouzou;	Président
. Ladrem Madjid;	Professeur;	ENS-Kouba, Alger;	Rapporteur
. Aurenche Patrick;	Directeur de Recherche au CNRS; LAPTH, Annecy;		Examinateur
. Abada Abdessamad;	Professeur;	ENS-Kouba, Alger;	Examinateur
. Amghar Abdelhamid;	Professeur;	Université de Boumerdes;	Examinateur

Soutenue le:

FINITE SIZE EFFECTS ON THE DECONFINEMENT PHASE TRANSITION TO A COLOR-SINGLET QGP

By

Amel AIT-EL-DJOUDI

Ecole Normale Supèrieure-Kouba

A Thesis Submitted to the Faculty of Science

in partial fulfillement of the requirements for the degree of

DOCTOR

Department of Physics

University of Mouloud Mammeri, Tizi-Ouzou

Jury:

. Omar Lamrous;	Professor;	Tizi-Ouzou University;	Chairman
. Madjid Ladrem;	Professor;	ENS-Kouba, Algiers;	Advisor
. Patrick Aurenche;	Research Director at CNRS; LAPTH, Annecy;		Examiner
. Abdessamad Abada;	Professor;	ENS-Kouba, Algiers;	Examiner
. Abdelhamid Amghar;	Professor;	Boumerdes University;	Examiner

Dedication

To my Father and my Mother

Acknowledgement

First of all, Praise to ALLAH the almighty who helped me to accomplish this work that I have done for his sake.

I would like to thank my advisor, Prof. M. Ladrem, for the help he provided me with, during his supervision of this work. I would like also to thank all members of the jury, Profs. O. Lamrous, A. Abada, P. Aurenche and A. Amghar for considering this thesis and taking the time to read the manuscript and enrich it with their suggestions which are welcome.

I take here the time to thank all people who supported me and contributed, in one way or an other, to the success of this work. A particular thank is to my parents who greatly helped me with their continuous presence and support, to my grand-parents for their permanent care that this work be successfully achieved, to my brothers and my sister for their help and support, and to all my friends.

A great thank is to my husband for his assistance and his patience, and for the time he gave me -likewise our son- during the achievement of this work.

Abstract

This thesis deals with the deconfinement phase transition of a finite system, using a simple model of coexisting hadron and QGP phases in a finite volume. The equations of state of infinite matter of the two phases are first used, and the finite-size effects on the deconfinement phase transition are investigated by probing the behavior of some useful quantities near the transition. It turns out that in a finite size system, all singularities occurring in the thermodynamic limit are smeared out and the transition is perfectly smooth.

Secondly, the color-singletness requirement is imposed to the QGP phase, to satisfy the color confinement property of QCD, introducing an additional finite-size effect, and leading to a shift of the transition point. A finite size scaling analysis is then carried out to determine the scaling critical exponents, characterizing the scaling behavior when approaching the thermodynamic limit ($V \longrightarrow \infty$), both in analytical and numerical ways.

Since hadrons are not pointlike because of their composite character, they should be treated as extended particles. To account for this, we then consider the excluded volume effects and examine their effects on the deconfinement phase transition.

The first chapter of this thesis is devoted to a review of the physics of phase transitions, as well as their classification, and the second one overviews the phase transitions

in finite systems.

In the third chapter, we study the deconfinement phase transition in a finite system within the phase coexistence model. Equations of state of infinite matter are used for a hadronic gas of pions and for a QGP consisting of gluons and massless quarks, then the color-singletness condition is implemented using the projection method. An approximate color-singlet partition function of the QGP is derived within the saddle point approximation and is used in a first step to calculate mean values of physical quantities. The expressions of these latter with T, μ and V are obtained, in these two cases, and both temperature-driven and density-driven deconfinement phase transitions are then studied, at fixed chemical potential and temperature respectively. In a second step, the exact integral expression of the color-singlet partition function of the QGP is used to accurately determine mean values of several quantities probing the phase transition in a finite volume, without explicitly calculating the color-singlet partition function itself.

The fourth chapter is dedicated to the numerical determination of the scaling critical exponents characterizing the studied phase transition, by the mean of a finite size scaling analysis.

In the fifth chapter, the excluded volume correction is considered for the hadronic phase, and his effects on the deconfinement phase transition are investigated.

Last, the obtained results are discussed and compared to results of other models and approaches.

Contents

List of Figures

List of Tables

Introduction

It is well established that QCD at finite temperature exhibits a typical behavior of a system with a phase transition. At sufficiently high temperatures and/or densities, quarks and gluons are no more confined into hadrons; strongly interacting matter seems to undergo a phase transition from hadronic state to what has been called the "Quark-Gluon Plasma" (QGP). This is logically a consequence of the quark-parton level of the matter structure and of the dynamics of strong interactions described by the QCD theory. The occurrence of this phase transition is important from a conceptual point of view, as it implies the existence of a novel state of matter, which was present in the early universe up to times $\sim 10^{-5}s$, and which could occur in the core of heavy neutron stars. The only available and experimental way to study the QCD deconfinement phase transition is to try to create in the laboratory, by ultra-relativistic heavy ion collisions, conditions similar to those in the early moments of the universe, right after the Big Bang.

If ever the QGP is created in ultra-relativistic heavy ion collisions, the volume within which the eventual formation would take place would certainly be finite. Also, in lattice QCD studies, the scale of the lattice space volume is finite. This motivates the study of the finite size effects on the expected deconfinement phase transition from a Hadronic Gas (HG) phase to a QGP phase. These effects are certainly important

since statistical fluctuations in a finite volume may hinder a sharp transition between the two phases. Phase transitions are known to be infinitely sharp, signaled by some singularities, only in the thermodynamic limit [1]. In general, finite size effects lead to a rounding of these singularities as pointed out in [2, 3]. However, even in such a situation, it is possible to obtain information on the critical behavior. Large but finite systems show a *universal* behavior called "Finite-Size Scaling" (FSS), allowing to put all the physical systems undergoing a phase transition in a certain number of universality classes. The systems in a given universality class display the same critical behavior, meaning that certain dimensionless quantities have the same values for all these systems. *Critical exponents* are an example of these universal quantities.

This thesis is devoted to the study of the finite size behavior for the deconfinement phase transition. For this purpose, we use a simple QCD model described in [4], based on the standard MIT bag model [5], and on the coexistence of hadronic and QGP phases in a finite system of volume V. The equations of state of the two phases are then used, and mean values of useful thermodynamic quantities can be calculated.

Additionally, we implement the color charge confinement property by requiring to the QGP phase to be a colorless object in the color space. The color-singlet partition function of the QGP is derived using the group theoretical projection technique formulated by Turko and Redlich [6], but can not be exactly determined and is usually calculated within the saddle point approximation in the limit $V_{QGP}T^3 >> 1$ as in [7, 8, 9, 10, 11]. It turns out, in our case, that the use of the obtained approximated partition function for the calculation of a mean value within the definition of our model, has as a consequence the absence of the deconfinement phase transition [12]. This is due to the fact that the approximation used for the calculation of the color-singlet partition

function breaks down at $V_{QGP}T^3 << 1$, and this limit is attained in our case. This has been noted in further works in which additional approximations have been used to carry out calculations, as in [4, 9]. We propose in the following a method which allows us to accurately calculate physical quantities describing well the deconfinement phase transition at finite volumes within the QCD model chosen, avoiding then the problem arising at $V_{QGP}T^3 << 1$ and without any approximation. We proceed by using the exact definition of the color-singlet partition function for Z_{QGP} in the definition of the mean value of a physical quantity. A first analytical step in the calculation of the mean value is then achieved, and an expression with integral coefficients is obtained. The double integrals are then carried out with a suitable numerical method at each value of temperature and volume, and the behavior of the physical quantity of the finite system can so be obtained on the whole range of temperature, for various volumes, without any restriction. Afterwards, scaling critical exponents characterizing the scaling behavior of some quantities are determined using a numerical FSS analysis.

Since hadrons are not pointlike, they should be treated as extended particles. To account for this, we then consider the excluded volume effects and examine their influence on the deconfinement phase transition.

This thesis is organized as follows. After the present introduction, the first chapter is mainly an overview of the physics of phase transitions, and the standard classification existing in literature. Besides, we have tried to achieve a more general classification of phase transitions.

In the second chapter, phase transitions in finite systems are reviewed. Finite-size effects are examined as well as finite-size scaling.

In the third chapter, we study the deconfinement phase transition in a finite system

within the phase coexistence model. Equations of state of infinite matter are first used for a hadronic gas of pions and for a QGP consisting of gluons and massless quarks, and some physical quantities are studied for both temperature and density driven deconfinement phase transition, since their expressions with T and μ are obtained [13, 14]. Then, the color-singletness requirement is implemented in the partition function of the QGP using the projection method. An approximate color-singlet partition function of the QGP has been derived within the saddle point approximation and used in a first step, in our works [15, 16], to calculate mean values of thermodynamical quantities. Secondly, the exact integral expression of the color-singlet partition function of the QGP is used to accurately determine mean values of several quantities probing the phase transition in a finite volume, without explicitly calculating the color-singlet partition function itself.

The fourth chapter is dedicated to the numerical determination of the scaling critical exponents characterizing the studied phase transition, by the mean of a finite size scaling analysis.

In the fifth chapter, the excluded volume correction is implemented for the hadronic phase, and their effects on the deconfinement phase transition are investigated.

Last is a discussion of the obtained results and a conclusion to our work.

Chapter 1

General Study of Phase Transitions

1.1 Introduction

The study of the physics of phase transitions phenomena occurring in nature is considered to be a subject of great interest to physicists. It is easy to understand the importance of this subject because firstly the list of systems exhibiting interesting phase transitions continues to expand, including the Universe itself, and secondly the theoretical framework of equilibrium statistical mechanics has found applications in very different areas of physics like string field theories, elementary particle physics, physics of the chaos, condensed matter ... etc.

Phase transitions are abrupt changes in the global behavior and in the qualitative properties of a system when certain parameters pass through particular values. Technically, phase transitions are characterized by the appearance of singularities in some thermodynamic quantities, in the thermodynamical limit where the volume V and the number of particles N go to infinity, while the density $\rho = \frac{N}{V}$ remains constant. That is, at the transition, some global behavior is not analytic in the infinite volume limit.

Examples of phase transitions are:

- The transitions between the solid, liquid, and gaseous phases (evaporation, boiling, melting, freezing, sublimation, etc.).
- The transition between the ferromagnetic and paramagnetic phases of magnetic materials at the Curie point.
- The emergence of superconductivity in certain metals when cooled below a critical temperature.
- Quantum condensation of bosonic fluids, such as Bose-Einstein condensation and the superfluid transition in liquid helium.
- The breaking of symmetries in the laws of physics during the early history of the universe as its temperature cooled.

In this chapter, we want to give an overview on the physics of phase transitions, and the related features. We'll look carefully at how the thermodynamic variables behave close to the transition point, in order to compare the behavior at first- and higher-order transitions, and to define the critical exponents. The QCD phase transition is also reviewed since it is subject of our study in this thesis, as well as some results of lattice QCD.

1.2 Review of Some Useful Thermodynamic Functions

The order of a phase transition is one of the basic thermodynamic classifications. It concerns the thermodynamic potential and its derivatives at the transition. In Tables (1.1) and (1.2), we recall the thermodynamic formulas for a magnet and a fluid [15], where $\beta = \frac{1}{T}$ with the units chosen as: $k_B = \hbar = c = 1$.

First derivatives of the physical potential (the free energy for the fluid system) with respect to T, H or V lead to the internal energy U, the entropy S, the magnetization M or the pressure P, according to the equations in Tables (1.1) and (1.2). On the second level of derivatives, we have the specific heat C at constant H or M (respectively at constant V or P for a fluid) and the isothermal susceptibility χ_T for a magnet (respectively the isothermal compressibility κ_T for a fluid).

In the infinite volume limit, a phase transition is signalled by a singularity (in the sense of non analyticity) in some thermodynamic function. On whether a discontinuity occurs in one of the first derivatives or of the second or higher derivatives of the thermodynamical potential Ω, depends the order of the transition and the class to which the phase transition belongs. But before enumerating the different classes of phase transitions, let us introduce in the following a characteristic quantity of the transition representing the main qualitative differences between the various phases, whose evolution allows the determination of the nature of the phase transition, namely *The Order Parameter.*

Thermodynamic variables for a magnet

First law: $dU = TdS - MdH$

Partition function

$$Z(T,H) = \sum_r e^{-\beta E_r}$$

$$\downarrow$$

Free energy

$$F = -T \ln Z$$

$$\swarrow \qquad \downarrow \qquad \searrow$$

Internal energy	*Entropy*	*Magnetization*
$U = \dfrac{-\partial \ln Z}{\partial \beta}$	$S = -\left(\dfrac{\partial F}{\partial T}\right)_H$	$M = -\left(\dfrac{\partial F}{\partial H}\right)_T$
$\downarrow$	$\downarrow$	$\downarrow$
Specific Heat (constant H)	*Specific Heat (constant $X = H, M$)*	*Isothermal susceptibility*
$C_H = \left(\dfrac{\partial U}{\partial T}\right)_H$	$C_X = T\left(\dfrac{\partial S}{\partial T}\right)_X$	$\chi_T = \left(\dfrac{\partial M}{\partial H}\right)_T$

Table 1.1: Thermodynamic variables for a magnetic system

Thermodynamic variables for a fluid

First law: $dU = TdS - PdV$

Partition function

$$Z(T,H) = \sum_r e^{-\beta E_r}$$

$$\downarrow$$

Free energy

$$F = -T \ln Z$$

$$\swarrow \qquad \downarrow \qquad \searrow$$

Internal energy	*Entropy*	*Pressure*
$U = \dfrac{-\partial \ln Z}{\partial \beta}$	$S = -\left(\dfrac{\partial F}{\partial T}\right)_V$	$P = -\left(\dfrac{\partial F}{\partial V}\right)_T$
$\downarrow$	$\downarrow$	$\downarrow$
Specific Heat (constant V)	*Specific Heat (constant $X = V, P$)*	*Isothermal compressibility*
$C_V = \left(\dfrac{\partial U}{\partial T}\right)_V$	$C_X = T\left(\dfrac{\partial S}{\partial T}\right)_X$	$\kappa_T = -\dfrac{1}{V}\left(\dfrac{\partial V}{\partial P}\right)_T$

Table 1.2: Thermodynamic variables for a fluid system

1.3 Order Parameter of a General x-driven phase transition

Thermodynamical systems can exist in various stable homogeneous states (phases) which might differ in their structure, symmetry, order and dynamics. We represent this stability by the presence of an order in the system. Any modification occurring in one parameter can lead to a macroscopic change in the state and alter its stability, and as a consequence there is a wholesale reorganization of matter, even locally. Then, the system undergoes an abrupt change from one phase to another, called a phase transition, whose signature is a singularity or discontinuity of some observable physical properties. A first mathematical description of phase transitions was given by Gibbs [16] who characterized a phase transition by a point of non-analyticity in one or more thermodynamic functions. The apparition of a phase transition is nowadays interpreted as coming from the strong fluctuations of the system close to the critical point. At the critical point, the system exhibits a singular behavior and the phase transition is known as a critical phenomenon. Kramers was the first who suggested that the singular behavior only appears when the thermodynamic limit is taken (the volume V and the number of particles N go to infinity, with a fixed density $\rho = \frac{N}{V}$). This view was demonstrated theoretically through the famous work of Lee and Yang published in 1952 [17].

If we consider a phase transition between two different phases, we have certainly one of the phases as statistically more ordered (Ordered Phase) than the other (Disordered Phase). In an other sense, we can speak about a disorder-order phase transition which results from the loss of stability of the disordered (parent) phase. The stability is

Transition	Order Parameter $\langle\mathcal{O}\rangle$
Ferromagnetic Transition	Spontaneous Magnetization
Water Gas-Liquid Transition	Density Difference between Liquid and Gas
Liquid Crystal Transition	Degree of Orientational Order
Superconducting Transition	Energy Gap between the Ground State and the Spectrum of Single-Particle Excitations

Table 1.3: Order parameters of some phase transitions

restored by a distortion of the parent phase and in this way a distorted (ordered) phase is created. The most useful function generally used to characterize this order is a some appropriate thermodynamical quantity which has a non-vanishing value in the ordered phase and a zero value in the disordered phase. We commonly call this quantity "*Order Parameter*", since its value reflects the strength and kind of ordering in the system, and we'll note it $\mathcal{O}$ in the following. Then by definition:

$$\begin{cases} \langle\mathcal{O}\rangle = \langle\mathcal{O}\rangle^{+} & \text{, the system is in an ordered phase} \\ \langle\mathcal{O}\rangle = \langle\mathcal{O}\rangle^{-} < \langle\mathcal{O}\rangle^{+} & \text{, the system is in a disordered phase} \end{cases}$$

in which $\langle ... \rangle$ means the statistical average.

An order parameter may be a scalar quantity or may be a multicomponent (or even complex) quantity and is defined differently in different kinds of physical systems. We give in Table (1.3) some examples of order parameters as defined in special known systems [18].

In both experimental and numerical Monte Carlo studies, a complete study of the behavior of a well chosen order parameter $\langle\mathcal{O}\rangle$ at the phase transition is usually a key to determine the nature of the phase transition and gives a good way to calculate its most important thermodynamical properties. When studying the phase transition, we need then to define the varying thermodynamical parameter x (temperature (T), magnetc field (H), chemical potential (μ), ...) whose change may cause the phase

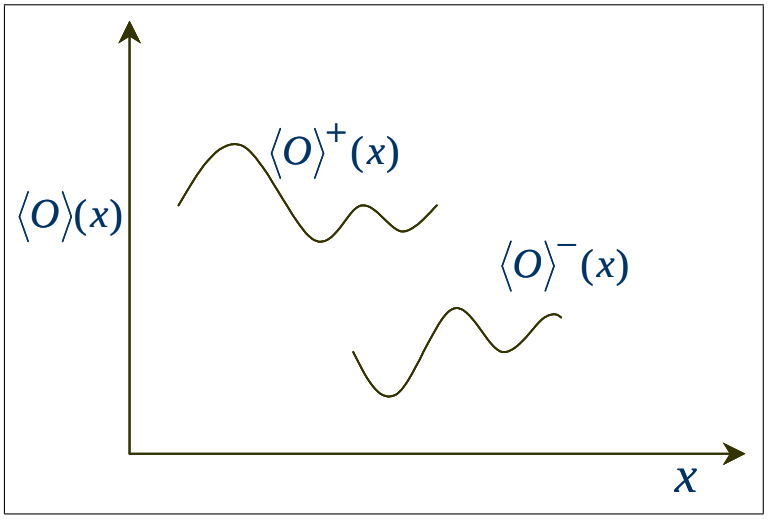

Figure 1.1: Evolution of the order parameter from the ordered phase to the disordered phase as a function of the thermodynamic $x-$variable driving the phase transition.

transition and then, on which it is interesting to study the dependence of $\langle\mathcal{O}\rangle$. We speak about an x-driven phase transition, and therefore we describe the phase transition with the help of diagrams where the order parameter is plotted against the respective thermodynamic parameter x, i. e., $\langle\mathcal{O}\rangle = \langle\mathcal{O}\rangle(x)$. Going from the ordered phase to the disordered phase, the evolution of $\langle\mathcal{O}\rangle(x)$ from $\langle\mathcal{O}\rangle^{+}(x)$ to $\langle\mathcal{O}\rangle^{-}(x)$, Fig. (1.1), can have mathematically different behaviors. According to this, we can distinguish three different classes of phase transitions, which have quite different qualitative properties near the transition point.

1.4 Standard Classification of Phase Transitions

Discontinuous or **First Order Phase Transitions** (**1st-OPT**) are characterized by a finite discontinuity in $\langle\mathcal{O}\rangle(x)$ (i. e. basically in anything except the free energy, which of course must be equal for the two phases at the transition point). The transition point

will be marked by a sudden and drastic jump from one phase ($\langle\mathcal{O}\rangle^{+}(x)$) to the other ($\langle\mathcal{O}\rangle^{-}(x)$) as illustrated in Fig. (1.2). For example, in the case of a ferromagnet there is a jump in the magnetization, if one passes through the transition temperature from the phase of broken symmetry to the symmetric phase, and the phase transition is then of first order.

Second Order Phase Transitions (**2^{nd}-OPT**), on the other hand, are characterized by a continuous but nonanalytic behavior of $\langle\mathcal{O}\rangle(x)$. A finite discontinuity appears in the first derivative of $\langle\mathcal{O}\rangle(x)$ as illustrated in Fig. (1.3). The transition to superconductivity without an external magnetic field is an example of phase transitions of this kind, where the discontinuity of the specific heat at T_c is due to a kink in the entropy. When the discontinuity in the first derivative of $\langle\mathcal{O}\rangle(x)$ becomes infinite as in Fig. (1.4), the phase transition is called a **continuous Phase Transition** (**c-PT**). Because of the characteristic shape of the first derivative of the order parameter in this case, such phase transitions are called **"$\lambda-$Transitions"**. An interesting example of such phase transitions is the transition to superfluidity in ^4He, in which the discontinuity in the specific heat is not due to a kink in the entropy but to a vertical tangent at T_c [19].

This is somewhat a resume of the Ehrenfest and Fisher classifications. The **Ehrenfest classification scheme** was the first attempt at classifying phase transitions, based on the degree of non-analyticity involved. Under this scheme, phase transitions were labelled by the lowest derivative of the thermodynamic potential that is discontinuous at the transition, such that is called of **n^{th}-Order** the phase transition for which there is a discontinuity at the **n^{th}-**order derivative of an appropriate thermodynamic potential. Though useful, Ehrenfest classification is flawed since it didn't account for

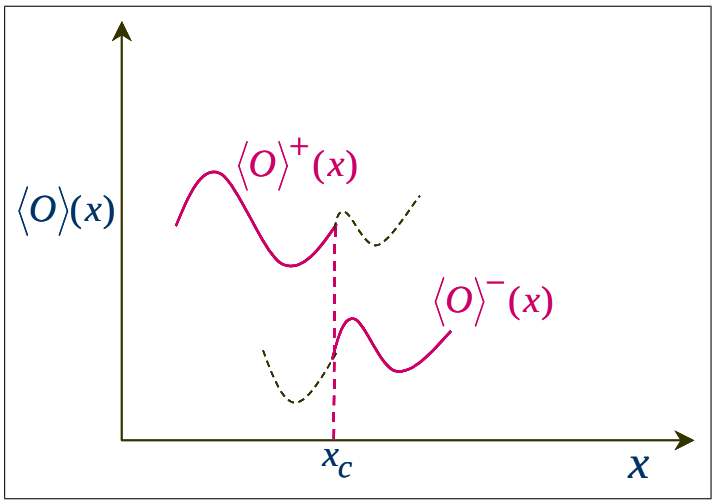

Figure 1.2: Behavior of the order parameter as a function of the thermodynamic $x-$variable driving the transition, for a first-order phase transition.

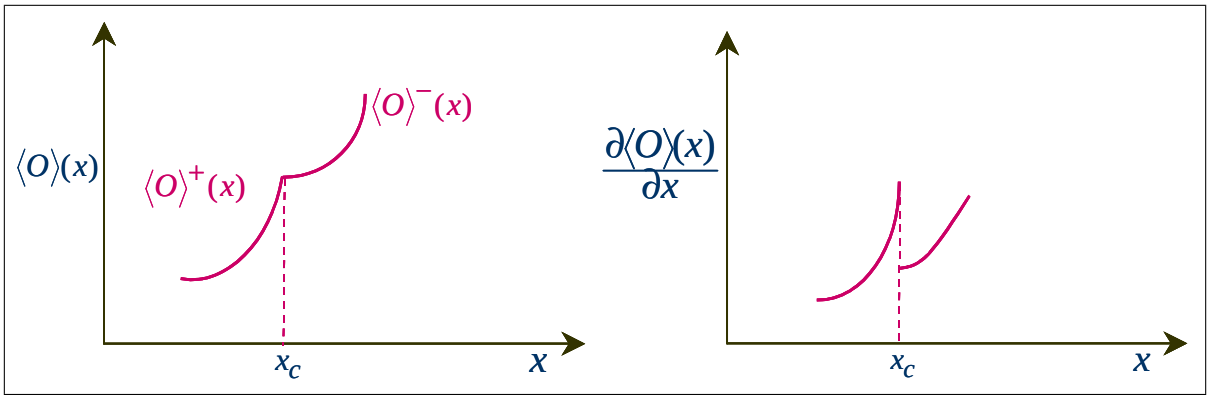

Figure 1.3: Behavior of the order parameter and its first derivative with respect to the thermodynamic $x-$variable driving the transition, near the critical point x_c for a second-order phase transition.

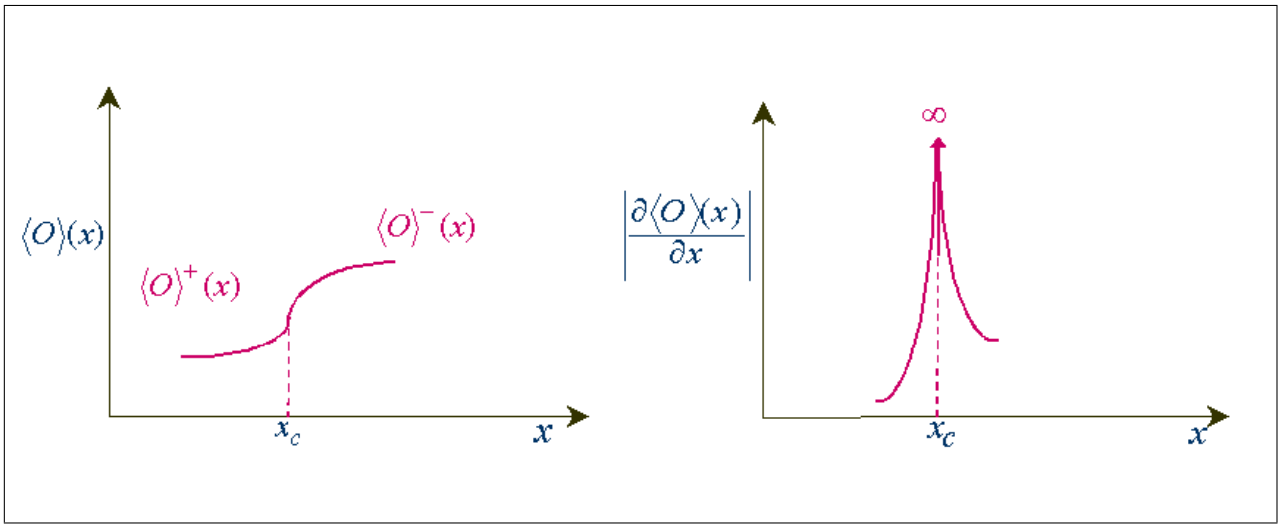

Figure 1.4: Behavior of the order parameter and its first derivative with respect to the thermodynamic $x-$variable driving the transition, near the critical point x_c for a $\lambda-$transition.

the case of a divergence in the derivatives of the thermodynamic potential. After this, a more complete classification which is **Fisher classification scheme** came, under which is denoted by **1st-Order phase transition** the case for which the **1st** derivative of the thermodynamic potential is discontinuous and by **"higher order phase transition"** or **"continuous phase transition"** the case for which the **1st** derivatives of the thermodynamic potential are continuous while the **2**nd derivatives are either discontinuous or infinitely divergent.

1.5 Mathematical description of general x-driven phase transitions and new approach to their classification

To achieve a more general classification of phase transitions, let us start from a general case of an x-driven phase transition described by an order parameter $\langle \mathcal{O} \rangle (x)$ having a behavior schematized in Fig. (1.2) in which we suppose a finite discontinuity at the transition point x_c . The parent phase is described by $\langle \mathcal{O} \rangle^{+} (x)$ and the final phase by $\langle \mathcal{O} \rangle^{-} (x)$. When the finite discontinuity becomes smaller getting close to zero, we can have a continuous Phase Transition (**c-PT)** case from the initial discontinuous Phase Transition (**d-PT)** case. This fact allows to consider the **d-PT** case as more general than the **c-PT** one. We can then write:

$$\begin{cases} \langle \mathcal{O} \rangle (x) = \langle \mathcal{O} \rangle^{-} (x) \ \text{ if } \ x \succ x_c \\ \langle \mathcal{O} \rangle (x) = \langle \mathcal{O} \rangle^{+} (x) \ \text{ if } \ x \prec x_c \ , \end{cases} \tag{1.1}$$

from which a formal analogy with the definition of the causal temporal green function as well known in the standard statistical quantum field theory is to be noted. Then by using the Heaviside step- function $\Theta(x)$, we rewrite eq. (1.1) in the compact form :

$$\langle \mathcal{O} \rangle (x) = [1 - \Theta(x - x_c)] \langle \mathcal{O} \rangle^{+} (x) + \Theta(x - x_c) \langle \mathcal{O} \rangle^{-} (x). \tag{1.2}$$

This formula will reveal a great importance in what follows since its mathematical manipulation, as we shall see, permits to construct a new classification of the existing phase transitions, which agrees very well with the Fisher's classification and gives a clarification to the Ehrenfest one.

We suppose now that the singular behavior manifested by the phase transition at

x_c appears in the $\mathbf{n^{th}}$**-order** derivative: $\frac{\partial^n \langle \mathcal{O} \rangle}{\partial x^n}(x \to x_c) \sim \infty$, the $\{(\mathbf{n-1})$**-order**$\}$ derivatives being all continuous functions. We need then to derive the $\mathbf{n^{th}}$**-order** derivative of $\langle \mathcal{O} \rangle (x)$:

$$\langle \mathcal{O} \rangle_n (x) = -\boldsymbol{\delta}(x - x_c)\Delta \langle \mathcal{O} \rangle_{n-1} (x) + [1 - \Theta(x - x_c)] \langle \mathcal{O} \rangle_n^+ (x) + \Theta(x - x_c) \langle \mathcal{O} \rangle_n^- (x), \tag{1.3}$$

with:

$$\begin{cases} \langle \mathcal{O} \rangle_n (x) = \dfrac{\partial^n \langle \mathcal{O} \rangle (x)}{\partial x^n} \\ \boldsymbol{\Delta} \langle \mathcal{O} \rangle_n (x) = \langle \mathcal{O} \rangle_n^+ (x) - \langle \mathcal{O} \rangle_n^- (x). \end{cases} \tag{1.4}$$

The possible mathematical cases in which we can have a singularity corresponding to our phase transition are the followings:

1. <u>**Case N°1**</u>: $\Delta \langle \mathcal{O} \rangle_{n-1} (x)$=finite and $\langle \mathcal{O} \rangle_n^{\pm} (x)$=finite. We have a finite discontinuity in $\langle \mathcal{O} \rangle_{n-1} (x)$ and the singularity is dominated by the $\delta(x - x_c)$ function:

$$\langle \mathcal{O} \rangle_n (x) \sim \delta(x - x_c), \tag{1.5}$$

   $\Rightarrow$ The phase transition is called $\mathbf{n^{th}}$**-Order d-PT.**

2. <u>**Case N°2**</u>: $\Delta \langle \mathcal{O} \rangle_{n-1} (x) = 0$ and $\langle \mathcal{O} \rangle_n^{\pm} (x) = \infty$. We have no discontinuity in $\langle \mathcal{O} \rangle_{n-1} (x)$ and the singularity is dominated by divergent $\langle \mathcal{O} \rangle_n^{\pm} (x)$:

$$\langle \mathcal{O} \rangle_n (x) \sim [1 - \Theta(x - x_c)] \langle \mathcal{O} \rangle_n^+ (x) + \Theta(x - x_c) \langle \mathcal{O} \rangle_n^- (x), \tag{1.6}$$

   $\Rightarrow$ The phase transition is called $\mathbf{n^{th}}$**-Order c-PT.**

3. <u>**Case N°3**</u> : $\Delta \langle \mathcal{O} \rangle_{n-1} (x)$ = finite and $\langle \mathcal{O} \rangle_n^{\pm} (x) = \infty$. We are opposite a special case, in which the singularity comes from both $\delta(x - x_c)$ and divergent $\langle \mathcal{O} \rangle_n^{\pm} (x)$. Until now, to our knowledge, we have not observed any experimental phase transition manifesting the two different kinds of singularities at the same time.

4. **Case N°4** : $\Delta \langle \mathcal{O} \rangle_{n-1}(x) = 0$ and $\langle \mathcal{O} \rangle_n^{\pm}(x) =$ finite. In this case the phase transition does not manifest any singularity in the $\langle \mathcal{O} \rangle_n(x)$. We must look for it in the $(\mathbf{n+1})$-order derivative, and then similar cases may appear at this level.

We can then summarize our classification by saying that we have in reality two different kinds of phase transitions: discontinuous phase transitions (**d-PT**) and continuous phase transitions (**c-PT**). The order of a **d-PT** is nothing but the order of the derivative of the order parameter at which the singularity appears as a δ-function:

$$\mathbf{n^{th}-Order\ d-PT\ class}$$

$$\langle \mathcal{O} \rangle_{n-1}(x) \sim \Theta(x - x_c), \quad \langle \mathcal{O} \rangle_n(x) \equiv \delta(x - x_c) \ ,$$

which agrees with the first and traditional classification formulated by Ehrenfest (1933).

For the **c-PT**, the singularity comes from a divergent $\langle \mathcal{O} \rangle_n^{\pm}(x)$ and with the same considerations, we can speak about the order of the **c-PT** as the order of the derivative $\langle \mathcal{O} \rangle_n(x)$ having a divergent behavior. We note that this case of an infinite singularity in the $\langle \mathcal{O} \rangle_n(x)$ fails to the Ehrenfest classification because :

$$\mathbf{n^{th}-Order\ c-PT\ class}$$

$$\underset{x \to x_c}{Lim} \langle \mathcal{O} \rangle_n(x) \equiv \infty, \quad \Leftrightarrow \quad \langle \mathcal{O} \rangle_{n-1}(x) \propto (x - x_c)^{\upsilon} \ ,$$

which gives a constraint on the value of the critical exponent υ : $\upsilon - 1 \prec 0$.

We finish our discussion by a diagrammatic view which may explain more clearly the different kinds of phase transitions existing in nature.

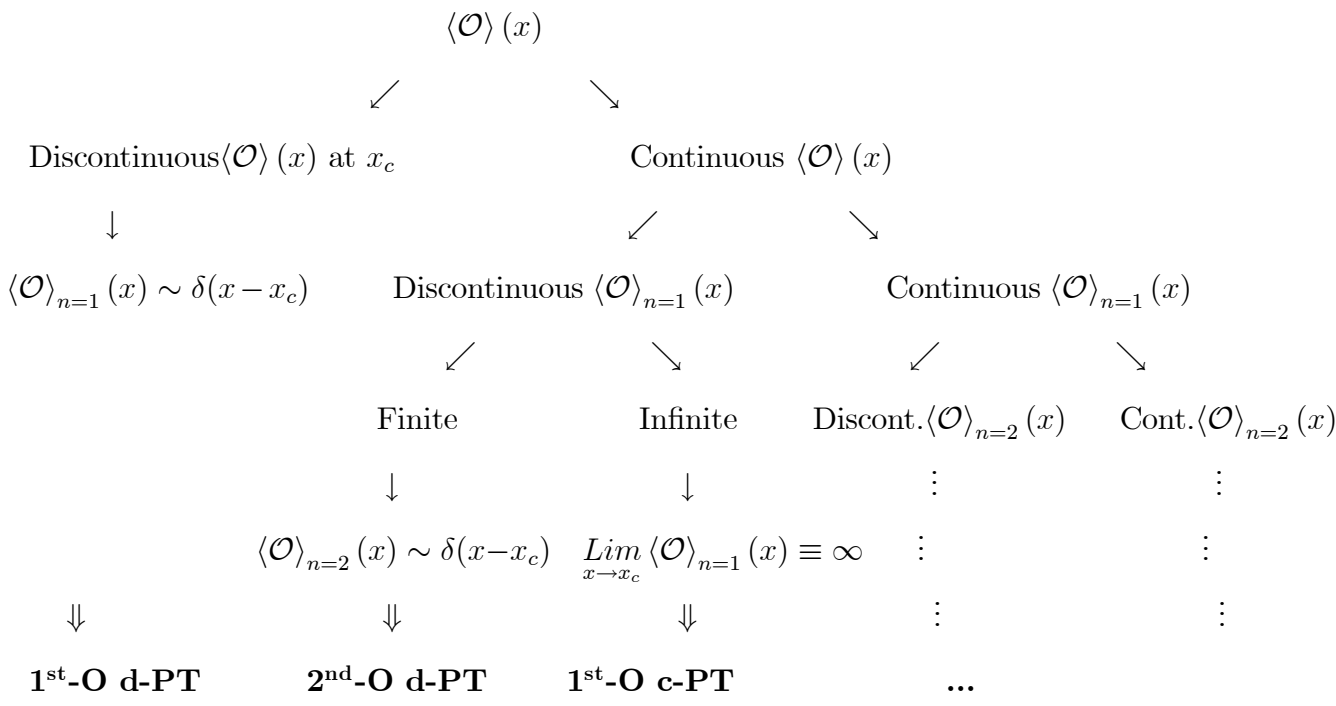

1.6 Critical Behavior and Exponents

From thermodynamical point of view, a critical point is characterized by the type of singularity of the thermodynamic potential and its derivatives with respect to the relevant variables at this point. It turns out to be very important to the theory of critical phenomena to understand more carefully the form of the singular behavior of these quantities near the critical point. Considering the critical behavior, it is convenient to speak in terms of the reduced distance from the critical point:

$$\widetilde{x} = \frac{x - x_c}{x_c}, \tag{1.7}$$

then, the thermodynamic functions have singularities at $\widetilde{x} = 0$. Data from multiple experiments as well as results from a number of exactly soluble models show that these thermodynamic functions can be described by a set of simple power laws in the vicinity

of the critical point x_c, characterized by powers, with a customary notation in terms of greek letters, called *Critical Exponents*. Then the critical exponent associated with a function $F(\widetilde{x})$ is:

$$\lambda = \lim_{\widetilde{x}\to 0} \frac{\ln|F(\widetilde{x})|}{\ln|\widetilde{x}|} \ , \tag{1.8}$$

assuming that the limit exists, or as it is more usually written:

$$F(\widetilde{x}) \sim |\widetilde{x}|^{\lambda} \ . \tag{1.9}$$

The proportionality sign $\sim$ is to remind that eq. (1.9) only represents the asymptotic behavior of the function $F(\widetilde{x})$ as $\widetilde{x} \to 0$, and is then an asymptotic law. More generally, one might expect:

$$F(\widetilde{x}) = A\,|\widetilde{x}|^{\lambda}\left(1 + b\widetilde{x}^{\lambda_1} + ...\right), \quad \lambda_1 > 0. \tag{1.10}$$

It can easily be seen that sufficiently near the critical point, the behavior of the leading term dominates.

Definitions of the most commonly used critical exponents connected to the most important quantities are given in the following, for thermally driven phase transitions in fluids and/or magnets.

- **The exponent $\boldsymbol{\alpha}$**

This exponent describes the divergence of the specific heat C_V for a fluid or C_H for a magnet near the critical point:

$$C_V \sim |t|^{-\alpha}, \quad C_H \sim |t|^{-\alpha}, \tag{1.11}$$

where the deviation in temperature from the critical temperature T_c has been noted t.

- **The exponent $\boldsymbol{\beta}$**

The critical exponent β is connected to the density difference $\left(\rho_l - \rho_g\right)$ for a fluid system or the spontaneous magnetization M for a magnetic system. It shows how the order parameter varies with the varying temperature T as T_c is approached.

$$\left(\rho_l - \rho_g\right) \sim (-t)^{\beta}, \quad M \sim (-t)^{\beta}. \tag{1.12}$$

- **The exponent γ**

This exponent describes the critical variation at $t \to 0$ of the isothermal compressibility κ_T for a fluid and the isothermal susceptibility χ_T for a magnet:

$$\kappa_T \sim |t|^{-\gamma}, \quad \chi_T \sim |t|^{-\gamma}. \tag{1.13}$$

- **The exponent δ**

The exponent δ describes the variation of the difference in Pressure $(P - P_c)$ with $\left(\rho_l - \rho_g\right)$ (fluid) and of the field H with magnetization M (magnet) along the critical isotherm $T = T_c$:

$$(P - P_c) \sim \left|\rho_l - \rho_g\right|^{\delta} sgn(\rho_l - \rho_g), \qquad H \sim |M|^{\delta} sgn(M), \tag{1.14}$$

where sgn is the sign function:

$$sgn(z) = \begin{cases} \dfrac{z}{|z|} \text{ if } z \neq 0 \\ 0 \text{ if } z = 0\ . \end{cases} \tag{1.15}$$

- **The exponent η**

The critical exponent η is associated to the critical variation at $t \to 0$ of the

connected two point correlation function $G(r)$ [1], where r denotes the separation of the two points, at $P = P_c$ for a fluid or at $H = 0$ for a magnet.

$$G(r) \sim r^{-(d-2+\eta)}. \tag{1.16}$$

Here d is the dimensionality of the system.

- **The exponent ν**

The last exponent concerns the correlation length which is a measure of the range of the correlation function.

$$\xi \sim |t|^{-\nu}, \qquad t \to 0,\ H = 0. \tag{1.17}$$

The exponent definitions are summarized for fluid and magnetic system in Tables (1.4) and (1.5) respectively [15, 20].

[1] Thermodynamic variables like the magnetization or the entropy are macroscopic properties. A much fuller understanding of phase transitions can be obtained by considering what happens on a microscopic level. To be able to do this in a more qualitative way, we introduce correlation functions [15]. Let the order parameter $\mathcal{O}$ be written as a volume integral over an order parameter density $\mathfrak{o}(\overrightarrow{r})$ as: $\mathcal{O} = \left\langle \int d^3r\ \mathfrak{o}(\overrightarrow{r}) \right\rangle$, where $\langle ... \rangle$ represents the statistical average by which one obtains thermodynamic functions. The correlation function defined as: $G(\overrightarrow{r}) = \langle \mathfrak{o}(\overrightarrow{r})\mathfrak{o}(0)\rangle - \langle \mathfrak{o}(\overrightarrow{r})\rangle \langle \mathfrak{o}(0)\rangle$, measures how the value of the order parameter at one point is correlated to its value at some other point. Away from the critical point, far away points ($r \to \infty$) become uncorrelated and hence the correlation length decays to zero. This decay is exponential with the form: $G(\overrightarrow{r}) \sim r^{-\tau} e^{-r/\xi}$, where τ is some number, and ξ the correlation length which is a measure of the range over which fluctuations in one region of space are correlated with those in another region. Experimentally, the correlation length is found to diverge at the critical point, which means that very far points become correlated. Thus the system near a second-order PT 'loses memory' of its microscopic structure and begins to display new long-range macroscopic correlations. Evidence form experiments and exactly soluble models shows that here the correlation function decays as a power law: $G(\overrightarrow{r}) \sim r^{-(d-2+\eta)}$.

Specific heat at constant volume	$C_V \sim \lvert t\rvert^{-\alpha}$
Liquid-gas density difference	$\left(\rho_l - \rho_g\right) \sim (-t)^{\beta}$
Isothermal compressibility	$\kappa_T \sim \lvert t\rvert^{-\gamma}$
Critical isotherm ($t = 0$)	$P - P_c \sim \left\lvert \rho_l - \rho_g \right\rvert^{\delta} sgn(\rho_l - \rho_g)$
Pair correlation function at T_c	$G(r) \sim r^{-(d-2+\eta)}$
Correlation length	$\xi \sim \lvert t\rvert^{-\nu}$

Table 1.4: Definitions of the most commonly used critical exponents for a fluid system

Zero-field specific heat	$C_H \sim \lvert t\rvert^{-\alpha}$
Zero-field magnetization	$M \sim (-t)^{\beta}$
Zero-field isothermal susceptibility	$\chi_T \sim \lvert t\rvert^{-\gamma}$
Critical isotherm ($t = 0$)	$H \sim \lvert M\rvert^{\delta} sgn(M)$
Pair correlation function at T_c	$G(r) \sim r^{-(d-2+\eta)}$
Correlation length	$\xi \sim \lvert t\rvert^{-\nu}$

Table 1.5: Definitions of the most commonly used critical exponents for a magnetic system

1.7 Universality, Scaling and Renormalization Group Theory

Having defined the critical exponents, we need to justify why they are interesting, and indeed why they are more interesting than the critical point itself. It turns out that, whereas the critical point depends sensitively on the details of the interatomic interactions, the critical exponents are to a large degree *universal* depending only on a few fundamental parameters, consisting in the dimensionality of space, the symmetry of the order parameter and the range of the interaction. Simple systems, or numerical models appropriate for computer simulations, are used to describe the critical behavior. The results are then extended to more complex systems: by making sure that one is working in the right dimension and that the symmetry is correctly represented by a model, it can be used to obtain critical exponents for *all* the systems within its *universality class*.

Universality Class	Symmetry of Order Parameter	α	β	γ	δ	ν	η
2-d Ising	2-component scalar	0 (log)	1/8	7/4	15	1	1/4
3-d Ising	2-component scalar	0.10	0.33	1.24	4.8	0.63	0.04
3-d X-Y	2-dimensional vector	0.01	0.34	1.30	4.8	0.66	0.04
3-d Heisenberg	3-dimensional vector	-0.12	0.36	1.39	4.8	0.71	0.04
2-d Potts, $q = 3$	q-component scalar	1/3	1/9	13/9	14	5/6	4/15
$q = 4$		2/3	1/12	7/6	15	2/3	1/4

Table 1.6: Examples of universality classes with the corresponding symmetry of the order parameter and the values of the critical exponents

Striking evidence for this comes when comparing the value of the critical exponent β for phase transitions in completely different systems, with a scalar order parameter, such as the liquid-gas phase transition, magnets with uniaxial anisotropy in spin space, phase separation in the binary fluid mixture and the lattice models of ± 1 spins (Ising models); in all these cases β is the same, 1/3, and thus all four systems fall in the same *universality class* in the sense that they are described by the same scaling relations. The Ising model, however, is much simpler than the other experimental systems, and it has been used extensively in numerical simulations [21].

Some universality classes are listed in Table (1.6) with a description of the symmetry of the corresponding order parameter and the values of the critical exponents [15].

Universality means that systems differing in microscopic details (e.g. different types of interaction potentials, ion species, ... etc) exhibit identical collective behavior, or as termed by Kadanoff [22]: *"All phase transition problems can be divided into a small number of different classes depending upon the dimensionality of the system and the symmetries of the ordered state. Within each class, all phase transitions have identical behavior in the critical region, only the names of thermodynamic variables are changed".*

Not all of the critical exponents defined in the previous section are independent

Rushbrooke's law	$\alpha + 2\beta + \gamma \geq 2$
Griffiths law	$\alpha + \beta\,(1 + \delta) \geq 2$
Fisher's law	$(2 - \eta)\,\nu \geq \gamma$
Josephson's law	$d\nu \geq 2 - \alpha$

Table 1.7: Scaling laws of critical exponents

and using a number of thermodynamic arguments one can derive a series of exponent relations called *scaling laws.* Rushbrooke (1963), Griffiths (1965), Josephson (1967) and Fisher (1969) were the first to find certain inequalities between the critical exponents. By experimental evidence, it turned out later that these are in fact equalities. Table (1.7) resumes these scaling laws.

Universality in critical phenomena is described by the *Renormalization Group Theory.* The first work describing the fundamental concepts of the renormalization group approach was the paper of K. G. Wilson published in 1971 [23]. The renormalization group works by changing the length scale of a system by removing degrees of freedom, using renormalization group transformations which relate a system with correlations on the scale ξ to another system with correlations on the scale ξ/b, where the scale factor $b > 1$. Only at criticality will the properties of the system remain unaltered by the change in scale and hence the critical behavior is described by the so-called fixed points of the transformation, and this leads to the important result that the thermodynamic functions can be written in a scaling form. The equality of the critical exponents above and below the critical temperature and the relations between them then follow immediately [15, 21, 24].

We note that the ideas of *Universality, Scaling* and *Renormalization* are important concepts from which a modern understanding of critical phenomena has emerged, and H.E. Stanley has recently pointed out in his famous article [25] that: *"Scaling, Univer-*

sality and Renormalization are the three pillars of the current understanding of modern critical phenomena".

1.8 QCD phase transition and the Hagedorn temperature

Today, we think that we arrived at a deep level of structure of matter. All matter in the universe is constructed from Quarks and Leptons: the Quark-Lepton Level. These fundamental particles are spin $\frac{1}{2}$: "fermions" and are classified into three "generations" (or families) and interact through the exchange of gauge bosons. Both quarks and leptons are structureless at the smallest distances currently probed by the highest energy accelerators (current limits of resolution or present observational limit $\sim 10^{-21}m = 10^{-6}fm$ [26]).

If we heat and/or compress very highly a strongly interacting (hadronic) matter, we arrive to such extreme conditions which do not permit the hadrons to survive, and above a certain high temperature T_c and/or high density n_c, the dissolution of the hadronic matter into its components can occur, and a weakly interacting system of nearly free quarks and gluons can be created. Since quarks and gluons play similar roles in Quantum Chromo-Dynamics (QCD) than the electrons and photons in Quantum Electro-Dynamics (QED), this phase is generally known as the Quark Gluon Plasma (QGP), Partonic Plasma or Non-Abelian Plasma. In this naive picture, the phase diagram of QCD contains two important regions:

- A Hadronic Gas (HG) phase at low temperature (density).
- A QGP phase at high temperature (density).

The qualitative differences between these two phases lead to speculate the existence of a phase transition connecting them, commonly called the QCD Deconfinement Phase Transition (DPT), which is as old as the quark structure of matter [27, 28, 29, 30].

The nature and the character of this QCD DPT are still much debated questions. Its existence, however, has been partly supported by Lattice QCD calculations and the Cosmological Standard Model predictions. Experimentally, the only way to study this QCD phase transition is to try to recreate, in ultra-relativistic heavy ion collisions, conditions similar to those which occurred in the early times of the universe ($\sim 10^{-6}s$), immediately after the big bang. To understand the physics of this QCD DPT, numerous studies have been performed using phenomenological approaches to the two-phase nature of strongly interacting matter; the "Statistical Bootstrap Model" (SBM) of Hagedorn is one of those [31, 32]. It is a statistical model based on the observation that hadrons not only form bound and resonance states but also decay statistically into such states if they are heavy enough. This leads to the concept of a sequence of heavier and heavier bound and resonance states, each being a possible constituent of a still heavier resonance, while at the same time being itself composed of lighter ones. We call these states "clusters" or "fireballs". The thermodynamical study of nuclei collisions shows that when the impact energy gets very high, the temperature in the collision, estimated from the energy distribution of the emitted fragments, does not increase as fast as the model suggests. The temperature seems to approach some kind of plateau as the collision energy grows. This is due to the fact that the energy in the collision is high enough to convert into mass, and then higher-mass hadrons are created: the temperature in the collision remains the same until the most massive hadron has been created, then it starts to increase again.

The same situation occurs during the liquid-vapor transition in water: the temperature of boiling water does not change during the phase transition when water enters its vapor phase. Hagedorn suggested that this limiting temperature, of the order of pion mass, characterizes the limit of existence of hadronic matter.

Several estimates of this temperature from the SBM have been given, and here are some of them [32]:

- The Frautschi-Yellin bootstrap equation (BE) yields with pions only:

$$T_0 \approx 0.145 GeV$$

- If K and N were added to the input: $T_0 \approx 0.135 GeV$

- Hamer and Frautschi solve their BE by numerical iteration and read off:

$$T_0 \approx 0.140 GeV$$

- Nahm derives a sum rule from which he found, under different assumptions:

$$T_0 \approx 0.154 GeV$$

$$\text{or } T_0 \approx 0.142 GeV$$

Actually, this singular temperature is interpreted as the temperature where (for chemical potential $\mu = 0$) the phase transition from hadronic matter to quark-gluon plasma occurs.

Another widely used model describing the QCD phase transition is the thermodynamic approach with two-phase matter equations of state, which will be used in the present work, from chapter 3 on.

1.9 Lattice QCD

In 1974, Wilson proposed a formulation of quantum chromodynamics (QCD) on a discrete space-time lattice [33]. A few years later, Creutz demonstrated that this formulation was a promising basis for the successful numerical simulation of the theory [34]. The simulation method is the most promising currently available method for deducing nonperturbative characteristics of QCD at finite temperature and/or density [35].

In the past several years, considerable progress has been made and lattice simulations continue providing results on the equation of state of QCD [36, 37, 38, 39], the transition temperature [40, 41], the order of the deconfinement phase transition [37, 40, 42, 43], as well as the QCD phase diagram [40, 44, 45]. It has been shown that the nature of this transition depends strongly on the number of colors (N_c), the number of flavors (N_f) and the current quark masses as revealed by several lattice QCD calculations (see for example [46, 47, 48, 49, 50, 51, 52, 53, 54, 55, 56, 57, 58, 59, 60]. For infinite or very large quark masses, the transition is a 1st order deconfining transition. In the opposite case of zero quark masses, one may have a 2nd order chiral phase transition for two flavors or a 1st order chiral phase transition for three flavors. For intermediate masses, the transition is just a rapid crossover, meaning that thermodynamic quantities change very rapidly in a narrow temperature interval [61].

Chapter 2

Phase Transitions in Finite-Size Systems

2.1 Introduction

Phase transitions in statistical physics are known to be infinitely sharp only in the thermodynamic limit, where the volume V and the number of particles N go to infinity, while the density $\rho = \frac{N}{V}$ remains constant. Only in this limit is the thermodynamical potential or any of its derivatives singular at the critical point. However, real systems and systems we simulate are finite.

In general, finite size effects lead to a mixed phase system and a rounding of the transition, rendering the order of the transition difficult to infer. The main care is then how to sign a possible phase transition in a finite system. It turns out that we can extract the true critical behavior of infinite systems from calculations on finite systems, by studying how some characteristic thermodynamical quantities vary with the size of the system, namely by a *Finite Size Scaling* (FSS) analysis. Studies in statisti-

cal physics have shown that despite the apparent diversity in the underlying structure of systems undergoing phase transitions, these latter take place with some *universal* global behavior, depending only on the range of interaction of the forces at play and the dimensionality of the problem. This means the singular behavior of some characteristic observables near criticality is identical for many systems when appropriately scaled. This *universality* allows the put of all the physical systems undergoing a phase transition in a certain number of universality classes. The systems in a given universality class display the same critical behavior, meaning that certain dimensionless quantities have the same values for all these systems. *Critical exponents* are an example of these universal quantities. The determination of critical exponents has long been one of the main interests for both analytical calculations and numerical simulations.

This chapter is mainly an overview of phase transitions in finite size systems. The finite size effects are examined and the finite size scaling analysis permitting the determination of the scaling critical exponents is reviewed for both first and second order phase transitions.

2.2 Thermodynamic Limit

In statistical mechanics, the existence of phase transitions is associated with singularities of the thermodynamic potential in some region of the thermodynamic space. These singularities occur only in the thermodynamic limit, where the volume V and particle number N go to infinity, with a constant density $\rho = \frac{N}{V}$. This fact could be understood by analyzing the partition function which contains all of the essential information about the system under consideration, and whose general form for a classical

system is:

$$Z = \sum_{all\ \ states} e^{-\beta\mathcal{H}}, \tag{2.1}$$

where $\mathcal{H}$ is the Hamiltonian of the system, $\beta = \frac{1}{T}$ with the units chosen as: $k_B = \hbar = c = 1$. The sum in eq. (2.1) is over all possible states of the system and thus depends upon the size of the system and the number of degrees of freedom for each particle. For a finite system, the partition function is a finite sum of analytical terms, and therefore it is itself an analytical function. It is necessary to take an infinite number of terms to obtain a singularity, and this has been demonstrated through the work of Lee and Yang in [17].

Thus, in a finite system no singularity occurs and, strictly speaking, no phase transition occurs. The question of why a finite system can apparently describe phase transitions and the relation of this phenomenon with true phase transitions in infinite systems is the main subject of the Finite Size Scaling (FSS) theory [2, 62, 63, 64, 65, 66]. Finite Size Scaling is not only a formal way to understand the asymptotic behavior of a system when the size goes to infinity. In fact, the theory gives us numerical methods capable of obtaining accurate results for infinite systems only by studying very small systems.

2.3 Finite Size Effects and Useful Thermodynamic $x-$Response Functions

In the thermodynamic limit and at criticality, the phase transition is signaled by a divergence (infinite singularity) manifested by some thermodynamic function $F(x, \infty)$. This singularity is according to our classification in chapter 1 given by the $\boldsymbol{\delta}(\tilde{x})-$function

for a discontinuous phase transition (d-PT), while for a continuous phase transition (c-PT), the singularity has the form of a power-law $\tilde{x}^{\upsilon}-$function. Now, if the volume is finite at least in one dimension with a characteristic size $L = V^{1/d}$, the singularity is smeared out into a peak with finite mathematical properties, and three effects can be observed [3, 62, 67, 68]:

1. **The rounding effect of the maximum of the infinite singularity**

   The Infinite height of the $x_c(\infty)$-singularity ($F(x_c(\infty), \infty) = \infty$) becomes finite ($F(x_c(L), L) = finite$)

2. **The shifting effect of the transition point position**

   The position of the $x_c(\infty)$-singularity is shifted to $x_c(L)$

3. **The widening of the transition region around the transition point**

   The $x_c(\infty)$-singularity acquires a finite width ($\delta x(L) = finite$) around the $x_c(L)$-maximum.

The most important feature in a finite volume is then the localization of the finite size transition point: $x_c(L)$. If we analyze the finite peak of $F(x, L)$ when approaching the thermodynamic limit, we see that it tends to the real initial singularity. It is then logical to say that the location of the maximum of the rounded peak of $F(x, L)$ determines the finite-size transition point $x_c(L)$, i. e.,

$$\left[\frac{\partial\langle F\,(x, L)\rangle}{\partial x}\right]_{x=x_c(L)} = 0\ . \tag{2.2}$$

For each of the FSE described previously, we may associate a scaling critical exponent according to the scaling law $\sim L^{\sigma}$. The value of the critical exponent σ may

certainly depend enormously on the kind of singularity occurring in the thermodynamic limit, and differ according to the phase transitions class, i. e., $\sigma(\text{d-PT}) \neq \sigma(\text{c-PT})$. The principal reason is the dependence of $\sigma(\text{c-PT})$ on the critical exponent υ which does not exist in the case of a d-PT [69]. Thus, we can say that the value of the scaling critical exponent σ can give an indication on the order of a phase transition and may be used as a criterion for its determination.

Now, we define the most useful two thermodynamical functions for the study of FSE on the more commonly encountered $x-$ driven phase transitions, namely the first-order phase transition and the second-order phase transition, and for the derivation of the associated scaling critical exponents. These two $x-$ response functions are:

1. The $x-$ susceptibility defined to be the first derivative of the order parameter with respect to the $x-$ variable, i. e.,

$$\chi(x, L) = \frac{\partial \langle \mathcal{O}(x, L) \rangle}{\partial x}, \tag{2.3}$$

2. The $x-$ specific heat density defined to be the first derivative of the energy density $\varepsilon(x, L)$ of the system with respect to the $x-$ variable, i. e.,

$$c(x, L) = \frac{\partial \langle \varepsilon(x, L) \rangle}{\partial x}. \tag{2.4}$$

A FSS analysis of the scaling behavior of the properties describing $\chi(x, L)$ and $c(x, L)$, namely of:

- **The height of the x-susceptibility maximum** $|\chi_x|^{\max}(L)$
- **The height of the x-specific heat maximum** $c_x^{\max}(L)$

- **The shift of the pseudo-critical point from the true critical point**: $\tau_x(L) = x_c(L) - x_c(\infty)$
- **The width of the transition region** $\delta x(L)$ over which the singularities occurring in $\chi(x, L)$ and $c(x, L)$ are rounded,

is used to study quantitatively the volume dependence of these finite size effects, and to recover the scaling critical exponents characterizing the phase transition in question.

2.4 Finite Size Scaling

The appreciable rounding of the critical point singularities induced by finite size effects render it difficult to infer the order of a phase transition. Fortunately, there are characteristic signatures in a finite volume which anticipate the behavior in the thermodynamic limit. A careful analysis of these signatures allows to determine the order of the transition, by performing measurements as function of a varying volume.

In the following, we discuss the finite size scaling behavior of singularities in thermodynamic functions for both $1^{\mathbf{st}}$-Order and 2^{nd}-Order phase transitions.

2.4.1 Finite-size scaling at $2^{\mathbf{nd}}$-Order phase transitions

Let us consider a thermodynamical function $F(\tilde{x}, \infty)$ which admits a critical singularity in the infinite volume limit (the susceptibility $\chi(\tilde{x}, V)$ or the specific heat $c(\tilde{x}, V)$), characterized by an index μ:

$$F(\tilde{x}, \infty) \sim A_F \ |\tilde{x}|^{-\mu} \quad . \tag{2.5}$$

For a system which is finite at least in one dimension with a characteristic size $L = V^{1/d}$, this function is $F(\tilde{x}, L)$. For large L and small $\tilde{x}$, the property of **Finite Size Scaling** means that $F(\tilde{x}, L)$ has the asymptotic form:

$$F(\tilde{x}, L) = |\tilde{x}|^{-\mu} f(L/\xi(\tilde{x}, \infty)), \tag{2.6}$$

where $\xi(\tilde{x}, \infty) \sim \xi_0 |\tilde{x}|^{-\nu}$ is the correlation length in the infinite volume limit.

We are interested in the limit $x \to x_c$ at fixed $L < \infty$, i. e., $\dfrac{L}{\xi(\tilde{x} \to 0, \infty)} \to 0$, at which $F(\tilde{x}, L)$ should be finite. Hence, the singularity of $F(\tilde{x}, \infty)$ has to be compensated by the scaling function $f(L/\xi(\tilde{x}, \infty))$ which may behave as:

$$f(L/\xi(\tilde{x}, \infty)) \sim (\frac{L}{\xi(\tilde{x}, \infty)})^{\mu/\nu} \qquad \text{for} \quad \frac{L}{\xi(\tilde{x}, \infty)} \to 0, \tag{2.7}$$

where $\xi(\tilde{x}, \infty) \sim |\tilde{x}|^{-\nu}$ for $\tilde{x} \to 0$. It follows then [70]:

$$F(x_c, L) = F(\tilde{x} = 0, L) \sim L^{\mu/\nu} \quad . \tag{2.8}$$

The last relation (2.8) predicts for instance for the susceptibility:

$$\chi(x_c, L) \sim L^{\gamma/\nu} \quad , \tag{2.9}$$

and for the specific heat:

$$c(x_c, L) \sim L^{\alpha/\nu} \quad . \tag{2.10}$$

For the width of the transition region $\delta x\,(L)$ and the shift of the transition point $\tau_x\,(L)$ which vanish at the infinite volume limit, their scaling behavior is characterized by the same critical index $1/\nu$, according to:

$$\delta x\,(L) \sim L^{-1/\nu}, \quad \tau_x\,(L) \sim L^{-1/\nu}\ , \tag{2.11}$$

while the scaling behavior of the correlation length in a finite volume is stated as [70]:

$$\xi(\tilde{x}, L) = \xi(\tilde{x}, \infty) f_\xi(L/\xi(\tilde{x}, \infty))\ . \tag{2.12}$$

2.4.2 Finite-size scaling at $1^{\mathbf{st}}$-Order phase transitions

Finally, we turn to finite-size scaling analysis at first-order phase transitions. In an infinite system, a $1^{\mathbf{st}}$-Order phase transition is characterized by delta function singularities in the second derivatives of the thermodynamical potential at the critical point $x_c\,(\infty)$. In finite systems, of course, these delta function singularities are rounded off into finite peaks. The finite-size scaling analysis for $1^{\mathbf{st}}$-Order phase transitions is more difficult than for 2^{nd}-Order phase transitions because $\dfrac{\xi(\tilde{x},\infty)}{L}$ is no longer a sensible scaling variable as in eq. (2.7) since the correlation length for a $1^{\mathbf{st}}$-Order phase transition stays finite even in the infinite volume limit as $x \to x_c$ [70]. Thus, since there is no diverging characteristic length to which the linear dimension could be compared at $1^{\mathbf{st}}$-Order phase transition, it is simply the volume L^d that controls the size effects.

The goal of the finite size scaling analysis for $1^{\mathbf{st}}$-Order phase transitions is to predict the rounding and shifting of $\delta-$function singularities in the second derivatives of a thermodynamical potential due to the finite volume, e.g., in the specific heat due to a latent heat, or in the susceptibility due to a jump in the order parameter (see [2, 3, 64, 71, 72]).

We plot in Fig. (2.1) a diagrammatic behavior of the susceptibility $\chi(L,x)$, the specific heat $c(L,x)$ as well as the $x-$derivative of the susceptibility $[\partial\chi(L,T)/\partial x]$ as function of x, and show the characteristic maxima of the rounded peaks $|\chi_x|^{\max}(L)$ and $c_x^{\max}(L)$, the width of the region over which the transition is rounded off $\delta x(L)$, and the shift of the transition point $x_c(L) - x_c(\infty)$, which scale with the volume according

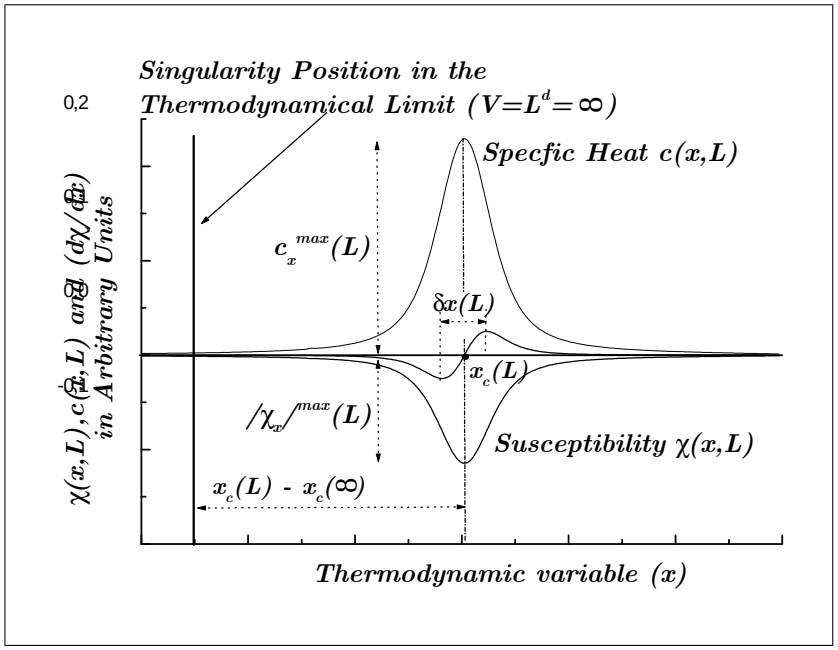

Figure 2.1: Behavior of the susceptibility $\chi(x,L)$, its first derivative $\frac{\partial \chi}{\partial x}$ and specific heat $c(x,L)$ versus the thermodynamic $x-$variable driving the transition, at the transition point x_c.

to:

$$\begin{cases} \delta x(L) \sim L^{-d\ \theta} = V^{-\theta} \\ (x_c(L) - x_c(\infty)) \sim L^{-d\ \lambda} = V^{-\lambda} \\ |\chi_x|^{\max}(L) \sim L^{d\ \gamma} = V^{\gamma} \\ C_x^{\max}(L) \sim L^{d\ \alpha} = V^{\alpha}\ . \end{cases} \tag{2.13}$$

It has been shown in the FSS theory [3, 64, 66, 67, 71] that in this case, the scaling exponents θ, λ, α and γ are all equal to unity, and it is only the dimensionality which controls the finite size effects.

As an example, we shall report on in the following the work in [3] to recover the scaling exponents for a first order phase transition. Using thermodynamic fluctuation

theory, finite-size effects at first order phase transitions have been worked out in Ising models below T_c, to discuss the rounding of the magnetization jump in the Ising ferromagnet as the field H is varied. In an infinite system, the magnetization jumps from $-M_{sp}$ as $H \to 0^+$ to $+M_{sp}$ reached for $H \to 0^-$. In a system with all linear dimensions L finite, however, no singularity can occur and the variation of the magnetization $\langle S \rangle_L$ with field is perfectly smooth. Rather than the infinitely steep variation of $\langle S \rangle_L$ with H from $H = 0^+$ to $H = 0^-$ occurring for $L \to \infty$, $\langle S \rangle_L$ has a large but finite slope of order $\dfrac{M_L^2 L^d}{kT}$, for a finite region of fields $-\dfrac{M_L L^d}{kT} \lesssim H \lesssim \dfrac{M_L L^d}{kT}$. Here $\pm M_L$ are the values of the magnetization where the probability distribution $P_L(s)$ at zero field is maximal, and d is the system's dimensionality.

The probability distribution of the magnetization of an Ising system below T_c at zero field can be approximated by two Gaussian curves, one centered on $-M$ and one on $+M$, as:

$$P_L(s) = \frac{1}{2} \frac{L^{d/2}}{\left(2\pi k T \chi_{(L)}\right)^{1/2}} \left\{ \exp\left[-\frac{(s - M_L)^2 L^d}{2kT\chi_{(L)}} \right] + \exp\left[-\frac{(s + M_L)^2 L^d}{2kT\chi_{(L)}} \right] \right\} . \quad (2.14)$$

The generalization to nonzero field H then simply is:

$$P_L(s) = A \left\{ \exp\left[-\frac{\left((s - M_{sp})^2 - 2\chi s H\right) L^d}{2kT\chi_{(L)}} \right] + \exp\left[-\frac{\left((s + M_L)^2 - 2\chi s H\right) L^d}{2kT\chi_{(L)}} \right] \right\} , \quad (2.15)$$

with A a normalization constant which can be written as:

$$A = \frac{1}{2} \frac{L^{d/2}}{\left(2\pi k T \chi_{(L)}\right)^{1/2}} \exp\left[-\frac{\chi H^{\,2} L^d}{2kT} \right] / \cosh\left[\frac{H M_{sp} L^d}{kT} \right] . \quad (2.16)$$

Eq. (2.15) can then be rewritten as:

$$\begin{aligned} P_L(s) \;=\; & \frac{1}{2} L^d \frac{\left(2\pi k T \chi_{(L)}\right)^{-1/2}}{\cosh\left[H M_{sp} L^d / kT\right]} \left\{ \exp\left[\frac{H M_{sp} L^d}{kT} \right] \exp\left[-\frac{(s - M_{sp} - \chi H)^2 L^d}{2kT\chi_{(L)}} \right] \right. \\ & \left. + \exp\left[\frac{H M_{sp} L^d}{kT} \right] \exp\left[-\frac{(s + M_L - \chi H)^2 L^d}{2kT\chi_{(L)}} \right] \right\} . \quad (2.17) \end{aligned}$$

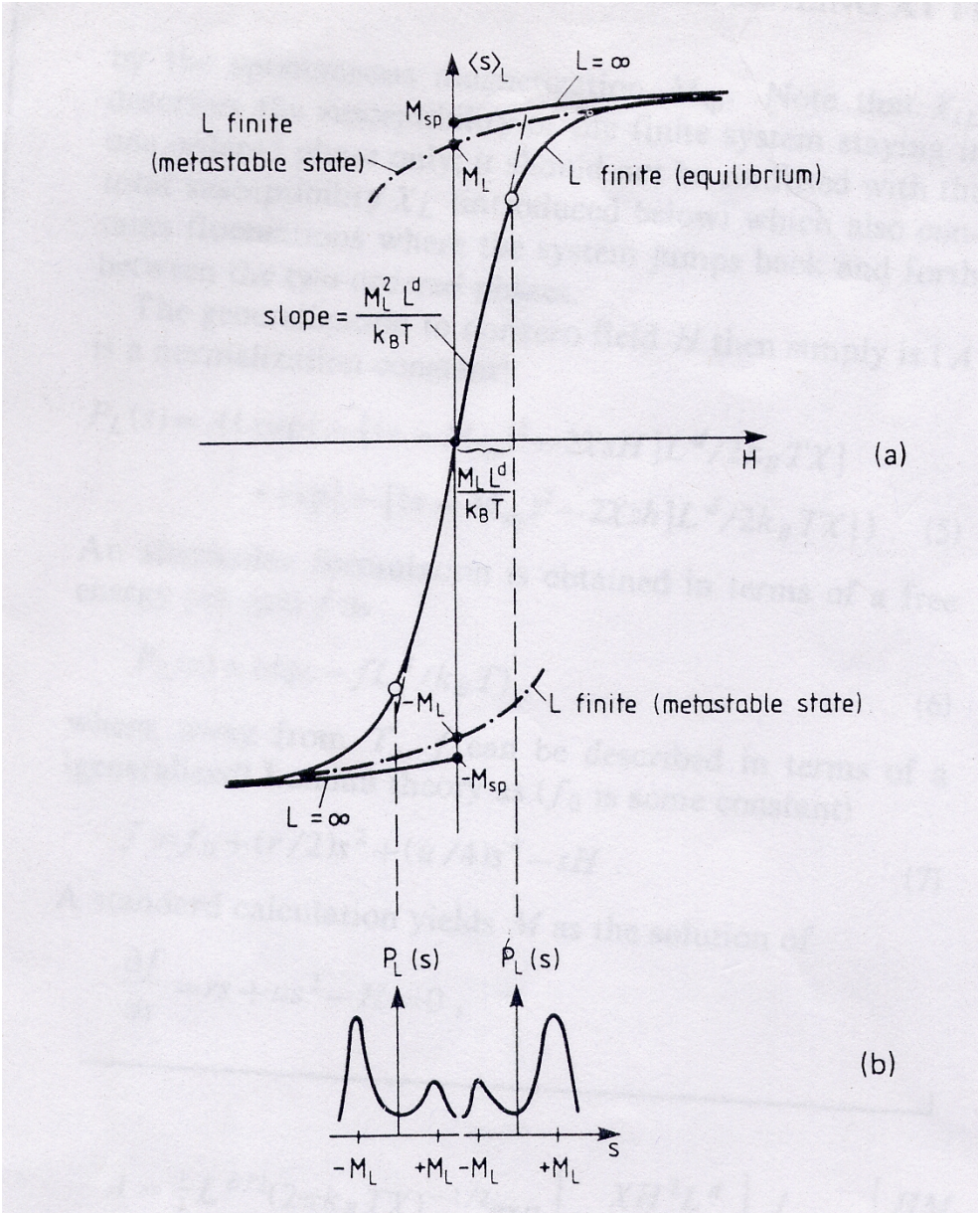

Figure 2.2: (a) Variation of magnetization $\langle s \rangle_L$ in a finite Ising ferromagnet plotted vs magnetic field H, as observed in thermal equilibrium (full curve) and in a Monte Carlo simulation with sufficiently short observation time where metastable branches occur (dash-dotted). The behavior of the infinite system is also indicated (schematized). M_{sp} is the spontaneous magnetization of the infinte system. M_L is the most probable value of the magnetization in the finite system at $T < T_c$. (b) Schematic probability distribution of the magnetization for two cases (open circles in (a)) where the magnetization is in between [3].

Thus, $P_L(s)$ still is a superposition of two Gaussians, now centered around the shifted magnetization $\pm M_{sp} + \chi H$.

From eq. (2.17), it is now easy to obtain the moments $\langle s^k \rangle_L$ of interest. The first moment $\langle s \rangle_L$ giving the magnetization is then:

$$\langle s \rangle_L = \chi H + M_{sp} \tanh \left[\frac{H M_{sp} L^d}{kT} \right], \tag{2.18}$$

and we conclude that for $\dfrac{H M_{sp} L^d}{kT} \gg 1$ we simply have the bulk behavior:

$$\langle s \rangle_L = \chi H + M_{sp}, \tag{2.19}$$

while in the limit $\dfrac{H M_{sp} L^d}{kT} \ll 1$, we have:

$$\langle s \rangle_L = \chi H + \frac{H M_{sp}^{\ 2} L^d}{kT}. \tag{2.20}$$

The width over which the transition is rounded is of the order of:

$$\Delta H_{round} \approx \frac{kT}{M_{sp} L^d}, \tag{2.21}$$

since, as can be seen from eq. (2.18), the field H has to exceed this value to find the behavior characteristic of the infinite system.

The susceptibility of the finite system χ_L becomes:

$$\chi_L = \left(\frac{\partial \langle s \rangle_L}{\partial H}\right)_T = \chi + \frac{M_{sp}^{\ 2} L^d}{kT \ \cosh^2 \left[\frac{H M_{sp} L^d}{kT} \right]}, \tag{2.22}$$

which shows that instead of the $\delta-$function singularity at $H = 0$, we now have a smooth peak of height proportional to L^d. Also, it is easy to show that:

$$\langle s^2 \rangle_L = M_{sp}^{\ 2} + \chi^2 H^2 + \frac{kT\chi}{L^d} + 2 M_{sp} \chi H \ \tanh \left[\frac{H M_{sp} L^d}{kT} \right], \tag{2.23}$$

and hence the fluctuation relation:

$$\langle s^2 \rangle_L - \langle s \rangle_L^2 = \frac{kT\chi_L}{L^d}, \tag{2.24}$$

holds as usual. Thus, the only scaling power of L which enters in the above relations of $\langle s \rangle_L$, χ_L, etc. comes via the volume L^d of the system. Hence, it is only the dimensionality of the system which controls the finite size effects.

In the following, Table (2.1) resumes the scaling behavior at the limit of an infinite volume and in the vicinity of the transition point for each of the previous four quantities of eq. (2.13), and shows how to relate the finite size effects on the singularities of thermodynamic quantities close to both $1^{\mathbf{st}}$-order and $2^{\mathbf{nd}}$-order phase transitions, to the critical exponents of the infinite system.

The difference between the scaling critical exponents for $1^{\mathbf{st}}$-Order and 2^{nd}-Order phase transitions allows to distinguish between the two classes, since for a $1^{\mathbf{st}}$-Order phase transition $\gamma = \alpha = \lambda = \theta = 1$ and for a 2^{nd}-Order phase transition γ, α and ν differ from 1. This is also revealed by the results found for the scaling critical exponents in theoretical, numerical and experimental studies, hence the use of the critical exponents as a criterion for the determination of the order of a phase transition [47, 48, 49, 50, 70, 73, 74].

2.5 Localization of the transition point in a finite volume

In addition to the two ways cited in section (2.3) for determining the transition point in a finite volume $x_c(L)$, from the localization of the extrema of the susceptibility $\chi(x, L)$

	1st-Order PT		**2nd-Order PT**	
	Infinite System (TL)	Finite-Size System	Infinite System (TL)	Finite-Size System
$\lvert\chi_x\rvert^{\max}(V)$	$\delta(\tilde{x})$	$L^{d\ \gamma}$	$\tilde{x}^{-\gamma}$	$L^{\gamma/\nu}$
$c_x^{\max}(V)$	$\delta(\tilde{x})$	$L^{d\ \alpha}$	$\tilde{x}^{-\alpha}$	$L^{\alpha/\nu}$
$\tau_x(V)$	★	$L^{-d\ \lambda}$	★	$L^{-1/\nu}$
$\delta x\,(V)$	★	$L^{-d\ \theta}$	★	$L^{-1/\nu}$

Table 2.1: Scaling behavior of characteristic quantities for 1st-order phase transition and 2nd-order phase transition in both infinite and finite systems.

and specific heat $c(x, L)$, another quantity has been proposed in [3, 66, 75] which is the fourth order cumulant of the order parameter, defined as:

$$B_4(L) = 1 - \frac{\langle \mathcal{O}(L) \rangle^4}{3\ \langle \mathcal{O}^2(L) \rangle^2}\ , \tag{2.25}$$

and which presents a minimum value at an effective transition point $x_c(L)$ whose shift from the true transition point $x_c(\infty)$ is of order L^{-d} for a first order transition. This cumulant is a finite size scaling function [3, 66, 67, 68, 76], and is widely used to indicate the order of the transition in a finite volume.

Other cumulants are also expected to give information on the transition point in a finite volume, and some of them (the second and third order ones) will be examined later in this work (chapter 4) to determine the effective transition temperature.

The speed of sound (squared) defined by: $c_s^2 = \dfrac{dP}{d\varepsilon}$, P being the pressure and ε the energy density, is also used to localize the transition point, since for a first order phase transition, occurring at the thermodynamic limit, c_s^2 has a vanishing minimum at the transition point $x_c(\infty)$. In a finite volume, c_s^2 decreases in the transition region and has a minimum at the effective transition point $x_c(L)$.

Chapter 3

Finite-Size Effects for the Deconfinement Phase Transition

3.1 Introduction and Motivation

If ever the QGP phase is created in ultra-relativistic heavy ion collisions, the volume in which its eventual formation may take place would certainly be finite. Naively, the formation of a quark-gluon plasma (QGP) in a relativistic heavy ion collision is generally assumed to take place in a reaction zone having a finite volume V, about $1\,fermi$ of width and a transverse area of colliding nuclei $\sim A^{2/3}$, which gives: $V \simeq A^{2/3} fm^3$. Since the AGS and SPS data are available, then the use of the Hanbury Brown Twiss (HBT) interferometry method to estimate the possible sizes of the QGP gives the results resumed in Table (3.1) (for the RHIC and LHC energies, simple entropy arguments have been used to predict the QGP sizes [77]) :

Also, the study of the phase transition from HG to QGP with lattice QCD calculations is necessarily performed in finite lattices [78]. In lattice QCD and if we consider

Accelerator	**AGS-SPS**	**RHIC**	**LHC**
QGP Volume (fm^3)	$\sim (34 - 268)$	$\sim (268 - 2144)$	$\sim (905 - 5575)$

Table 3.1: QGP volumes realised at AGS-SPS and RHIC and expected at LHC.

References	[79]	[80]	[81]	[82]	[83]	[78]
QCD Lattice Volume $V_{\max}$ (fm^3)	$\lesssim 40$	~ 7	~ 8	~ 21	~ 37	~ 14

Table 3.2: Values of some lattice volumes used in lattice-QCD calculations

a 4-dimensional lattice, of lattice spacing a, on which we want to perform Monte-carlo simulations of QCD, the lattice sizes are $T \times L \times L \times L$.

Effects of the finite volume are certainly important, since statistical fluctuations in a finite volume are considerable and may hinder a sharp transition between the two phases. Indeed, phase transitions are known to be infinitely sharp only in the thermodynamic limit. In general, finite size effects lead to a mixed phase system, a rounding of the transition and a broadened transition region.

This chapter is devoted to the study of a finite system undergoing a deconfinement phase transition from a hadronic gas phase to a QGP. The finite size effects are studied within a simple thermodynamic model used in [4], based on the assumption of the co-existence of confined and deconfined phases in a finite volume, and using the equations of state of the two phases. For the HG phase, we consider the partition function of a pionic gas. For the QGP phase, we first consider the partition function of a free gas of quarks and gluons derived simply within the bag model.

After this, to account for the 'color neutrality' of the observed free particles, and then of the total QGP, we require that all physical states be color-singlet with respect to the SU(3) color gauge group. Hence, we include the exact color-singletness con-

dition in the calculation of the QGP partition function using the Group Theoretical Projection Technique [6]. This color-singlet partition function can not be exactly calculated and is usually calculated within the saddle point and Gaussian approximations in the limit $VT^3 >> 1$ [7, 8]. It turns out that the use of the such obtained partition function, within the phase coexistence model, has as a consequence the absence of the deconfinement phase transition. We show that this is due to the fact that the approximations used for the calculation of the color-singlet partition function break down at $VT^3 << 1$, and this limit is attained using the phase coexistence model, since the fractional volume V_{QGP} occupied by the QGP is allowed to take small and even zero values.

In view to analyze the finite-size effects in such a model, we first proposed in [13, 14] the calculation of an adequate color-singlet partition function expanded in a power series of the QGP volume fraction, using some approximations but avoiding the problem arising at $VT^3 << 1$. The color-singlet partition function derived in this way allowed us to accurately calculate physical quantities describing well the deconfinement phase transition at finite volumes, and to probe the behavior of the phase transition at criticality, for both temperature-driven and density-driven deconfinement phase transition. This part of the work will not be exposed in this thesis.

After this, we proceeded in a different way for calculating the mean values of physical quantities numerically and without any approximation, by including the exact definition of the color-singlet partition function within the phase coexistence model, without explicitly calculating this latter [84]. The effects of finiteness of the system size are then studied by examining the behavior of several physical quantities with varying volume. This is the main object of the present chapter.

3.2 The Deconfinement Phase Transition in a Finite Volume

3.2.1 The Deconfinement Phase Transition within the Phase Coexistence Model

To study the QCD deconfinement phase transition in a finite volume, we consider a simple phase coexistence model used in [4], in which the mixed HG-QGP phase system has a finite volume: $V = V_{HG} + V_{QGP}$. The parameter $\mathfrak{h}$ representing the fraction of volume occupied by the HG: $V_{HG} = \mathfrak{h}V$, is then defined. Thus, the value: $\mathfrak{h} = 1$ corresponds to a total HG phase and when $\mathfrak{h} = 0$, the system is completely in the QGP phase. Assuming non-interacting phases (separability of the energy spectra of the two phases), the total partition function of the system can be approximately written as:

$$Z\left(\mathfrak{h},T,\mu,V\right) = Z_{QGP}\left(\mathfrak{h},T,\mu,V\right) Z_{HG}\left(\mathfrak{h},T,\mu,V\right), \tag{3.1}$$

and the probability to find the system in the state $\mathfrak{h}$, as defined in [4], is then given by:

$$p\left(\mathfrak{h},T,\mu,V\right) = \frac{Z\left(\mathfrak{h},T,\mu,V\right)}{\int\limits_0^1 Z\left(\mathfrak{h},T,\mu,V\right) d\mathfrak{h}}. \tag{3.2}$$

The mean value of any thermodynamic quantity $\mathcal{A}(T,\mu,V)$ of the system can then be calculated by:

$$\begin{aligned} \left\langle \mathcal{A}(T,\mu,V) \right\rangle &= \int\limits_0^1 \mathcal{A}\left(\mathfrak{h},T,\mu,V\right) p\left(\mathfrak{h},T,\mu,V\right) d\mathfrak{h} \\ &= \frac{\int\limits_0^1 \mathcal{A}\left(\mathfrak{h},T,\mu,V\right) Z\left(\mathfrak{h},T,\mu,V\right) d\mathfrak{h}}{\int\limits_0^1 Z\left(\mathfrak{h},T,\mu,V\right) d\mathfrak{h}}, \end{aligned} \tag{3.3}$$

where $\mathcal{A}(\mathfrak{h},T,\mu,V)$ is the total thermodynamic quantity in the state $\mathfrak{h}$, given in the case of an extensive quantity by:

$$\mathcal{A}(\mathfrak{h},T,\mu,V) = \mathcal{A}_{HG}(T,\mu,\mathfrak{h}V) + \mathcal{A}_{QGP}(T,\mu,(1-\mathfrak{h})\,V), \tag{3.4}$$

and in the case of an intensive quantity, by:

$$\mathcal{A}(\mathfrak{h},T,\mu,V) = \mathfrak{h}\mathcal{A}_{HG}(T,\mu,\mathfrak{h}V) + (1-\mathfrak{h})\mathcal{A}_{QGP}(T,\mu,(1-\mathfrak{h})\,V), \tag{3.5}$$

with $\mathcal{A}_{QGP}$ and $\mathcal{A}_{HG}$ the thermodynamic quantities relative to the individual QGP and HG phases, respectively.

Let us note that the coexistence of two phases in a finite system undergoing a phase transition taken alone seems not to be sufficient for anticipating the first order nature of the phase transition when approaching the thermodynamic limit. A similar confusion can arise in the case of a correlation length scaling with the volume and suggesting a second order nature of the transition in the thermodynamic limit. This subtle situation has been noticed and clarified in several works [46, 70, 85, 86, 87, 88, 89, 90, 91, 92, 93, 94, 95, 96]. Then, for a firm determination of the order of a phase transition in a finite system, a full and detailed finite size scaling analysis of different response functions simultaneously, yielding various scaling critical exponents, seems to be necessary. This is not all in our case, since other basic parameters of QCD like the number of flavors and the current quark masses have a strong influence on how the phase transition occurs. A clear sensitivity of the order of the QCD deconfinement phase transition to these parameters has been revealed by several lattice QCD calculations (see for example [46]-[60]).

The partition functions of both HG and QGP phases are calculated, and their final expressions are given in the following. For a pionic gas, the partition function is simply

given by:

$$Z_{HG}\left(T, V_{HG}\right) = e^{\frac{\pi^2}{30}T^3 V_{HG}}, \tag{3.6}$$

and for a QGP consisting of gluons and two flavors of massless quarks (up, down), with a chemical potential μ, within the bag model [5], the partition function is given by [97]:

$$Z_{QGP}(T, \mu, V_{QGP}) = \exp\left(\left(\frac{37\pi^2}{90}T^3 + \mu^2 T + \frac{1}{2\pi^2}\frac{\mu^4}{T} - \frac{B}{T}\right)V_{QGP}\right), \tag{3.7}$$

where B is the bag constant accounting for the real vacuum pressure exerted on the perturbative vacuum. Let us note that taking the same chemical potential for quarks, i.e., $\mu_u = \mu_d = \mu$, is just an approximation for simplification, and is usually used [98]. The chemical potential depends on several parameter as the bath temperature and the particle masses, since it determines the energy required to add/remove a particle at fixed pressure, energy and entropy [99].

The pressure of the QGP can then be derived directly as:

$$P_{QGP} = \frac{37\pi^2}{90}T^4 + \mu^2 T^2 + \frac{1}{2\pi^2}\mu^4 - B. \tag{3.8}$$

and that of the hadronic matter is given by:

$$P_{HG} = \frac{\pi^2}{30}T^4. \tag{3.9}$$

From the Gibbs criteria, the two matter phases are in equilibrium when the temperature, the chemical potential and the pressure of both of them are equal [100]. The phase transition parameters in our simple model come then from setting:

$$P_{HG}\left(\mu_c, T_c\right) = P_{QGP}\left(\mu_c, T_c\right), \tag{3.10}$$

which gives the following expression relating between T_c and μ_c:

$$\frac{17\pi^2}{45}T_c^4 + \mu_c^2 T_c^2 + \frac{1}{2\pi^2}\mu_c^4 = B. \tag{3.11}$$

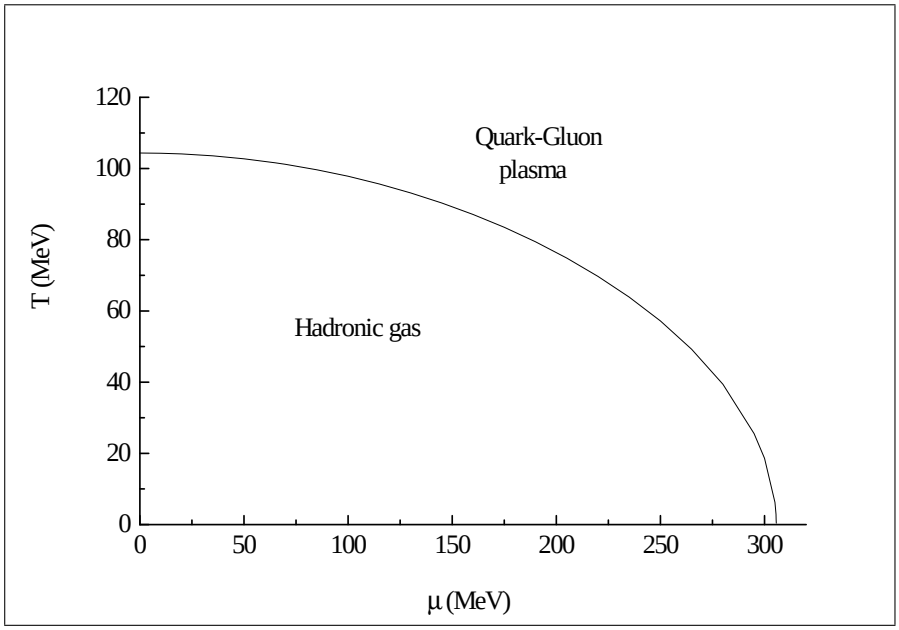

Figure 3.1: Phase diagram in the $\mu - T$ plane.

Fig. (3.1) shows the phase diagram in the $\mu - T$ plane [101], separating between hadronic and QGP phases, and giving at each point the transition parameters (μ_c, T_c) for two flavors ($N_f = 2$), with the common value of the bag constant $B^{1/4} = 145MeV$.

The extreme case $\mu = 0$ could be attained in heavy-ion collisions at high energy (i. e., at high temperature), and the critical temperature evaluated in this case is:

$$T_c = \frac{B^{1/4}}{\left(\frac{17\pi^2}{45}\right)^{\frac{1}{4}}} , \tag{3.12}$$

so the QGP is favored at high temperature ($T > T_c$), and the hadronic phase is favored at low temperature ($T < T_c$) .

The second extreme case $T = 0$ could be reached in the core of some neutron stars

where the density is high, and the critical chemical potential is then given by:

$$\mu_c = \frac{B^{1/4}}{\left[\frac{1}{2\pi^2}\right]^{\frac{1}{4}}}, \tag{3.13}$$

so the QGP is favored at large baryon density, i. e., large chemical potential ($\mu > \mu_c$), and the hadronic phase is favored at low baryon density ($\mu < \mu_c$).

3.2.2 Finite Size Rounding of the Deconfinement Phase Transition

As it is known, the deconfined quark matter state can be obtained at extreme conditions of temperature and/or density, i. e., either by raising temperature or chemical potential. The deconfinement phase transition is then temperature-driven or density-driven. We'll study in the following the FSE for a temperature driven deconfinement phase transition, at a vanishing chemical potential ($\mu = 0$), and for a density driven deconfinement phase transition at a fixed temperature ($T = 100MeV$), using the common value $B^{1/4} = 145MeV$ for the bag constant. To study these effects of volume finiteness, we'll examine the behavior of some thermodynamic quantities with temperature and chemical potential for varying volume. The main quantities of interest are the order parameter, which is simply in this case the mean value of the hadronic volume fraction, the entropy density and the energy density. The mean values of these latter, i. e., $\langle s(T,\mu,V)\rangle$ and $\langle \varepsilon(T,\mu,V)\rangle$ are related to the order parameter $\langle \mathfrak{h}(T,\mu,V)\rangle$ by the expressions:

$$\begin{aligned} \langle s(T,\mu,V)\rangle &= \mathfrak{s}_{QGP} + (\mathfrak{s}_{HG} - \mathfrak{s}_{QGP})\ \langle \mathfrak{h}(T,\mu,V)\rangle \\ \langle \varepsilon(T,\mu,V)\rangle &= \mathfrak{e}_{QGP} + (\mathfrak{e}_{HG} - \mathfrak{e}_{QGP})\ \langle \mathfrak{h}(T,\mu,V)\rangle, \end{aligned} \tag{3.14}$$

where:

$$\langle \mathfrak{h}\,(T,\mu,V)\rangle = \frac{\left(-\frac{1}{T}(f_{HG}-f_{QGP})V-1\right)e^{-\frac{1}{T}(f_{HG}-f_{QGP})V}+1}{-\frac{1}{T}(f_{HG}-f_{QGP})V\left(e^{-\frac{1}{T}(f_{HG}-f_{QGP})V}-1\right)}, \tag{3.15}$$

with:

$$\begin{cases} f_{QGP} = -\frac{37\pi^2}{90}T^4 - \mu^2T^2 - \frac{1}{2\pi^2}\mu^4 + B;\ f_{HG} = -\frac{\pi^2}{30}T^4 \\ \mathfrak{s}_{QGP} = \frac{74\pi^2}{45}T^3 + 2\mu^2T;\ \mathfrak{s}_{HG} = \frac{2\pi^2}{15}T^3 \\ \mathfrak{e}_{QGP} = B + \frac{37\pi^2}{30}T^4 + \mu^2T^2 - \frac{\mu^4}{2\pi^2};\ \mathfrak{e}_{HG} = \frac{\pi^2}{10}T^4. \end{cases} \tag{3.16}$$

Fig. (3.2) shows the three-dimensional plots of the order parameter, energy density $\langle \varepsilon\,(T,V)\rangle$ and entropy density $\langle s\,(T,V)\rangle$, vs temperature and system volume, at a vanishing chemical potential ($\mu = 0$), with $B^{1/4} = 145MeV$ for the bag constant, and Fig. (3.3) illustrates those of the normalized energy density $\frac{\langle \varepsilon\,(T,V)\rangle}{T^4}$ and entropy density $\frac{\langle s\,(T,V)\rangle}{T^3}$. The first-order character of the transition is showed by the step-like rise or sharp discontinuity of each of the order parameter, as well as the normalized energy and entropy densities, when approaching the thermodynamic limit, at a transition temperature $T_c\,(\infty) \simeq 104.35MeV$, which reflects the existence of a latent heat accompanying the phase transition. The quantities $\frac{\langle \varepsilon\rangle}{T^4}$ and $\frac{\langle s\rangle}{T^3}$ are traditionally interpreted as a measure of the number of effective degrees of freedom [102]; the temperature increase causes then a "melting" of the constituent degrees of freedom "frozen" in the hadronic state, making the energy and entropy densities attain their plasma values. In small systems, the phase transition is rounded since the probability of presence of the QGP phase below T_c, and of the hadron phase above T_c are finite because of the considerable thermodynamical fluctuations. The transition region around the transition temperature $T_c\,(\infty)$ is then broadened, acquiring a bigger width $\delta T(V)$, smaller is the volume.

Similarly, Fig. (3.4) shows the variations of the order parameter, the energy and

entropy densities with chemical potential and system volume, at the temperature $T = 100MeV$. The first-order character of the transition can, also in this case, clearly be seen from the sharp discontinuity of the three quantities at a transition chemical potential $\mu_c(\infty) \simeq 81.8MeV$, at the large volume limit. In small systems, the transition is perfectly smooth over a broadened region of chemical potential of width $\delta\mu(V)$. Let us note that in the QGP phase at $\mu > \mu_c(V)$, the energy and entropy densities grow with chemical potential like in Fig. (3.2) with temperature, but in this case it is no more possible to normalize in view to obtain the number of degrees of freedom because of the existence of both chemical potential and temperature in the expressions.

3.3 The QCD Deconfinement Phase Transition in a Finite Volume Including the Color-Singletness Requirement

3.3.1 The Color-Singlet Partition Function of the QGP

For the QGP phase, we consider a free gas of quarks and gluons with the exact color-singletness requirement. To implement the color-singletness constraint into the quantum statistical description of the system, we use the group theoretical projection technique formulated by Turko and Redlich [6], as done in several works [7, 8, 103, 104, 105, 106, 107, 108, 109, 110, 111, 112, 113]. The projected partition function for a system of quarks, antiquarks and gluons in a volume V, at temperature T and quark chemical potential μ is given by:

$$Z_j(T,\mu,V) = Tr(\widehat{\mathcal{P}}_j e^{-\beta\widehat{H}}), \tag{3.17}$$

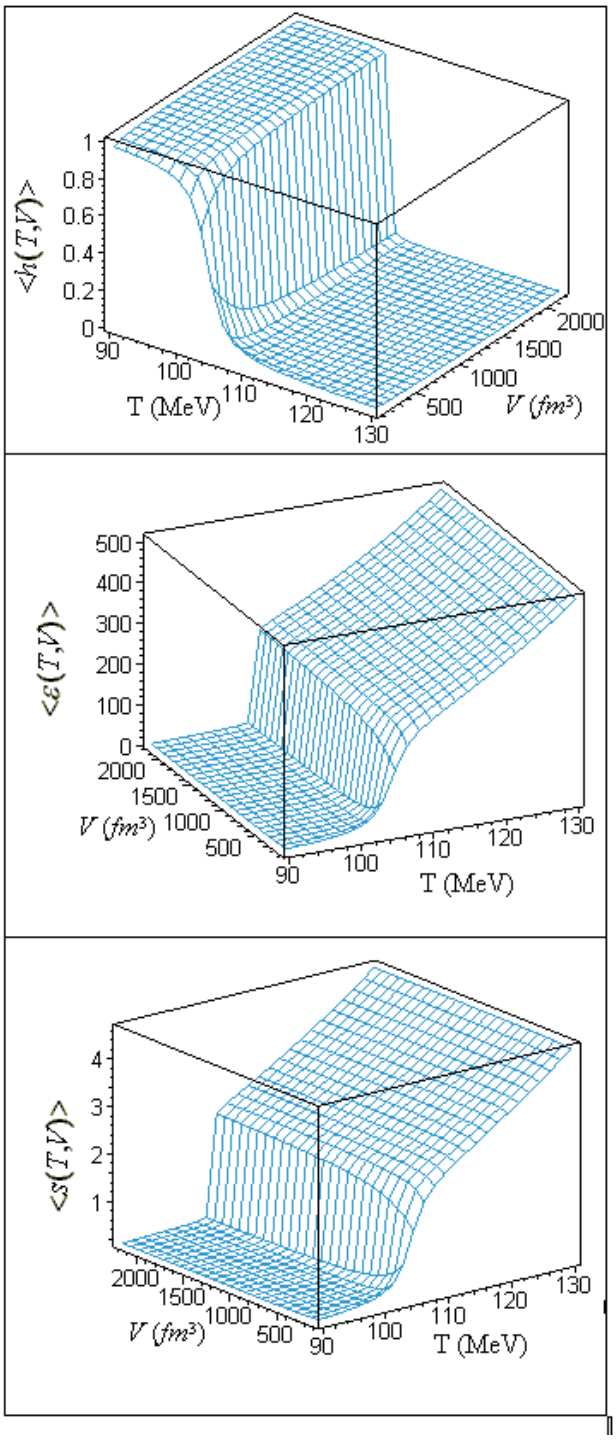

Figure 3.2: Mean values of (top) the order parameter, (middle) the energy density and (bottom) the entropy density as functions of temperature T and system size V, at $\mu = 0$.

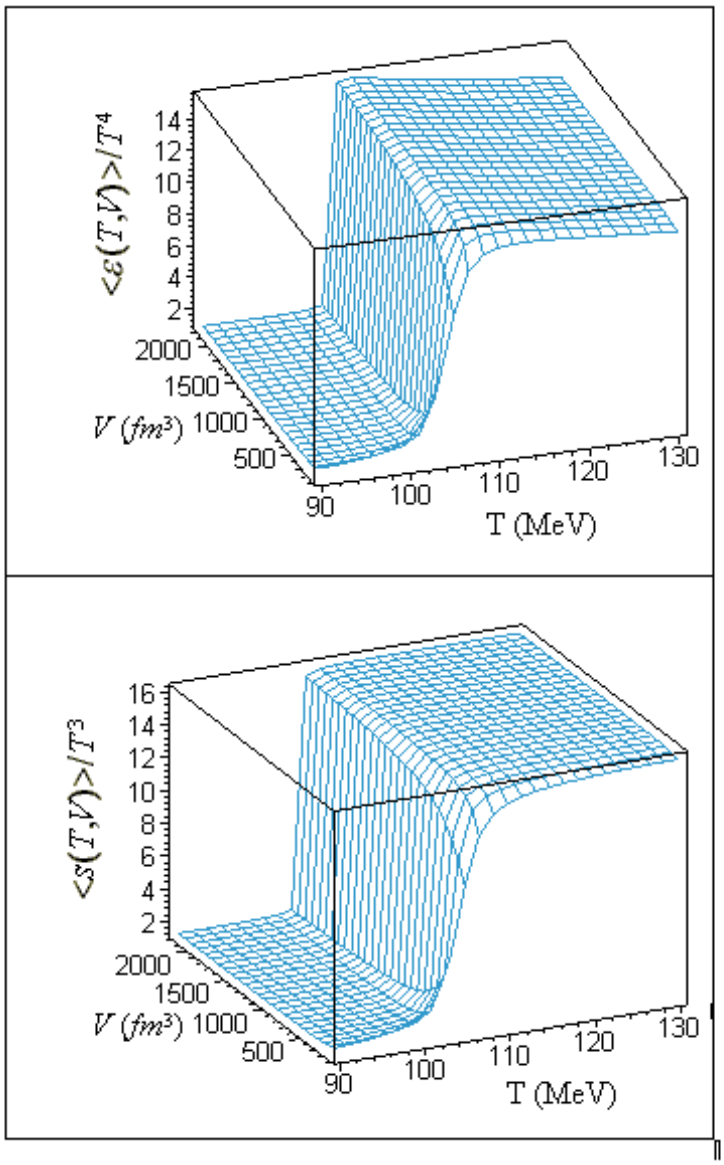

Figure 3.3: Mean values of (top) the energy density normalized by T^4 and (bottom) the entropy density normalized by T^3as functions of temperature T and system size V, at $\mu = 0$.

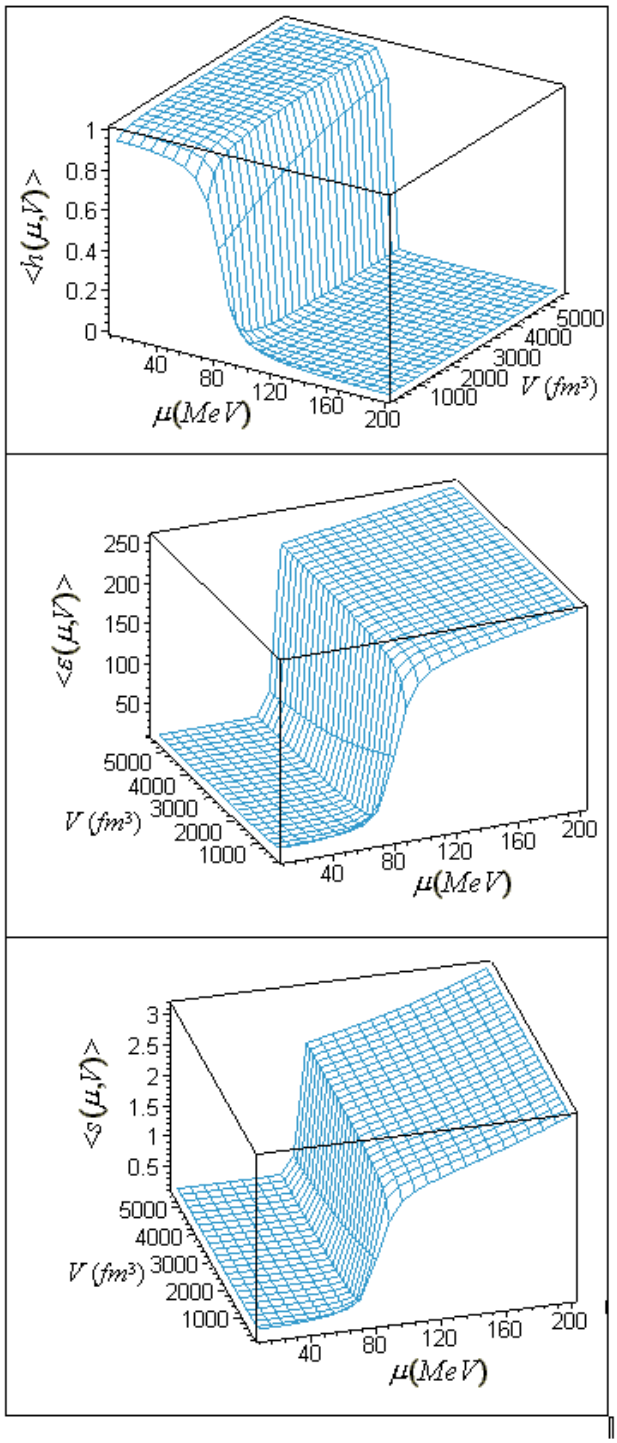

Figure 3.4: Mean values of (top) the order parameter, (middle) the energy density and (bottom) the entropy density as functions of chemical potential μ and system size V, at the temperature $T = 100MeV$.

where: $\beta = \frac{1}{T}$ with the units chosen as: $k_B = \hbar = c = 1$, $\widehat{H}$ is the Hamiltonian of the system and $\widehat{\mathcal{P}}_j$ is a projection operator for a symmetry group $\mathcal{G}$ (compact Lie group) having a unitary representation $\widehat{U}(g)$ in a Hilbert space $\mathcal{H}$,

$$\widehat{\mathcal{P}}_j = d_j \int_{\mathcal{G}} d\mu(g) \chi_j^*(g) \widehat{U}(g), \tag{3.18}$$

$d\mu(g)$ being the normalized Haar measure in $\mathcal{G}$, d_j the dimension and $\chi_j^*(g)$ the character of the irreducible representation "j" of $\mathcal{G}$.

For $SU(3)$ color-singlet configuration, $d_j = 1$, $\chi_j = 1$, and the explicit form of the Haar measure is:

$$\int_{SU(N_c)} d\mu(g) = \frac{1}{N_c!} \left(\prod_{c=1}^{N_c-1} \int_{-\pi}^{+\pi} \frac{d\theta_c}{2\pi} \right) \left[\prod_{i<k}^{N_c} \left(2 \sin \frac{\theta_i - \theta_k}{2} \right)^2 \right], \tag{3.19}$$

θ_l being a class parameter obeying the periodicity condition $\sum_{l=1}^{N_c} \theta_l = 0 \pmod{2\pi}$ and insuring that the group element is $SU(N_c)$. Hence, eq. (3.17) becomes:

$$Z_c(T, \mu, V) = \int_{SU(3)} d\mu(g) \mathcal{T}r(\widehat{U}(g) e^{-\beta \widehat{H}}). \tag{3.20}$$

The Hilbert space $\mathcal{H}$ of the composite system has the structure of a tensor product of their individual Fock spaces as:

$$\mathcal{H} = \mathcal{H}_q \otimes \mathcal{H}_{\overline{q}} \otimes \mathcal{H}_{\mathbf{g}}, \tag{3.21}$$

where the subscripts q, $\overline{q}$ and $\mathbf{g}$ denote respectively the quark, antiquark and gluon. The trace involved in eq. (3.20) decomposes then into the product of 3 traces as:

$$Z_c(T, \mu, V) = \int_{SU(3)} d\mu(g) \mathcal{T}r(\widehat{U_q}(g) e^{-\beta \widehat{H}_q}) \mathcal{T}r(\widehat{U_{\overline{q}}}(g) e^{-\beta \widehat{H_{\overline{q}}}}) \mathcal{T}r(\widehat{U_{\mathbf{g}}}(g) e^{-\beta \widehat{H_{\mathbf{g}}}}). \tag{3.22}$$

Now, the trace operations may be performed, and one can then write Z_c as:

$$Z_c(T,\mu,V) = \int\limits_{SU(3)} d\mu(g)\widetilde{Z}_{quark}\widetilde{Z}_{glue}, \tag{3.23}$$

with the quark and gluon contributions individually given by:

$$\begin{aligned}\widetilde{Z}_{quark} &= \prod_{q=r,g,b}\prod_{\alpha}\left[1+e^{-\beta(\epsilon_q^\alpha-\mu_q)+i\theta_q}\right]\left[1+e^{-\beta(\epsilon_{\overline{q}}^\alpha-\mu_{\overline{q}})-i\theta_q}\right] \\ &= \prod_{q=r,g,b}\prod_{\alpha}\left[1+e^{-\beta(\epsilon^\alpha-\mu)+i\theta_q}\right]\left[1+e^{-\beta(\epsilon^\alpha+\mu)-i\theta_q}\right], \end{aligned}\tag{3.24}$$

where ϵ^α are single-particle energies, the explicit expressions of the angles θ_q ($q = r,\ b,\ g$) in $SU(3)$ are:

$$\theta_r = \frac{\varphi}{2}+\frac{\psi}{3},\ \ \theta_g = -\frac{\varphi}{2}+\frac{\psi}{3},\ \ \theta_b = -\frac{2\psi}{3}, \tag{3.25}$$

and in the second factor arising from the antiquarks, we have replaced: $\epsilon_{\overline{q}}^\alpha = \epsilon_q^\alpha = \epsilon^\alpha$ and $\mu_{\overline{q}} = -\mu_q = -\mu$; and:

$$\widetilde{Z}_{glue} = \prod_{\mathbf{g}=1,2,3,4}\prod_{\alpha}\left[1-e^{-\beta\epsilon_\alpha+i\theta_{\mathbf{g}}}\right]^{-1}\left[1-e^{-\beta\epsilon_\alpha-i\theta_{\mathbf{g}}}\right]^{-1}, \tag{3.26}$$

with the angles $\theta_{\mathbf{g}}$ ($\mathbf{g} = 1, ...4$) being:

$$\theta_1 = \theta_r-\theta_g,\ \ \theta_2 = \theta_g-\theta_b,\ \ \theta_3 = \theta_b-\theta_r,\ \ \theta_4 = 0. \tag{3.27}$$

In the continuum approximation for the single-particle energy levels, one can replace $\sum\limits_\alpha$ by $\int\rho(\epsilon)d\epsilon$ where: $\rho(\epsilon) = d_{Q/g}\frac{V}{2\pi^2}\epsilon^2$ is the single-particle density of states, $d_{Q/G}$ is the spin-isospin degeneracy factor for quarks or gluons, with $d_Q = 2N_f$ and $d_G = 2$. After integration, the quark contribution is given by:

$$\widetilde{Z}_{Quark}\left(T,V,\mu;\varphi,\psi\right) = \exp\left[\frac{\pi^2}{12}T^3Vd_Q\sum_{q=r,g,b}\left(\frac{7}{30}-\left(\frac{\theta_q-i(\frac{\mu}{T})}{\pi}\right)^2+\frac{1}{2}\left(\frac{\theta_q-i(\frac{\mu}{T})}{\pi}\right)^4\right)\right], \tag{3.28}$$

and the gluon contribution by:

$$\widetilde{Z}_{Gluon}\left(T,V;\varphi,\psi\right)=\exp\left[\frac{\pi^2}{12}T^3Vd_G\sum_{\mathbf{g}=1}^{4}\left(-\frac{7}{30}+\left(\frac{\theta_{\mathbf{g}}-\pi}{\pi}\right)^2-\frac{1}{2}\left(\frac{\theta_{\mathbf{g}}-\pi}{\pi}\right)^4\right)\right]. \tag{3.29}$$

Thus, the partition function for a color-singlet quark-gluon plasma can be written as [7, 8]:

$$Z(T,V,\mu)=\frac{8}{3\pi^2}e^{-\frac{BV}{T}}\int_{-\pi}^{+\pi}\int_{-\pi}^{+\pi}d\left(\frac{\varphi}{2}\right)d\left(\frac{\psi}{3}\right)M(\varphi,\psi)\widetilde{Z}(T,V,\mu;\varphi,\psi), \tag{3.30}$$

where $M(\varphi,\psi)$ is explicitly given by:

$$M(\varphi,\psi)=\left(\sin\left(\frac{1}{2}(\psi+\frac{\varphi}{2})\right)\sin(\frac{\varphi}{2})\sin\left(\frac{1}{2}(\psi-\frac{\varphi}{2})\right)\right)^2, \tag{3.31}$$

B being the bag constant.

Let us write $\widetilde{Z}$ on the form:

$$\widetilde{Z}\left(T,V,\mu;\varphi,\psi\right)=e^{VT^3g(\varphi,\psi,\frac{\mu}{T})}, \tag{3.32}$$

with:

$$\begin{aligned}g(\varphi,\psi,\frac{\mu}{T}) &= \frac{\pi^2}{12}(\frac{21}{30}d_Q+\frac{16}{15}d_G)+\frac{\pi^2}{12}\frac{d_Q}{2}\sum_{q=r,b,g}\left\{-1+\left(\frac{\left(\theta_q-i(\frac{\mu}{T})\right)^2}{\pi^2}-1\right)^2\right\}\\ &\quad -\frac{\pi^2}{12}\frac{d_G}{2}\sum_{\mathbf{g}=1}^{4}\left(\frac{(\theta_{\mathbf{g}}-\pi)^2}{\pi^2}-1\right)^2,\end{aligned} \tag{3.33}$$

then eq. (3.30) becomes:

$$Z(T,V,\mu)=\frac{8}{3\pi^2}e^{-\frac{BV}{T}}\int_{-\pi}^{+\pi}\int_{-\pi}^{+\pi}d\left(\frac{\varphi}{2}\right)d\left(\frac{\psi}{3}\right)M(\varphi,\psi)e^{VT^3g(\varphi,\psi,\frac{\mu}{T})}. \tag{3.34}$$

3.3.2 Calculation of the Color-Singlet Partition Function of the QGP, within the Saddle Point Approximation

The analytic calculation of the color-singlet partition function of the QGP in eq. (3.34) being not possible to be effectuated exactly, an approximated calculus is usually carried

out using the saddle point approximation as in [8, 9, 10]. Let's derive in the following such an approximate color-singlet partition function at zero chemical potential ($\mu = 0$).

In this case, we have:

$$\begin{aligned} g_{\mu=0}(\varphi,\psi) &= \frac{\pi^2}{12}(\frac{21}{30}d_Q + \frac{16}{15}d_G) + \frac{\pi^2}{12}\frac{d_Q}{2}\sum_{q=r,b,g}\left(\left(\frac{\alpha_q^2}{\pi^2}-1\right)^2-1\right) \\ &\quad -\frac{\pi^2}{12}\frac{d_G}{2}\sum_{\mathbf{g}=1}^{4}\left(\frac{(\alpha_{\mathbf{g}}-\pi)^2}{\pi^2}-1\right)^2, \end{aligned} \tag{3.35}$$

and then the color-singlet partition function for a quark-gluon plasma contained in a volume V_{QGP} becomes:

$$Z(T,V_{QGP}) = \frac{8}{3\pi^2}e^{-\frac{BV_{QGP}}{T}}\int_{-\pi}^{+\pi}\int_{-\pi}^{+\pi} d\left(\frac{\varphi}{2}\right) d\left(\frac{\psi}{3}\right) M(\varphi,\psi)\exp\left(V_{QGP}T^3 g_{\mu=0}(\varphi,\psi)\right). \tag{3.36}$$

The integral in (3.36) can be evaluated by a saddle point approximation around the maximum of the integrand at $(\varphi,\psi) = (0,0)$. For that purpose, we expand the weight function M to leading order in the angular variables, and expand the argument of the exponential to second order in φ and ψ (gaussian approximation). The measure function has then the following form:

$$M(\varphi,\psi) \approx M^{(0,0)}(\varphi,\psi) = \frac{1}{64}\varphi^2\left(\psi^2 - \frac{\varphi^2}{4}\right)^2, \tag{3.37}$$

and $g_{\mu=0}(\varphi,\psi)$ becomes for two flavors ($N_f = 2$) (up and down quarks):

$$g_{\mu=0}(\varphi,\psi) \approx g_{\mu=0}^{(0,0)}(\varphi,\psi) = S_0 - \frac{2}{3}\left(\varphi^2 + \frac{4}{3}\psi^2\right), \tag{3.38}$$

with:

$$S_0 = \frac{\pi^2}{12}(\frac{7N_f}{5} + \frac{32}{15}). \tag{3.39}$$

Therefore, we have integrals like:

$$\int_0^a e^{-\alpha x^2}dx \approx \int_0^\infty e^{-\alpha x^2}dx = \sqrt{\pi/\alpha}, \tag{3.40}$$

with $\alpha \gg 1$.

From all these considerations, the partition function can then be rewritten as:

$$Z(T, V_{QGP}) = \frac{8}{3\pi^2} e^{-\frac{BV_{QGP}}{T}} \int_{-\infty}^{+\infty} \int_{-\infty}^{+\infty} d\left(\frac{\varphi}{2}\right) d\left(\frac{\psi}{3}\right) M^{(0,0)}(\varphi, \psi) \exp\left(g_{\mu=0}^{(0,0)}(\varphi, \psi) V_{QGP} T^3\right), \tag{3.41}$$

which gives after calculation:

$$Z(T, V_{QGP}) = \frac{A_0 e^{\left(S_0 T^3 - \frac{B}{T}\right) V_{QGP}}}{\left(V_{QGP} T^3\right)^4}, \tag{3.42}$$

where:

$$A_0 = \frac{27\sqrt{3}}{8192\pi}. \tag{3.43}$$

We mention here a similar result obtained in [9] given for a zero baryon density as:

$$Z_{QGP}(T, V_{QGP}) = A\, C^{-4} u^{-3/2} \frac{\exp\left(\frac{1}{3} u V_{QGP} T^3\right)}{\left(V_{QGP} T^3\right)^{13/2}} \exp(-\frac{B V_{QGP}}{T}), \tag{3.44}$$

with:

$$\begin{cases} A = \dfrac{3\sqrt{2\pi}}{4} \\ C = 2 + \dfrac{N_f}{3} \\ u = \left(\dfrac{8}{15} + \dfrac{7N_f}{20}\right) \pi^2. \end{cases} \tag{3.45}$$

3.3.3 Problem with the Use of the Color-Singlet Partition Function Derived within the Saddle Point Approximation, in the Phase Coexistence Model

Let us incorporate such an approximate partition function, eqs. (3.42-43), for the QGP in the phase coexistence model. The order parameter can then be expressed as:

$$\langle \mathfrak{h}(T, V) \rangle = 1 - \left(\int_0^1 \mathfrak{q}^{-3} e^{K\mathfrak{q}} d\mathfrak{q} \; / \; \int_0^1 \mathfrak{q}^{-4} e^{K\mathfrak{q}} d\mathfrak{q} \right), \tag{3.46}$$

where $\mathfrak{q}$ is the QGP volume fraction defined as: $\mathfrak{q} = 1 - \mathfrak{h}$, and: $K = \left(S_0 - \frac{\pi^2}{30}\right) T^3 V - \frac{BV}{T}$.

By expanding the exponential $e^{K\mathfrak{q}}$, and taking the limit $\mathfrak{q}_0$ for $\mathfrak{q}$ instead of 0 in the integral above (i.e., $\mathfrak{h} \longrightarrow \mathfrak{h}_0$), we obtain the following expression for the mean value of the hadronic volume fraction:

$$\langle \mathfrak{h}(T,V) \rangle = 1 - \mathfrak{q}_0 \left(\sum_{p=0}^{\infty} \frac{K^p}{p!\,(p-2)} \left(\mathfrak{q}_0^p - \mathfrak{q}_0^2\right) / \sum_{p=0}^{\infty} \frac{K^p}{p!\,(p-3)} \left(\mathfrak{q}_0^p - \mathfrak{q}_0^3\right) \right). \tag{3.47}$$

We can easily show that for $\mathfrak{q}_0 \longrightarrow 0$ (i. e., $\mathfrak{h}_0 \longrightarrow 1$), the mean value of the hadronic volume fraction is equal to 1 for all values of temperature and volume [12].

Hence, the use of the obtained approximate total partition function $Z(\mathfrak{h})$ in the definition (3.3), has as a consequence the absence of the deconfinement phase transition. This is due to the fact that the saddle point approximation, used for the calculation of the color-singlet partition function, breaks down at $V_{QGP}T^3 << 1$. We propose in the following, first, a new method for calculating an exact color-singlet partition function with the unique disadvantage of necessitating very long times for numerical calculations.

3.3.4 Remedy to the problem

To remedy to the problem exposed above in a first step, we have tried to do the expansion of the exponential $e^{V_{QGP}T^3 g(\varphi,\psi,\frac{\mu}{T})}$ as:

$$e^{V_{QGP}T^3 g(\varphi,\psi,\frac{\mu}{T})} = \sum_{j=0}^{\infty} \frac{(V_{QGP}T^3)^j}{j!} \left(g(\varphi,\psi,\frac{\mu}{T}) \right)^j, \tag{3.48}$$

then (3.34) becomes:

$$Z_{QGP}(T,\mu,V_{QGP}) = \frac{8}{3\pi^2} \int_{-\pi}^{+\pi} \int_{-\pi}^{+\pi} d(\varphi/2) d(\psi/3) M(\varphi,\psi) \sum_{j=0}^{\infty} \frac{(V_{QGP}T^3)^j}{j!} \left(g(\varphi,\psi,\frac{\mu}{T}) \right)^j, \tag{3.49}$$

and by putting:

$$\alpha_j = \frac{4}{9\pi^2}\int_{-\pi}^{+\pi}\int_{-\pi}^{+\pi} d\varphi d\psi M(\varphi,\psi)\frac{\left(g(\varphi,\psi,\frac{\mu}{T})\right)^j}{j!}, \tag{3.50}$$

the partition function becomes:

$$Z_{QGP}(T,\mu,V_{QGP}) = \sum_{j=0}^{\infty}\alpha_j(V_{QGP}T^3)^j = \sum_{j=0}^{\infty}\alpha_j z^j, \tag{3.51}$$

where: $z = V_{QGP}T^3$. It can be seen that the series (3.51) giving the color-singlet partition function is convergent and causes no more problems at $z \to 0$ since for $V_{QGP}T^3 = 0$, $Z\left(V_{QGP}T^3 = 0\right) = \alpha_0$. It can then be incorporated in the phase coexistence model to probe the critical behavior of thermodynamic quantities characterizing the system which undergoes a deconfinement phase transition. Because of numerical difficulties, it was not possible for us to illustrate this exact calculus at the present time. Indeed, the integral coefficients α_j have been calculated to high ranks ($j = 175$) using a numerical integration program with fortran, and the series giving Z_{QGP} has been calculated for values of T and V_{QGP} such that $V_{QGP}T^3 \leq 5$; for example, for $V_{QGP}T^3 = 2$ the value of Z_{QGP} is stable at $j \approx 110$. But it turned out that for large volumes and/or temperatures, the rank j at which the convergence of Z_{QGP} is attained is very high, and since the values of the coefficients α_j are largely increasing and due to the insufficient precision offered by fortran, the convergence of Z_{QGP} couldn't be attained.

After this, we have tried to use Mathematica 4.0 for the numerical calculation of α_j, since this software can insure much more precision but it turned out that the time of calculus at ranks $j \gtrsim 13$ begins to become too long, rendering the use of such a method practically a waste of time.

In order to get a first understanding of the deconfinement phase transition in a

finite volume, we have proceeded, in a second step of the work, by effectuating some approximations to derive a suitable color-singlet partition function, which allowed us to accurately calculate physical quantities describing well the deconfinement phase transition at finite volumes. This part of the work can be found in [13, 14].

A more rigorous calculus then followed, where the color-singlet partition function of the QGP has not been calculated explicitly, but has just been used with its exact expression (3.34) in order to calculate mean values of physical quantities of the system using the definition (3.3) [84]. Details are given in the following.

3.4 Finite-Size Effects with the Exact Color-Singlet Partition Function within the L_{mn} *Method*

In the following, we'll derive the mean values of the order parameter, and then of other thermodynamic quantities, directly from the definition (3.3) of the mean value of any physical quantity within the phase coexistence model, using the exact definition (3.34) of the QGP color-singlet partition function. The exact total partition function given by:

$$Z\left(\mathfrak{q}\right)=\frac{4}{9\pi^{2}}e^{\frac{\pi^{2}}{30}VT^{3}}\int_{-\pi}^{+\pi}\int_{-\pi}^{+\pi}d\varphi d\psi M(\varphi,\psi)e^{\mathfrak{q}VT^{3}\left(g(\varphi,\psi,\frac{\mu}{T})-\frac{\pi^{2}}{30}-\frac{B}{T^{4}}\right)}, \tag{3.52}$$

will not be calculated itself exactly, but the integration on $\mathfrak{q}$ in the calculation of the mean values using this exact partition function will first be effectuated, then the integrations on φ and ψ will be done at last [84].

Let's first illustrate the variations of the probability density $p(\mathfrak{h})=\frac{Z(\mathfrak{h})}{\int_{0}^{1}Z(\mathfrak{h})d\mathfrak{h}}$ with the hadron fraction $\mathfrak{h}$, for various system volumes, at the temperature $T=105MeV$

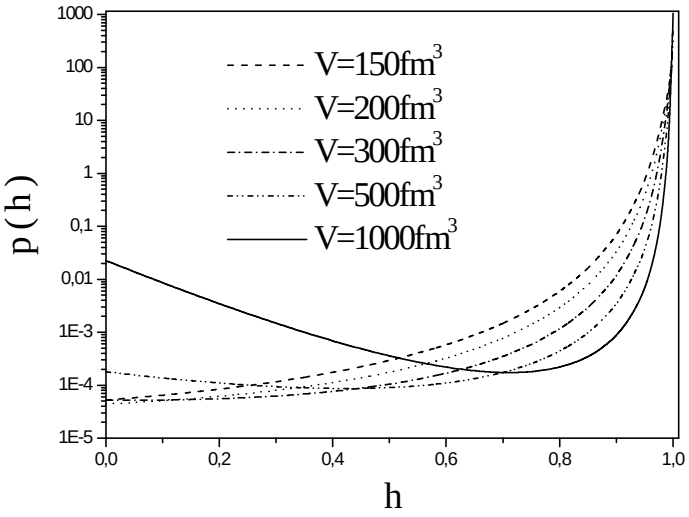

Figure 3.5: Probability density as a function of the hadron fraction for different system volumes, at the temperature $T = 105MeV$.

(Fig. (3.5)). The probability density exhibits a "two hump" structure at the extremal values of the hadron fraction $\mathfrak{h}$, more accentuated for big volumes. This structure indicates the dominance of one phase in the mixed phase system. It has been shown in [3] that such a structure is expected in the case of first order phase transitions.

The probability distribution at a fixed value of $\mathfrak{h}$ is also plotted versus temperature at different volumes in Fig. (3.6), which shows that the probability at fixed $\mathfrak{h}$ and V is peaked at a certain temperature tending to the true transition temperature $T_c(\infty)$ with increasing volume, at which it is maximal. This temperature is shifted to bigger values for small volumes. It can also be noted that the probability distribution looks to be symmetric for $\mathfrak{h} = 0.5$, while for $\mathfrak{h} = 0.1$ and $\mathfrak{h} = 0.9$ it is not symmetric. The tail of the distribution is heavier on the right for $\mathfrak{h} = 0.1$ and heavier on the left for $\mathfrak{h} = 0.9$. This is easily understandable, since at $\mathfrak{h} = 0.1$ it is the QGP which is dominant and

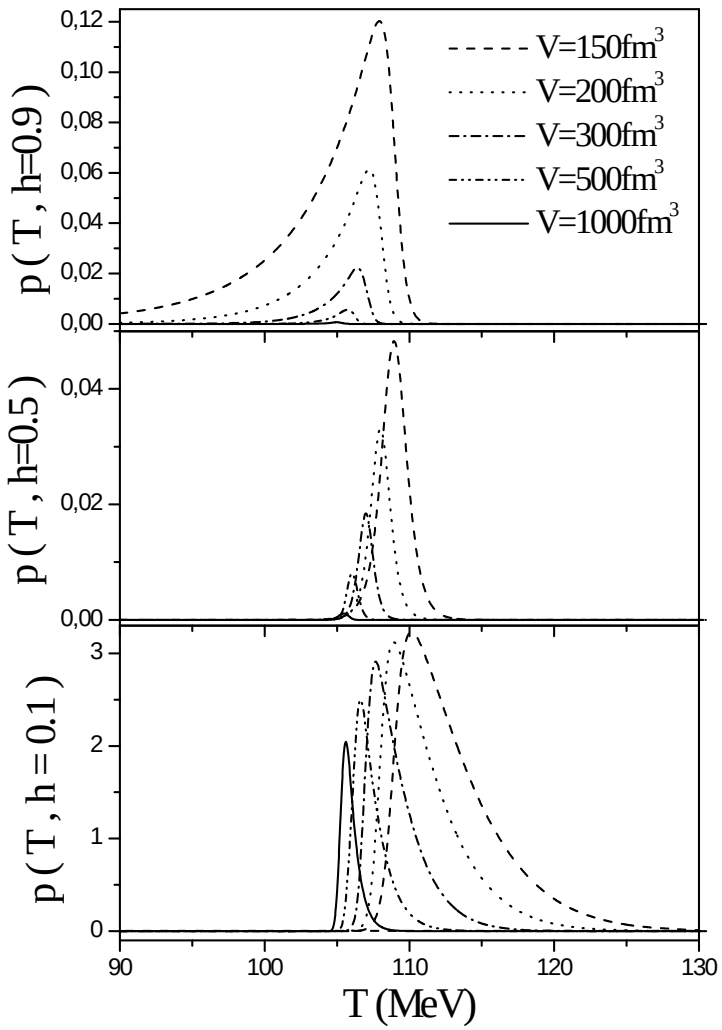

Figure 3.6: Variations of the probability of finding the system (of volume V) in a state (bottom) $\mathfrak{h}$ =0.1, (middle) $\mathfrak{h}$ =0.5, and (top) $\mathfrak{h}$ =0.9 with temperature T, for different system volumes.

this occurs above the transition temperature, and at $\mathfrak{h} = 0.9$ it is the hadronic gas phase which is dominant and this occurs below the transition temperature.

3.4.1 Order Parameter, Energy and Entropy Densities

Like in the case without including the color-singletness requirement, let's calculate now the order parameter at zero chemical potential ($\mu = 0$), using the total partition function (3.52). Its expression is in this case:

$$< \mathfrak{h}(T,V) >^{*} = 1 - \frac{\int_{-\pi}^{+\pi}\int_{-\pi}^{+\pi} d\varphi d\psi M(\varphi,\psi) \int_{0}^{1} \mathfrak{q} e^{\mathfrak{q}\ \mathfrak{R}(\varphi,\psi;T,V)} d\mathfrak{q}}{\int_{-\pi}^{+\pi}\int_{-\pi}^{+\pi} d\varphi d\psi M(\varphi,\psi) \int_{0}^{1} e^{\mathfrak{q}\ \mathfrak{R}(\varphi,\psi;T,V)} d\mathfrak{q}}, \tag{3.53}$$

with:

$$\mathfrak{R}\left(\varphi,\psi;T,V\right) = \left(g_{\mu=0}(\varphi,\psi) - \frac{\pi^2}{30} - \frac{B}{T^4}\right) VT^3. \tag{3.54}$$

After effectuation of the integrations on $\mathfrak{q}$, the order parameter can be written on the form:

$$< \mathfrak{h}(T,V) >^{*} = \frac{L_{01}\left(0\right) + L_{02}\left(0\right) - L_{02}\left(1\right)}{L_{01}\left(0\right) - L_{01}\left(1\right)}, \tag{3.55}$$

where the general form of the integrals on φ and ψ appearing in this expression is:

$$L_{mn}\left(\mathfrak{q}\right) = \int_{-\pi}^{+\pi}\int_{-\pi}^{+\pi} d\varphi d\psi M(\varphi,\psi)(g_{\mu=0}(\varphi,\psi))^m \frac{e^{\mathfrak{q}\ \mathfrak{R}(\varphi,\psi;T,V)}}{\left(\mathfrak{R}\left(\varphi,\psi;T,V\right)\right)^n}. \tag{3.56}$$

The integrals L_{mn} represent in themselves state functions, and they have been chosen in a judicious way so that all thermodynamic quantities can, in one way or the other, be written as function of these L_{mn}'s. They can be calculated numerically at each temperature T and volume V, and the mean values of physical quantities can therefore be illustrated on the hole range of temperature for varying volume. Fig. (3.7) illustrates the variations of some L_{mn}'s with temperature at fixed volume.

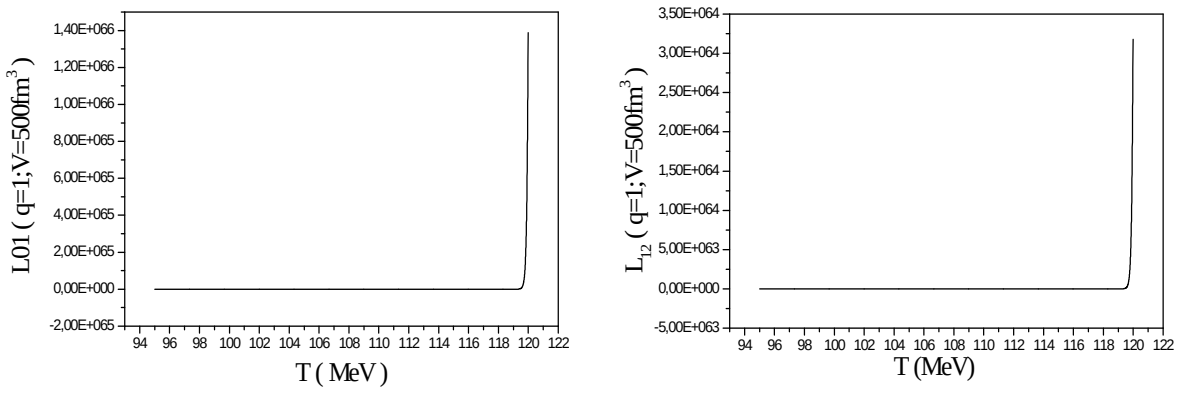

Figure 3.7: Variations of $L_{01}\,(\mathfrak{q}=1)$ and $L_{12}\,(\mathfrak{q}=1)$ with temperature at the volume $V = 500 fm^3$.

The mean value of the energy density is also calculated in the same way, and is found to be related to $<\mathfrak{h}(T,V)>^*$ by the expression:

$$<\varepsilon(T,V)>^* = B-(B-e_{HG})<\mathfrak{h}(T,V)>^* -3T^4\,\frac{L_{12}\,(0)+L_{11}\,(1)-L_{12}\,(1)}{L_{01}\,(0)-L_{01}\,(1)}. \quad (3.57)$$

Let us note that we have used "Mathematica 4.0" to evaluate the integrals L_{mn} numerically, and then the mean values of the order parameter and energy density. The evaluation of the order parameter at a given temperature and volume takes an approximate time of about 13 minutes, and that of $<\varepsilon(T,V)>^*$ about 25 minutes, on a (PentiumIII, 500MHz). For the illustration of both $<\mathfrak{h}(T,V)>^*$ and $<\varepsilon(T,V)>^*$, the calculations are done on an interval of temperature $(95-120 MeV)$ with a temperature step $(dT = 0.1 MeV)$ and are repeated for various volumes.

The entropy can be obtained from the thermodynamic relation: $s = \frac{1}{T}(\varepsilon - f)$, knowing the free energy $F = fV$, which is defined as: $F = -T\ln Z$. The mean value

of this latter involves then an integral $\int_0^1 d\mathfrak{h} Z(\mathfrak{h}) \ln Z(\mathfrak{h})$ as given by the expression:

$$\begin{aligned}\langle F(T,V)\rangle^* &= -T\left[\ln(\frac{4}{9\pi^2}) + \frac{\pi^2}{30}VT^3\right. \\ &\left. + \frac{\int_0^1 d\mathfrak{q}\left(\int_{-\pi}^{+\pi}\int_{-\pi}^{+\pi} d\varphi d\psi M(\varphi,\psi) e^{\mathfrak{q}\ \mathfrak{R}(\varphi,\psi;T,V)}\right)\ln\left(\int_{-\pi}^{+\pi}\int_{-\pi}^{+\pi} d\varphi d\psi M(\varphi,\psi) e^{\mathfrak{q}\ \mathfrak{R}(\varphi,\psi;T,V)}\right)}{\int_0^1 d\mathfrak{q}\int_{-\pi}^{+\pi}\int_{-\pi}^{+\pi} d\varphi d\psi M(\varphi,\psi) e^{\mathfrak{q}\ \mathfrak{R}(\varphi,\psi;T,V)}}\right] \end{aligned} \quad (3.58)$$

and can not be evaluated as $< \mathfrak{h}(T,V) >^*$ and $< \varepsilon(T,V) >^*$ simply with the L_{mn}'s. Hence, it is evaluated with a numerical integration of the numerator in the last term of eq. (3.58).

The entropy density can also be obtained from the definitions of the specific heat at constant V (see section 1.2): $C_V = \left(\frac{\partial U}{\partial T}\right)_V = T\left(\frac{\partial S}{\partial T}\right)_V$. We have then the specific heat density related to both energy and entropy densities as:

$$c = \left(\frac{\partial \langle\varepsilon\rangle^*}{\partial T}\right)_V = T\left(\frac{\partial \langle s\rangle^*}{\partial T}\right)_V. \quad (3.59)$$

Hence, the entropy density can be obtained from:

$$\langle s(T,V)\rangle^* = \int \frac{1}{T}\left(\frac{\partial \langle\varepsilon\rangle^*}{\partial T}\right) dT = \int \frac{c(T,V)}{T}\ dT, \quad (3.60)$$

by the mean of a numerical integration of the specific heat density, whose expression after differentiation of the energy density in (3.57) with respect to temperature, is given

by:

$$\begin{aligned} c(T,V) &= \frac{2\pi^2}{5}T^3\left\langle \mathfrak{h}(T,V)\right\rangle^* + \left(\frac{\pi^2}{10}T^4 - B\right)\chi(T,V) + 12T^3\frac{\left(L_{11}\left(1\right) - L_{12}\left(1\right) + L_{12}\left(0\right)\right)}{L_{01}\left(1\right) - L_{01}\left(0\right)} \\ &+3T^6V\left[\frac{1}{L_{01}\left(1\right) - L_{01}\left(0\right)}\left(3(L_{21}\left(1\right) - 2L_{22}\left(1\right) + 2L_{23}\left(1\right) - 2L_{23}\left(0\right)\right)\right. \\ &\left.-(\frac{B}{T^4} - \frac{\pi^2}{10})(L_{11}\left(1\right) - 2L_{12}\left(1\right) + 2L_{13}\left(1\right) - 2L_{13}\left(0\right))\right) \\ &-\frac{L_{11}\left(1\right) - L_{12}\left(1\right) + L_{12}\left(0\right)}{\left(L_{01}\left(1\right) - L_{01}\left(0\right)\right)^2}\left(3(L_{11}\left(1\right) - L_{12}\left(1\right) + L_{12}\left(0\right)\right) \\ &\left.+(\frac{B}{T^4} - \frac{\pi^2}{10})(L_{01}\left(1\right) - L_{02}\left(1\right) + L_{02}\left(0\right))\right)\Bigg], \end{aligned} \tag{3.61}$$

with:

$$\begin{aligned} \chi\left(T,V\right) &= T^2V\left[\frac{1}{L_{01}\left(0\right) - L_{01}\left(1\right)}\left(-3(L_{12}\left(0\right) + 2L_{13}\left(0\right) + L_{12}\left(1\right) - 2L_{13}\left(1\right)\right)\right. \\ &\left.-(\frac{B}{T^4} - \frac{\pi^2}{10})(L_{02}\left(0\right) + 2L_{03}\left(0\right) + L_{02}\left(1\right) - 2L_{03}\left(1\right))\right) \\ &+\frac{L_{01}\left(0\right) + L_{02}\left(0\right) - L_{02}\left(1\right)}{\left(L_{01}\left(0\right) - L_{01}\left(1\right)\right)^2}\left(3(L_{11}\left(1\right) - L_{12}\left(1\right) + L_{12}\left(0\right)\right) \\ &\left.+(\frac{B}{T^4} - \frac{\pi^2}{10})(L_{01}\left(1\right) - L_{02}\left(1\right) + L_{02}\left(0\right))\right)\Bigg]. \end{aligned} \tag{3.62}$$

Our results for the variations of each of the order parameter, the energy density normalized by T^4 and the entropy density normalized by T^3, with temperature at different system sizes are presented in the plots on Fig. (3.8). A pronounced size dependence of these quantities can be noted over almost the entire temperature range. The main and striking difference, comparatively with Fig. (3.2), is the shift of the transition temperature to higher values for small sizes. This is due to the effect of the color-singletness requirement which was found to lead to a gradual freezing of the effective number of degrees of freedom in the QGP [7]. In a finite volume, the pressure at a given temperature has a lower value and the equilibrium between the two phases according to the Gibbs criterion is then reached at temperatures greater than $T_c\left(\infty\right)$.

This freezing in the QGP degrees of freedom can more clearly be seen on Fig. (3.9) where we compare the normalized energy density $\frac{\langle \varepsilon (T,V) \rangle}{T^4}$, representing the effective number of degrees of freedom as yet mentioned, with (dashed line) and without (solid line) color-singletness requirement at the volume $V = 150 fm^3$ for example. It can also be noted that the smearing due to the fluctuations including the color-singletness is less pronounced than in the case without color-singletness, maybe because of the reduction of the QGP degrees of freedom.

Let's note that as it was the case in Fig. (3.3), the variations of the normalized energy and entropy densities, including color singletness are not exactly the same,. This can better be seen in Fig. (3.10) where the normalized energy density vs temperature at different volumes is illustrated more clearly. The difference from the normalized entropy density, which can be approximated by a step function, can easily be observed.

3.4.2 Susceptibility and Specific Heat Density

It is also worth to illustrate two additional thermal response functions relevant to this case, which are the specific heat density $c(T,V) = \frac{\partial \langle \varepsilon(T,V) \rangle^*}{\partial T}$ and susceptibility $\chi(T,V) = \frac{\partial \langle \mathfrak{h}(T,V) \rangle^*}{\partial T}$, obtained by differentiating the energy density in (3.57) and the order parameter in (3.55-56) with respect to temperature. Their expressions have been obtained in (3.61) and (3.62) respectively.

In the following, the variations of the thermal susceptibility and specific heat density with temperature are illustrated on Figs. (3.11) and (3.12) respectively, for various sizes. It can clearly be seen that the delta function singularity of both quantities occurring in the thermodynamical limit is smeared, in a finite volume, into a finite peak of width $\delta T(V)$. This result is expected, since the derivative of the step function

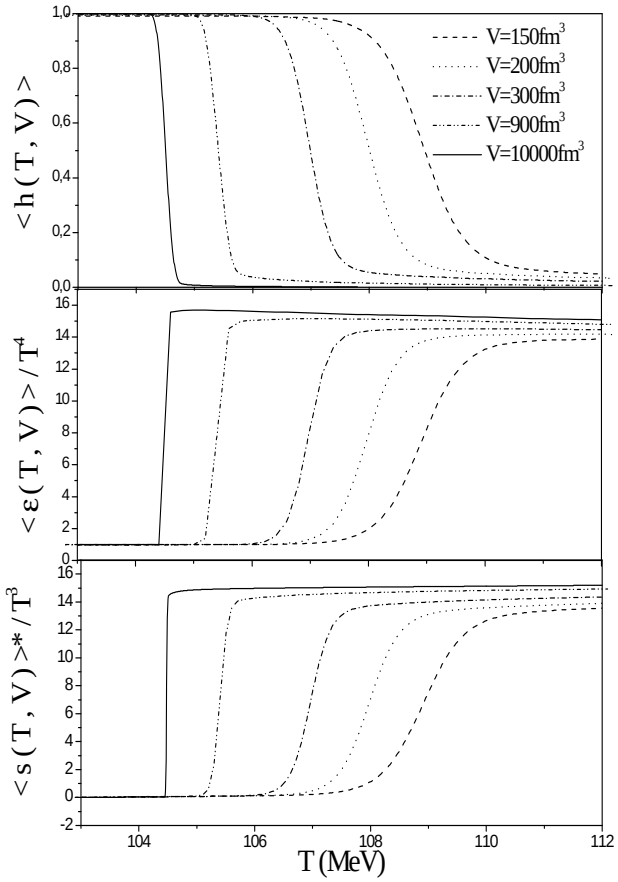

Figure 3.8: Temperature variation of the order parameter (bottom), the energy density normalized by T^4 (middle) and the entropy density normalized by T^3 (top) at $\mu = 0$, for different system volumes.

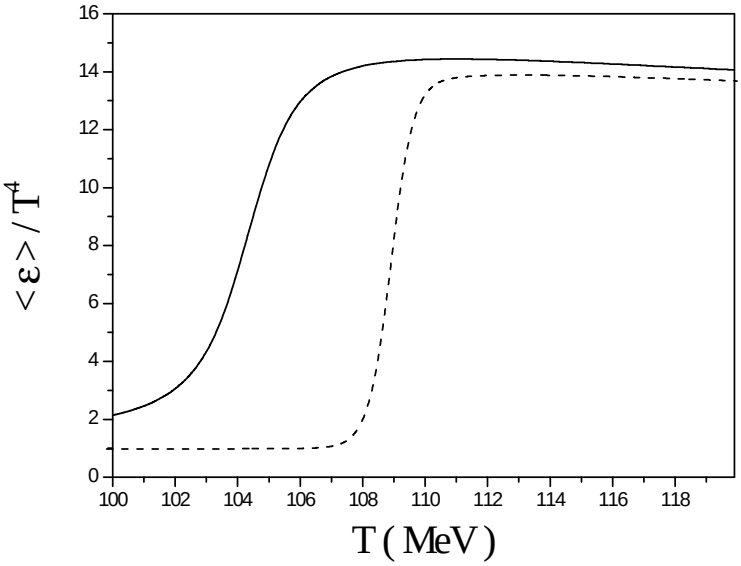

Figure 3.9: Normalized energy density $\frac{\langle \varepsilon(T,V)\rangle}{T^4}$, versus temperature, with (dashed line) and without (solid line) color-singletness requirement at the volume $V = 150 fm^3$.

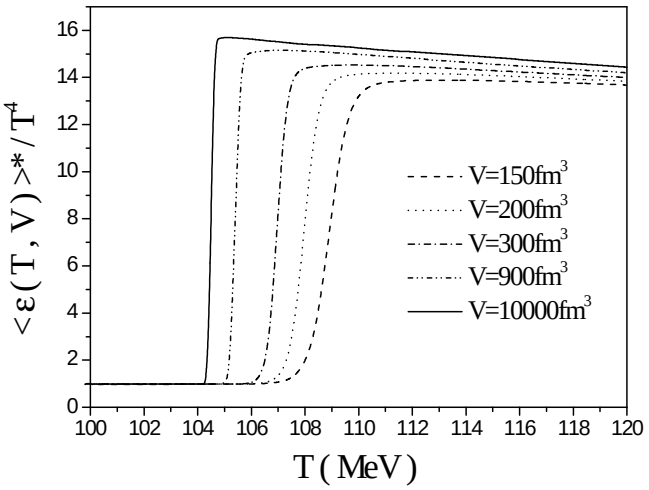

Figure 3.10: Normalized energy density $\frac{\langle \varepsilon(T,V)\rangle *}{T^4}$ with the color-singletness requirement versus temperature at various volumes.

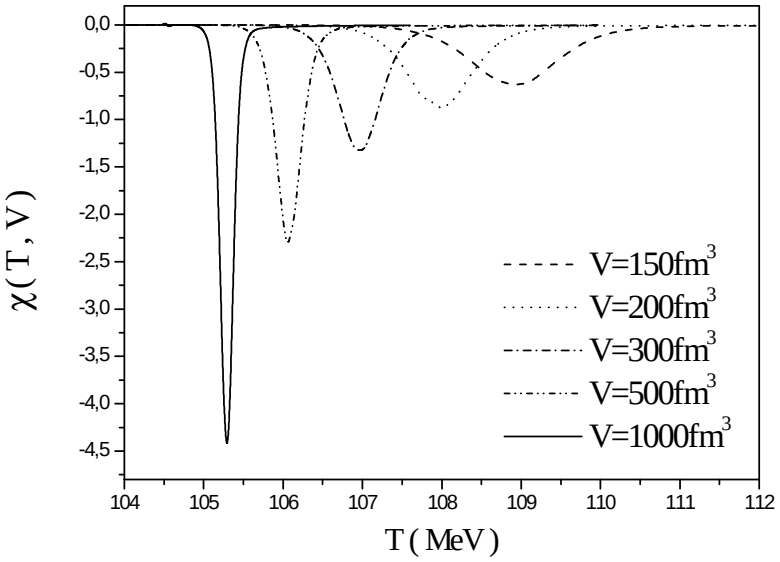

Figure 3.11: Plot of the susceptibility $\chi\,(T,V)$ versus temperature for different system volumes.

is a delta function, as well known. The rounding of each of $\langle \mathfrak{h}\,(T,V)\rangle^*$ and $\langle \varepsilon(T,V)\rangle^*$ manifests then at the level of their first derivatives as a smearing of the delta function. For decreasing volume, the width of the peaks gets larger while their heights, noted $\mid \chi_T \mid^{\max}(V)$ and $c_T^{\max}(V)$, decrease, occurring at effective transition temperatures $T_c(V)$ shifted away from the true transition temperature $T_c\,(\infty)$.

3.4.3 Pressure and Sound Velocity

In what follows, let's examine the behavior of the pressure for the system undergoing a deconfinement phase transition. Its mean value can be determined, and is simply in this case related to both energy density and order parameter by:

$$\langle P(T,V)\rangle^* = \frac{1}{3}\left(\langle \varepsilon(T,V)\rangle^* - 4\ B\ \left(1 - \langle \mathfrak{h}(T,V)\rangle^*\right)\right). \tag{3.63}$$

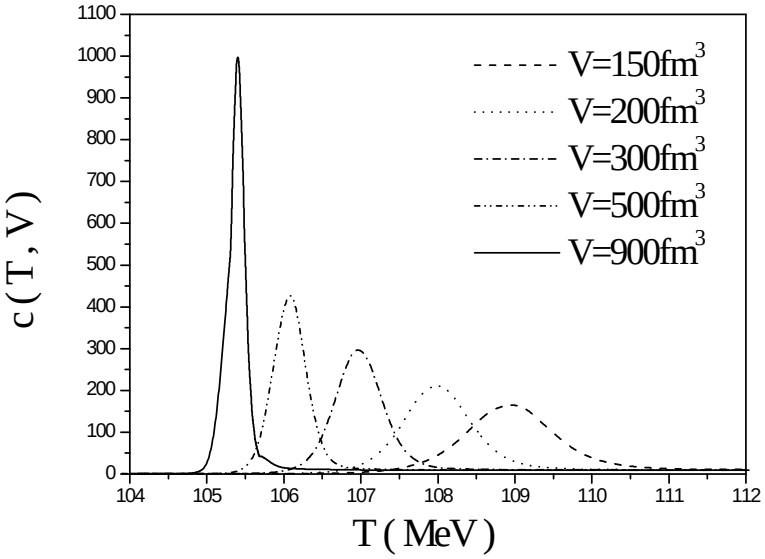

Figure 3.12: Plot of the specific heat density $c\,(T, V)$ versus temperature for different system volumes.

An other quantity, determined by the pressure gradient dP for a given gradient in the energy density $d\varepsilon$, is the sound velocity squared, defined as [114]:

$$c_s^2 = \left(\frac{\mathfrak{v}_s}{c}\right)^2 = \frac{dP}{d\varepsilon}, \tag{3.64}$$

which is the most relevant measure of the system's tendency to expand [115]. After a straightforward calculation, c_s^2 can be related to both thermal susceptibility $\chi(T,V)$ and specific heat density $c(T,V)$, by the relation:

$$c_s^2 = \frac{1}{3}\left(1 + 4B\frac{\chi}{c}\right). \tag{3.65}$$

Fig. (3.13) illustrates the variations of the pressure normalized by T^4 with temperature for different volumes, and it can clearly be seen that below the transition temperature, the pressure is constant with the Stefan-Boltzmann value for a hadronic gas, then it abruptly increases around $T_c(V)$ and continues increasing, rather slowly this time.

The velocity of sound squared is plotted on Fig. (3.14) as a function of temperature, for different sizes, and it is obvious from the curves that for temperatures well below and/or above a transition temperature, it approaches the value for an ultra-relativistic ideal gas $c_s^2 = \frac{1}{3}$. In a finite volume, c_s decreases in the transition region, and has a minimum at the effective transition temperature $T_c(V)$. For a first order phase transition, occurring at the thermodynamic limit, this minimum is zero at $T_c(\infty)$.

It is more common and useful to plot thermodynamic quantities as a function of the energy density $\langle\varepsilon\rangle^*$, especially in hydrodynamics, as in [115, 116, 117]. The graph of the pressure $\langle P\rangle^*$ vs $\langle\varepsilon\rangle^*$ in Fig. (3.15-top) shows that for large volumes, $\langle P\rangle^*$ increases with increasing energy density below a value ε_{HG} and above ε_{QGP}. On a range of energy density $\varepsilon_{HG} \leq \varepsilon \leq \varepsilon_{QGP}$, the pressure remains constant meaning that

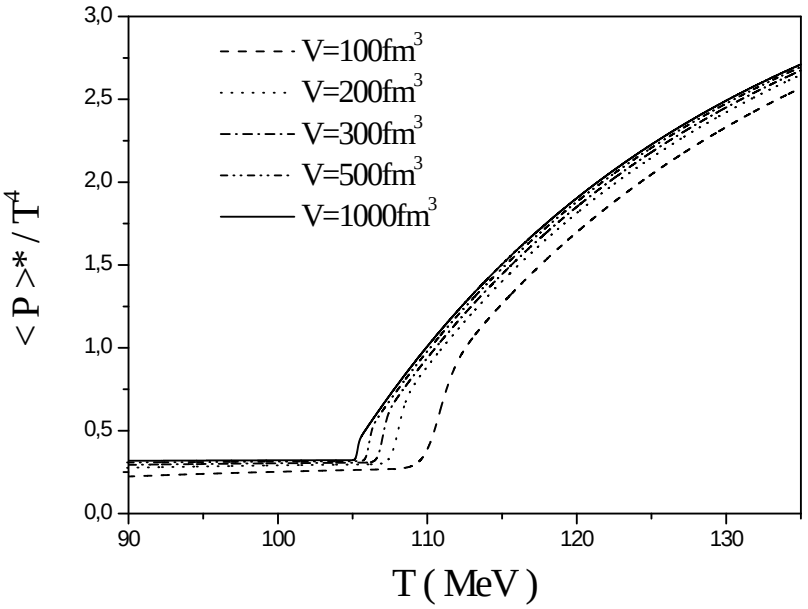

Figure 3.13: Plot of the normalized pressure $\frac{\langle P \rangle^*}{T^4}$ versus temperature for different system volumes.

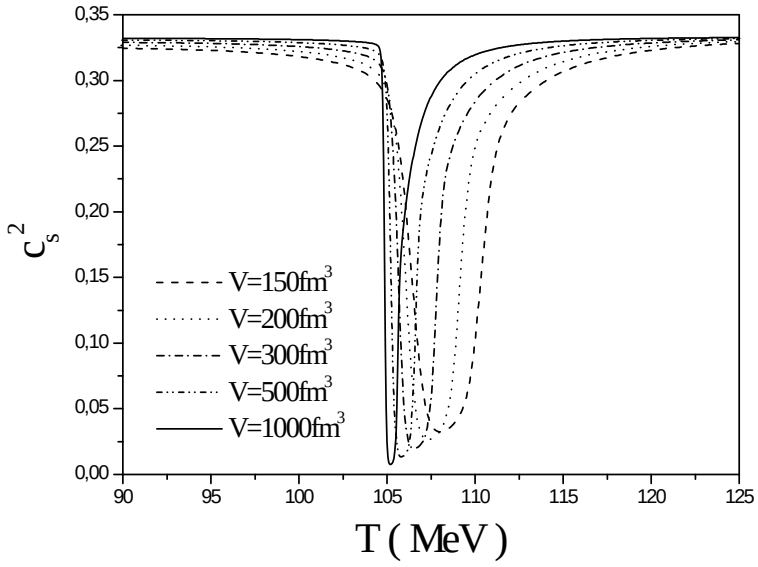

Figure 3.14: Velocity of sound squared c_s^2 as a function of temperature at different system volumes.

the system does not perform mechanical work. This region is referred to as the *soft region* of the equation of state [115, 116, 117, 118]. For small systems, it can clearly be seen that the pressure increases continuously with increasing energy density. The notions of *soft region* and *softest point* can better be seen by illustrating the ratio $\frac{\langle P\rangle^*}{\langle\varepsilon\rangle^*}$ as a function of $\langle\varepsilon\rangle^*$. The minimum of this latter occurs at the point $\langle\varepsilon\rangle^* = \varepsilon_{QGP}$ which is called the *softest point* of the equation of state. Fig. (3.15-middle) shows that for large volumes, the ratio $\frac{\langle P\rangle^*}{\langle\varepsilon\rangle^*} = \frac{1}{3} = c_s^2$ in the hadronic phase, then it starts to decrease at ε_{HG}, since $\langle P\rangle^*$ is constant in the mixed phase while $\langle\varepsilon\rangle^*$ increases. At the softest point ε_{QGP}, $\frac{\langle P\rangle^*}{\langle\varepsilon\rangle^*}$ takes its minimum value then resumes increasing in the QGP phase ($\langle\varepsilon\rangle^* \geq \varepsilon_{QGP}$) to reach again the asymptotic value $\frac{1}{3}$ for $\langle\varepsilon\rangle^* \to \infty$. For small volumes, the minimum of $\frac{\langle P\rangle^*}{\langle\varepsilon\rangle^*}$ increases and the softening of the equation of state is less pronounced.

Fig. (3.15-bottom) illustrates the variations of the speed of sound squared with the energy density for different system volumes, and shows that for big volumes, the speed of sound takes the value for an ultra-relativistic ideal gas $c_s^2 = \frac{1}{3}$ at $\langle\varepsilon\rangle^* \leq \varepsilon_{HG}$ and $\langle\varepsilon\rangle^* \geq \varepsilon_{QGP}$. On a range of energy density between ε_{HG} and ε_{QGP}, i.e., in the mixed phase, the speed of sound is nearly vanishing, reflecting the first order character of the transition. It has been interpreted in [115, 116, 117, 118] that mixed phase matter does not expand at all on account of its internal pressure, even if there are strong gradients in the energy density, and this has, in turn, the consequence that it does not perform mechanical work and therefore cools less rapidly. Thus, the expansion of the system is delayed and its lifetime is considerably prolonged. For small systems, the sound velocity is damped in a larger domain of energy density and does not vanish, since pressure gradients are finite, but they are still smaller than for an ideal gas equation

of state, and therefore the tendency of the system to expand is also reduced.

3.4.4 Second Derivative of the Order Parameter

The second derivative of the order parameter $\frac{\partial^2}{\partial T^2}\langle \mathfrak{h}\,(T,V)\rangle^*$ is also worth to be studied. Its expression is given by:

$$
\begin{aligned}
\frac{\partial^2}{\partial T^2}\langle \mathfrak{h}\,(T,V)\rangle^* \;=\; & \frac{2\chi}{T} + \frac{\left(T^2V\right)^2}{L_{01}(0)-L_{01}(1)}\left[18L_{23}(0)+54L_{24}(0)-9L_{22}(1)+36L_{23}(1)\right. \\
& -54L_{24}(1)+\left(\tfrac{B}{T^4}-\tfrac{\pi^2}{10}\right)\left(12L_{13}(0)+36L_{14}(0)-6L_{12}(1)+24L_{13}(1)-36L_{14}(1)\right) \\
& \left.+\left(\tfrac{B}{T^4}-\tfrac{\pi^2}{10}\right)^2\left(2L_{03}(0)+6L_{04}(0)-L_{02}(1)+4L_{03}(1)-6L_{04}(1)\right)\right] \\
& + \frac{4BV}{T^3}\,\frac{L_{02}(0)+2L_{03}(0)+L_{02}(1)-2L_{03}(1)}{L_{01}(0)-L_{01}(1)} \\
& + \frac{\left(T^2V\right)^2}{\left(L_{01}(0)-L_{01}(1)\right)^2}\left[\left(-3L_{12}(0)-3L_{11}(1)+3L_{12}(1)+\left(\tfrac{B}{T^4}-\tfrac{\pi^2}{10}\right)\left(-L_{02}(0)-L_{01}(1)\right.\right.\right. \\
& \left.\left.+L_{02}(1)\right)\right)\left(3L_{12}(0)+6L_{13}(0)+3L_{12}(1)-6L_{13}(1)+\left(\tfrac{B}{T^4}-\tfrac{\pi^2}{10}\right)\left(L_{02}(0)+2L_{03}(0)\right.\right. \\
& \left.\left.+L_{02}(1)-2L_{03}(1)\right)\right)+\left(L_{01}(0)+L_{02}(0)-L_{02}(1)\right)\left(9L_{21}(1)-18L_{22}(1)+18L_{23}(1)\right. \\
& -18L_{23}(0)+\left(\tfrac{B}{T^4}-\tfrac{\pi^2}{10}\right)\left(6L_{11}(1)-12L_{12}(1)+12L_{13}(1)-12L_{13}(0)\right) \\
& \left.+\left(\tfrac{B}{T^4}-\tfrac{\pi^2}{10}\right)^2\left(L_{01}(1)-2L_{02}(1)+2L_{03}(1)-2L_{03}(0)\right)-\tfrac{4B}{T^{\,7}V}\left(L_{01}(1)-L_{02}(1)+L_{02}(0)\right)\right) \\
& +\left(3L_{11}(1)-3L_{12}(1)+3L_{12}(0)+\left(\tfrac{B}{T^4}-\tfrac{\pi^2}{10}\right)\left(L_{01}(1)-L_{02}(1)+L_{02}(0)\right)\right) \\
& \times\left(6L_{13}(1)-3L_{12}(1)-3L_{12}(0)-6L_{13}(0)+\left(\tfrac{B}{T^4}-\tfrac{\pi^2}{10}\right)\left(2L_{03}(1)-L_{02}(1)-L_{02}(0)\right.\right. \\
& \left.\left.-2L_{03}(0)\right)\right)]+\frac{2\left(T^2V\right)^2}{\left(L_{01}(0)-L_{01}(1)\right)^3}\left(L_{01}(0)+L_{02}(0)-L_{02}(1)\right) \\
& \times\left(3L_{12}(0)+3L_{11}(1)-3L_{12}(1)+\left(\tfrac{B}{T^4}-\tfrac{\pi^2}{10}\right)\left(L_{02}(0)+L_{01}(1)-L_{02}(1)\right)\right)^2, \qquad (3.66)
\end{aligned}
$$

and its variations with temperature for various system sizes are illustrated in Fig. (3.16). It can be seen that this quantity takes its extrema at two temperatures $T_1(V)$

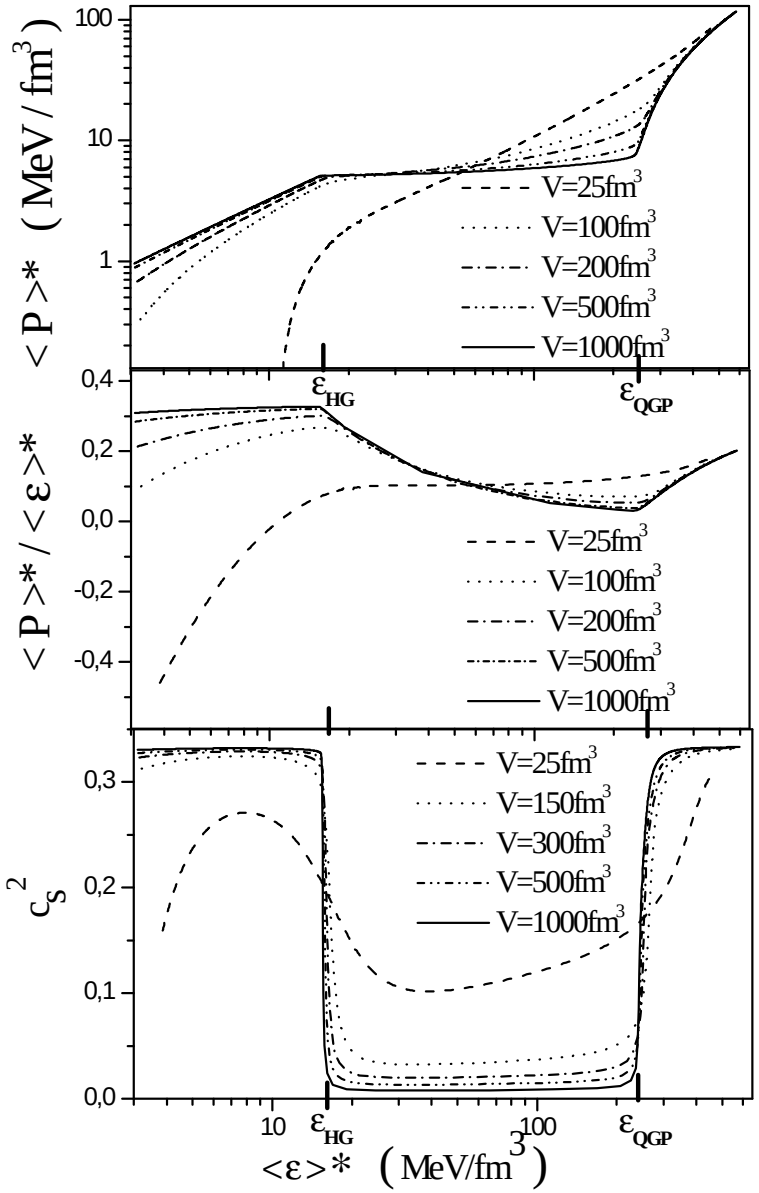

Figure 3.15: (Top) Pressure, (middle) Pressure over energy density and (bottom) Sound velocity vs energy density, for different volumes of the system.

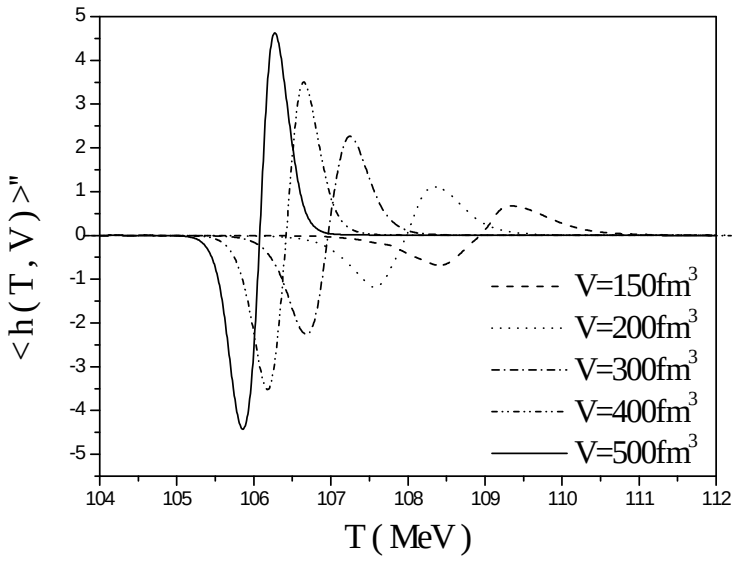

Figure 3.16: Plot of the second derivative of the order parameter, $\langle \mathfrak{h}\,(T,V)\rangle'' = \partial^2\langle \mathfrak{h}\,(T,V)\rangle/\partial T^2$, versus temperature for different system volumes.

and $T_2(V)$, so that the gap $T_2(V) - T_1(V)$, which represents the broadening of the transition region $\delta T(V)$, decreases with increasing volume.

Thus, from the illustration of all these response functions for the studied deconfinement phase transition, the three effects of finiteness of the volume evoked in section (2.3) have been recovered. A finite size scaling analysis will then be carried out in the next chapter to determine the corresponding scaling behavior and determine the relevant scaling critical exponents.

Chapter 4

Numerical Determination of the Scaling Critical Exponents for the Deconfinement Phase Transition

4.1 Introduction

In the precedent chapter, we have seen that finite-size effects have led to a rounding of the deconfinement phase transition over a range of temperature $\delta T(V)$, around a transition temperature $T_c(V)$. This effective transition temperature is shifted relative to the true one $T_c(\infty)$ in such a way that the shift $T_c(V) - T_c(\infty)$ increases for small volumes. This smearing makes the order of the transition difficult to infer. It turns out that the analysis of some known characteristic signatures as functions of varying volume allows one to go up to the order of the transition.

In finite systems, the shift of the effective transition temperature $T_c(V)$ relative to the true one $T_c(\infty)$, the width $\delta T(V)$ of the critical region over which the transition

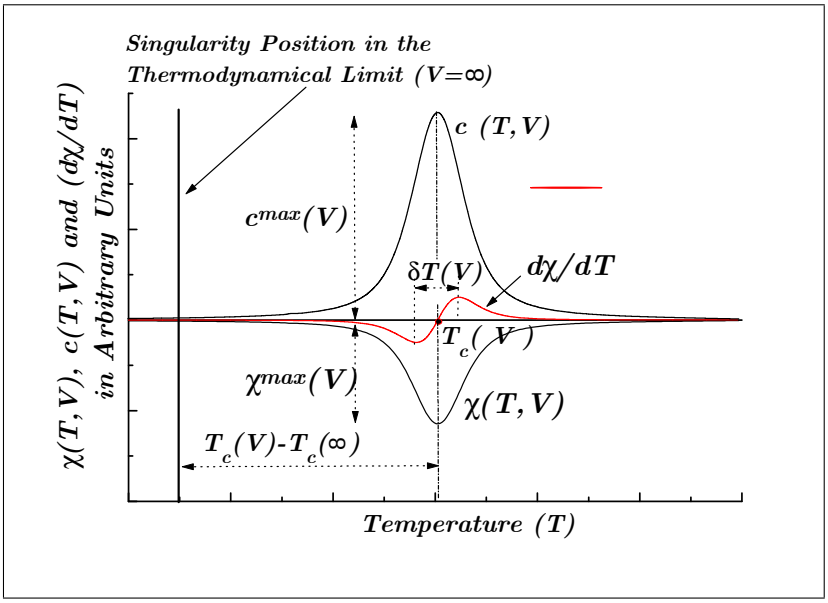

Figure 4.1: Illustration of the finite size behavior of the susceptibility $\chi(T,V)$, the specific heat density $c(T,V)$ and the second derivative of the order parameter $\partial\chi/\partial T$.

is smeared out and the maxima of the rounded peaks of the thermal susceptibility $\chi(T,V) = \dfrac{\partial\langle \mathfrak{h}(T,V)\rangle^*}{\partial T}$ and specific heat density $c(T,V) = \dfrac{\partial\langle \varepsilon(T,V)\rangle^*}{\partial T}$, which are illustrated on Fig. (4.1), are expected to behave like powers of the volume V, respectively, as:

$$\begin{cases} \tau_T(V) = T_c(V) - T_c(\infty) \sim V^{-\lambda_T} \\ \delta T(V) \sim V^{-\theta_T} \\ |\chi_T|^{\max}(V) \sim V^{\gamma_T} \\ c_T^{\max}(V) \sim V^{\alpha_T} \ , \end{cases} \tag{4.1}$$

where the scaling critical exponents λ_T, θ_T, γ_T and α_T characterize their dependence on the volume in a d-space, and are expected to be all equal to unity [2, 3, 66, 67], i.e., $\lambda_T = \theta_T = \gamma_T = \alpha_T = 1$.

These results have been recovered in our work [119] where an analytic determination

of the scaling critical exponents relevant to a thermally driven deconfinement phase transition has been carried out.

In the following, we shall determine numerically these scaling critical exponents. For this purpose, a FSS analysis of characteristic quantities for a system which undergoes a thermal deconfinement phase transition, from a pionic gas to a QGP consisting of two massless quarks at zero chemical potential, may be used.

4.2 Numerical Determination of the Critical Exponents for the Thermal Deconfinement Phase Transition with the Exact Color-Singlet Partition Function

In the following, we use a FSS analysis to recover the scaling exponents θ_T, λ_T, α_T and γ_T for the thermally driven deconfinement phase transition. For this purpose, we proceed by studying the thermal susceptibility and specific heat density. We examine the behavior of their maxima, their rounding as well as the shift of the effective transition temperature with varying volume. Let's note that the determination of the location of the maxima of the finite size peaks as well as their heights is done in a numerical way, and this yields a systematic error, which is estimated and given for the determined scaling exponents.

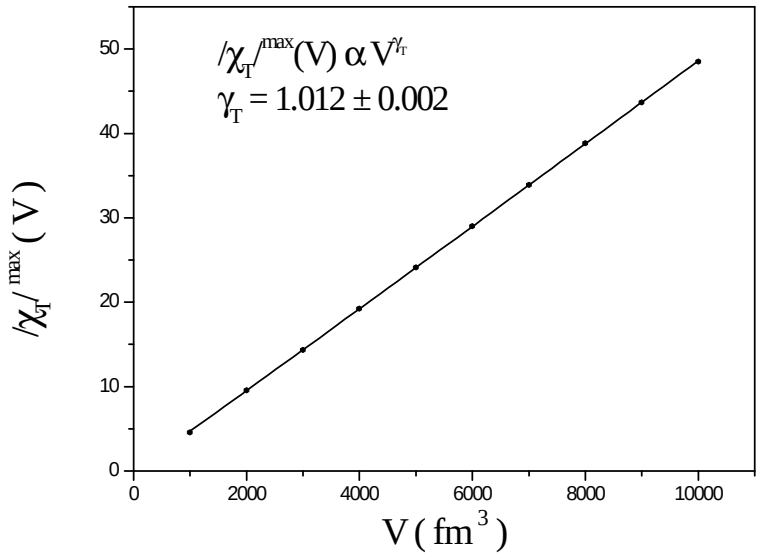

Figure 4.2: Linear fit of the results for the maxima of the susceptibility vs volume.

4.2.1 The susceptibility critical exponent

Fig. (4.2) illustrates the plot of the maxima of the thermal susceptibility peaks, $\mid \chi_T \mid^{\max}(V)$ versus volume. The linearity of the data with V can clearly be noted. A numerical parametrization with the power-law form: $\mid \chi_T \mid^{\max}(V) \sim V^{\gamma_T}$, gives the value of the susceptibility critical exponent: $\gamma_T = 1.012 \pm 0.002$.

4.2.2 The specific heat critical exponent

As in the precedent case, the data of the maxima of the specific heat $c_T^{\max}(V)$ are plotted in Fig. (4.3), and are fitted to the power-law form: $c_T^{\max}(V) \sim V^{\alpha_T}$. The obtained specific heat critical exponent is: $\alpha_T = 1.0075 \pm 0.0007$.

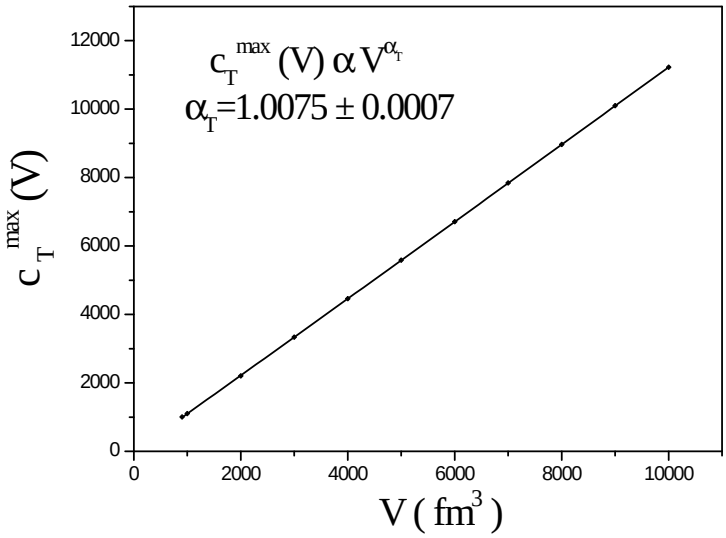

Figure 4.3: Variations of the maxima of the specific heat density with the volume.

4.2.3 The smearing critical exponent

The width of the transition region can be defined by the gap: $\delta T(V) = T_2(V) - T_1(V)$ with $T_1(V)$ and $T_2(V)$ the temperatures at which the second derivative of the order parameter reaches its extrema, or in other terms the temperatures at which the third derivative of the order parameter vanishes, i. e., $\frac{\partial^3}{\partial T^3}\langle \mathfrak{h}\,(T,V)\rangle^*\Big|_{T_1(V),T_2(V)} = 0$. To localize $T_1(V)$ and $T_2(V)$, we'll then search for the locations of the extrema of $\frac{\partial^2}{\partial T^2}\langle \mathfrak{h}\,(T,V)\rangle^*$, whose expression was given in (3.66).

The results for the widths $\delta T\,(V)$, plotted in Fig. (4.4) vs the inverse of the volume, were fitted to the power law form: $\delta T\,(V) \sim V^{-\theta_T}$, and the obtained smearing critical exponent is: $\theta_T = 1.03 \pm 0.02$.

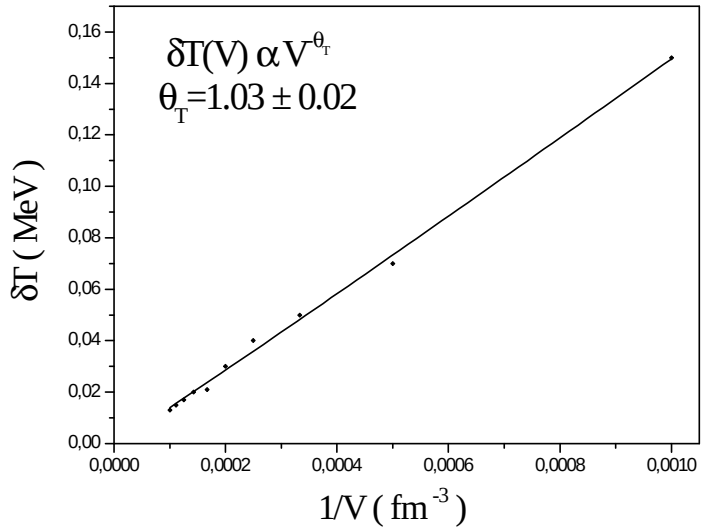

Figure 4.4: Data of the width of the temperature region over which the transition is smeared, fitted to a power-law of the inverse volume.

4.2.4 The shift critical exponent

For the study of the shift of the transition temperature $\tau_T(V) = T_c(V) - T_c(\infty)$, we need to locate the effective transition temperature in a finite volume $T_c(V)$. A way to define $T_c(V)$ is to locate the maxima of the rounded peaks of the susceptibility and the specific heat, shifted away from the true transition temperature $T_c(\infty)$.

Results of the shift of the transition temperature obtained in this way are plotted in Fig. (4.5) versus inverse volume. The shift critical exponent obtained from a fit to the form: $\tau_T(V) \sim V^{-\lambda}$, is : $\lambda = 0.876 \pm 0.041$. Such a value $\neq 1$ suggests the contribution of non-leading terms in the expression of the volume variation of the shift. Different forms of the fit of $\tau_T(V)$ including additional terms with higher powers of V^{-1}, such as $A_1 V^{-\lambda} + A_2 V^{-2}$, and $A_1 V^{-\lambda} + A_2 V^{-2} + A_3 V^{-3}$, have been tested, and the obtained results show that effectively, the shift critical exponent λ increases from the value 0.876

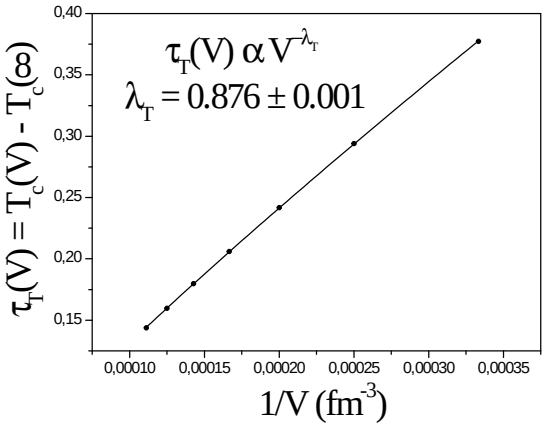

Figure 4.5: Plot of the shift of the transition temperature (from the maxima of $\chi(T,V)$ and $c(T,V)$) vs inversed volume.

and tends to 1, with a better $\boldsymbol{\chi}^2$. Other forms have been tested, where the value of the shift exponent has been fixed to 1, and finite-size correction terms have been included. In this case also, we note that we obtain a better $\boldsymbol{\chi}^2$ value with the presence of the non-leading terms.

The effective transition temperature can also be obtained from the minimum of the velocity of sound, as explained in subsection (3.5.3). Data of the locations of the minima of the sound velocity at different volumes $T_c^{(c_s^{2\ (\min)})}(V)$ are collected, and their shifts away from the true transition temperature $T_c(\infty)$ are plotted vs inversed volume in Fig. (4.6). A fit of this shift to the form: $\tau_T^{(c_s^{2\ (\min)})}(V) = T_c^{(c_s^{2\ (\min)})}(V) - T_c(\infty) \sim V^{-\lambda'_T}$, gives the shift critical exponent : $\lambda'_T = 0.841 \pm 0.004$. Such a value suggests, in turn, the contribution of non-leading terms to the expression of the shift as a function of the volume.

Other ways for defining the transition temperature are investigated and the details are given in the two next subsections.

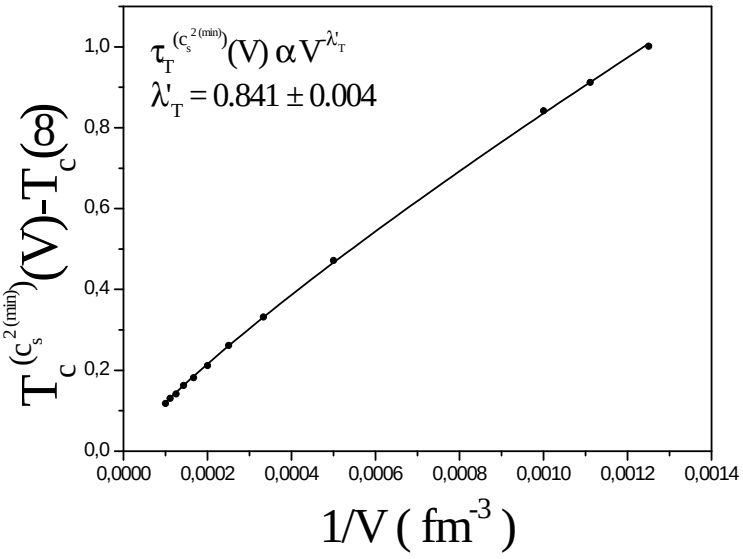

Figure 4.6: Plot of the shift of the transition temperature, from the minima of the sound velocity c_s^2, vs inversed volume.

4.2.5 Parametrization of the Order Parameter and the Susceptibility

Within the model used in this work, the order parameter in the limit of infinite volume being equal to 1 below the transition temperature and zero above it, it can then be expressed in a simple way using the Heaviside step-function Θ as:

$$\langle \mathfrak{h}\,(T, V \longrightarrow \infty)\rangle = 1 - \Theta\,(T - T_c\,(\infty))\,. \tag{4.2}$$

Such a parametrization has been used first in [120], for a similar case of a system of coexisting hadronic matter and QGP phases, then in other works as [121]. Using one of the known mathematical representations of the smoothed step function $\Theta\,(T - T_c)$,

the order parameter may then be expressed as:

$$\langle \mathfrak{h}\,(T,V)\rangle = \frac{1}{2}\left(1-\tanh\left(\frac{T-T_c\,(V)}{\Gamma_T\,(V)}\right)\right), \tag{4.3}$$

where $T_c\,(V)$ is the effective transition temperature and $\Gamma_T\,(V)$ the half-width of the rounded transition region, which leads to the susceptibility expression :

$$\chi\,(T,V) = \frac{-1}{2\Gamma_T\,(V)\ \ \cosh^2\left(\frac{T-T_c(V)}{\Gamma_T(V)}\right)}. \tag{4.4}$$

The parametrization choice (4.3) is the most accepted physically, and it can be understood phenomenologically in the context of the Double Gaussian Peaks model where the obtained expressions of the order parameter and the susceptibility are very similar to (4.3) and (4.4) [3, 70, 122].

An illustration of such parametrizations of the order parameter at the volume $V = 4000fm^3$, and the susceptibility at the volume $V = 900fm^3$ are presented in Figs. (4.7-left) and (4.7-right) respectively, and the parameters $T_c\,(V)$ and $\Gamma_T\,(V)$ obtained from each fit are given.

The results for the width of the transition region and the shift of the transition temperature from the parametrizations of the order parameter and the susceptibility are fitted to power law forms: ${\tau_T}^{fit(1)}(V) \sim V^{-\lambda_1}$, ${\tau_T}^{fit(2)}(V) \sim V^{-\lambda_2}$, $\delta T^{\,fit(1)}\,(V) \sim V^{-\theta_1}$ and $\delta T^{\,fit(2)}\,(V) \sim V^{-\theta_2}$ which give the scaling critical exponents: $\lambda_1 = 0.830 \pm 0.013$, $\lambda_2 = 0.857 \pm 0.006$, $\theta_1 = 0.990 \pm 0.015$ and $\theta_2 = 1.032 \pm 0.003$.

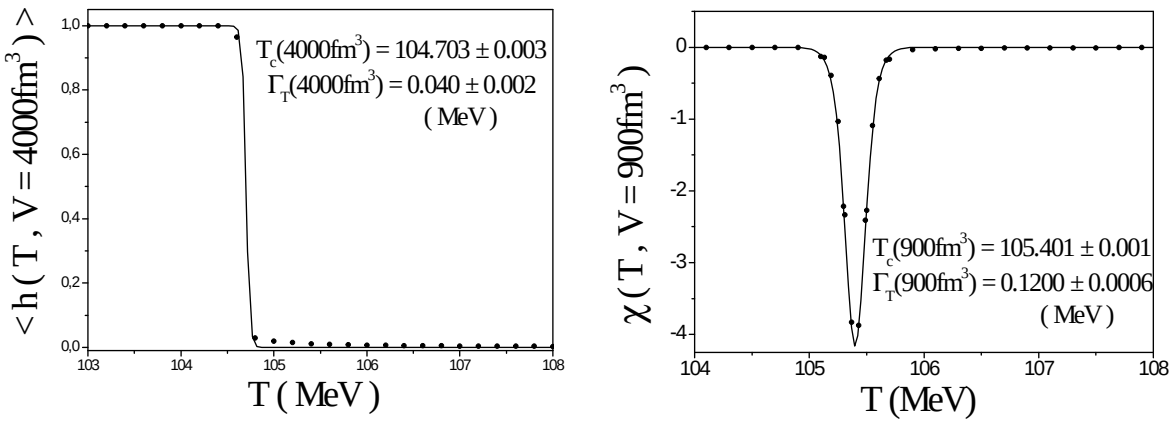

Figure 4.7: Parametrization of the order parameter to the form (4.3) at the volume $V = 4000 fm^3$, and of the susceptibility to the form (4.4) at the volume $V = 900 fm^3$.

4.2.6 Shift of the transition temperature and width of the transition region from cumulants

A way for locating $T_c\,(V)$ is to consider the fourth order cumulant:

$$B_4\,(T,V) = 1 - \frac{\langle \mathfrak{h}\,(T,V)\rangle^{*4}}{3\,\langle \mathfrak{h}^2\,(T,V)\rangle^{*2}}, \tag{4.5}$$

introduced by Binder [75, 3], and which is known to present a minimum at an effective transition temperature whose shift from the true transition temperature $T_c(\infty)$ is of order V^{-1} for a first order transition. This cumulant is a finite size scaling function [3, 66, 67, 68, 76], and is widely used to indicate the order of the transition in a finite volume.

The expression of $B_4\,(T,V)$ as function of the integral terms, for this case of the

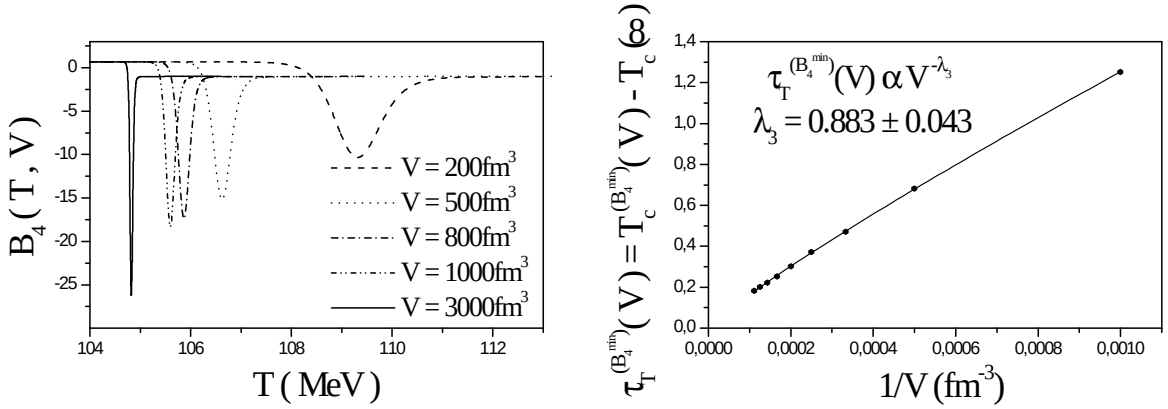

Figure 4.8: (Left) Binder Cumulant B_4 vs temperature at different system volumes. (Right) Shift of the transition temperature obtained from the minimum of the Binder cumulant vs inversed volume.

deconfinement transition, is after calculation:

$$B_4(T,V) = 1 - \frac{(L_{01}(1) - L_{01}(0))}{3\ (2L_{03}(1) - 2L_{03}(0) - 2L_{02}(0) - L_{01}(0))^2} \times (24\,(L_{05}(1) - L_{05}(0) - L_{04}(0)) - 12L_{03}(0) - 4L_{02}(0) - L_{01}(0)) \quad (4.6)$$

Fig. (4.8-left) illustrates the variations of the Binder cumulant with temperature for various volumes, and shows that the locations of the minima in finite sizes $T_{\min}(V)$ are shifted to higher values from $T_c(\infty)$. Data of the shift of the transition temperature obtained in this way are plotted in Fig. (4.8-right) versus inversed volume, and the scaling shift critical exponent obtained from a fit to the form: $\tau_T^{(B_4^{\min})}(V) = T_c^{(B_4^{\min})}(V) - T_c(\infty) \sim V^{-\lambda_3}$, is: $\lambda_3 = 0.883 \pm 0.043$. In this case also, non-leading terms appear in the expression of $\tau_T^{(B_4^{\min})}(V)$.

We can also calculate the Binder cumulant defined from the 4^{th} normalized central moment as:

$$B_4'(T,V) = 1 - \frac{\langle(\mathfrak{h} - \langle\mathfrak{h}\rangle^*)^4\rangle^*}{3\ \langle(\mathfrak{h} - \langle\mathfrak{h}\rangle^*)^2\rangle^{*2}}, \quad (4.7)$$

which is directly related to the kurtosis $K(T,V)$, which will be defined in the following, by:

$$B_4'(T,V) = \frac{-K(T,V)}{3} \ . \tag{4.8}$$

The locations of the extrema of both $B_4'(T,V)$ and $K(T,V)$ are then the same.

In the same context, we have thought to examine the second and third cumulants for the case of the probability distribution $p(\mathfrak{h})$ used in the present work. For this purpose, let's first begin with some definitions.

Definitions of the Moments

The n^{th} moment of a function $f(x)$ of a variable x about a value x_0 is mathematically defined by:

$$\mathcal{M}_n = \int_0^1 (x - x_0)^n f(x) dx \ \ . \tag{4.9}$$

The moments about zero are usually referred to simply as the *moments* of a function. Usually, the function will be a probability density function. The n^{th} moment (about zero) of a probability density function $f(x)$ is the *expected value* of x^n. The moments about its mean $\mathcal{M}$ are called *central moments*; these describe the shape of the function, independently of translation.

Significance of the Moments

The first moment about zero, if it exists, is the *expectation* of x, i.e., the *mean* of the probability distribution of x, designated $\mathcal{M}$. In higher orders, the central moments are more interesting than the moments about zero.

The n^{th} central moment of the probability distribution of a random variable x is

then given by:

$$\mathcal{M}_n = \langle (x - \mathcal{M})^n \rangle = \langle (x - \langle x \rangle)^n \rangle. \tag{4.10}$$

The first central moment is thus 0; the second central moment is the *variance* σ^2, the square root of which is the *standard deviation* σ defined as:

$$\sigma = \left(\langle (x - \langle x \rangle)^2 \rangle \right)^{1/2}. \tag{4.11}$$

The normalized n^{th} central moment is the n^{th} central moment divided by σ^n. These normalized central moments are dimensionless quantities, which represent the distribution independently of any linear change of scale.

The third central moment is a measure of symmetry, or more precisely, the lack of symmetry. A distribution, or data set, is symmetric if it looks the same to the left and right of the center point. The 3^{rd} central moment for a normal distribution is zero, and any symmetric distribution will have a third central moment, if defined, near zero. The normalized 3^{rd} central moment is called the *skewness* Σ :

$$\Sigma = \frac{\langle (x - \langle x \rangle)^3 \rangle}{\sigma^3}. \tag{4.12}$$

A distribution that is skewed to the left (the tail of the distribution is heavier on the left) will have a negative skewness. A distribution that is skewed to the right (the tail of the distribution is heavier on the right) will have a positive skewness.

The fourth central moment is a measure of whether the distribution is peaked or flat relative to a normal distribution. Since it is the expectation of a fourth power, the fourth central moment, where defined, is always positive. The fourth central moment of a normal distribution is $3\sigma^4$.

The *Kurtosis* is defined to be the normalized 4^{th} central moment minus 3:

$$K = \frac{\langle (x - \langle x \rangle)^4 \rangle}{\sigma^4} - 3, \tag{4.13}$$

so that the standard normal distribution has a kurtosis of zero. Positive kurtosis indicates a "peaked" distribution and negative kurtosis indicates a "flat" distribution. That is, distributions or data sets with high kurtosis tend to have a distinct peak near the mean, decline rather rapidly, and have heavy tails. Data sets with low kurtosis tend to have a flat top near the mean rather than a sharp peak

Cumulants

The first moment and the second and third unnormalized central moments are linear in the sense that if x and y are independent random variables, then:

$$\mathcal{M}_1(x+y) = \mathcal{M}_1(x) + \mathcal{M}_1(y) \ , \tag{4.14}$$

and:

$$\mathcal{M}_2(x+y) = \mathcal{M}_2(x) + \mathcal{M}_2(y) \ , \tag{4.15}$$

and:

$$\mathcal{M}_3(x+y) = \mathcal{M}_3(x) + \mathcal{M}_3(y) \ . \tag{4.16}$$

This is true because these moments are the first three cumulants; the fourth cumulant is the kurtosis times σ^4.

The four first cumulants for the probability density $p(\mathfrak{h})$

For this case of probability distribution $p(\mathfrak{h})$, the first cumulant is the order parameter $\langle\mathfrak{h}\rangle^*$, the second is the variance given by:

$$\sigma^2\left(T,V\right) = \langle(\mathfrak{h} - \langle\mathfrak{h}\rangle^*)^2\rangle^* = \langle\mathfrak{h}^2\rangle^* - \langle\mathfrak{h}\rangle^{*2}, \tag{4.17}$$

which is expressed by mean of the L_{mn}'s as:

$$\begin{aligned}\sigma^2(T,V) &= \frac{1}{\left(L_{01}(1)-L_{01}(0)\right)^2}\left[\left(2L_{03}(1)-2L_{03}(0)-2L_{02}(0)-L_{01}(0)\right)\right.\\ &\left.\times\left(L_{01}(1)-L_{01}(0)\right)-\left(L_{01}(0)+L_{02}(0)-L_{02}(1)\right)^2\right]. \qquad (4.18)\end{aligned}$$

The third cumulant is the skewness times σ^3, with the skewness given by:

$$\Sigma(T,V)=\frac{\langle(\mathfrak{h}-\langle\mathfrak{h}\rangle^*)^3\rangle^*}{\sigma^3}=\frac{\langle\mathfrak{h}^3\rangle^*-3\langle\mathfrak{h}\rangle^*\langle\mathfrak{h}^2\rangle^*+2\langle\mathfrak{h}\rangle^{*3}}{\left(\langle\mathfrak{h}^2\rangle^*-\langle\mathfrak{h}\rangle^{*2}\right)^{3/2}}, \qquad (4.19)$$

which can be written as function of the L_{mn}'s as:

$$\begin{aligned}\Sigma(T,V) &= \left[\left(L_{01}(1)-L_{01}(0)\right)^2\left(6L_{04}(1)-6L_{04}(0)-6L_{03}(0)-3L_{02}(0)-L_{01}(0)\right)\right.\\ &+3\left(L_{01}(1)-L_{01}(0)\right)\left(L_{01}(0)+L_{02}(0)-L_{02}(1)\right)\left(2L_{03}(1)-2L_{03}(0)-2L_{02}(0)-L_{01}(0)\right)\\ &\left.-2\left(L_{01}(0)+L_{02}(0)-L_{02}(1)\right)^3\right]/\left[\left(2L_{03}(1)-2L_{03}(0)-2L_{02}(0)-L_{01}(0)\right)\right.\\ &\left.\times\left(L_{01}(1)-L_{01}(0)\right)-\left(L_{01}(0)+L_{02}(0)-L_{02}(1)\right)^2\right]^{3/2}. \qquad (4.20)\end{aligned}$$

The fourth cumulant is the kurtosis times σ^4, where the kurtosis is given by:

$$K(T,V)=\frac{\langle(\mathfrak{h}-\langle\mathfrak{h}\rangle^*)^4\rangle^*}{\sigma^4}-3=\frac{\langle\mathfrak{h}^4\rangle^*-4\langle\mathfrak{h}\rangle^*\langle\mathfrak{h}^3\rangle^*+6\langle\mathfrak{h}\rangle^{*2}\langle\mathfrak{h}^2\rangle^*-3\langle\mathfrak{h}\rangle^{*4}}{\left(\langle\mathfrak{h}^2\rangle^*-\langle\mathfrak{h}\rangle^{*2}\right)^2}-3, \qquad (4.21)$$

whose expression with the L_{mn}'s is:

$$\begin{aligned}K(T,V) &= \left\{\left[\left(L_{01}(1)-L_{01}(0)\right)^3\left(24L_{05}(1)-24L_{05}(0)-24L_{04}(0)-12L_{03}(0)\right)\right.\right.\\ &-4L_{02}(0)-L_{01}(0))+4\left(L_{01}(1)-L_{01}(0)\right)^2\left(L_{01}(0)+L_{02}(0)-L_{02}(1)\right)\\ &\times\left(6L_{04}(1)-6L_{04}(0)-6L_{03}(0)-3L_{02}(0)-L_{01}(0)\right)-3\left(L_{01}(0)+L_{02}(0)-L_{02}(1)\right)^4\Big]\\ &/\left[\left(2L_{03}(1)-2L_{03}(0)-2L_{02}(0)-L_{01}(0)\right)\left(L_{01}(1)-L_{01}(0)\right)\right.\\ &\left.\left.-\left(L_{01}(0)+L_{02}(0)-L_{02}(1)\right)^2\right]^2\right\}-3\,. \qquad (4.22)\end{aligned}$$

with:

$$\langle \mathfrak{h}^2 \rangle^* = \frac{2L_{03}(1) - 2L_{03}(0) - 2L_{02}(0) - L_{01}(0)}{L_{01}(1) - L_{01}(0)}, \tag{4.23}$$

$$\langle \mathfrak{h}^3 \rangle^* = \frac{6L_{04}(1) - 6L_{04}(0) - 6L_{03}(0) - 3L_{02}(0) - L_{01}(0)}{L_{01}(1) - L_{01}(0)}, \tag{4.24}$$

$$\langle \mathfrak{h}^4 \rangle^* = \frac{24L_{05}(1) - 24L_{05}(0) - 24L_{04}(0) - 12L_{03}(0) - 4L_{02}(0) - L_{01}(0)}{L_{01}(1) - L_{01}(0)}. \tag{4.25}$$

As it can clearly be observed on Fig. (4.9), the plots of the variance versus temperature for different system volumes look like bell functions, with the peaks broadened, smaller is the volume. These peaks are located at temperatures $T^{(\sigma^{2^{\max}})}(V)$, seemingly tending to $T_c(\infty)$ with increasing volume.

Similarly, Fig. (4.10) illustrates the variations of skewness with temperature at different sizes. The curves of skewness show that this latter vanishes at a temperature $T_c^{(\Sigma=0)}$, being negative for $T < T_c^{(\Sigma=0)}$ and positive for $T > T_c^{(\Sigma=0)}$, and the probability distribution seems then to be skewed to the left for $T < T_c^{(\Sigma=0)}$, and skewed to the right for $T > T_c^{(\Sigma=0)}$. The temperature at which skewness vanishes is expected to represent the transition temperature, and tends apparently to $T_c(\infty)$ with increasing volume, while the temperature gap between the two maxima is expected to give the width of the transition region.

Finally, the plots of kurtosis versus temperature are represented on Fig. (4.11), as usual at different sizes, but because of the high values taken by the kurtosis at large volumes, information on a part of the temperature range is lost. To see the detailed kurtosis, an individual plot at the volume $V = 300fm^3$ is illustrated on Fig. (4.12), which shows that kurtosis is positively peaked around a temperature $T_c^{(K^{\max_1})}(V)$ attaining high values, vanishes then takes negative values on a narrow interval of temperatures with a minimum at a temperature $T_c^{(K^{\min})}(V)$ and vanishes again, then takes positive

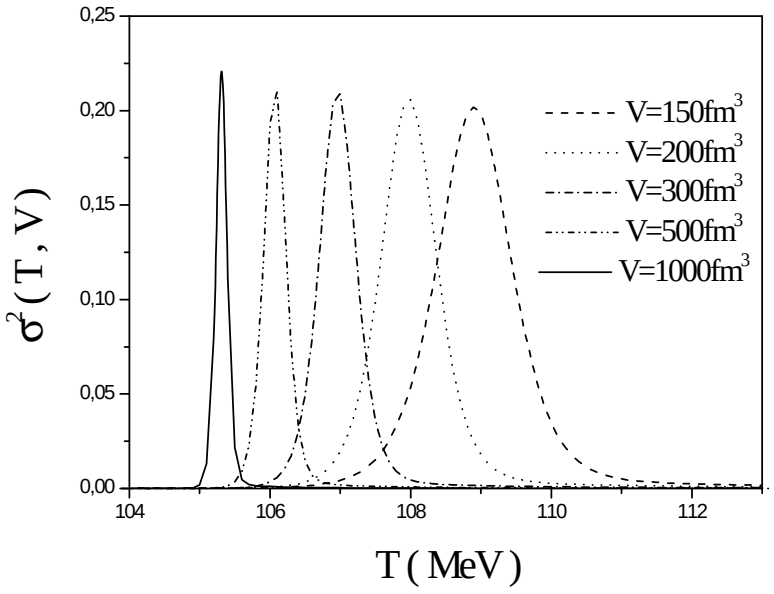

Figure 4.9: Variance vs Temperature at different system volumes.

but low values with a peak around a temperature $T_c^{(K^{\max_2})}(V)$. In this case, we expect the transition temperature to occur at the minimum of kurtosis.

To verify the validity of the assumptions that the transition temperatures can be defined at the maximum of the variance, at vanishing skewness and at the minimum of kurtosis, we plot the variations of the shifts of the such obtained transition temperatures, relative to $T_c(\infty)$, with inversed volume and fit to a power law, like in eq. (4.1). The numerical values of the shift critical exponents obtained in this way are:

$$\begin{aligned}
\tau_T^{(Var)}(V) &= T^{(\sigma^{2^{\max}})}(V) - T_c(\infty) \sim V^{-\lambda_4}, \quad \lambda_4 = 0.861 \pm 0.002, \\
\tau_T^{(Skew)}(V) &= T^{(\Sigma=0)}(V) - T_c(\infty) \sim V^{-\lambda_5}, \quad \lambda_5 = 0.862 \pm 0.002, \\
\tau_T^{(Kurt)}(V) &= T^{(K^{\min})}(V) - T_c(\infty) \sim V^{-\lambda_6}, \quad \lambda_6 = 0.861 \pm 0.002,
\end{aligned} \tag{4.26}$$

and are very close to the values of the shift critical exponent previously obtained

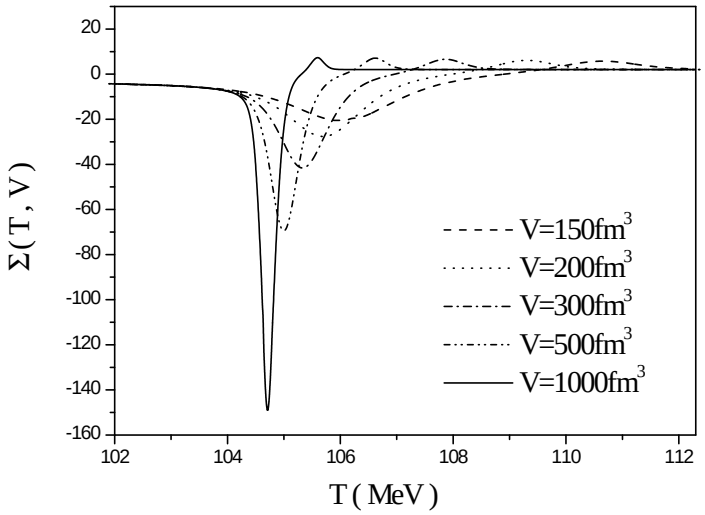

Figure 4.10: Skewness vs Temperature at different system volumes.

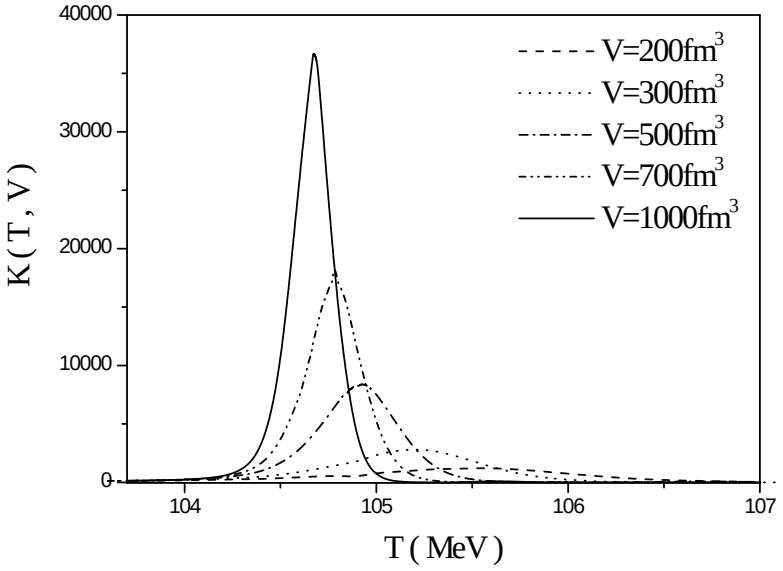

Figure 4.11: Kurtosis vs Temperature at different system volumes.

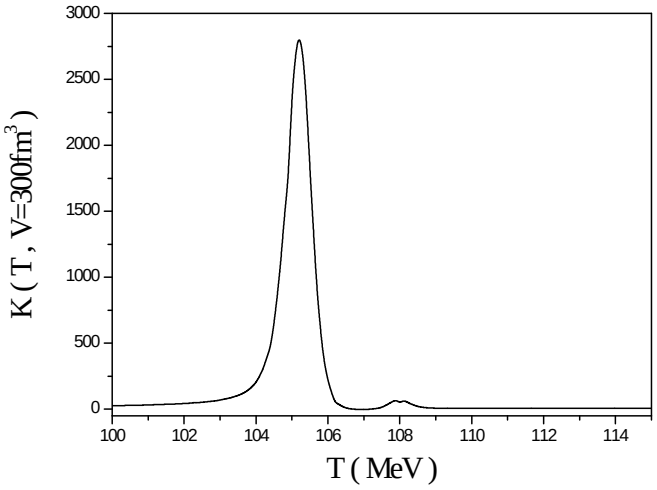

Figure 4.12: Kurtosis vs Temperature at the volume $V = 300fm^3$.

(subsections 4.2.4 to 4.2.6), and which are $\neq 1$ suggesting the contribution of non-leading terms in the expression of the volume variation of the shift, as yet mentioned.

For the width of the transition region, data are obtained from skewness as the gap in temperature between the two extrema, and are fitted to power laws of the inversed volume. The smearing critical exponent obtained in this case is:

$$\delta T^{(Skew)}(V) \sim V^{-\theta'_T}; \quad \theta'_T = 0.903 \pm 0.011 \ . \tag{4.27}$$

For more accuracy, we'll search in the next section for the correlation between the such obtained shifts and the shift of the transition temperature obtained from the value 0.5 of the order parameter, or equivalently from the peaks of the susceptibility. A linear relation between the two, with a slope equal to 1 will indicate whether the transition temperature is effectively that determined from each cumulant.

Cumulant	Value of a	Value of b
Variance maximum $c^{(\sigma^2_{\max})}$	0.0019 ± 0.0098	0.971 ± 0.024
Vanishing skewness ($\Sigma = 0$)	0.000593 ± 0.000078	0.9941 ± 0.0002
First kurtosis maximum	0.00152 ± 0.00344	0.3331 ± 0.0008
Kurtosis minimum	0.00105 ± 0.00027	0.99150 ± 0.00067
Second kurtosis maximum	-0.00569 ± 0.00105	1.30045 ± 0.00259
Binder cumulant minimum	-0.0117 ± 0.0018	1.0008 ± 0.0002

Table 4.1: Numerical values of the fit parameters a and b, with the formula (4.28).

4.3 Correlation between the cumulants and the susceptibility

In the following, we shall examine the correlation between the temperatures at the locations of the different cumulant peaks and the transition temperatures obtained from the maxima of the peaks of the thermal susceptibility $\mid \chi_T \mid^{\max}$. For this, we plot the shift $T_c^{(Cum)}(V) - T_c(\infty)$ with $T_c^{(Cum)}(V)$ obtained from the peaks of each of the dispersion σ^2 and the kurtosis K, versus $T_c^{(|\chi_T|^{\max})}(V) - T_c(\infty)$. For the skewness Σ, $T_c^{(Cum)}(V)$ is obtained at the vanishing value $\Sigma(V) = 0$.

The different plots are illustrated on Figs. (4-13) to (4.17), and the linearity of the variations can clearly be observed. Fits with the linear forms:

$$T_c^{(Cum)}(V) - T_c(\infty) = a + b(T_c^{(|\chi_T|^{\max})}(V) - T_c(\infty)) \ , \tag{4.28}$$

give the values of the fit parameters a and b presented in Table 4.1.

Results of these fits show exact linear variations of the shifts of the transition temperatures from cumulants with the shifts of the transition temperatures from the susceptibility maxima, except for the kurtosis maxima, indicating that the most appropriate way for defining the transition temperature from kurtosis is at the location of its minimum, while its definition from the maximum of the variance and the vanishing

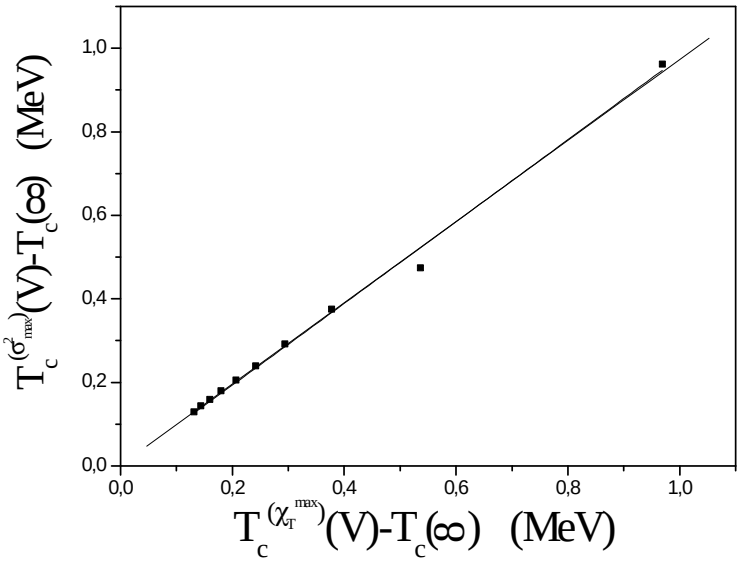

Figure 4.13: Linear fit of the data of the shift of the transition temperature defined as the location of the variance maximum vs the shift of the transition temperature obtained from $\mid \chi_T \mid^{\max}$.

skewness are well justified and can be adopted.

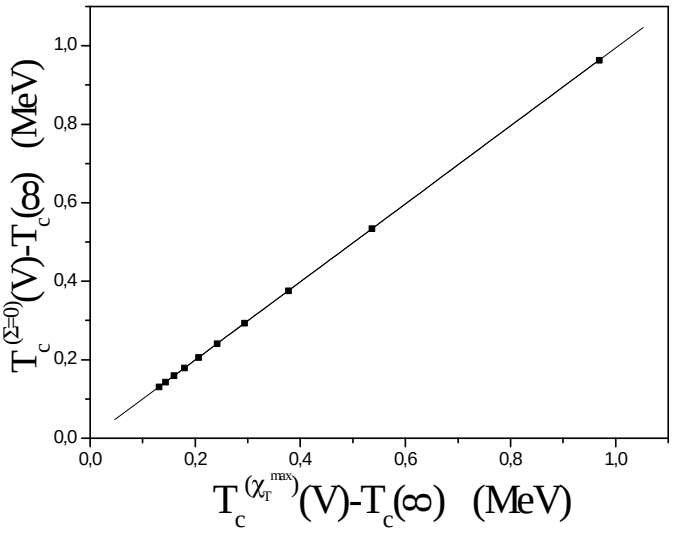

Figure 4.14: Linear fit of the data of the shift of the transition temperature defined at a vanishing skewness vs the shift of the transition temperature obtained from $\mid \chi_T \mid^{\max}$.

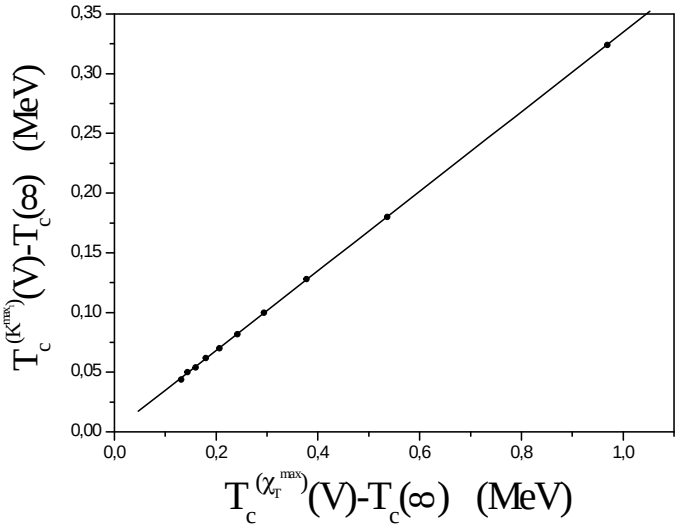

Figure 4.15: Linear fit of the data of the shift of the transition temperature defined at the first maximum of kurtosis vs the shift of the transition temperature obtained from $\mid \chi_T \mid^{\max}$.

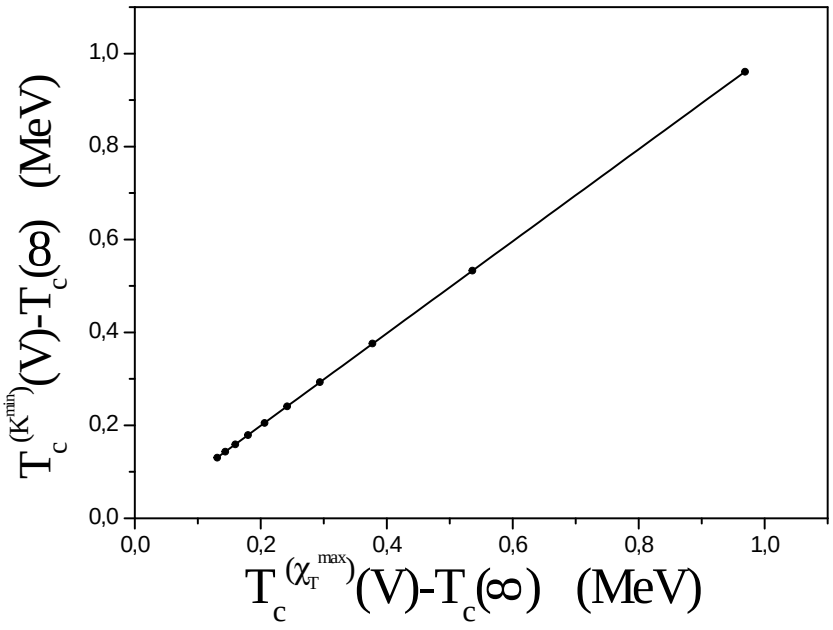

Figure 4.16: Linear fit of the data of the shift of the transition temperature defined at the minimum of kurtosis vs the shift of the transition temperature obtained from $\mid \chi_T \mid^{\max}$.

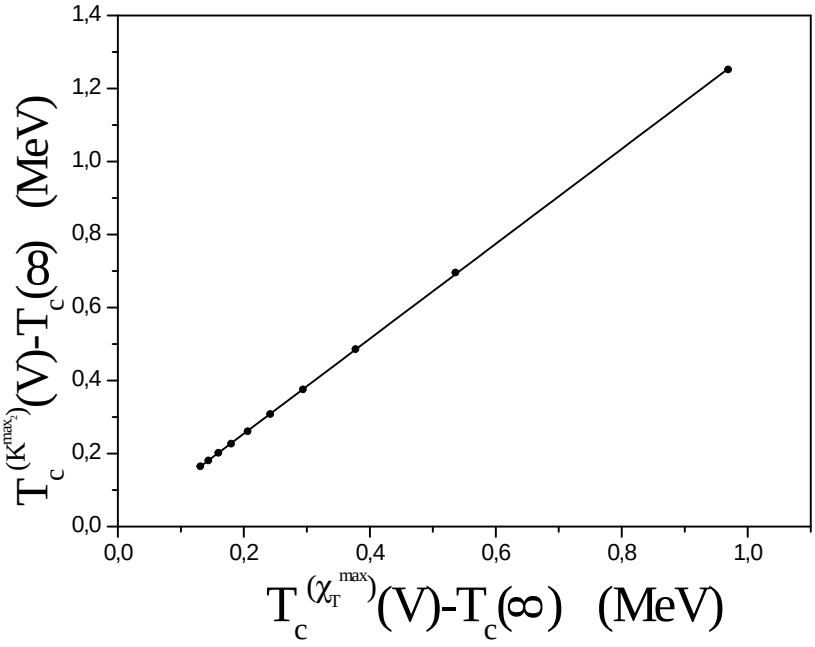

Figure 4.17: Linear fit of the data of the shift of the transition temperature defined at the second maximum of kurtosis vs the shift of the transition temperature obtained from $\mid \chi_T \mid^{\max}$.

Chapter 5

Finite-Size Effects and Scaling of the Deconfinement Phase Transition within the Excluded Volume Effects

5.1 Introduction

So far in this work, hadrons have been considered as point particles, and the considered finite size effects were those due to the finiteness of the system undergoing a phase transition, additionally to those induced by the color-singletness requirement. But, since hadrons are composed of quarks, they are extended particles and have finite volumes.

In the present chapter, such excluded volume effects are considered within the

phase coexistence model, using the color-singlet partition function for the QGP. Their effects on the studied deconfinement phase transition are then examined by probing the behavior of some physical quantities, as in the two previous chapters. It has been shown in [123] that "*dense nuclear matter can go through a second order phase transition into a QGP when the finite extensions of hadronic constituents are taken into account*".

5.2 The role of the finite volume of particles and their interactions: Hagedorn correction

The Hagedorn model described in section (1.8) represents a nonperturbative, analytically soluble model of a strongly interacting many-particle system. It predicts either the existence of a limiting temperature or a phase transition at high energy density. If the latter is true, the new phase cannot be treated in the framework of this model. Much progress has also been achieved in the mathematical understanding of the bootstrap constraint, mostly due to its reformulation in a relativistically covariant way. An excellent review of these results can be found in [124]. There were, however, two important questions to be answered. First, why can the fireball be treated as an ideal gas of hadron resonances? Second, how to take into account the finite proper volumes of the hadrons in the fireball? As to the first question, it has been argued that the rest masses of the observed hadron resonances arise as a result of strong interaction and with the inclusion of the total mass spectrum, the interaction (more precisely, its attractive part) is entirely taken into account [125]. According to this point of view, the observed hadron resonances are considered as quasiparticles among which only some residual interaction can be imagined, and which is neglected.

The second problem has been addressed by differentiating between the volume V_{ext} of the gas and the volume V available for the particles [126, 127];

$$V = V_{ext} - \sum_{i=1}^{N_p} V_i \tag{5.1}$$

where V_i are the proper volumes of the resonances. From the consistent, relativistically covariant treatment, it follows that the proper volume of the resonances must be proportional to their mass, $V_i = \frac{m_i}{4B}$. This is precisely the relation derived in the MIT bag model. Therefore, the constant B can be identified with the bag constant. The particles occupy an available volume,

$$V = V_{ext} - \frac{E}{4B} \tag{5.2}$$

depending on their energy. Thus, V is the volume in which the particles move as if they were pointlike, while in reality they have finite proper volumes and move in V_{ext}.

Treating the hadrons as extended particles leads to important consequences in the thermodynamical behavior of the gas. If the gas of hadron resonances is a real gas with some repulsion among the particles represented by the impenetrability of their proper volumes, then there is no limiting temperature, but the gas undergoes a phase transition and the energy density becomes too large. We can explain what happens as follows: The thermodynamical problem can be solved at first for a gas of fictitious point particles enclosed in the available volume V and one gets the corresponding equations of state. Then one can express the energy density of the real gas through the energy density of the gas of fictitious particles by means of the formula:

$$\frac{E}{V_{ext}} = \frac{(E/V)}{1 + \frac{(E/V)}{4B}} \ . \tag{5.3}$$

Even if the energy density (E/V) of the gas of fictitious point particles diverges in the limit $T \to T_c$, the energy density of the real gas remains constant and tends to the energy density of the hadronic bag, $(E/V_{ext}) \to 4B$.

In order to take into account the repulsive interactions between hadrons, all thermodynamical quantities in the hadronic phase may be corrected by the Hagedorn factor [126, 99]:

$$\eta_{Hag} = \frac{1}{1 + \frac{\varepsilon_{HG}}{4B}}, \tag{5.4}$$

where $\varepsilon_{HG}(T, V)$ is the energy density of the hadronic matter. The corrected thermodynamical quantities of the hadronic gas phase are then written as:

$$A_{HG\ cor}(T, V) = \eta_{Hag}\, A_{HG}(T, V). \tag{5.5}$$

5.3 Finite Size Rounding of the Deconfinement Phase Transition within the Excluded Volume Effects

Taking the excluded volume effects into account, the phase transition between the hadronic and QGP phases then occurs when:

$$P_{HG\ cor}\ (\mu_c, T_c) = P_{QGP}\ (\mu_c, T_c)\,, \tag{5.6}$$

with:

$$P_{QGP} = \frac{37\pi^2}{90} T^4 + \mu^2 T^2 + \frac{1}{2\pi^2}\mu^4 - B, \tag{5.7}$$

and:

$$P_{HG\ cor} = \eta_{Hag} \frac{\pi^2}{30} T^4. \tag{5.8}$$

Thus, the relation between T_c and μ_c is:

$$\frac{127}{12}T_c^4+\frac{37\pi^2}{120}\frac{T_c^8}{B}+\frac{30}{\pi^2}\mu_c^2T_c^2+\frac{3}{4}\frac{\mu_c^2T_c^6}{B}+\frac{15}{\pi^4}\mu_c^4+\frac{3}{8\pi^2}\frac{\mu_c^4T_c^4}{B}-\frac{30}{\pi^2}B=0. \tag{5.9}$$

The phase diagram in the $\mu-T$ plane, separating between hadronic and QGP phases, and giving at each point the transition parameters (μ_c, T_c) for two flavors $(N_f=2)$, with the common value of the bag constant $B^{1/4}=145MeV$, can also be illustrated in this case when the volume of the hadrons is considered. The extreme values of the transition parameters at $\mu=0$ and $T=0$ are: $T_c'(\mu=0;V=\infty)=104.21MeV$; $\mu_c'(T=0;V=\infty)=305.63MeV$.

We'll study in the following the FSE for a temperature driven deconfinement phase transition, at a vanishing chemical potential $(\mu=0)$, and for a density driven deconfinement phase transition at a fixed temperature $(T=100MeV)$, taking into account these excluded volume effects. For this purpose, we'll examine, like in chapter 3, the behavior of the order parameter, the entropy and energy densities with temperature and chemical potential for varying volume, when the volume of the hadrons is considered.

The corrected mean values of the energy and entropy densities are then related to the corrected order parameter by:

$$\begin{aligned}\langle s\left(T,\mu,V\right)\rangle_{cor} &= \mathfrak{s}_{QGP}+\left(\mathfrak{s}_{HG\ cor}-\mathfrak{s}_{QGP}\right)\ \langle\mathfrak{h}\left(T,\mu,V\right)\rangle_{cor}\\ \langle\varepsilon\left(T,\mu,V\right)\rangle_{cor} &= \mathfrak{e}_{QGP}+\left(\mathfrak{e}_{HG\ cor}-\mathfrak{e}_{QGP}\right)\ \langle\mathfrak{h}\left(T,\mu,V\right)\rangle_{cor},\end{aligned} \tag{5.10}$$

where:

$$\langle\mathfrak{h}\left(T,\mu,V\right)\rangle_{cor}=\frac{\left(-\frac{1}{T}(f_{HG\ cor}-f_{QGP})V-1\right)e^{-\frac{1}{T}(f_{HG\ cor}-f_{QGP})V}+1}{-\frac{1}{T}(f_{HG\ cor}-f_{QGP})V\left(e^{-\frac{1}{T}(f_{HG\ cor}-f_{QGP})V}-1\right)}. \tag{5.11}$$

In Fig. (5.1), we compare the order parameters without and with the Hagedorn correction, for two volumes, $V=150fm^3$ and $V=1000fm^3$, and for more clearness let's rather illustrate the variations of the relative difference between the order

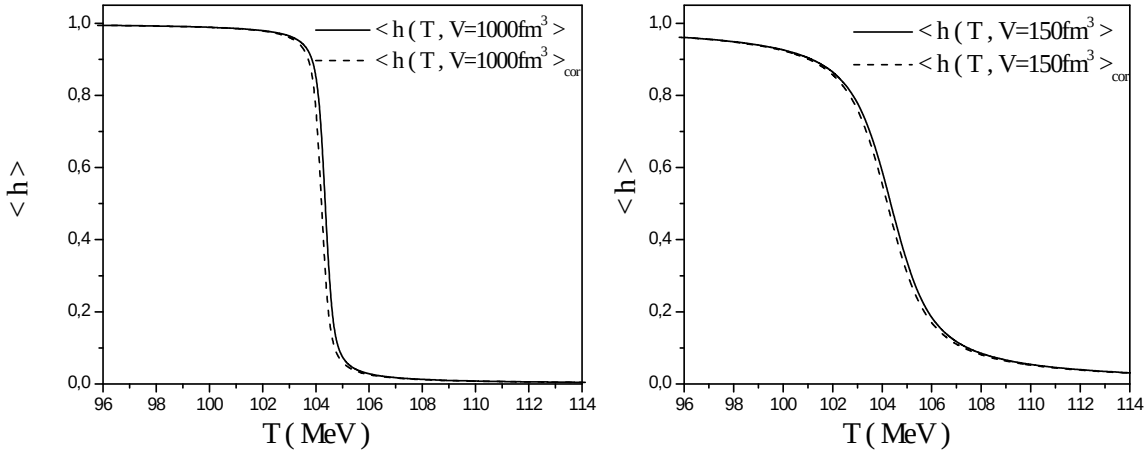

Figure 5.1: Order parameter versus temperature without (solid line) and with (dashed line) the Hagedorn correction, for the volumes, (left) $V = 1000fm^3$ and (right) $V = 150fm^3$.

parameters with and without the hagedorn correction $\frac{\langle h\rangle - \langle h\rangle_{cor}}{\langle h\rangle_{cor}}$, with temperature at different volumes in Fig. (5.2). We can notice that the difference is mostly notable in a temperature region around a temperature at which it is maximal, and which tends to $T_c(\infty)$ with increasing volume. This relative difference is more and more appreciable for big volumes, meaning that the transition region is the more sensitive to the extended volume correction

The three-dimensional plots of the corrected order parameter, entropy density scaled by T^3, $\frac{\langle s(T,V)\rangle_{cor}}{T^3}$, and energy density scaled by T^4, $\frac{\langle \varepsilon(T,V)\rangle_{cor}}{T^4}$ are illustrated, respectively, in the top, middle and bottom of Fig. (5.3). Like for the non-corrected quantities in Figs. (3.2), these plots exhibit a discontinuity at a critical temperature $T_c'(\infty) \simeq 104.21MeV$ for big volumes ($V \geq 1000fm^3$), indicating a first-order phase transition, while rounded curves are obtained when the volume decreases.

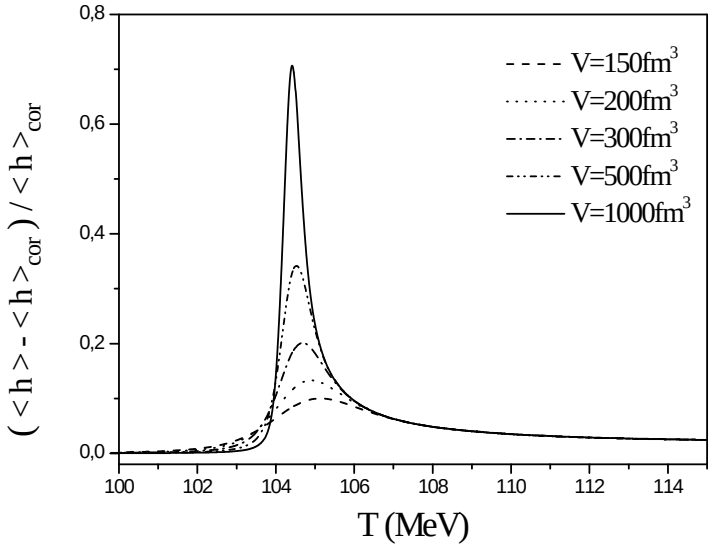

Figure 5.2: Relative difference $\frac{\langle h\rangle - \langle h\rangle_{cor}}{\langle h\rangle_{cor}}$ versus temperature for different volumes.

Similarly, Fig. (5.4) shows the variations of the corrected order parameter, normalized energy and entropy densities with chemical potential and system volume, at the temperature $T = 100MeV$. The first-order character of the transition can, also in this case, clearly be seen from the sharp discontinuity of the three quantities at a transition chemical potential $\mu_c'(\infty) \simeq 80.81MeV$, at the large volume limit. In small systems, the transition is perfectly smooth over a broadened region of chemical potential.

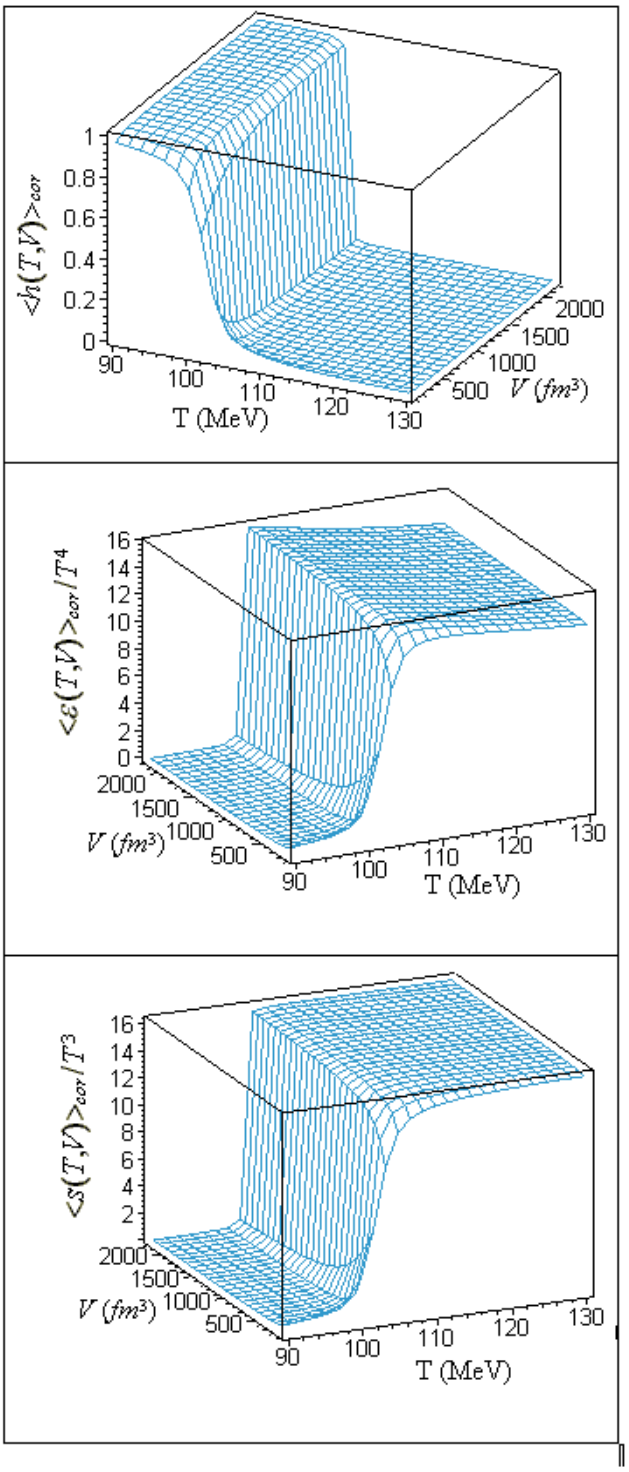

Figure 5.3: Three-dimensional plots of the corrected (top) order parameter, (middle) entropy density scaled by T^3, and (bottom) energy density scaled by T^4, with temperature and volume, at $\mu = 0$.

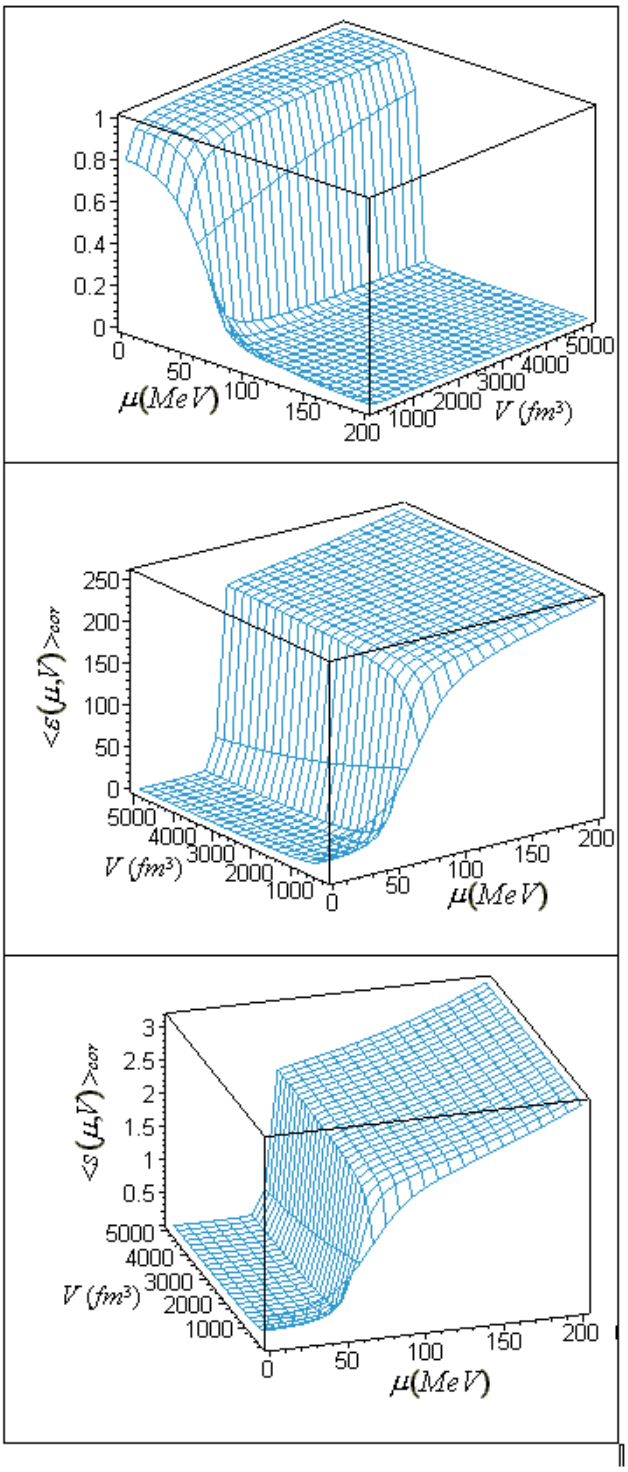

Figure 5.4: Three-dimensional plots of the corrected (top) order parameter, (middle) entropy density and (bottom) energy density with chemical potential and volume, at the temperature $T = 100MeV$.

5.4 Finite-Size Effects with the Exact Color-Singlet Partition Function and the Excluded Volume Correction

Hereafter, we shall consider the excluded volume correction for hadrons, as well as the color-singletness condition for the QGP phase within the phase coexistence model. The effects on the thermal deconfinement phase transition are then investigated by illustrating, first, each of the order parameter, energy and entropy densities calculated in this case.

The corrected mean value of the order parameter at zero chemical potential ($\mu = 0$) is calculated from the expression:

$$< \mathfrak{h}(T,V) >^{*}_{cor} = 1 - \frac{\int_{-\pi}^{+\pi}\int_{-\pi}^{+\pi} d\varphi d\psi M(\varphi,\psi) \int\limits_{0}^{1} \mathfrak{q} e^{\mathfrak{q}\mathsf{R}_{cor}(\varphi,\psi;T,V)} d\mathfrak{q}}{\int_{-\pi}^{+\pi}\int_{-\pi}^{+\pi} d\varphi d\psi M(\varphi,\psi) \int\limits_{0}^{1} e^{\mathfrak{q}\mathsf{R}_{cor}(\varphi,\psi;T,V)} d\mathfrak{q}}, \tag{5.12}$$

with:

$$\mathfrak{R}_{cor}\left(\varphi,\psi;T,V\right) = \left(g_{\mu=0}(\varphi,\psi) - \eta_{Hag}\,\frac{\pi^2}{30} - \frac{B}{T^4}\right) VT^3. \tag{5.13}$$

After effectuation of the integrations on $\mathfrak{q}$, the order parameter can be written on the form:

$$< \mathfrak{h}(T,V) >^{*}_{cor} = \frac{L_{01\ cor}\left(0\right) + L_{02\ cor}\left(0\right) - L_{12\ cor}\left(1\right)}{L_{01\ cor}\left(0\right) - L_{11\ cor}\left(1\right)}, \tag{5.14}$$

where the general form of the corrected integral coefficients appearing in this expression is:

$$L_{mn\ cor}\left(\mathfrak{q}\right) = \int_{-\pi}^{+\pi}\int_{-\pi}^{+\pi} d\varphi d\psi M(\varphi,\psi)(g_{\mu=0}(\varphi,\psi))^{m} \frac{\left(e^{\mathsf{R}_{cor}(\varphi,\psi;T,V)}\right)^{n}}{\mathfrak{R}_{cor}\left(\varphi,\psi;T,V\right)}. \tag{5.15}$$

The corrected mean value of the energy density is then related to $< \mathfrak{h}(T,V) >^*_{cor}$ by the expression:

$$< \varepsilon(T,V) >^*_{cor} = B + \left(e_{HG}\, \eta_{Hag} \left(1 - \frac{e_{HG}\, \eta_{Hag}}{3B} \right) - B \right) < \mathfrak{h}(T,V) >^*_{cor} - 3T^4\, \frac{L_{12\ cor}(0) + L_{11\ cor}(1) - L_{12\ cor}(1)}{L_{01\ cor}(0) - L_{01\ cor}(1)} \ . \tag{5.16}$$

Also in this case, as in (3.5.1), the corrected mean value of the entropy density will be calculated numerically by integrating $\frac{1}{T}(\frac{d<\varepsilon(T,V)>^*_{cor}}{dT})$, since it can not be expressed simply by the mean of the $L_{mn\ cor}$'s.

Fig. (5.5) shows the variations of the corrected order parameter, energy density over T^4 and entropy density over T^3 with temperature for various volumes. The same behavior as in Fig. (3.8) is observed, with the shifting effect induced by the color-singletness requirement.

5.5 Scaling Critical Exponents for the Deconfinement Phase Transition with the Exact Color-Singletness Condition and the Excluded Volume Correction

In the following, we shall carry out a finite size scaling analysis in order to determine the scaling critical exponents, given in eqs. (4.1), characterizing the deconfinement phase transition, when both excluded volume effects and color-singletness requirement are taken into account. For this purpose, each of the corrected thermal susceptibility, specific heat density and second derivative of the order parameter are first derived,

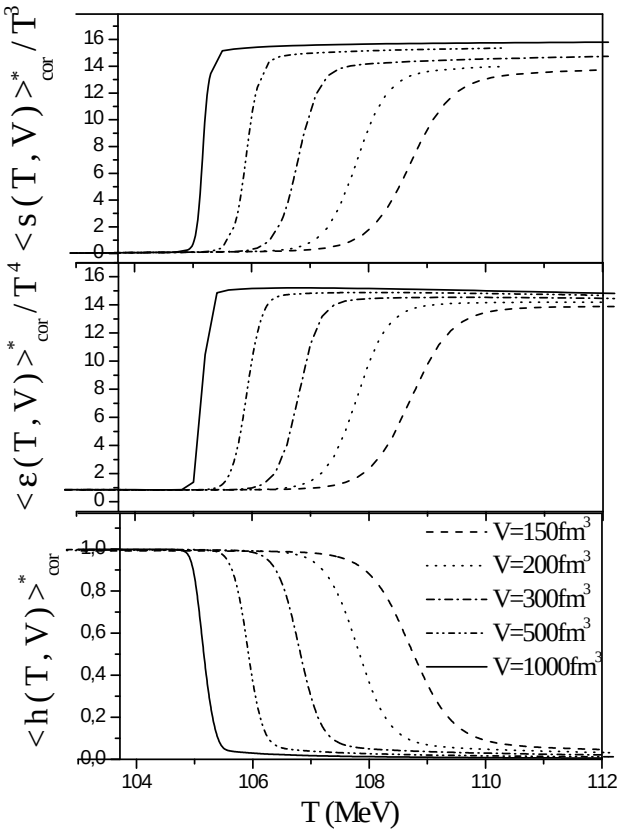

Figure 5.5: Variations of the corrected order parameter, normalized energy density $< \varepsilon(T,V) >^*_{cor} /T^4$ and normalized entropy density $< s(T,V) >^*_{cor} /T^3$ with temperature, at various volumes.

then analyzed in the transition region.

5.5.1 The susceptibility critical exponent

The obtained expression of the corrected thermal susceptibility is:

$$\begin{aligned}\chi_{cor}(T,V) &= \frac{T^2V}{L_{01}(0)-L_{01}(1)}\left[-3(L_{12\ cor}(0)+2L_{13\ cor}(0)+L_{12\ cor}(1)-2L_{13\ cor}(1))\right.\\ &\left.-(\frac{B}{T^4}-\frac{\pi^2}{10}\eta_{Hag}+\frac{\pi^4}{300}\frac{T^4}{B}\eta_{Hag}^2)(L_{02\ cor}(0)+2L_{03\ cor}(0)+L_{02\ cor}(1)-2L_{03\ cor}(1))\right]\\ &-T^2V\frac{L_{01\ cor}(0)+L_{02\ cor}(0)-L_{02\ cor}(1)}{(L_{01\ cor}(0)-L_{01\ cor}(1))^2}\left[-3(L_{12\ cor}(0)-L_{11\ cor}(1)+L_{12\ cor}(1))\right.\\ &\left.-(\frac{B}{T^4}-\frac{\pi^2}{10}\eta_{Hag}+\frac{\pi^4}{300}\frac{T^4}{B}\eta_{Hag}^2)(L_{02\ cor}(0)-L_{01\ cor}(1)+L_{02\ cor}(1))\right]\ , \qquad (5.17)\end{aligned}$$

and its variations with temperature at different volumes are represented on Fig. (5.6). Exactly the same behavior as in chapter 3 is found, and the difference between the values of the corrected and non corrected susceptibility at fixed temperature and volume is extremely small.

The data of the minima of the susceptibility at different system volumes are then extracted, and fitted to a power law of the volume: $\mid \chi_T \mid^{\max}(V) \sim V^{\gamma'_T}$, with the susceptibility scaling critical exponent: $\gamma'_T = 1.029 \pm 0.003$.

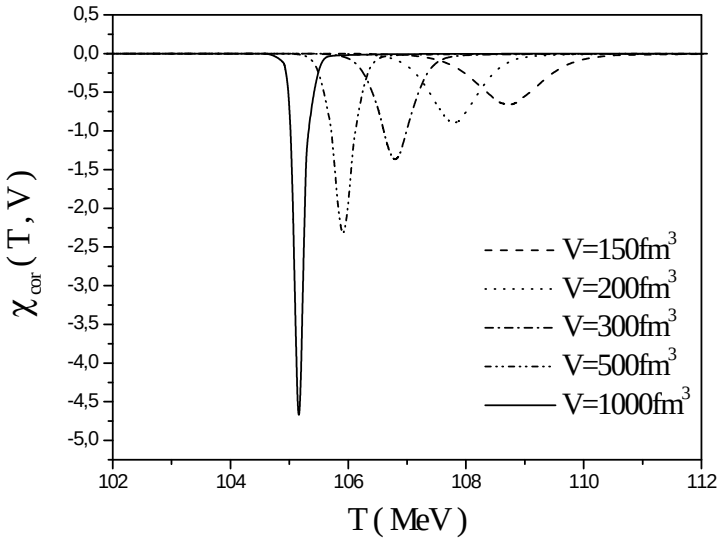

Figure 5.6: Variations of the corrected susceptibility with temperature for various volumes.

5.5.2 The specific heat critical exponent

The corrected thermal specific heat density given by:

$$
\begin{aligned}
c_{cor}\left(T,V\right) &= \left(\frac{2\pi^2}{5}\eta_{Hag}-\frac{\pi^2}{10}\eta_{Hag}^2\frac{\varepsilon_{HG}}{B}\right)T^3\ \left\langle \mathfrak{h}\left(T,V\right)\right\rangle^*_{cor} \\
&+\left(e_{HG}\ \eta_{Hag}\left(1-\frac{e_{HG}\ \eta_{Hag}}{3B}\right)-B\right)\ \chi_{cor}\left(T,V\right)+12T^3\frac{L_{11\ cor}(1)-L_{12\ cor}(1)+L_{12\ cor}(0)}{L_{11\ cor}(1)-L_{01\ cor}(0)} \\
&+\frac{3T^6V}{L_{01\ cor}(1)-L_{01\ cor}(0)}\left[-6L_{23\ cor}(0)+3L_{21\ cor}(1)-6L_{22\ cor}(1)+6L_{23\ cor}(1)\right. \\
&\left.+(\frac{B}{T^4}-\frac{\pi^2}{10}\eta_{Hag}+\frac{\pi^4}{300}\frac{T^4}{B}\eta_{Hag}^2)(-2L_{13\ cor}(0)+L_{11\ cor}(1)-2L_{12\ cor}(1)+2L_{13\ cor}(1))\right] \\
&-3T^6V\frac{L_{11\ cor}(1)-L_{12\ cor}(1)+L_{12\ cor}(0)}{\left(L_{01\ cor}(1)-L_{01\ cor}(0)\right)^2}\left[3(L_{12\ cor}(0)+L_{11\ cor}(1)-L_{12\ cor}(1))\right. \\
&\left.+(\frac{B}{T^4}-\frac{\pi^2}{10}\eta_{Hag}+\frac{\pi^4}{300}\frac{T^4}{B}\eta_{Hag}^2)(L_{02\ cor}(0)+L_{01\ cor}(1)-L_{02\ cor}(1))\right], \qquad (5.18)
\end{aligned}
$$

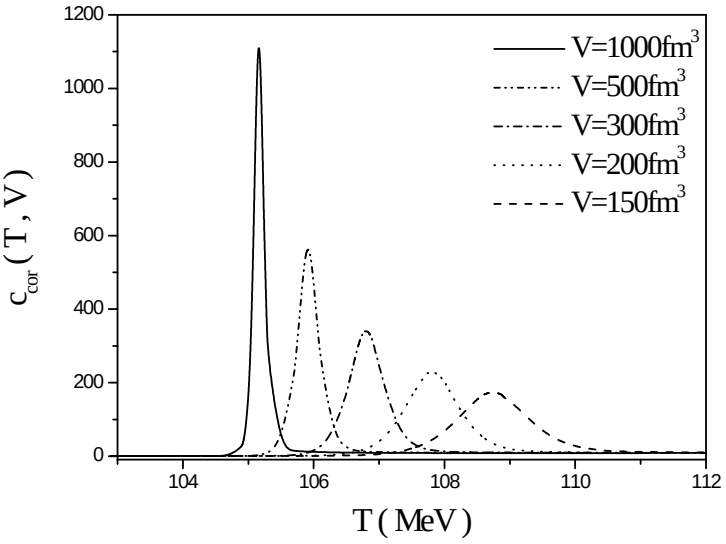

Figure 5.7: Variations of the corrected specific heat density with temperature for various volumes.

is illustrated in Fig. (5.7) versus temperature at various volumes. Here also, the same behavior as for the specific heat density in Fig. (3.12) is observed. Results of the maxima of the corrected specific heat density $c^{\max}_{T_{cor}}(V)$ are fitted to the power-law form: $c^{\max}_{T_{cor}}(V) \sim V^{\alpha'_T}$, and the obtained specific heat scaling exponent is: $\alpha'_T = 0.996 \pm 0.005$.

5.5.3 The smearing critical exponent

The width of the transition region is given by the difference: $\delta T'(V) = T'_2(V) - T'_1(V)$ with $T'_1(V)$ and $T'_2(V)$ the locations of the extrema of the corrected second derivative of the order parameter $\frac{\partial^2}{\partial T^2}\langle \mathfrak{h}(T,V)\rangle^*_{cor}$. The expression of this latter is:

$$
\begin{aligned}
\frac{\partial^2\langle\mathfrak{h}\,(T,V)\rangle^*_{cor}}{\partial T^2} &= \frac{2\chi_{cor}}{T} + \frac{\left(T^2V\right)^2}{L_{01_{cor}}(0)-L_{01_{cor}}(1)}\times \\
&[18L_{23_{cor}}(0)+54L_{24_{cor}}(0)-9L_{22_{cor}}(1)+36L_{23_{cor}}(1)-54L_{24_{cor}}(1) \\
&+\left(\tfrac{B}{T^4}-\tfrac{\pi^2}{10}\eta_{Hag}+\tfrac{\pi^4}{300}\tfrac{T^4}{B}\eta^2_{Hag}\right)(12L_{13_{cor}}(0)+36L_{14_{cor}}(0)-6L_{12_{cor}}(1)+24L_{13_{cor}}(1) \\
&-36L_{14_{cor}}(1))+\left(\tfrac{B}{T^4}-\tfrac{\pi^2}{10}\eta_{Hag}+\tfrac{\pi^4}{300}\tfrac{T^4}{B}\eta^2_{Hag}\right)^2(2L_{03_{cor}}(0)+6L_{04_{cor}}(0)-L_{02_{cor}}(1) \\
&+4L_{03_{cor}}(1)-6L_{14_{cor}}(1))-(L_{02_{cor}}(0)+2L_{03_{cor}}(0)+L_{02_{cor}}(1)-2L_{03_{cor}}(1)) \\
&\times\left(\tfrac{-4B}{T^7V}+\tfrac{7\pi^4}{300}\tfrac{T}{BV}\eta^2_{Hag}-\tfrac{\pi^6}{1500}\tfrac{T^5}{B^2V}\eta^3_{Hag}\right)]-\frac{\left(T^2V\right)^2}{\left(L_{01_{cor}}(0)-L_{01_{cor}}(1)\right)^2} \\
&\times[(3L_{12_{cor}}(0)+3L_{11_{cor}}(1)-3L_{12_{cor}}(1)+\left(\tfrac{B}{T^4}-\tfrac{\pi^2}{10}\eta_{Hag}+\eta_{Hag}+\tfrac{\pi^4}{300}\tfrac{T^4}{B}\eta^2_{Hag}\eta^2_{Hag}\right) \\
&\times(L_{02_{cor}}(0)+L_{01_{cor}}(1)-L_{02_{cor}}(1)))\,(3L_{12_{cor}}(0)+6L_{13_{cor}}(0)+3L_{12_{cor}}(1)-6L_{13_{cor}}(1) \\
&+\left(\tfrac{B}{T^4}-\tfrac{\pi^2}{10}\eta_{Hag}+\tfrac{\pi^4}{300}\tfrac{T^4}{B}\eta^2_{Hag}\right)(L_{02_{cor}}(0)+2L_{03_{cor}}(0)+L_{02_{cor}}(1)-2L_{03_{cor}}(1))\Big) \\
&+(L_{01_{cor}}(0)+L_{02_{cor}}(0)-L_{02_{cor}}(1))\,(-9L_{21_{cor}}(1)+18L_{22_{cor}}(1)-18L_{23_{cor}}(1)+18L_{23_{cor}}(0) \\
&-\left(\tfrac{B}{T^4}-\tfrac{\pi^2}{10}\eta_{Hag}+\tfrac{\pi^4}{300}\tfrac{T^4}{B}\eta^2_{Hag}\right)(6L_{11_{cor}}(1)-12L_{12_{cor}}(1)+12L_{13_{cor}}-12L_{13_{cor}}(0)) \\
&-\left(\tfrac{B}{T^4}-\tfrac{\pi^2}{10}\eta_{Hag}+\tfrac{\pi^4}{300}\tfrac{T^4}{B}\eta^2_{Hag}\right)^2(L_{11_{cor}}(1)-2L_{12_{cor}}(1)+2L_{13_{cor}}(1)-2L_{03_{cor}}(0)) \\
&-\left(\tfrac{-4B}{T^7V}+\tfrac{7\pi^4}{300}\tfrac{T}{BV}\eta^2_{Hag}-\tfrac{\pi^6}{1500}\tfrac{T^5}{B^2V}\eta^3_{Hag}\right)(L_{01}(1)-L_{02_{cor}}(1)+L_{02_{cor}}(0))\Big) \\
&-\Big(3L_{11_{cor}}(1)-3L_{12_{cor}}(1)+3L_{12_{cor}}(0)+\left(\tfrac{B}{T^4}-\tfrac{\pi^2}{10}\eta_{Hag}+\tfrac{\pi^4}{300}\tfrac{T^4}{B}\eta^2_{Hag}\right) \\
&\times(L_{01_{cor}}(1)-L_{02_{cor}}(1)+L_{02_{cor}}(0)))\,(6L_{13_{cor}}(1)-3L_{12_{cor}}(1)-3L_{12_{cor}}(0)-6L_{13_{cor}}(0) \\
&+\left(\tfrac{B}{T^4}-\tfrac{\pi^2}{10}\eta_{Hag}+\tfrac{\pi^4}{300}\tfrac{T^4}{B}\eta^2_{Hag}\right)(2L_{03_{cor}}(1)-L_{02_{cor}}(1)-L_{02_{cor}}(0)-2L_{03_{cor}}(0))\Big)\Big] \\
&+\frac{2\left(T^2V\right)^2}{\left(L_{01_{cor}}(0)-L_{01_{cor}}(1)\right)^3}\;(L_{01_{cor}}(0)+L_{02_{cor}}(0)-L_{02_{cor}}(1))\,(3L_{12_{cor}}(0)+3L_{11_{cor}}(1) \\
&-3L_{12_{cor}}(1)+\left(\tfrac{B}{T^4}-\tfrac{\pi^2}{10}\eta_{Hag}+\tfrac{\pi^4}{300}\tfrac{T^4}{B}\eta^2_{Hag}\right)(L_{02_{cor}}(0)+L_{01_{cor}}(1)-L_{02_{cor}}(1))\Big)^2\,, \qquad (5.19)
\end{aligned}
$$

and its variations with temperature at various system sizes are represented in Fig. (5.8).

The results of the width $\delta T(V)$ are fitted to the power-law form: $\delta T\,(V) \sim V^{-\theta'_T}$,

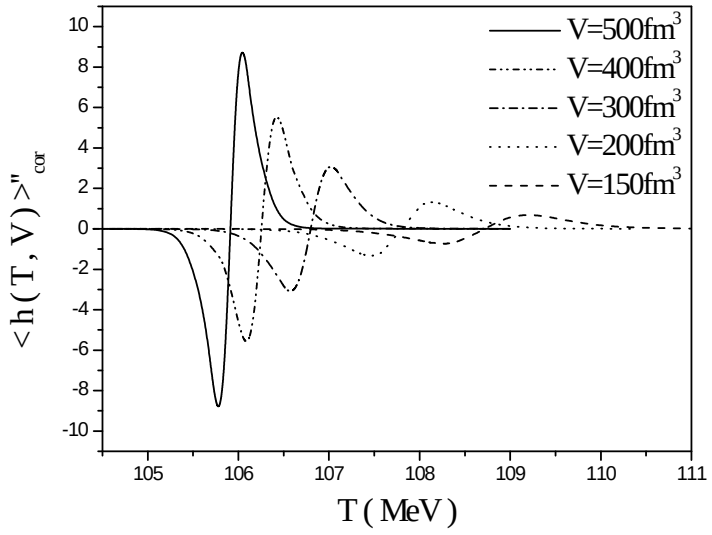

Figure 5.8: Second derivative of the corrected order parameter versus temperature at different volumes.

and the obtained value of the smearing scaling critical exponent is: $\theta'_T = 0.998 \pm 0.005$.

5.5.4 The shift critical exponent

The transition temperature can, also in this case, be obtained by several ways as in chapter 4. Extracting the data of $T_c(V)$ from the locations of the peaks of the thermal susceptibility $\mid \chi_T \mid^{\max} (V)$, and fitting them to a power-law function of the volume: $\tau_T(V) \sim V^{-\lambda'_T}$, gives the shift scaling critical exponent: $\lambda'_T = 0.812 \pm 0.003$.

The obtained results for the scaling critical exponents in this case are akin to those obtained previously in chapter 4 without the excluded volume correction. The phase transition is then still of first order, and has not been affected by the finite extention of the hadrons, as in [123].

Conclusion

The present work dealt with the study of the finite-size effects on the deconfinement phase transition, using a simple model of coexisting hadronic and QGP phases in a finite volume. Our model has shown the influence of the finiteness of the system size on the behavior of some response functions in the vicinity of the transition point. A sharp transition is observed in the thermodynamical limit, signaled by discontinuities in the order parameter, the entropy density s and the energy density ε at a transition temperature $T_c(\infty)$ for a thermally driven deconfinement phase transition (at $\mu = 0$), and at a transition chemical potential $\mu_c(\infty)$ for a density driven deconfinement phase transition (at $T = 100MeV$). In other terms, the deconfinement phase transition is labelled by a rapid rise in the effective degrees of freedom, represented by the ratios $\frac{\varepsilon}{T^4}$ and $\frac{s}{T^3}$ for a thermal deconfinement phase transition. Such a step-like rise behavior reflects a first-order phase transition. In finite volumes, the transition is rounded off and the variations of these thermodynamic quantities are perfectly smooth on the whole range of temperature. The delta function singularities appearing in the first derivatives of these discontinuous quantities, i.e., in the susceptibility $\chi = \frac{\partial \langle \mathsf{h} \rangle}{\partial T}$ and the specific heat density $c = \frac{\partial \langle \varepsilon \rangle}{\partial T}$, are then smeared out into finite peaks of widths $\delta T(V)$.

When the color-singlet character of physical states is exactly treated in the equation of state for the QGP in a finite volume, then a gradual "'freezing" of internal degrees

of freedom appears, as compared to the equation of state for infinite matter. This is reflected by a shift of the transition temperature $T_c(V)$ at which the thermal deconfinement phase transition from hadronic to QGP phases occurs, for finite systems. The maxima of the peaks of both susceptibility and specific heat density occur at effective transition temperatures $T_c\left(V\right)$ shifted away from the true transition temperature $T_c\left(\infty\right)$.

Our work has also shown that temperature and chemical potential play the same role when they drive the deconfinement phase transition. For a density driven deconfinement phase transition at a fixed temperature, the sharp transition occurring at the thermodynamic limit is smeared out in finite volumes over a range of chemical potential $\delta\mu\left(V\right)$ around the transition chemical potential $\mu_c\left(\infty\right)$, and when the color-singletness requirement is included for the QGP, the effective transition chemical potential $\mu_c\left(V\right)$ is shifted away from $\mu_c\left(\infty\right)$.

Other physical quantities can also be examined, which carry informations on the transition. Examples of such quantities are the sound velocity, rate of fluctuations and the second, third and fourth cumulants of the used probability distribution, each giving the transition temperature at some defined point. An other quantity of interest is the second derivative of the order parameter from which the width of the transition region can be obtained.

For a thermal deconfinement phase transition, finite size scaling analysis of the behavior of the maxima of the rounded peaks of the thermal susceptibility $\chi_T^{\max}\left(V\right)$ and specific heat density $c_T^{\max}\left(V\right)$, the width of the transition region $\delta T\left(V\right)$, and the shift of the effective transition temperature relative to the true one $\tau_T\left(V\right)=T_c\left(V\right)-T_c\left(\infty\right)$, shows their power-law variations with the volume characterized by the scaling critical

exponents γ, α, θ, and λ respectively. Numerical results of these scaling exponents have been determined in chapter 4, where the transition temperature has been obtained from various quantities as well from parametrizations of the order parameter and the susceptibility. These results are in good agreement with the analytical ones: $\gamma = \alpha = \theta = \lambda = 1$ obtained in our work [97], except for the shift critical exponent which slightly deflects from the analytical value 1. This may be due on one hand to the difficulty of locating accurately the peaks of the physical quantities, especially in the case of large volumes for which the peaks become very sharp, and on the other hand to the non-leading terms which contribute to the expression of the shift $\tau_T(V)$. However, a first estimate of the scaling critical exponents for the thermal deconfinement phase transition within this model has been obtained, and our result expressing the equality between all scaling exponents and the space dimensionality is a consequence of the singularity characterizing a first order phase transition and agrees very well with the predictions of the standard finite size scaling theoretical approaches to a first order phase transition [49, 50, 55, 106, 107, 108, 109] and with those obtained in a rather different and rigorous way, generalizing the finite size scaling description of a first order phase transition [110]. Also, we note a good agreement with the results of calculations using Monte Carlo methods in both lattice QCD [78, 111, 112, 113, 114] and other models in statistical physics [57, 115, 116].

A supplementary volume effect due to the finite hadron volumes has been considered in a part of this work. Wether the excluded volume effects influence the deconfinement phase transition has been examined, since it has been demonstrated that they can alter the kind of the transition. It has been shown in [100] that when the finite volume extensions of constituents in a hadronic gas are taken into account, for certain values of

the parameters of the used model, namely the QCD coupling constant α_s and the bag constant B, a smooth evolution from nuclear matter to a quark plasma phase through a second order transition becomes possible. In our model, we have found that such a correction does not affect the order of the transition.

Bibliography

[1] C. N. Yang and T. D. Lee, Phys. Rev. **87** (1952) 404; Phys. Rev. **87** (1952) 410.

[2] J. Imry, Phys. Rev. B **21** (1980) 2042.

[3] K. Binder and D. P. Landau, Phys. Rev. B **30** (1984) 1477.

[4] C. Spieles, H. Stöcker and C. Greiner, Phys. Rev. C **57** (1998) 908.

[5] A. Chodos and al., Phys. Rev. D **9** (1974) 3471; J. Cleymans, R. V. Gavai & E. Suhonen, Phys. Rep. **130** (1986) 217.

[6] K. Redlich and L. Turko, Z. Phys. C **5** (1980) 201; L.Turko, Phys. Lett. B **104** (1981) 153.

[7] H.-Th. Elze, W. Greiner and J. Rafelski , Phys. Lett. B **124** (1983) 515; Zeit. Phys. C **24** (1984) 361.

[8] H.-Th. Elze and W. Greiner, Phys. Lett. B **179** (1986) 385.

[9] A. Tounsi, J. Letessier and J. Rafelski, hep-ph/9811290.

[10] M. G. Mustafa, D. K. Srivastava and B. Sinha, Eur. Phys. J. C **5** (1998) 711; nucl-th/9712014.

[11] J. Madsen, D. M. Jensen and M. B. Christiansen, Phys. Rev. C **53** (1996) 1883.

[12] G. Yezza, Magister thesis in theoretical physics, Ecole Normale Supérieure-Kouba, Algiers (March 2002).

[13] A. Ait-El-Djoudi, M. Ladrem and G. Yezza, communication at the international conference *The Sixth Constantine High Energy Physics School*, held in Constantine-Algeria from 06 to 12 April 2002.

[14] M. Ladrem, A. Ait-El-Djoudi and G. Yezza, communication at the international conference Quark Matter 2002, held in Nantes-France from 18 to 24 July 2002.

[15] J. M. Yeomans, *Statistical Mechanics of Phase Transitions*, (Oxford University Press, 1992).

[16] J. W. Gibbs, Elementary Principles of Statistical Mechanics, The Collected Works of J. W. Gibbs, vol. II, Yale University Press, New Haven, CT, 1948.

[17] C. N. Yang and T. D. Lee, Phys. Rev. **87** (1952) 404; T. D. Lee and C. N. Yang, Phys. Rev. **87** (1952) 410.

[18] D. P. Landau & K. Binder, *A Guide to Monte Carlo Simulations in Statistical Physics,* Cambridge University Press (2000).

[19] W. Greiner, L. Neise and H. Stöcker, *Thermodynamics and Statistical Mechanics*, Springer-Verlag (1995).

[20] H. E. Stanley, *Introduction to Phase Transitions and Critical Phenomena*, Clarendon Press-Oxford (1971).

[21] V. Privman, Encycl. Appl. Phys. 23 (1998) 31.

[22] L. P. Kadanoff, in Proc. School of Physics "Enrico Fermi", Corso LI, edited by M. S. Green (Academic Press, New York, 1971).

[23] K.G. Wilson, Phys. Rev. **B4** (1971) 3174; **B4** (1971) 3184.

[24] M.E. Fisher, Rev. Mod. Phys. **46** (1974) 597; **70** (1998) 653.

[25] H. E. Stanley, Reviews of Modern Physics, Vol 71, 2, (1999) S358.

[26] http://d0server1.fnal.gov/users/gll/public/edpublic.htm .

[27] Ya. B. Zeldovitch, JETP 37 (1959) 569.

[28] Ya. B. Zeldovitch, L. B. Okun and S. B. Pikelner, Usp. Fiz. Nauk 87 (1965) 113.

[29] D. Ivanenko and D. E. Kurdgelaidze, Nuovo Cimento Lett.2 (1969) 13.

[30] N. Itoh, Progr. Theoret. Phys. 44 (1970) 291.

[31] R. Hagedorn, Nuovo Cim. Suppl. 3 (1965) 147.

[32] R. Hagedorn, Lectures given at the “Advanced NATO Workshop: Hot Hadronic matter, Theory and experiment.”, Divonne-les-Bois, France, preprint CERN-TH.7190 (1994).

[33] K. G. Wilson, Phys. Rev. **D10** (1974) 2445.

[34] M. Creutz, Phys. Rev. Lett. **43** (1979) 553; Phys. Rev. **D21** (1980) 2308.

[35] C. DeTar, hep-ph/9504325.

[36] S. Ejiri et al., hep-lat/0408046.

[37] F. Karsch, J. Phys. G31 (2005) S633, hep-lat/0412038.

[38] S. Ejiri et al., Nucl. Phys. A774 (2006) 837, hep-ph/0509361.

[39] S. Ejiri, F. Karsch,c, E. Laermann and C. Schmidt, Phys. Rev. D73 (2006) 054506, hep-lat/0512040.

[40] F. Karsch, AIP Conf. Proc. 602 (2001) 323, hep-lat/0109017.

[41] M. Cheng et al., Phys. Rev. D74 (2006) 054507, hep-lat/0608013.

[42] F. Karsch, E. Laermann and Ch. Schmidt, Phys. Lett. B520 (2001) 41, hep-lat/0107020.

[43] Ch. Schmidt, F. Karsch and E. Laermann, Nucl. Phys. Proc. Suppl. 106 (2002) 423, hep-lat/0110039.

[44] F. Karsch, hep-lat/0601013.

[45] F. Karsch, J. Phys. Conf. Ser. 46 (2006) 122, hap-lat/0608003.

[46] M. Fukugita, Nucl. Phys. Proc. Suppl. **9** (1989) 291.

[47] F. Karsch, Nucl. Phys. A **590** (1995) 367c-382c.

[48] F. Karsch, Nucl. Phys. A **698** (2002) 199c-208c.

[49] F. Karsch et al., Nucl. Phys. (Proc. Suppl.) B **94** (2001) 411-414.

[50] F. Karsch et al., Nucl. Phys. B **605** (2001) 579-599.

[51] M. Fukugita, RIFP-703 (June 1987).

[52] M. Fukugita et al., Phys. Rev. Lett. **58** (1987) 2515; UTHEP-168 (August 1987).

[53] M. Fukugita et al.,Phys. Rev. Lett. **60** (1988) 178.

[54] M. Fukugita, Nucl. Phys. Proc. Suppl. **4** (1988) 105.

[55] M. Fukugita & A. Ukawa, Phys. Rev. D **38** (1988) 1971.

[56] R. V. Gavai et al., Phys. Lett. B **200** (1988) 137.

[57] F. R. Brown et al., Phys. Rev. Lett. **65** (1990) 2491.

[58] S. Aoki et al. (JLQCD Coll.), Nucl. Phys. B **63**A-C (1998) 403, **60**A (1998) 188.

[59] B. Lucini et al., Phys. Lett. B **545** (2002) 197.

[60] P. Cea et al., Nucl. Phys. (Proc. Suppl.) B **129, 130** (2004) 751.

[61] M. Cheng et al., Phys.Rev. D75 (2007) 034506; hep-lat/0612001.

[62] M. E. Fisher and M. N. Barber, Phys. Rev. Lett. 28 (1972) 1516.

[63] D. P. Landau, Phys. Rev. B vol. 14, N° 1 (1976) 255.

[64] M. E. Fisher and A. N. Berker, Phys. Rev. B **26** N° 5 (1982) 2507.

[65] M. N. Barber, in *Phase Transitions and Critical Phenomena*, Vol. 8, C. Domb and J. L. Lebowitz eds. (Academic Press, New York, 1983) 145.

[66] M. S. Challa, D. P. Landau and K. Binder, Phys. Rev. **B34** (1986) 1841.

[67] K. Binder and D. W. Heermann, *Monte Carlo Simulations in Statistical Physics*, (Springer-Verlag, 1988, 2nd edition 2002).

[68] K. Binder, Rep. Prog. Phys. **60** (1997) 487.

[69] P. Forcrand and O. Philipsen, hep-lat/ 0205016.

[70] H. Meyer-Ortmanns, Rev. Mod. Phys. **68** (1996) 473.

[71] V. Privman et M. E. Fischer, J. Stat. Phys. Vol 33, N° 2 (1983) 385; J. App. Phys. Vol 57, N° 1 (1985) 3327.

[72] A. Billoire, hep-lat/9208026.

[73] M. Fukugita et al., KEK-TH-233 (1989).

[74] M. Henkel, *Conformal Invariance and Critical Phenomena*, (Springer-Verlag, 1999).

[75] K. Binder, Phys. Rev. Lett. **47** (1981) 693; Z. Phys. **B43** (1981) 119.

[76] D. P. Landau & K. Binder, *A Guide to Monte Carlo Simulation in Statistical Physics, (*Cambridge University Press, 2000).

[77] Q.H. Zhang, hep-ph/0106242.

[78] J. Fingberg, U. Heller, and F. Karsch, Preprint HLRZ-92-39.

[79] G. S. Bali and K. Schilling, Phys. Rev. **D46** (1992) 2636.

[80] K. D. Born, et al., Phys. Lett. **B329** (1994) 325.

K. D. Born, et al., Phys. Lett. **B329** (1994) 332.

[81] C. Allton et al. (RBC and UKQCD Collaborations), hep-lat/0701013, BNL-HET-07/1, CU-TP-1175, Edinburgh 2007/1, KEK-TH-1132, RBRC-637, SHEP-0701, SWAT/07/502.

[82] A. Ukawa, preprint CERN-TH 5266/88.

[83] J. Engels, F. Karsch, H. Satz and I. Montvay, Nucl. Phys. **B205** [$FS5$] (1982) 545.

[84] A. Ait-El-Djoudi, M. Ladrem and G. Yezza, communication at the international conference *The Seventh Constantine High Energy Physics School on Theoretical Physics and Cosmology*, held in Constantine-Algeria from 03 to 08 April 2004.

[85] D. P. Landau and R. H. Swendsen, Phys. Rev. Lett. **46** (1981) 1437

[86] F. R. Brown et al., Phys. Rev. Lett. **61** (1988) 2058.

[87] P. Bacilieri et al., Phys. Rev. Lett. **61** (1988) 1545.

[88] J. F. McCarthy, Indiana University Preprint IUHET 164 (1989).

[89] M. Fukugita et al., Phys. Rev. Lett. **63** (1989) 1768.

[90] P. Bacilieri et al., Phys. Lett. **B220** (1989) 607.

[91] R. V. Gavai, F. Karsch and B. Petersson, Nucl. Phys. **B322** (1989) 738.

[92] M. Fukugita, Phys. Rev. Lett. **63** (1989) 13.

[93] M. Fukugita et al., Nucl. Phys. Proc. Suppl. **17** (1990) 204.

[94] S. Gupta et al., Nucl. Phys. **B329** (1990) 263.

[95] M. Fukugita et al., J. Phys. **A23** (1990) L561-L566.

[96] N. A. Alves et al., Phys. Rev. Lett. **64** (1990) 3107.

[97] A. Ait-El-Djoudi, Magister thesis in theoretical physics, Ecole Normale Supérieure-Kouba, Algiers (October 1999).

[98] C. Schmidt, Proceedings of Science (Lat2006) 021; hep-lat/0610116v2.

[99] J. Letessier and J. Rafelski, *Hadrons and Quark-Gluon Plasma*, (Cambridge University Press, 2002).

[100] S. A. Chin, Phys. Lett. **78B** (1978) 552.

[101] M. LeBellac, Lectures given at the XXX^{th} Schladming winter school, Austria, preprint INLN 1991/8.

[102] C. Barter, D. Blaschke and H. Voss, preprint CERN-TH. 6499/92.

[103] G. Auberson et al., J. Math. Phys. **27** (1986) 1658.

[104] F. Savatier, J. Math. Phys. **32** (1991) 2243.

[105] M. I. Gorenstein, O. A. Mogilevsky, V. K. Petrov, G. M. Zinovjev, Z. Phys. C **18** (1983) 13.

[106] Bo-Sture K. Skagerstam, Phys. Lett. **B133** (1983) 419.

[107] Bo-Sture K. Skagerstam, Z. Phys. **C24** (1984) 97.

[108] Ramesh Anishetty, J. Phys. **G10** (1984) 439.

[109] J. C. Anjos, J. Sá Borges, A. P. C. Malbouisson, F. R. A. Simão, Z. Phys. **C23** (1984) 243.

[110] S. I. Azakov, P. Salomonson and B. -S. Skagerstam, Phys. Rev. **D36** (1987) 2137.

[111] S. I. Azakov, Teor. Mat. Fiz, Vol. **76** N○ 3 (1988) 362.

[112] P. Von Brentano and Winfried Frank, Am. J. Phys. **64** (1996) 589.

[113] M. G. Mustafa and A. Ansari, Phys. Rev. **C55** (1997) 2005.

[114] L. Landau and E. M. Lifshitz, Hydrodynamics, (Pergamon Press, London, 1959).

[115] D. H. Rischke, Nucl. Phys. A610 (1996) 88c-101c; nucl-th/9608024

[116] D. H. Rischke and M. Gyulassy, Nucl. Phys. **A597** (1996) 701.

[117] D. H. Rischke, nucl-th/9809044.

[118] C. M. Hung and E. V. Shuryak, Phys. Rev. Lett. **75** (1995) 4003.

[119] M. Ladrem, A. Ait-El-Djoudi and G. Yezza, in the Proceedings of the international conference "Quark Confinement and the Hadron Spectrum" held in Gargnano-Italy from 10-14 September 2002.

[120] J. P. Blaizot and J. Y. Ollitraut, Phys. Rev. **D36** (1987) 916.

[121] M. Asakawa and T. Hatsuda, Phys.Rev. **D55** (1997) 4488.

[122] K. Binder, Phys. Rev. Lett. **47** (1981) 693; Zeit. Phys. **B43** (1981) 119.

[123] T. Çelik and Y. Gündüç, Preprint IC/85/296.

[124] R. Hagedorn, in Quark matter'84, Helsinki, 1984 (Springer, Berlin, 1985).

[125] S. Z. Belenky, Nucl. Phys. **2** (1956) 259.

[126] R. Hagedorn and J. Rafelski, Phys. Lett. **97B** (1980) 136.

[127] R. Hagedorn, I. Montvay and J. Rafelski, in Quark matter'84.

[128] K. Binder, Ferroelectrics 73 (1987) 43; in Computational Methods in Field Theory, H. Gausterer and C. B. Lang, (Eds. Springer, Berlin 1992) 59.

[129] W. Janke, Phys. Rev. B **47** (1993) 14757.

[130] K. Vollmayr, J.D. Reger, M. Scheucher, and K. Binder, Z. Phys. B **91** (1993) 113.

[131] J. G. Brankov, D. M. Danchev and N. S. Tonchev, *Theory of Critical Phenomena in Finite-Size Systems - Scaling and Quantum Effects*, (World Scientific, 2000).

[132] C. Borgs and R. Kotecky, J. Stat. Phys. **61** (1991) 79; C. Borgs, R. Kotecky and S. Miracle-Solé, J. Stat. Phys. **62** (1991) 529.

[133] B. Beinlich, F. Karsch, E. Laermann and A. Peikert, Eur. Phys. J. C **6** (1999) 133.

[134] K. Bitar et al., Nucl. Phys. B **337** (1990) 245.

[135] R. V. Gavai, Nucl. Phys. Proc. Suppl. **106** (2002) 480; Nucl. Phys. B **633** (2002) 127.

[136] M. Mathur et R. V. Gavai, Nucl. Phys. B **448** (1995) 399.

[137] D. Loison and K. D. Schotte, Eur. Phys. J. B **5** (1998) 735, B **14** (2000) 125.

[138] O. Dillmann, W. Janke and K. Binder, J. Stat. Phys. **92** 1/2 (1998) 57.

Eur. Phys. J. C (2005)
Digital Object Identifier (DOI) 10.1140/epjc/s2005-02357-y

THE EUROPEAN PHYSICAL JOURNAL C

Finite-size effects and scaling for the thermal QCD deconfinement phase transition within the exact color-singlet partition function

M. Ladrem[a], A. Ait-El-Djoudi[b]

Laboratoire de Physique des Particules et Physique Statistique, Ecole Normale Supérieure-Kouba, B.P. 92, 16050, Vieux-Kouba, Algiers, Algeria

Received: 11 January 2005 / Revised version: 7 July 2005 /
Published online: ♣ 2005 –

Abstract. We study the finite-size effects for the thermal quantum chromodynamics (QCD) deconfinement phase transition, and use a numerical finite-size scaling analysis to extract the scaling exponents characterizing its scaling behavior when approaching the thermodynamic limit ($V \longrightarrow \infty$). For this, we use a simple model of coexistence of hadronic gas and color-singlet quark gluon plasma (QGP) phases in a finite volume. The color-singlet partition function of the QGP cannot be exactly calculated and is usually derived within the saddle-point approximation. When we try to do calculations with such an approximate color-singlet partition function, a problem arises in the limit of small temperatures and/or volumes $\left(VT^3 << 1\right)$, requiring additional approximations if we want to carry out calculations. We propose in this work a method for an accurate calculation of any quantity of the finite system, without any approximation. By probing the behavior of some useful thermodynamic response functions on the whole range of temperature, it turns out that, in a finite-size system, all singularities in the thermodynamic limit are smeared out and the transition point is shifted away. A numerical finite-size scaling (FSS) analysis of the obtained data allows us to determine the scaling exponents of the QCD deconfinement phase transition. Our results expressing the equality between their values and the space dimensionality is a consequence of the singularity characterizing a first-order phase transition and agree very well with the predictions of other FSS theoretical approaches to a first-order phase transition and with the results of calculations using Monte Carlo methods in both lattice QCD and statistical physics models.

1 Introduction

It is generally believed that at sufficiently high temperatures and/or densities a new phase of matter called the quark gluon plasma (QGP) can be created. This is logically a consequence of the quark–parton level of the matter structure and of the dynamics of strong interactions described by the quantum chromodynamics (QCD) theory. Its existence, however, has been partly supported by lattice QCD calculations and cosmological standard model predictions. The only available and experimental way to study the QCD deconfinement phase transition is to try to create it in ultra-relativistic heavy-ion collision conditions similar to those in the early moments of the universe, right after the Big Bang. If ever the QGP is created in ultra-relativistic heavy-ion collisions, the volume within which the eventual formation would take place would certainly be finite. Also, in lattice QCD studies, the scale of the lattice space volume is finite. This motivates the study of finite-size effects on the expected deconfinement phase transition from a hadronic gas (HG) phase to a QGP phase. These effects are certainly important since statistical fluctuations in a finite volume may hinder a sharp transition between the two phases. Phase transitions are known to be infinitely sharp, signaled by some singularities, only in the thermodynamic limit [1]. In general, finite-size effects lead to a rounding of these singularities, as pointed out in [2, 3]. However, even in a such situation, it is possible to obtain information on the critical behavior. Large but finite systems show a *universal* behavior called "finite-size scaling" (FSS), allowing one to put all the physical systems undergoing a phase transition in a certain number of universality classes. The systems in a given universality class display the same critical behavior, meaning that certain dimensionless quantities have the same values for all these systems. *Critical exponents* are an example of these universal quantities.

In the present work, we study the finite-size behavior for the thermally driven deconfinement phase transition within a simple QCD model as used in [4]. The model is based on the standard MIT bag model with a mixed phase system having a finite total volume V [5]. The fraction of volume (defined by the parameter $\mathfrak{h}$) occupied by the HG phase is given by: $V_{HG} = \mathfrak{h}V$, and the remaining volume: $V_{QGP} = (1-\mathfrak{h})V$ then contains the QGP phase. Addition-

[a] e-mail: Ladrem@eepad.dz
[b] e-mail: Aitamel@eepad.dz

ally, we implement the color-charge confinement property by requiring that the QGP phase is a colorless object in the color space. Then, if we assume noninteracting phases (separability of the energy spectra of the two phases), the total partition function of the system can be written as the product:

$$Z(\mathfrak{h}) = Z_{\mathrm{QGP}}(\mathfrak{h}) Z_{\mathrm{HG}}(\mathfrak{h}) Z_{\mathrm{Vac}}(\mathfrak{h}), \tag{1}$$

where:

$$\begin{aligned} Z_{\mathrm{Vac}}(T,\mathfrak{h}) &= \exp(-BV_{\mathrm{QGP}}/T) \\ &= \exp(-BV(1-\mathfrak{h})/T), \end{aligned} \tag{2}$$

accounts for the confinement of quarks and gluons by the real vacuum pressure exerted on the perturbative vacuum (B) of the bag model. For the HG phase, the partition function is calculated just for a pionic gas and is simply given by:

$$Z_{\mathrm{HG}} = e^{\frac{\pi^2}{30} T^3 V_{HG}}. \tag{3}$$

The partition function $Z_{\mathrm{QGP}}(\mathfrak{h})$ of the QGP phase is calculated by considering a free gas of quarks and gluons with the exact color-singletness requirement. We can then perform calculation of the mean value of any thermodynamic quantity of the system $\langle \mathcal{A}(T,\mu,V) \rangle$, as defined in [4], by:

$$\langle \mathcal{A}(T,\mu,V) \rangle = \frac{\int_0^1 \mathcal{A}(\mathfrak{h},T,\mu,V)\, Z(\mathfrak{h})\, d\mathfrak{h}}{\int_0^1 Z(\mathfrak{h})\, d\mathfrak{h}}, \tag{4}$$

where $\mathcal{A}(\mathfrak{h},T,\mu,V)$ is the total thermodynamic quantity in the state $\mathfrak{h}$, given in the case of an extensive quantity by:

$$\begin{aligned} \mathcal{A}(\mathfrak{h},T,\mu,V) &= \mathcal{A}_{\mathrm{HG}}(T,\mu,\mathfrak{h}V) \\ &\quad + \mathcal{A}_{\mathrm{QGP}}(T,\mu,(1-\mathfrak{h})V), \end{aligned} \tag{5}$$

and in the case of an intensive quantity, by:

$$\begin{aligned} \mathcal{A}(\mathfrak{h},T,\mu,V) &= \mathfrak{h}\mathcal{A}_{\mathrm{HG}}(T,\mu,\mathfrak{h}V) \\ &\quad + (1-\mathfrak{h})\mathcal{A}_{\mathrm{QGP}}(T,\mu,(1-\mathfrak{h})V), \end{aligned} \tag{6}$$

with $\mathcal{A}_{\mathrm{QGP}}$ and $\mathcal{A}_{\mathrm{HG}}$ being the contributions relative to the individual QGP and HG phases, respectively.

Let us note that the coexistence of two phases in a finite system undergoing a phase transition taken alone seems not to be sufficient for anticipating the first-order nature of the phase transition when approaching the thermodynamic limit. A similar confusion can arise in the case of a correlation-length scaling with the volume and suggesting a second-order nature of the transition in the thermodynamic limit. This subtle situation has been noticed and clarified in several works [6–9]. Then, for a firm determination of the order of a phase transition in a finite system, a full and detailed finite-size scaling analysis of different response functions simultaneously, yielding various scaling critical exponents, seems to be necessary. This is not all in our case, since other basic parameters of QCD like the number of flavors and the current quark masses have a strong influence on how the phase transition occurs. A clear sensitivity of the order of the QCD deconfinement phase transition to these parameters has been revealed by several lattice QCD calculations (see, for example, [7,10,11]).

The color-singlet partition function of the QGP derived using the group-theoretical projection technique formulated by Turko and Redlich [12] cannot be exactly calculated and is usually calculated within the saddle-point approximation in the limit $V_{QGP}T^3 >> 1$ as in [13–16]. It turns out that the use of the obtained approximated partition function for the calculation of a mean value within the definition (4), has as a consequence the absence of the deconfinement phase transition [17]. This is due to the fact that the approximation used for the calculation of the color-singlet partition function breaks down at $V_{QGP}T^3 << 1$, and this limit is attained in our case. This has been emphasized in further works in which additional approximations have been used to carry out calculations, as in [4,14]. We propose in the following a method which allows us to calculate physical quantities accurately describing well the deconfinement phase transition at finite volumes within the QCD model chosen, thus avoiding then the problem arising at $V_{QGP}T^3 << 1$ without any approximation. We proceed by using the exact definition of the color-singlet partition function for Z_{QGP} in the definition (4) of the mean value of a physical quantity. A first analytical step in the calculation of the mean value is then achieved, and an expression with integral coefficients is obtained. The double integrals are then carried out with a suitable numerical method at each value of temperature and volume, and the behavior of the physical quantity of the finite system can so be obtained on the whole range of temperature, for various volumes, without any restriction. Afterwards, scaling critical exponents characterizing the scaling behavior of some quantities are determined using a numerical FSS analysis.

2 Exact color-singlet partition function of the QGP

The exact partition function for a color-singlet QGP contained in a volume V_{QGP}, at temperature T and quark chemical potential μ, is determined by [13]:

$$\begin{aligned} &Z_{\mathrm{QGP}}(T,V_{\mathrm{QGP}},\mu) \\ &= \frac{8}{3\pi^2} \int_{-\pi}^{+\pi}\int_{-\pi}^{+\pi} d\left(\tfrac{\varphi}{2}\right) d\left(\tfrac{\psi}{3}\right) M(\varphi,\psi) \widetilde{Z}(T,V_{\mathrm{QGP}},\mu;\varphi,\psi), \end{aligned} \tag{7}$$

$M(\varphi,\psi)$ is the weight function (Haar measure) given by:

$$M(\varphi,\psi) = \left(\sin\left(\tfrac{1}{2}(\psi+\tfrac{\varphi}{2})\right) \sin(\tfrac{\varphi}{2}) \sin\left(\tfrac{1}{2}(\psi-\tfrac{\varphi}{2})\right)\right)^2, \tag{8}$$

and $\widetilde{Z}$ the generating function defined by:

$$\widetilde{Z}(T,V_{\rm QGP},\mu;\varphi,\psi) \quad (9)$$
$$= Tr\left[\exp\left(-\beta\left(\widehat{H}_0-\mu\left(\widehat{N}_q-\widehat{N}_{\overline{q}}\right)\right)+i\varphi\widehat{I}_3+i\psi\widehat{Y}_8\right)\right],$$

where $\beta=\dfrac{1}{T}$ (with the units chosen as: $k_B=\hbar=c=1$), $\widehat{H}_0$ is the free quark–gluon Hamiltonian, $\widehat{N}_q\left(\widehat{N}_{\overline{q}}\right)$ denotes the (anti-) quark number operator, and $\widehat{I}_3$ and $\widehat{Y}_8$ are the color "isospin" and "hypercharge" operators respectively. Its final expression, in the massless limit, can be put in the form:

$$Z_{\rm QGP}(T,V_{\rm QGP},\mu) \quad (10)$$
$$=\frac{4}{9\pi^2}\int_{-\pi}^{+\pi}\int_{-\pi}^{+\pi}d\varphi d\psi M(\varphi,\psi)e^{V_{\rm QGP}T^3 g\left(\varphi,\psi,\frac{\mu}{T}\right)},$$

with:

$$g(\varphi,\psi,\frac{\mu}{T})$$
$$=\frac{\pi^2}{12}(\frac{21}{30}d_{\rm Q}+\frac{16}{15}d_{\rm G})$$
$$+\frac{\pi^2}{12}\frac{d_{\rm Q}}{2}\sum_{q=r,b,g}\left\{-1+\left(\frac{\left(\alpha_q-i(\frac{\mu}{T})\right)^2}{\pi^2}-1\right)^2\right\}$$
$$-\frac{\pi^2}{12}\frac{d_{\rm G}}{2}\sum_{g=1}^{4}\left(\frac{(\alpha_g-\pi)^2}{\pi^2}-1\right)^2, \quad (11)$$

$d_{\rm Q}=2N_f$ and $d_{\rm G}=2$ being the degeneracy factors of quarks and gluons respectively, α_q ($q=r,\,b,\,g$) the angles determined by the eigenvalues of the color charge operators in (9):

$$\alpha_r=\tfrac{\varphi}{2}+\tfrac{\psi}{3},\quad \alpha_g=-\tfrac{\varphi}{2}+\tfrac{\psi}{3},\quad \alpha_b=-\tfrac{2\psi}{3}, \quad (12)$$

and α_g ($g=1,\ldots,4$) being:

$$\alpha_1=\alpha_r-\alpha_g,\ \alpha_2=\alpha_g-\alpha_b,\ \alpha_3=\alpha_b-\alpha_r,\ \alpha_4=0. \quad (13)$$

3 Finite-size effects

To study the effects of volume finiteness on the thermal deconfinement phase transition within the QCD model chosen, we will examine in the following the behavior of some thermodynamic quantities of the system with temperature, at a vanishing chemical potential ($\mu=0$), considering the two lightest quarks u and d ($N_f=2$), and using the common value $B^{1/4}=145MeV$ for the bag constant.

The first quantity of interest for our study is the mean value of the hadronic volume fraction $<\mathfrak{h}(T,V)>$, which can be considered as representing the order parameter for the studied deconfinement phase transition. According to (4), $<\mathfrak{h}(T,V)>$ is expressed as:

$$<\mathfrak{h}(T,V)>=1-\frac{\int_{-\pi}^{+\pi}\int_{-\pi}^{+\pi}d\varphi d\psi M(\varphi,\psi)\int_0^1\mathfrak{q}e^{\mathfrak{q}\Re(\varphi,\psi;T,V)}d\mathfrak{q}}{\int_{-\pi}^{+\pi}\int_{-\pi}^{+\pi}d\varphi d\psi M(\varphi,\psi)\int_0^1 e^{\mathfrak{q}\Re(\varphi,\psi;T,V)}d\mathfrak{q}}, \quad (14)$$

with: $\Re\left(\varphi,\psi;T,V\right)=\left(g_{\mu=0}(\varphi,\psi)-\frac{\pi^2}{30}-\frac{B}{T^4}\right)VT^3$. After integration on the $\mathfrak{q}$ variable representing the QGP volume fraction, the order parameter can be written as:

$$<\mathfrak{h}(T,V)>=\frac{L_{01}+L_{02}-L_{12}}{L_{01}-L_{11}}, \quad (15)$$

where the general form of the integral terms appearing in this expression is:

$$L_{nm}=\int_{-\pi}^{+\pi}\int_{-\pi}^{+\pi}d\varphi d\psi M(\varphi,\psi)\frac{\left(e^{\Re(\varphi,\psi;T,V)}\right)^n}{\left(\Re\left(\varphi,\psi;T,V\right)\right)^m}. \quad (16)$$

These integrals are then carried out using a suitable numerical method at each fixed temperature and volume.

The second quantity of interest is the energy density $\varepsilon(T,V)$, whose mean value is related to $<\mathfrak{h}(T,V)>$ by:

$$<\varepsilon(T,V)>=\varepsilon_{HG}<\mathfrak{h}(T,V)>+B\left[1-<\mathfrak{h}(T,V)\right]$$
$$-3T^4\left[\frac{\widetilde{L}_{11}-\widetilde{L}_{12}+\widetilde{L}_{02}}{L_{01}-L_{11}}\right], \quad (17)$$

where the new integrals on φ and ψ , noted by $\widetilde{L}_{nm}$, are given by:

$$\widetilde{L}_{nm}=\int_{-\pi}^{+\pi}\int_{-\pi}^{+\pi}d\varphi d\psi M(\varphi,\psi)g_{\mu=0}(\varphi,\psi)$$
$$\times\frac{\left(e^{\Re(\varphi,\psi;T,V)}\right)^n}{\left(\Re\left(\varphi,\psi;T,V\right)\right)^m}, \quad (18)$$

and: $\varepsilon_{\rm HG}=\frac{\pi^2}{10}T^4$.

We can also examine the effects of volume finiteness by illustrating two more quantities representing the first derivatives of the two previous ones, that is, the susceptibility χ defined as:

$$\chi\left(T,V\right)=\frac{\partial\langle\mathfrak{h}\left(T,V\right)\rangle}{\partial T}, \quad (19)$$

and the specific heat density $c\left(T,V\right)$ defined as:

$$c\left(T,V\right)=\frac{\partial\langle\varepsilon\left(T,V\right)\rangle}{\partial T}. \quad (20)$$

Our results for the variations of these four response functions with temperature at different system sizes are presented in the plots on Figs. 1 and 2 and show a pronounced size dependence over almost the entire temperature range. The curves show that, in the limit of an infinite volume, both $\langle\mathfrak{h}\rangle$ and $\dfrac{<\varepsilon>}{T^4}$ exhibit a finite sharp

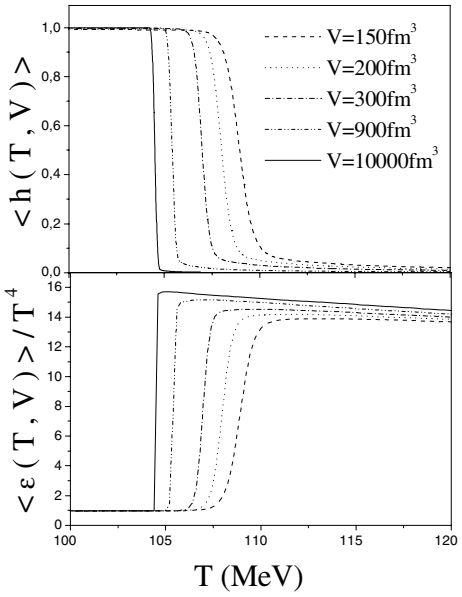

Fig. 1. Temperature variation of the order parameter (top) and the energy density normalized by T^4 (bottom) at $\mu = 0$, for different system volumes

discontinuity, which is related to the latent heat of the deconfinement phase transition, at a bulk transition temperature $T_c(\infty) \simeq 104.35\,\mathrm{MeV}$, reflecting the first-order character of the transition. The quantity $\frac{\langle\varepsilon\rangle}{T^4}$ is traditionally interpreted as a measure of the number of effective degrees of freedom; the temperature increase then causes a "melting" of the constituent degrees of freedom "frozen" in the hadronic state, making the energy density attain its plasma value. This finite discontinuity can be mathematically described by a step function, which transforms to a δ-function in χ and c. When the volume decreases, the four quantities vary continuously such that the finite sharp jump is rounded off and the δ-peaks are smeared out into finite peaks over a range of temperature $\delta T(V)$. This is due to the finite probability of the presence of the QGP phase below T_c and of the hadron phase above T_c, induced by the considerable thermodynamical fluctuations.

Another feature which can be noted is that the maxima of these rounded peaks occur at effective transition temperatures $T_c(V)$ shifted away from the bulk transition temperature for infinite volume $T_c(\infty)$. This shift is a consequence of the color-singletness requirement since the effective number of internal degrees of freedom for a color-singlet QGP is drastically reduced with decreasing volume, as can clearly be seen from the curves, and has been shown in [13]. Thus, the pressure of the QGP phase is lower at a given temperature, and the mechanical Gibbs equilibrium between the two phases would then be reached for $T_c(V) > T_c(\infty)$.

It can also be noted that, for decreasing volume, while the height of the peak decreases, its width gets larger. To see this in more detail, we illustrate in the following the second derivative of the order parameter $\langle \mathfrak{h}(T,V)\rangle'' = \frac{\partial^2\langle \mathfrak{h}(T,V)\rangle}{\partial T^2}$, which reaches its extrema at thetemperatures $T_1(V)$ and $T_2(V)$. The width of the transition region can simply be defined by the gap between these two temperatures, that is, $\delta T(V) = T_2(V) - T_1(V)$. The variations of $\langle \mathfrak{h}(T,V)\rangle''$ with temperature for various sizes are illustrated in Fig. 3, from which it can clearly be seen that the gap between the two extrema decreases with increasing volume.

Finally from the obtained results for the finite size response functions, four finite-size effects can be observed:

- the rounding effect of the discontinuities,
- the smearing effect of the singularities,
- the shifting effect of the transition point,
- the broadening effect of the transition region,

and to study quantitatively the volume dependence of these effects, a numerical scaling analysis is carried out, which will be presented in the next section.

4 Finite-size scaling analysis

4.1 Finite-size scaling

In statistical mechanics, it is known that only in the thermodynamic limit are phase transitions characterized by the appearance of singularities in some second derivatives of the thermodynamic potential, such as the susceptibility and the specific heat. For a first-order phase transition, the divergences are δ-function singularities, corresponding to the

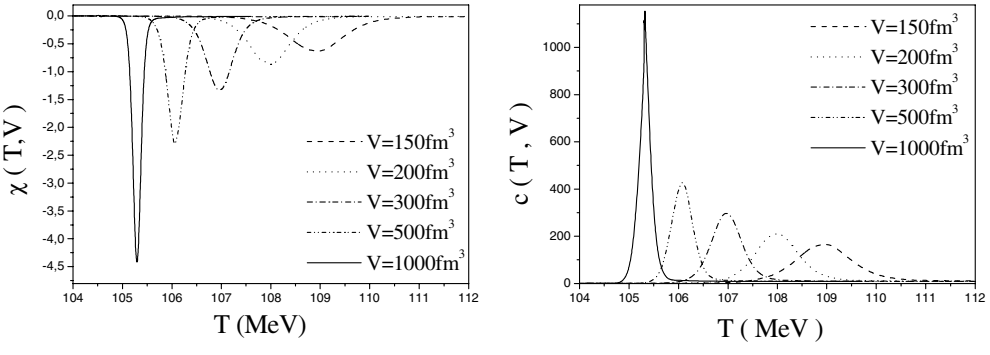

Fig. 2. Plot of (left) the susceptibility $\chi(T,V)$ and (right) the specific heat density $c(T,V)$, versus temperature for different system volumes

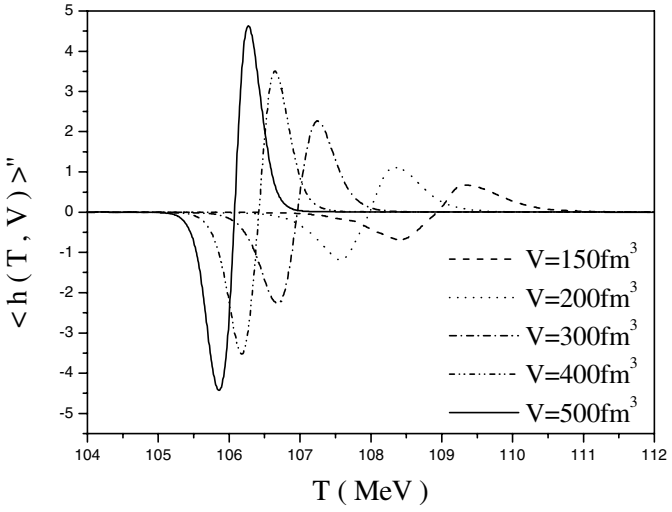

Fig. 3. Plot of the second derivative of the order parameter $\langle \mathfrak{h}(T,V)\rangle'' = \frac{\partial^2 \langle \mathfrak{h}(T,V)\rangle}{\partial T^2}$ versus temperature for different system volumes

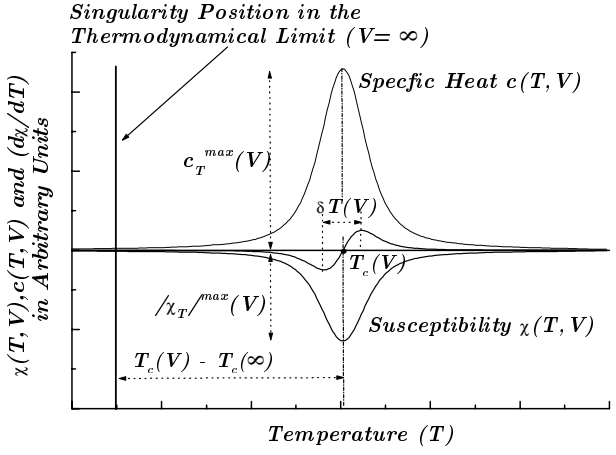

Fig. 4. Illustration of the finite-size behavior of the susceptibility $\chi\,(T,V)$, the specific-heat density $c\,(T,V)$ and the second derivative of the order parameter $\partial\chi/\partial\ T$

finite discontinuities in the first derivatives of the thermodynamic potential, while for a second-order phase transition the singularity has a power-law form. For the QCD model of the thermal deconfinement phase transition studied in this work, δ-singularities appear in the susceptibility χ and in the specific heat density c in the thermodynamic limit. In finite volumes, these δ-functions are found to be smeared out into finite peaks. To the finite-size effects, four useful characteristic quantities can be associated as illustrated on Fig. 4: the maxima of the peaks of the susceptibility $\chi_T^{\max}(V)$ and the specific heat density $c_T^{\max}(V)$, the shift of the transition temperature $\tau_T(V) = T_c\,(V) - T_c\,(\infty)$ and the width of the transition region $\delta T\,(V)$. Each of these quantities can be considered as a signature which may anticipate the behavior in the thermodynamic limit, and is expected to present a scaling behavior described by a power law of the volume $V = L^d$, where L is the linear extension of the volume and d the space dimensionality, characterized by a *scaling critical exponent*. For a first-order phase transition, the set of power laws is:

$$\begin{cases} \chi_T^{\max}(V) \sim V^{\gamma}\,, \\ c_T^{\max}(V) \sim V^{\alpha}\,, \\ \delta T\,(V) \sim V^{-\theta}\,, \\ \tau_T(V) = T_c\,(V) - T_c\,(\infty) \sim V^{-\lambda}\,, \end{cases} \tag{21}$$

and it has been shown in the FSS theory [18–21] that in this case, the scaling exponents θ, λ, α and γ are all equal to unity, and it is only the dimensionality which controls the finite-size effects.

At a second-order phase transition, the correlation length diverges as $\xi \propto |T - T_c|^{-\nu}$, and this we predict the same power-law behavior as for a first-order transition, but with different scaling critical exponents, usually given as:

$$\begin{cases} \chi_T^{\max}(V) \sim V^{\gamma/d\nu}\,, \\ c_T^{\max}(V) \sim V^{\alpha/d\nu}\,, \\ \delta T\,(V) \sim V^{-1/d\nu}\,, \\ \tau_T(V) = T_c\,(V) - T_c\,(\infty) \sim V^{-1/d\nu}\,. \end{cases} \tag{22}$$

The values of the scaling critical exponents may then give an indication on the order of a phase transition and are usually used as a criterion for the determination of this latter [9, 11, 22, 23].

4.2 Numerical determination of the scaling critical exponents for the thermal deconfinement phase transition

In the following, we use a FSS analysis to recover the scaling exponents θ, λ, α and γ for the thermally driven deconfinement phase transition. For this purpose, we proceed by studying the behavior of the response-function maxima, their rounding as well as the shift of the effective transition temperature with varying volume. Let us note that the determination of the location of the maxima of the finite-size peaks as well as their heights is done in a numerical way, and this yields a systematic error, which is estimated and given for the determined scaling exponents.

4.2.1 Susceptibility, specific heat and smearing scaling exponents

The data of the maxima of the rounded peaks of the susceptibility $\mid \chi_T \mid^{\max}(V)$ and the specific heat density $c_T^{\max}(V)$ are plotted versus volume in Fig. 5 (left) and Fig. 5 (right),respectively, and their linearity with V can clearly be noted. A numerical parameterization with the power-law forms: $\mid \chi_T \mid^{\max}(V) \sim V^{\gamma}$ and: $c_T^{\max}(V) \sim V^{\alpha}$, gives the values of the susceptibility scaling exponent: $\gamma = 1.01 \pm 0.03$, and the specific-heat scaling exponent: $\alpha = 1.007 \pm 0.031$, where the associated errors are systematic.

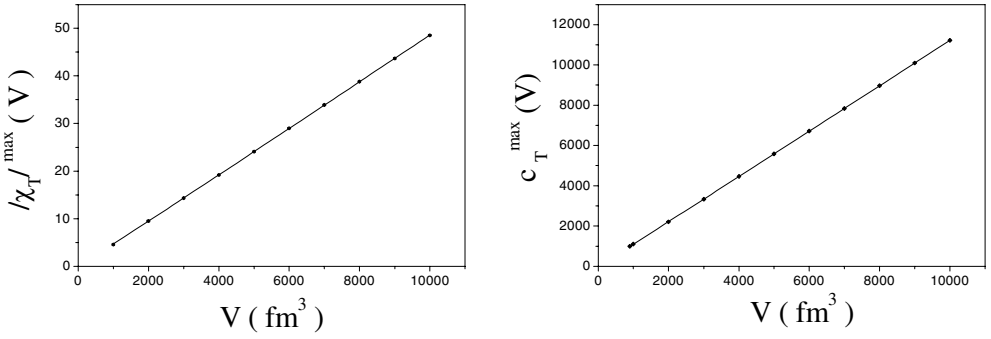

Fig. 5. Variation of (left) the susceptibility maxima $\mid \chi_T \mid^{\max}(V)$ and (right) the specific-heat density maxima ${c_T}^{\max}(V)$ with volume

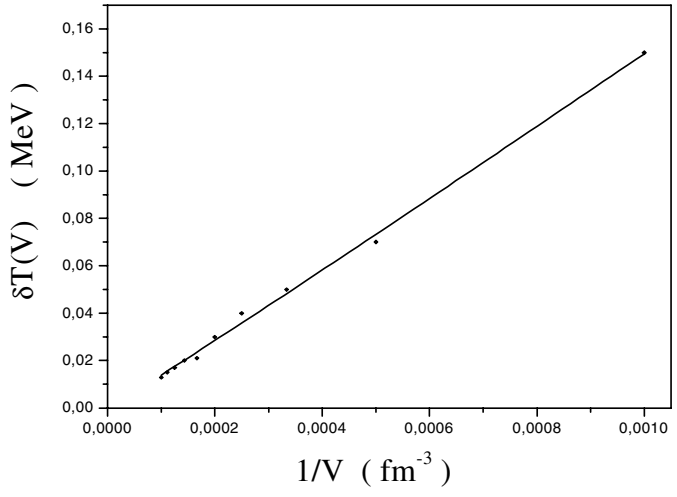

Fig. 6. Variation of the width of the temperature region over which the transition is smeared $\delta T(V)$ with inverse volume

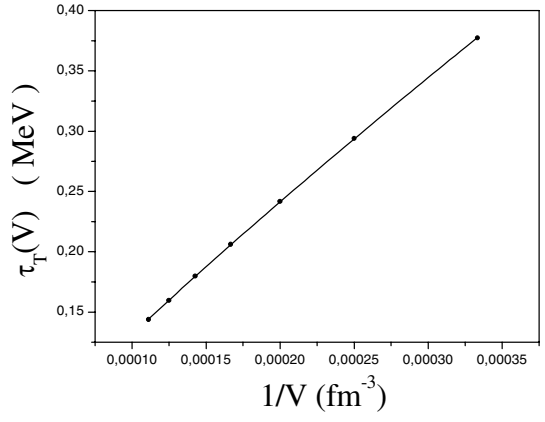

Fig. 7. Variation of the shift of the transition temperature $\tau_T(V)$ (from the maxima of $\chi(T,V)$ and $c(T,V)$) with inverse volume

Figure 6 illustrates the plot of the results of the width $\delta T(V)$ with the inverse of the volume, and their fit to the power-law form: $\delta T(V) \sim V^{-\theta}$. The obtained smearing scaling exponent is: $\theta = 1.03 \pm 0.03$.

4.2.2 The shift scaling exponent

For the study of the shift of the transition temperature $\tau_T(V) = T_c(V) - T_c(\infty)$, we need to locate the effective transition temperature in a finite volume $T_c(V)$. A way to define $T_c(V)$ is to locate the maxima of the rounded peaks of the susceptibility and the specific heat, shifted away from the true transition temperature $T_c(\infty)$. Results of the shift of the transition temperature obtained in this way are plotted in Fig. 7 versus inverse volume. The shift critical exponent obtained from a fit to the form: $\tau_T(V) \sim V^{-\lambda}$, is: $\lambda = 0.876 \pm 0.041$. Such a value $\neq 1$ suggests the contribution of non-leading terms in the expression of the volume variation of the shift. Different forms of the fit of $\tau_T(V)$, including additional terms with higher powers of V^{-1}, such as $A_1 V^{-\lambda} + A_2 V^{-2}$, and $A_1 V^{-\lambda} + A_2 V^{-2} + A_3 V^{-3}$, have been tested, and the obtained results show that effectively, the shift critical exponent λ increases from the value 0.876 and tends to 1, with a better χ^2. Other forms have been tested, where the value of the shift exponent has been fixed to 1, and finite-size correction terms have been included. In this case also, we note that we obtain a better χ^2 value with the presence of the non-leading terms.

4.2.3 The shift from the binder cumulant

Another way of locating $T_c(V)$ is to consider the fourth-order cumulant of the order parameter proposed in [3,19] and defined as:

$$B_4(T,V) = 1 - \frac{\langle \mathfrak{h}^4(T,V) \rangle}{3 \langle \mathfrak{h}^2(T,V) \rangle^2}, \tag{23}$$

which presents a minimum value at an effective transition temperature whose shift from the true transition temperature is of the order V^{-1} for a first-order transition. This cumulant is a finite-size scaling function [3,19,20,24,25], and has been proven to be a suitable indicator of the order of the transition in a finite volume.

The expression for $B_4(T,V)$ as function of the integral terms, for this case of the deconfinement transition, is after calculation:

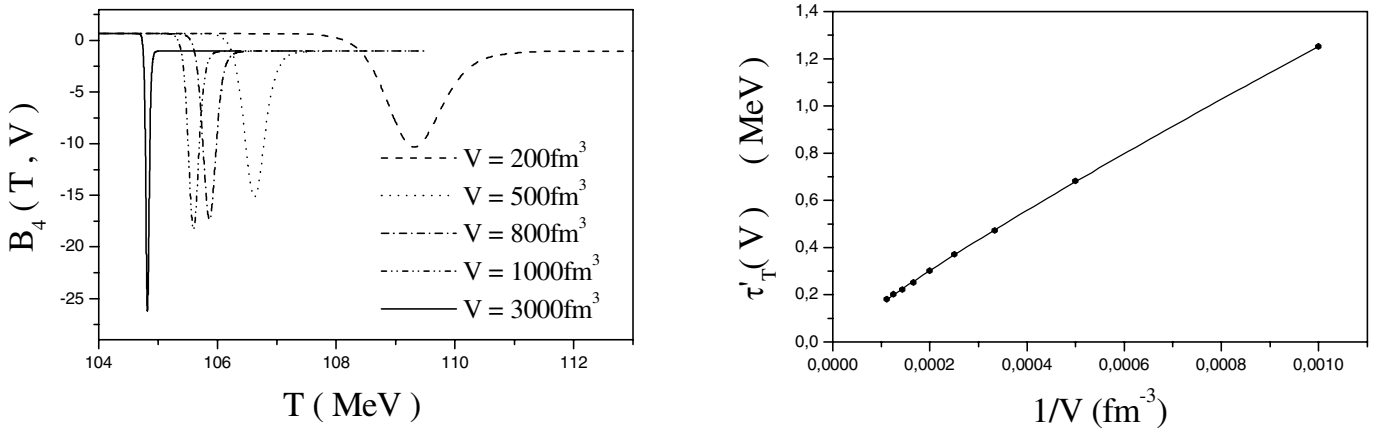

Fig. 8. Plot of the Binder cumulant $B_4(T,V)$ (left) versus temperature for different system volumes, and (right) variation of the shift of the transition temperature $\tau'_T(V)$ (from the minimum of $B_4(T,V)$) with inverse volume

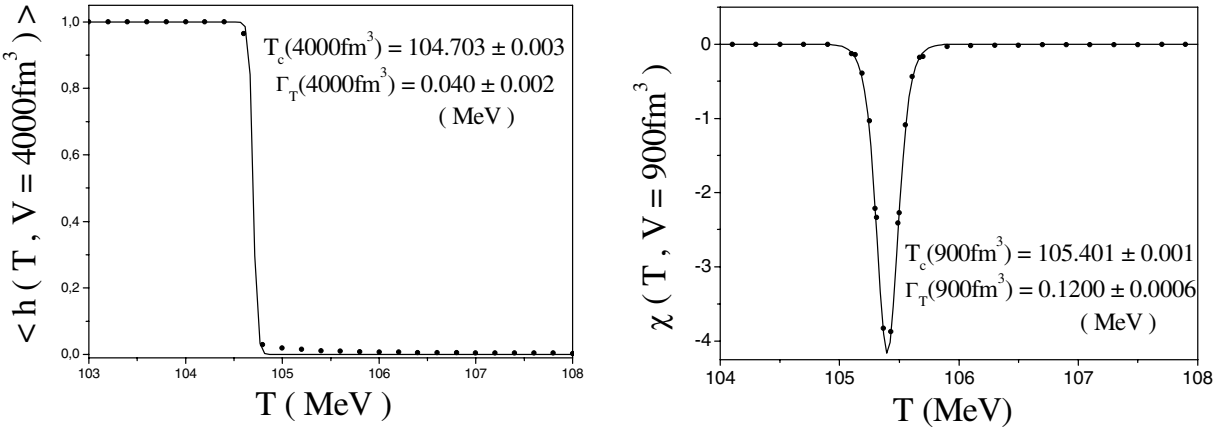

Fig. 9. Illustration of the fits of the order parameter to the form (26) at the volume $V = 4000 fm^3$, and of the susceptibility to the form (27) at the volume $V = 900\,\mathrm{fm}^3$

$$B_4(T,V) = 1 - \frac{(L_{11}-L_{01})(24(L_{15}-L_{05}-L_{04})-12L_{03}-4L_{02}-L_{01})}{3\,(2L_{13}-2L_{03}-2L_{02}-L_{01})^2}\,. \tag{24}$$

Figure 8 (left) illustrates the variations of the fourth cumulant of the order parameter with temperature for various volumes, and shows that the locations of the minima in finite sizes $T_{\min}(V)$ are shifted to higher values from $T_c(\infty)$. Data of the shift of the transition temperature obtained in this way are plotted in Fig. 8 (right) versus inverse volume, and the scaling shift critical exponent obtained from a fit to the form: $\tau'_T(V) = T_{\min}(V) - T_c(\infty) \sim V^{-\lambda'}$, is $\lambda' = 0.883 \pm 0.043$. In this case also, non-leading terms appear in the expression of $\tau'_T(V)$.

4.2.4 Parameterization of the order parameter and the susceptibility

Within the model used in this work, the order parameter in the limit of infinite volume being equal to 1 below the transition temperature and zero above, it can then be expressed in a simple way using the Heaviside step function as:

$$\langle \mathfrak{h}(T, V \longrightarrow \infty)\rangle = 1 - \Theta(T - T_c(\infty))\,. \tag{25}$$

Such a parameterization has been used in [26], for a similar case of a system of coexisting hadronic matter and QGP phases. Using one of the known mathematical representations of the smoothed step function $\Theta(T-T_c)$, the order parameter may then be expressed as:

$$\langle \mathfrak{h}(T,V)\rangle = \frac{1}{2}\left(1 - \tanh\left(\frac{T - T_c(V)}{\Gamma_T(V)}\right)\right), \tag{26}$$

where $T_c(V)$ is the effective transition temperature and $\Gamma_T(V)$ is the half-width of the rounded transition region, which leads to the susceptibility expression :

$$\chi(T,V) = \frac{-1}{2\Gamma_T(V)\ \cosh^2\left(\frac{T-T_c(V)}{\Gamma_T(V)}\right)}. \tag{27}$$

The parameterization choice (26) is the most accepted physically, and can be understood phenomenologically in the context of the double Gaussian peaks model where the obtained expressions of the order parameter and the susceptibility are very similar to (26) and (27) [3,9,27].

An illustration of such parameterizations of the order parameter at the volume $V = 4000\,\mathrm{fm}^3$, and the susceptibility at the volume $V = 900\,\mathrm{fm}^3$ are presented in Fig. 9

(left) and Fig. 9 (right), respectively, and the parameters $T_c(V)$ and $\Gamma_T(V)$ obtained from each fit are given.

The results for the width of the transition region and the shift of the transition temperature from the parameterizations of the order parameter and the susceptibility are fitted to power-law forms: ${\tau_T}^{\mathrm{fit}(1)}(V) \sim V^{-\lambda_1}$, ${\tau_T}^{\mathrm{fit}(2)}(V) \sim V^{-\lambda_2}$, $\delta T^{\mathrm{fit}(1)}(V) \sim V^{-\theta_1}$, and $\delta T^{\mathrm{fit}(2)}(V) \sim V^{-\theta_2}$ which give the scaling critical exponents: $\lambda_1 = 0.830 \pm 0.013$, $\lambda_2 = 0.857 \pm 0.006$, $\theta_1 = 0.990 \pm 0.015$, and $\theta_2 = 1.032 \pm 0.003$.

5 Conclusion

Our model has shown the influence of the finiteness of the system size on the behavior of some response functions in the vicinity of the transition point. The sharp transition observed in the thermodynamical limit, signaled by discontinuities in the order parameter and in the energy density at a transition temperature $T_c(\infty)$, is rounded off in finite volumes, and the variations of these thermodynamic quantities are perfectly smooth on the whole range of temperature. The delta function singularities appearing in the first derivatives of these discontinuous quantities, i.e., in the susceptibility and specific heat density, are then smeared out into finite peaks of widths $\delta T(V)$. The maxima of these peaks occur at effective transition temperatures $T_c(V)$ shifted away from the true transition temperature $T_c(\infty)$. An FSS analysis of the behavior of the maxima of the rounded peaks of the susceptibility $\chi_T^{\max}(V)$ and the specific heat density $c_T^{\max}(V)$, the width of the transition region $\delta T(V)$, and the shift of the effective transition temperature relative to the true one $\tau_T(V) = T_c(V) - T_c(\infty)$, shows their power-law variations with the volume characterized by the scaling critical exponents γ, α, θ, and λ, respectively. Numerical results for these scaling exponents are obtained and are in good agreement with our analytical results: $\gamma = \alpha = \theta = \lambda = 1$ obtained in [28], except for the shift critical exponent which slightly deflects from the analytical value 1. This may be due, on one hand, to the difficulty of locating accurately the peaks of χ, c and B_4, especially in the case of large volumes for which the peaks become very sharp and, on the other hand, to the non-leading terms which contribute to the expression of $\tau_T(V)$. However, a first estimate of the scaling critical exponents for the thermal deconfinement phase transition within this model has been obtained, and our result expressing the equality between all scaling exponents and the space dimensionality is a consequence of the singularity characterizing a first-order phase transition and agrees very well with the predictions of the standard FSS theoretical approaches to a first-order phase transition [19, 21, 29–33] and with those obtained in a rather different and rigorous way, generalizing the FSS description of a first-order phase transition [34]. Also, we note the good agreement with the results of calculations using Monte Carlo methods in both lattice QCD [8, 35–38] and other models in statistical physics [22, 39, 40].

References

1. C.N. Yang, T.D. Lee, Phys. Rev. **87**, 404 (1952); Phys. Rev. **87**, 410 (1952)
2. J. Imry, Phys. Rev. B **21**, 2042 (1980)
3. K. Binder, D.P. Landau, Phys. Rev. B **30**, 1477 (1984)
4. C. Spieles, H. Stöcker, C. Greiner, Phys. Rev. C **57**, 908 (1998)
5. A. Chodos et al., Phys. Rev. D **9**, 3471 (1974); J. Cleymans, R.V. Gavai, E. Suhonen, Phys. Rep. **130**, 217 (1986)
6. D.P. Landau, R.H. Swendsen, Phys. Rev. Lett. **46**, 1437 (1981); F.R. Brown et al., Phys. Rev. Lett. **61**, 2058 (1988); P. Bacilieri et al., Phys. Rev. Lett. **61**, 1545 (1988); J.F. McCarthy, Indiana University Preprint IUHET 164 (1989); M. Fukugita et al., Phys. Rev. Lett. **63**, 1768 (1989); P. Bacilieri et al., Phys. Lett. B **220**, 607 (1989); R.V. Gavai, F. Karsch, B. Petersson, Nucl. Phys. B **322** , 738 (1989); M. Fukugita, Phys. Rev. Lett. **63**, 13 (1989); M. Fukugita et al., Nucl. Phys. Proc. Suppl. **17**, 204 (1990); S. Gupta et al., Nucl. Phys. B **329**, 263 (1990); M. Fukugita et al., J. Phys. A **23**, L561–L566 (1990)
7. M. Fukugita, Nucl. Phys. Proc. Suppl. **9**, 291 (1989)
8. N.A. Alves et al., Phys. Rev. Lett. **64**, 3107 (1990)
9. H. Meyer-Ortmanns, Rev. Mod. Phys. **68**, 473 (1996)
10. F. Karsch, Nucl. Phys. A **590**, 367c–382c (1995); Nucl. Phys. A **698**, 199c–208c (2002); F. Karsch et al., Nucl. Phys. (Proc. Suppl.) B **94**, 411–414 (2001); Nucl. Phys. B **605**, 579–599 (2001)
11. M. Fukugita, RIFP-703 (June 1987); M. Fukugita et al., Phys. Rev. Lett. **58**, 2515 (1987); UTHEP-168 (August 1987); Phys. Rev. Lett. **60**, 178 (1988); M. Fukugita, Nucl. Phys. Proc. Suppl. **4**, 105 (1988), M. Fukugita, A. Ukawa, Phys. Rev. D **38**, 1971 (1988); R.V. Gavai et al., Phys. Lett. B **200**, 137 (1988); F.R. Brown et al., Phys. Rev. Lett. **65**, 2491 (1990); S. Aoki et al. (JLQCD Coll.), Nucl. Phys. B **63**A–C, 403 (1998), **60**A, 188 (1998); B. Lucini et al., Phys. Lett. B **545**, 197 (2002); P. Cea et al., Nucl. Phys. (Proc. Suppl.) B **129–130**, 751 (2004)
12. K. Redlich, L. Turko, Z. Phys. C **5**, 201 (1980); L.Turko, Phys. Lett. B **104**, 153 (1981)
13. H.-Th. Elze, W. Greiner, J. Rafelski, Phys. Lett. B **124**, 515 (1983); Z. Phys. C **24**, 361 (1984); H.-Th. Elze, W. Greiner, Phys. Lett. B **179**, 385 (1986)
14. A. Tounsi, J. Letessier, J. Rafelski, hep-ph/9811290
15. M.G. Mustafa, D.K. Srivastava, B. Sinha, Eur. Phys. J. C **5**, 711 (1998); nucl-th/9712014
16. J. Madsen, D.M. Jensen, M.B. Christiansen, Phys. Rev. C **53**, 1883 (1996)
17. G. Yezza, Magister thesis in theoretical physics, Ecole Normale Supérieure, Kouba, Algiers (March 2002)
18. M.E. Fisher, A.N. Berker, Phys. Rev. B **26**, 2507 (1982).
19. M.S. Challa, D.P. Landau, K. Binder, Phys. Rev. B **34**, 1841 (1986)
20. K. Binder, D.W. Heermann, Monte Carlo Simulations in Statistical Physics, (Springer-Verlag, 1988, 2nd ed. 2002)
21. V. Privman, M.E. Fischer, J. Stat. Phys. **33**(2), 385 (1983)
22. M. Fukugita et al., KEK-TH-233 (1989)
23. M. Henkel, Conformal Invariance and Critical Phenomena, (Springer-Verlag, 1999)
24. K. Binder, Rep. Prog. Phys. **60**, 487 (1997)
25. D.P. Landau, K. Binder, A Guide to Monte Carlo Simulation in Statistical Physics, (Cambridge University Press, 2000)

26. J.P. Blaizot, J.Y. Ollitraut, Phys. Rev. D **36**, 916 (1987)
27. K. Binder, Phys. Rev. Lett. **47**, 693 (1981); Z. Phys. B **43**, 119 (1981)
28. M. Ladrem, A. Ait-El-Djoudi, G. Yezza, communication at the international conference 'Quark Confinement and the Hadron spectrum', held in Gargnano, Italy, 10–14 September 2002
29. M.N. Barber, in Phase Transitions and Critical Phenomena, Vol. 8, edited by C.Domb, J.L. Lebowitz (Academic, New York, 1983) 145
30. K. Binder, Ferroelectrics **73**, 43 (1987); in Computational Methods in Field Theory, H. Gausterer, C.B. Lang, (Eds. Springer, Berlin 1992) 59
31. W. Janke, Phys. Rev. B **47**, 14757 (1993)
32. K. Vollmayr, J.D. Reger, M. Scheucher, K. Binder, Z. Phys. B **91**, 113 (1993)
33. J.G. Brankov, D.M. Danchev, N.S. Tonchev, Theory of Critical Phenomena in Finite-Size Systems – Scaling and Quantum Effects, (World Scientific, 2000)
34. C. Borgs, R. Kotecky, J. Stat. Phys. **61**, 79 (1991); C. Borgs, R. Kotecky, S. Miracle-Solé, J. Stat. Phys. **62**, 529 (1991)
35. B. Beinlich, F. Karsch, E. Laermann, A. Peikert, Eur. Phys. J. C **6**, 133 (1999)
36. K. Bitar et al., Nucl. Phys. B **337**, 245 (1990)
37. R.V. Gavai, Nucl. Phys. Proc. Suppl. **106**, 480 (2002); Nucl. Phys. B **633**, 127 (2002)
38. M. Mathur, R.V. Gavai, Nucl. Phys. B **448**, 399 (1995)
39. D. Loison, K.D. Schotte, Eur. Phys. J. B **5**, 735 (1998); B **14**, 125 (2000)
40. O. Dillmann, W. Janke, K. Binder, J. Stat. Phys. **92**, 1/2, 57 (1998)

FINITE SIZE EFFECTS ON THE DECONFINEMENT PHASE TRANSITION TO A COLOR-SINGLET QGP

By

Amel AIT-EL-DJOUDI

Ecole Normale Supèrieure-Kouba

A Thesis Submitted to the Faculty of Science

in partial fulfillement of the requirements for the degree of

DOCTOR

Department of Physics

University of Mouloud Mammeri, Tizi-Ouzou

Jury:

. Omar Lamrous;	Professor;	Tizi-Ouzou University;	Chairman
. Madjid Ladrem;	Professor;	ENS-Kouba, Algiers;	Advisor
. Patrick Aurenche;	Research Director at CNRS; LAPTH, Annecy;		Examiner
. Abdessamad Abada;	Professor;	ENS-Kouba, Algiers;	Examiner
. Abdelhamid Amghar;	Professor;	Boumerdes University;	Examiner

Dedication

To my Father and my Mother

Acknowledgement

First of all, Praise to ALLAH the almighty who helped me to accomplish this work that I have done for his sake.

I would like to thank my advisor, Prof. M. Ladrem, for the help he provided me with, during his supervision of this work. I would like also to thank all members of the jury, Profs. O. Lamrous, A. Abada, P. Aurenche and A. Amghar for considering this thesis and taking the time to read the manuscript and enrich it with their suggestions which are welcome.

I take here the time to thank all people who supported me and contributed, in one way or an other, to the success of this work. A particular thank is to my parents who greatly helped me with their continuous presence and support, to my grand-parents for their permanent care that this work be successfully achieved, to my brothers and my sister for their help and support, and to all my friends.

A great thank is to my husband for his assistance and his patience, and for the time he gave me -likewise our son- during the achievement of this work.

Abstract

This thesis deals with the deconfinement phase transition of a finite system, using a simple model of coexisting hadron and QGP phases in a finite volume. The equations of state of infinite matter of the two phases are first used, and the finite-size effects on the deconfinement phase transition are investigated by probing the behavior of some useful quantities near the transition. It turns out that in a finite size system, all singularities occurring in the thermodynamic limit are smeared out and the transition is perfectly smooth.

Secondly, the color-singletness requirement is imposed to the QGP phase, to satisfy the color confinement property of QCD, introducing an additional finite-size effect, and leading to a shift of the transition point. A finite size scaling analysis is then carried out to determine the scaling critical exponents, characterizing the scaling behavior when approaching the thermodynamic limit ($V \longrightarrow \infty$), both in analytical and numerical ways.

Since hadrons are not pointlike because of their composite character, they should be treated as extended particles. To account for this, we then consider the excluded volume effects and examine their effects on the deconfinement phase transition.

The first chapter of this thesis is devoted to a review of the physics of phase transitions, as well as their classification, and the second one overviews the phase transitions

in finite systems.

In the third chapter, we study the deconfinement phase transition in a finite system within the phase coexistence model. Equations of state of infinite matter are used for a hadronic gas of pions and for a QGP consisting of gluons and massless quarks, then the color-singletness condition is implemented using the projection method. An approximate color-singlet partition function of the QGP is derived within the saddle point approximation and is used in a first step to calculate mean values of physical quantities. The expressions of these latter with T, μ and V are obtained, in these two cases, and both temperature-driven and density-driven deconfinement phase transitions are then studied, at fixed chemical potential and temperature respectively. In a second step, the exact integral expression of the color-singlet partition function of the QGP is used to accurately determine mean values of several quantities probing the phase transition in a finite volume, without explicitly calculating the color-singlet partition function itself.

The fourth chapter is dedicated to the numerical determination of the scaling critical exponents characterizing the studied phase transition, by the mean of a finite size scaling analysis.

In the fifth chapter, the excluded volume correction is considered for the hadronic phase, and his effects on the deconfinement phase transition are investigated.

Last, the obtained results are discussed and compared to results of other models and approaches.

Contents

List of Figures

List of Tables

Introduction

It is well established that QCD at finite temperature exhibits a typical behavior of a system with a phase transition. At sufficiently high temperatures and/or densities, quarks and gluons are no more confined into hadrons; strongly interacting matter seems to undergo a phase transition from hadronic state to what has been called the "Quark-Gluon Plasma" (QGP). This is logically a consequence of the quark-parton level of the matter structure and of the dynamics of strong interactions described by the QCD theory. The occurrence of this phase transition is important from a conceptual point of view, as it implies the existence of a novel state of matter, which was present in the early universe up to times $\sim 10^{-5}s$, and which could occur in the core of heavy neutron stars. The only available and experimental way to study the QCD deconfinement phase transition is to try to create in the laboratory, by ultra-relativistic heavy ion collisions, conditions similar to those in the early moments of the universe, right after the Big Bang.

If ever the QGP is created in ultra-relativistic heavy ion collisions, the volume within which the eventual formation would take place would certainly be finite. Also, in lattice QCD studies, the scale of the lattice space volume is finite. This motivates the study of the finite size effects on the expected deconfinement phase transition from a Hadronic Gas (HG) phase to a QGP phase. These effects are certainly important

since statistical fluctuations in a finite volume may hinder a sharp transition between the two phases. Phase transitions are known to be infinitely sharp, signaled by some singularities, only in the thermodynamic limit [1]. In general, finite size effects lead to a rounding of these singularities as pointed out in [2, 3]. However, even in such a situation, it is possible to obtain information on the critical behavior. Large but finite systems show a *universal* behavior called "Finite-Size Scaling" (FSS), allowing to put all the physical systems undergoing a phase transition in a certain number of universality classes. The systems in a given universality class display the same critical behavior, meaning that certain dimensionless quantities have the same values for all these systems. *Critical exponents* are an example of these universal quantities.

This thesis is devoted to the study of the finite size behavior for the deconfinement phase transition. For this purpose, we use a simple QCD model described in [4], based on the standard MIT bag model [5], and on the coexistence of hadronic and QGP phases in a finite system of volume V. The equations of state of the two phases are then used, and mean values of useful thermodynamic quantities can be calculated.

Additionally, we implement the color charge confinement property by requiring to the QGP phase to be a colorless object in the color space. The color-singlet partition function of the QGP is derived using the group theoretical projection technique formulated by Turko and Redlich [6], but can not be exactly determined and is usually calculated within the saddle point approximation in the limit $V_{QGP}T^3 >> 1$ as in [7, 8, 9, 10, 11]. It turns out, in our case, that the use of the obtained approximated partition function for the calculation of a mean value within the definition of our model, has as a consequence the absence of the deconfinement phase transition [12]. This is due to the fact that the approximation used for the calculation of the color-singlet partition

function breaks down at $V_{QGP}T^3 << 1$, and this limit is attained in our case. This has been noted in further works in which additional approximations have been used to carry out calculations, as in [4, 9]. We propose in the following a method which allows us to accurately calculate physical quantities describing well the deconfinement phase transition at finite volumes within the QCD model chosen, avoiding then the problem arising at $V_{QGP}T^3 << 1$ and without any approximation. We proceed by using the exact definition of the color-singlet partition function for Z_{QGP} in the definition of the mean value of a physical quantity. A first analytical step in the calculation of the mean value is then achieved, and an expression with integral coefficients is obtained. The double integrals are then carried out with a suitable numerical method at each value of temperature and volume, and the behavior of the physical quantity of the finite system can so be obtained on the whole range of temperature, for various volumes, without any restriction. Afterwards, scaling critical exponents characterizing the scaling behavior of some quantities are determined using a numerical FSS analysis.

Since hadrons are not pointlike, they should be treated as extended particles. To account for this, we then consider the excluded volume effects and examine their influence on the deconfinement phase transition.

This thesis is organized as follows. After the present introduction, the first chapter is mainly an overview of the physics of phase transitions, and the standard classification existing in literature. Besides, we have tried to achieve a more general classification of phase transitions.

In the second chapter, phase transitions in finite systems are reviewed. Finite-size effects are examined as well as finite-size scaling.

In the third chapter, we study the deconfinement phase transition in a finite system

within the phase coexistence model. Equations of state of infinite matter are first used for a hadronic gas of pions and for a QGP consisting of gluons and massless quarks, and some physical quantities are studied for both temperature and density driven deconfinement phase transition, since their expressions with T and μ are obtained [13, 14]. Then, the color-singletness requirement is implemented in the partition function of the QGP using the projection method. An approximate color-singlet partition function of the QGP has been derived within the saddle point approximation and used in a first step, in our works [15, 16], to calculate mean values of thermodynamical quantities. Secondly, the exact integral expression of the color-singlet partition function of the QGP is used to accurately determine mean values of several quantities probing the phase transition in a finite volume, without explicitly calculating the color-singlet partition function itself.

The fourth chapter is dedicated to the numerical determination of the scaling critical exponents characterizing the studied phase transition, by the mean of a finite size scaling analysis.

In the fifth chapter, the excluded volume correction is implemented for the hadronic phase, and their effects on the deconfinement phase transition are investigated.

Last is a discussion of the obtained results and a conclusion to our work.

Chapter 1

General Study of Phase Transitions

1.1 Introduction

The study of the physics of phase transitions phenomena occurring in nature is considered to be a subject of great interest to physicists. It is easy to understand the importance of this subject because firstly the list of systems exhibiting interesting phase transitions continues to expand, including the Universe itself, and secondly the theoretical framework of equilibrium statistical mechanics has found applications in very different areas of physics like string field theories, elementary particle physics, physics of the chaos, condensed matter ... etc.

Phase transitions are abrupt changes in the global behavior and in the qualitative properties of a system when certain parameters pass through particular values. Technically, phase transitions are characterized by the appearance of singularities in some thermodynamic quantities, in the thermodynamical limit where the volume V and the number of particles N go to infinity, while the density $\rho = \frac{N}{V}$ remains constant. That is, at the transition, some global behavior is not analytic in the infinite volume limit.

Examples of phase transitions are:

- The transitions between the solid, liquid, and gaseous phases (evaporation, boiling, melting, freezing, sublimation, etc.).
- The transition between the ferromagnetic and paramagnetic phases of magnetic materials at the Curie point.
- The emergence of superconductivity in certain metals when cooled below a critical temperature.
- Quantum condensation of bosonic fluids, such as Bose-Einstein condensation and the superfluid transition in liquid helium.
- The breaking of symmetries in the laws of physics during the early history of the universe as its temperature cooled.

In this chapter, we want to give an overview on the physics of phase transitions, and the related features. We'll look carefully at how the thermodynamic variables behave close to the transition point, in order to compare the behavior at first- and higher-order transitions, and to define the critical exponents. The QCD phase transition is also reviewed since it is subject of our study in this thesis, as well as some results of lattice QCD.

1.2 Review of Some Useful Thermodynamic Functions

The order of a phase transition is one of the basic thermodynamic classifications. It concerns the thermodynamic potential and its derivatives at the transition. In Tables (1.1) and (1.2), we recall the thermodynamic formulas for a magnet and a fluid [15], where $\beta = \frac{1}{T}$ with the units chosen as: $k_B = \hbar = c = 1$.

First derivatives of the physical potential (the free energy for the fluid system) with respect to T, H or V lead to the internal energy U, the entropy S, the magnetization M or the pressure P, according to the equations in Tables (1.1) and (1.2). On the second level of derivatives, we have the specific heat C at constant H or M (respectively at constant V or P for a fluid) and the isothermal susceptibility χ_T for a magnet (respectively the isothermal compressibility κ_T for a fluid).

In the infinite volume limit, a phase transition is signalled by a singularity (in the sense of non analyticity) in some thermodynamic function. On whether a discontinuity occurs in one of the first derivatives or of the second or higher derivatives of the thermodynamical potential Ω, depends the order of the transition and the class to which the phase transition belongs. But before enumerating the different classes of phase transitions, let us introduce in the following a characteristic quantity of the transition representing the main qualitative differences between the various phases, whose evolution allows the determination of the nature of the phase transition, namely *The Order Parameter.*

Thermodynamic variables for a magnet

First law: $dU = TdS - MdH$

Partition function

$$Z(T,H) = \sum_r e^{-\beta E_r}$$

$$\downarrow$$

Free energy

$$F = -T \ln Z$$

$$\swarrow \qquad \downarrow \qquad \searrow$$

Internal energy	*Entropy*	*Magnetization*
$U = \dfrac{-\partial \ln Z}{\partial \beta}$	$S = -\left(\dfrac{\partial F}{\partial T}\right)_H$	$M = -\left(\dfrac{\partial F}{\partial H}\right)_T$
$\downarrow$	$\downarrow$	$\downarrow$
Specific Heat (constant H)	*Specific Heat (constant $X = H, M$)*	*Isothermal susceptibility*
$C_H = \left(\dfrac{\partial U}{\partial T}\right)_H$	$C_X = T\left(\dfrac{\partial S}{\partial T}\right)_X$	$\chi_T = \left(\dfrac{\partial M}{\partial H}\right)_T$

Table 1.1: Thermodynamic variables for a magnetic system

Thermodynamic variables for a fluid

First law: $dU = TdS - PdV$

Partition function

$$Z(T,H) = \sum_r e^{-\beta E_r}$$

$$\downarrow$$

Free energy

$$F = -T \ln Z$$

$$\swarrow \qquad \downarrow \qquad \searrow$$

Internal energy	*Entropy*	*Pressure*
$U = \dfrac{-\partial \ln Z}{\partial \beta}$	$S = -\left(\dfrac{\partial F}{\partial T}\right)_V$	$P = -\left(\dfrac{\partial F}{\partial V}\right)_T$
$\downarrow$	$\downarrow$	$\downarrow$
Specific Heat (constant V)	*Specific Heat (constant $X = V, P$)*	*Isothermal compressibility*
$C_V = \left(\dfrac{\partial U}{\partial T}\right)_V$	$C_X = T\left(\dfrac{\partial S}{\partial T}\right)_X$	$\kappa_T = -\dfrac{1}{V}\left(\dfrac{\partial V}{\partial P}\right)_T$

Table 1.2: Thermodynamic variables for a fluid system

1.3 Order Parameter of a General x-driven phase transition

Thermodynamical systems can exist in various stable homogeneous states (phases) which might differ in their structure, symmetry, order and dynamics. We represent this stability by the presence of an order in the system. Any modification occurring in one parameter can lead to a macroscopic change in the state and alter its stability, and as a consequence there is a wholesale reorganization of matter, even locally. Then, the system undergoes an abrupt change from one phase to another, called a phase transition, whose signature is a singularity or discontinuity of some observable physical properties. A first mathematical description of phase transitions was given by Gibbs [16] who characterized a phase transition by a point of non-analyticity in one or more thermodynamic functions. The apparition of a phase transition is nowadays interpreted as coming from the strong fluctuations of the system close to the critical point. At the critical point, the system exhibits a singular behavior and the phase transition is known as a critical phenomenon. Kramers was the first who suggested that the singular behavior only appears when the thermodynamic limit is taken (the volume V and the number of particles N go to infinity, with a fixed density $\rho = \frac{N}{V}$). This view was demonstrated theoretically through the famous work of Lee and Yang published in 1952 [17].

If we consider a phase transition between two different phases, we have certainly one of the phases as statistically more ordered (Ordered Phase) than the other (Disordered Phase). In an other sense, we can speak about a disorder-order phase transition which results from the loss of stability of the disordered (parent) phase. The stability is

Transition	Order Parameter $\langle\mathcal{O}\rangle$
Ferromagnetic Transition	Spontaneous Magnetization
Water Gas-Liquid Transition	Density Difference between Liquid and Gas
Liquid Crystal Transition	Degree of Orientational Order
Superconducting Transition	Energy Gap between the Ground State and the Spectrum of Single-Particle Excitations

Table 1.3: Order parameters of some phase transitions

restored by a distortion of the parent phase and in this way a distorted (ordered) phase is created. The most useful function generally used to characterize this order is a some appropriate thermodynamical quantity which has a non-vanishing value in the ordered phase and a zero value in the disordered phase. We commonly call this quantity "*Order Parameter*", since its value reflects the strength and kind of ordering in the system, and we'll note it $\mathcal{O}$ in the following. Then by definition:

$$\begin{cases} \langle\mathcal{O}\rangle = \langle\mathcal{O}\rangle^{+} & \text{, the system is in an ordered phase} \\ \langle\mathcal{O}\rangle = \langle\mathcal{O}\rangle^{-} < \langle\mathcal{O}\rangle^{+} & \text{, the system is in a disordered phase} \end{cases}$$

in which $\langle ... \rangle$ means the statistical average.

An order parameter may be a scalar quantity or may be a multicomponent (or even complex) quantity and is defined differently in different kinds of physical systems. We give in Table (1.3) some examples of order parameters as defined in special known systems [18].

In both experimental and numerical Monte Carlo studies, a complete study of the behavior of a well chosen order parameter $\langle\mathcal{O}\rangle$ at the phase transition is usually a key to determine the nature of the phase transition and gives a good way to calculate its most important thermodynamical properties. When studying the phase transition, we need then to define the varying thermodynamical parameter x (temperature (T), magnetc field (H), chemical potential (μ), ...) whose change may cause the phase

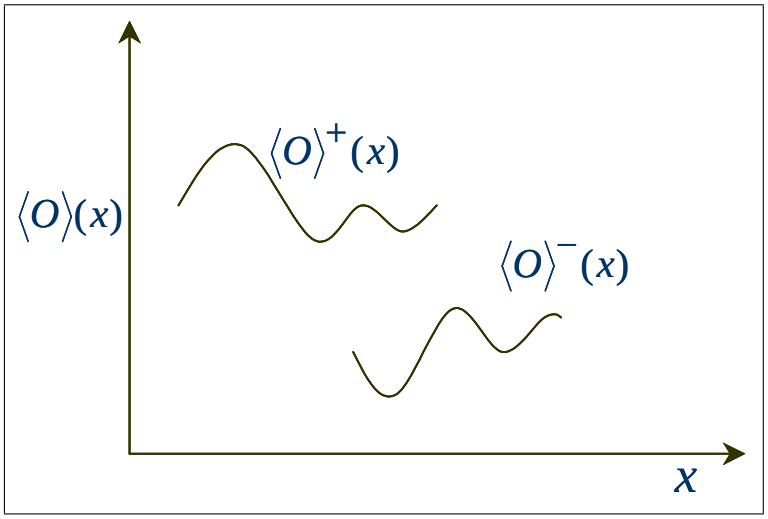

Figure 1.1: Evolution of the order parameter from the ordered phase to the disordered phase as a function of the thermodynamic $x-$variable driving the phase transition.

transition and then, on which it is interesting to study the dependence of $\langle\mathcal{O}\rangle$. We speak about an x-driven phase transition, and therefore we describe the phase transition with the help of diagrams where the order parameter is plotted against the respective thermodynamic parameter x, i. e., $\langle\mathcal{O}\rangle = \langle\mathcal{O}\rangle(x)$. Going from the ordered phase to the disordered phase, the evolution of $\langle\mathcal{O}\rangle(x)$ from $\langle\mathcal{O}\rangle^{+}(x)$ to $\langle\mathcal{O}\rangle^{-}(x)$, Fig. (1.1), can have mathematically different behaviors. According to this, we can distinguish three different classes of phase transitions, which have quite different qualitative properties near the transition point.

1.4 Standard Classification of Phase Transitions

Discontinuous or **First Order Phase Transitions** (**1st-OPT**) are characterized by a finite discontinuity in $\langle\mathcal{O}\rangle(x)$ (i. e. basically in anything except the free energy, which of course must be equal for the two phases at the transition point). The transition point

will be marked by a sudden and drastic jump from one phase ($\langle\mathcal{O}\rangle^{+}(x)$) to the other ($\langle\mathcal{O}\rangle^{-}(x)$) as illustrated in Fig. (1.2). For example, in the case of a ferromagnet there is a jump in the magnetization, if one passes through the transition temperature from the phase of broken symmetry to the symmetric phase, and the phase transition is then of first order.

Second Order Phase Transitions (**2^{nd}-OPT**), on the other hand, are characterized by a continuous but nonanalytic behavior of $\langle\mathcal{O}\rangle(x)$. A finite discontinuity appears in the first derivative of $\langle\mathcal{O}\rangle(x)$ as illustrated in Fig. (1.3). The transition to superconductivity without an external magnetic field is an example of phase transitions of this kind, where the discontinuity of the specific heat at T_c is due to a kink in the entropy. When the discontinuity in the first derivative of $\langle\mathcal{O}\rangle(x)$ becomes infinite as in Fig. (1.4), the phase transition is called a **continuous Phase Transition** (**c-PT**). Because of the characteristic shape of the first derivative of the order parameter in this case, such phase transitions are called **"$\lambda-$Transitions"**. An interesting example of such phase transitions is the transition to superfluidity in ^4He, in which the discontinuity in the specific heat is not due to a kink in the entropy but to a vertical tangent at T_c [19].

This is somewhat a resume of the Ehrenfest and Fisher classifications. The **Ehrenfest classification scheme** was the first attempt at classifying phase transitions, based on the degree of non-analyticity involved. Under this scheme, phase transitions were labelled by the lowest derivative of the thermodynamic potential that is discontinuous at the transition, such that is called of **n^{th}-Order** the phase transition for which there is a discontinuity at the **n^{th}-**order derivative of an appropriate thermodynamic potential. Though useful, Ehrenfest classification is flawed since it didn't account for

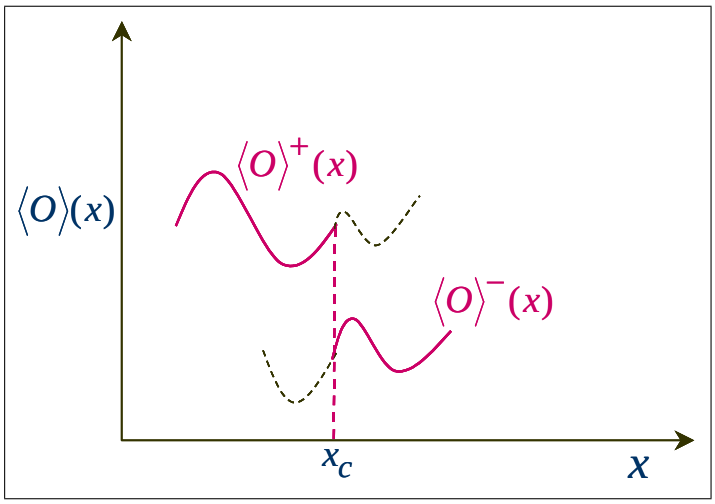

Figure 1.2: Behavior of the order parameter as a function of the thermodynamic $x-$variable driving the transition, for a first-order phase transition.

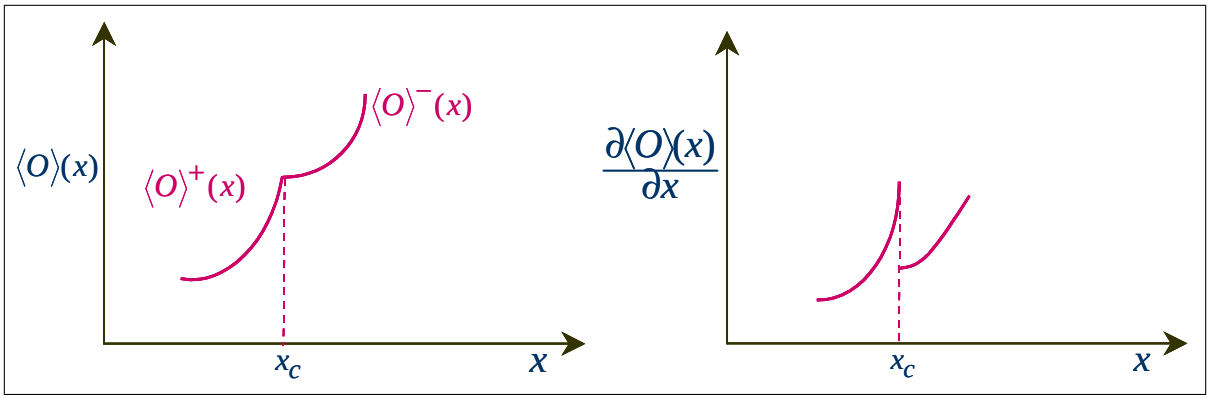

Figure 1.3: Behavior of the order parameter and its first derivative with respect to the thermodynamic $x-$variable driving the transition, near the critical point x_c for a second-order phase transition.

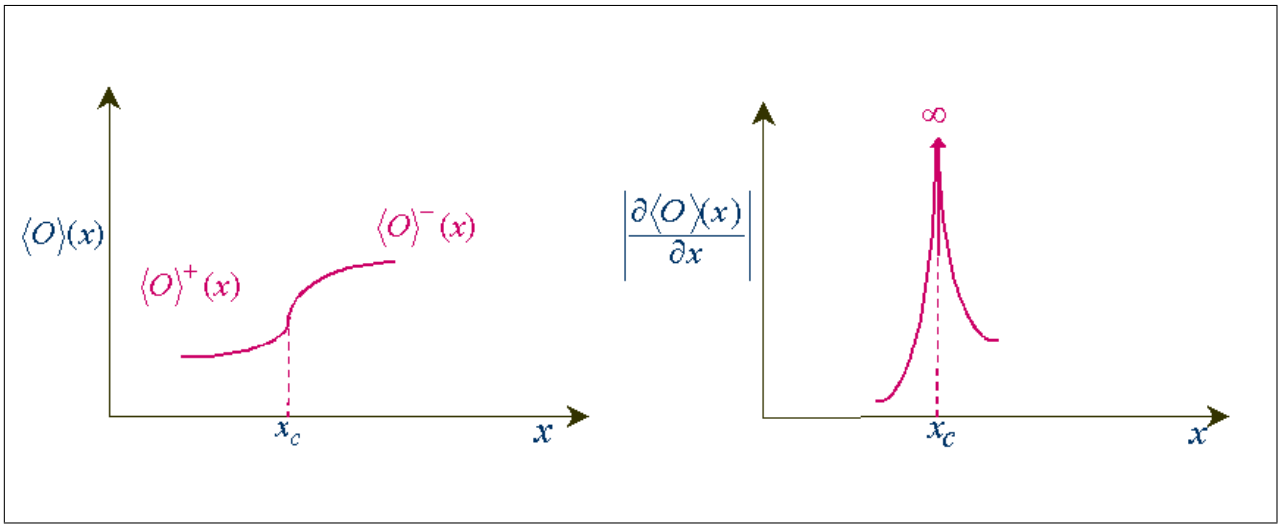

Figure 1.4: Behavior of the order parameter and its first derivative with respect to the thermodynamic $x-$variable driving the transition, near the critical point x_c for a $\lambda-$transition.

the case of a divergence in the derivatives of the thermodynamic potential. After this, a more complete classification which is **Fisher classification scheme** came, under which is denoted by **1st-Order phase transition** the case for which the **1st** derivative of the thermodynamic potential is discontinuous and by **"higher order phase transition"** or **"continuous phase transition"** the case for which the **1st** derivatives of the thermodynamic potential are continuous while the **2**nd derivatives are either discontinuous or infinitely divergent.

1.5 Mathematical description of general x-driven phase transitions and new approach to their classification

To achieve a more general classification of phase transitions, let us start from a general case of an x-driven phase transition described by an order parameter $\langle \mathcal{O} \rangle (x)$ having a behavior schematized in Fig. (1.2) in which we suppose a finite discontinuity at the transition point x_c . The parent phase is described by $\langle \mathcal{O} \rangle^{+} (x)$ and the final phase by $\langle \mathcal{O} \rangle^{-} (x)$. When the finite discontinuity becomes smaller getting close to zero, we can have a continuous Phase Transition (**c-PT)** case from the initial discontinuous Phase Transition (**d-PT)** case. This fact allows to consider the **d-PT** case as more general than the **c-PT** one. We can then write:

$$\begin{cases} \langle \mathcal{O} \rangle (x) = \langle \mathcal{O} \rangle^{-} (x) \ \text{ if } \ x \succ x_c \\ \langle \mathcal{O} \rangle (x) = \langle \mathcal{O} \rangle^{+} (x) \ \text{ if } \ x \prec x_c \ , \end{cases} \tag{1.1}$$

from which a formal analogy with the definition of the causal temporal green function as well known in the standard statistical quantum field theory is to be noted. Then by using the Heaviside step- function $\Theta(x)$, we rewrite eq. (1.1) in the compact form :

$$\langle \mathcal{O} \rangle (x) = [1 - \Theta(x - x_c)] \langle \mathcal{O} \rangle^{+} (x) + \Theta(x - x_c) \langle \mathcal{O} \rangle^{-} (x). \tag{1.2}$$

This formula will reveal a great importance in what follows since its mathematical manipulation, as we shall see, permits to construct a new classification of the existing phase transitions, which agrees very well with the Fisher's classification and gives a clarification to the Ehrenfest one.

We suppose now that the singular behavior manifested by the phase transition at

x_c appears in the $\mathbf{n^{th}}$**-order** derivative: $\frac{\partial^n \langle \mathcal{O} \rangle}{\partial x^n}(x \to x_c) \sim \infty$, the $\{(\mathbf{n-1})$**-order**$\}$ derivatives being all continuous functions. We need then to derive the $\mathbf{n^{th}}$**-order** derivative of $\langle \mathcal{O} \rangle (x)$:

$$\langle \mathcal{O} \rangle_n (x) = -\boldsymbol{\delta}(x - x_c)\Delta \langle \mathcal{O} \rangle_{n-1} (x) + [1 - \Theta(x - x_c)] \langle \mathcal{O} \rangle_n^+ (x) + \Theta(x - x_c) \langle \mathcal{O} \rangle_n^- (x), \tag{1.3}$$

with:

$$\begin{cases} \langle \mathcal{O} \rangle_n (x) = \dfrac{\partial^n \langle \mathcal{O} \rangle (x)}{\partial x^n} \\ \boldsymbol{\Delta} \langle \mathcal{O} \rangle_n (x) = \langle \mathcal{O} \rangle_n^+ (x) - \langle \mathcal{O} \rangle_n^- (x). \end{cases} \tag{1.4}$$

The possible mathematical cases in which we can have a singularity corresponding to our phase transition are the followings:

1. <u>**Case N°1**</u>: $\Delta \langle \mathcal{O} \rangle_{n-1} (x)$=finite and $\langle \mathcal{O} \rangle_n^{\pm} (x)$=finite. We have a finite discontinuity in $\langle \mathcal{O} \rangle_{n-1} (x)$ and the singularity is dominated by the $\delta(x - x_c)$ function:

$$\langle \mathcal{O} \rangle_n (x) \sim \delta(x - x_c), \tag{1.5}$$

   $\Rightarrow$ The phase transition is called $\mathbf{n^{th}}$**-Order d-PT.**

2. <u>**Case N°2**</u>: $\Delta \langle \mathcal{O} \rangle_{n-1} (x) = 0$ and $\langle \mathcal{O} \rangle_n^{\pm} (x) = \infty$. We have no discontinuity in $\langle \mathcal{O} \rangle_{n-1} (x)$ and the singularity is dominated by divergent $\langle \mathcal{O} \rangle_n^{\pm} (x)$:

$$\langle \mathcal{O} \rangle_n (x) \sim [1 - \Theta(x - x_c)] \langle \mathcal{O} \rangle_n^+ (x) + \Theta(x - x_c) \langle \mathcal{O} \rangle_n^- (x), \tag{1.6}$$

   $\Rightarrow$ The phase transition is called $\mathbf{n^{th}}$**-Order c-PT.**

3. <u>**Case N°3**</u> : $\Delta \langle \mathcal{O} \rangle_{n-1} (x)$ = finite and $\langle \mathcal{O} \rangle_n^{\pm} (x) = \infty$. We are opposite a special case, in which the singularity comes from both $\delta(x - x_c)$ and divergent $\langle \mathcal{O} \rangle_n^{\pm} (x)$. Until now, to our knowledge, we have not observed any experimental phase transition manifesting the two different kinds of singularities at the same time.

4. **Case N°4** : $\Delta \langle \mathcal{O} \rangle_{n-1}(x) = 0$ and $\langle \mathcal{O} \rangle_n^{\pm}(x) =$ finite. In this case the phase transition does not manifest any singularity in the $\langle \mathcal{O} \rangle_n(x)$. We must look for it in the $(\mathbf{n+1})$-order derivative, and then similar cases may appear at this level.

We can then summarize our classification by saying that we have in reality two different kinds of phase transitions: discontinuous phase transitions (**d-PT**) and continuous phase transitions (**c-PT**). The order of a **d-PT** is nothing but the order of the derivative of the order parameter at which the singularity appears as a δ-function:

$$\mathbf{n^{th}-Order\ d-PT\ class}$$

$$\langle \mathcal{O} \rangle_{n-1}(x) \sim \Theta(x - x_c), \quad \langle \mathcal{O} \rangle_n(x) \equiv \delta(x - x_c) \ ,$$

which agrees with the first and traditional classification formulated by Ehrenfest (1933).

For the **c-PT**, the singularity comes from a divergent $\langle \mathcal{O} \rangle_n^{\pm}(x)$ and with the same considerations, we can speak about the order of the **c-PT** as the order of the derivative $\langle \mathcal{O} \rangle_n(x)$ having a divergent behavior. We note that this case of an infinite singularity in the $\langle \mathcal{O} \rangle_n(x)$ fails to the Ehrenfest classification because :

$$\mathbf{n^{th}-Order\ c-PT\ class}$$

$$\underset{x \to x_c}{Lim} \langle \mathcal{O} \rangle_n(x) \equiv \infty, \quad \Leftrightarrow \quad \langle \mathcal{O} \rangle_{n-1}(x) \propto (x - x_c)^{\upsilon} \ ,$$

which gives a constraint on the value of the critical exponent υ : $\upsilon - 1 \prec 0$.

We finish our discussion by a diagrammatic view which may explain more clearly the different kinds of phase transitions existing in nature.

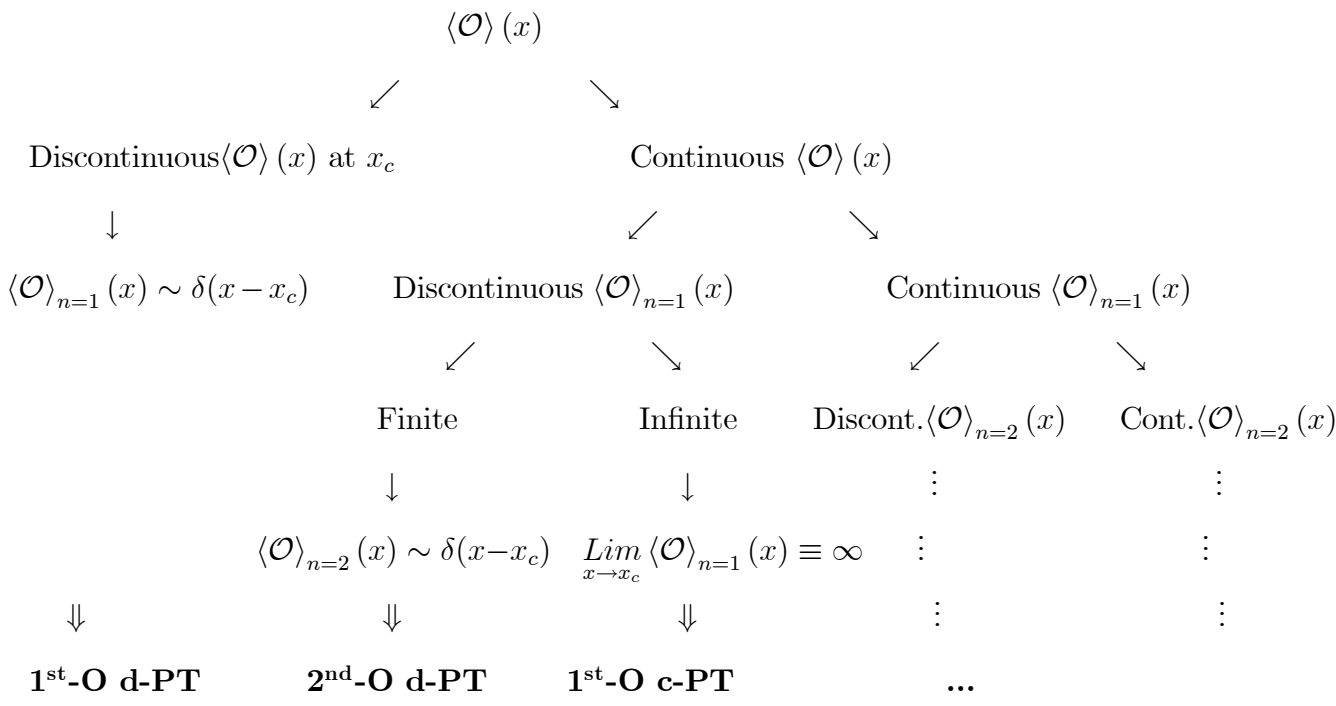

1.6 Critical Behavior and Exponents

From thermodynamical point of view, a critical point is characterized by the type of singularity of the thermodynamic potential and its derivatives with respect to the relevant variables at this point. It turns out to be very important to the theory of critical phenomena to understand more carefully the form of the singular behavior of these quantities near the critical point. Considering the critical behavior, it is convenient to speak in terms of the reduced distance from the critical point:

$$\widetilde{x} = \frac{x - x_c}{x_c}, \tag{1.7}$$

then, the thermodynamic functions have singularities at $\widetilde{x} = 0$. Data from multiple experiments as well as results from a number of exactly soluble models show that these thermodynamic functions can be described by a set of simple power laws in the vicinity

of the critical point x_c, characterized by powers, with a customary notation in terms of greek letters, called *Critical Exponents*. Then the critical exponent associated with a function $F(\widetilde{x})$ is:

$$\lambda = \lim_{\widetilde{x}\to 0} \frac{\ln|F(\widetilde{x})|}{\ln|\widetilde{x}|} \ , \tag{1.8}$$

assuming that the limit exists, or as it is more usually written:

$$F(\widetilde{x}) \sim |\widetilde{x}|^{\lambda} \ . \tag{1.9}$$

The proportionality sign $\sim$ is to remind that eq. (1.9) only represents the asymptotic behavior of the function $F(\widetilde{x})$ as $\widetilde{x} \to 0$, and is then an asymptotic law. More generally, one might expect:

$$F(\widetilde{x}) = A\,|\widetilde{x}|^{\lambda}\left(1 + b\widetilde{x}^{\lambda_1} + ...\right), \quad \lambda_1 > 0. \tag{1.10}$$

It can easily be seen that sufficiently near the critical point, the behavior of the leading term dominates.

Definitions of the most commonly used critical exponents connected to the most important quantities are given in the following, for thermally driven phase transitions in fluids and/or magnets.

- **The exponent $\boldsymbol{\alpha}$**

This exponent describes the divergence of the specific heat C_V for a fluid or C_H for a magnet near the critical point:

$$C_V \sim |t|^{-\alpha}, \quad C_H \sim |t|^{-\alpha}, \tag{1.11}$$

where the deviation in temperature from the critical temperature T_c has been noted t.

- **The exponent $\boldsymbol{\beta}$**

The critical exponent β is connected to the density difference $\left(\rho_l - \rho_g\right)$ for a fluid system or the spontaneous magnetization M for a magnetic system. It shows how the order parameter varies with the varying temperature T as T_c is approached.

$$\left(\rho_l - \rho_g\right) \sim (-t)^{\beta}, \quad M \sim (-t)^{\beta}. \tag{1.12}$$

- **The exponent γ**

This exponent describes the critical variation at $t \to 0$ of the isothermal compressibility κ_T for a fluid and the isothermal susceptibility χ_T for a magnet:

$$\kappa_T \sim |t|^{-\gamma}, \quad \chi_T \sim |t|^{-\gamma}. \tag{1.13}$$

- **The exponent δ**

The exponent δ describes the variation of the difference in Pressure $(P - P_c)$ with $\left(\rho_l - \rho_g\right)$ (fluid) and of the field H with magnetization M (magnet) along the critical isotherm $T = T_c$:

$$(P - P_c) \sim \left|\rho_l - \rho_g\right|^{\delta} sgn(\rho_l - \rho_g), \qquad H \sim |M|^{\delta} sgn(M), \tag{1.14}$$

where sgn is the sign function:

$$sgn(z) = \begin{cases} \dfrac{z}{|z|} \text{ if } z \neq 0 \\ 0 \text{ if } z = 0\ . \end{cases} \tag{1.15}$$

- **The exponent η**

The critical exponent η is associated to the critical variation at $t \to 0$ of the

connected two point correlation function $G(r)$ [1], where r denotes the separation of the two points, at $P = P_c$ for a fluid or at $H = 0$ for a magnet.

$$G(r) \sim r^{-(d-2+\eta)}. \tag{1.16}$$

Here d is the dimensionality of the system.

- **The exponent ν**

The last exponent concerns the correlation length which is a measure of the range of the correlation function.

$$\xi \sim |t|^{-\nu}, \qquad t \to 0,\ H = 0. \tag{1.17}$$

The exponent definitions are summarized for fluid and magnetic system in Tables (1.4) and (1.5) respectively [15, 20].

[1] Thermodynamic variables like the magnetization or the entropy are macroscopic properties. A much fuller understanding of phase transitions can be obtained by considering what happens on a microscopic level. To be able to do this in a more qualitative way, we introduce correlation functions [15]. Let the order parameter $\mathcal{O}$ be written as a volume integral over an order parameter density $\mathfrak{o}(\overrightarrow{r})$ as: $\mathcal{O} = \left\langle \int d^3r\ \mathfrak{o}(\overrightarrow{r}) \right\rangle$, where $\langle ... \rangle$ represents the statistical average by which one obtains thermodynamic functions. The correlation function defined as: $G(\overrightarrow{r}) = \langle \mathfrak{o}(\overrightarrow{r})\mathfrak{o}(0)\rangle - \langle \mathfrak{o}(\overrightarrow{r})\rangle \langle \mathfrak{o}(0)\rangle$, measures how the value of the order parameter at one point is correlated to its value at some other point. Away from the critical point, far away points ($r \to \infty$) become uncorrelated and hence the correlation length decays to zero. This decay is exponential with the form: $G(\overrightarrow{r}) \sim r^{-\tau} e^{-r/\xi}$, where τ is some number, and ξ the correlation length which is a measure of the range over which fluctuations in one region of space are correlated with those in another region. Experimentally, the correlation length is found to diverge at the critical point, which means that very far points become correlated. Thus the system near a second-order PT 'loses memory' of its microscopic structure and begins to display new long-range macroscopic correlations. Evidence form experiments and exactly soluble models shows that here the correlation function decays as a power law: $G(\overrightarrow{r}) \sim r^{-(d-2+\eta)}$.

Specific heat at constant volume	$C_V \sim \lvert t\rvert^{-\alpha}$
Liquid-gas density difference	$\left(\rho_l - \rho_g\right) \sim (-t)^{\beta}$
Isothermal compressibility	$\kappa_T \sim \lvert t\rvert^{-\gamma}$
Critical isotherm ($t = 0$)	$P - P_c \sim \left\lvert \rho_l - \rho_g \right\rvert^{\delta} sgn(\rho_l - \rho_g)$
Pair correlation function at T_c	$G(r) \sim r^{-(d-2+\eta)}$
Correlation length	$\xi \sim \lvert t\rvert^{-\nu}$

Table 1.4: Definitions of the most commonly used critical exponents for a fluid system

Zero-field specific heat	$C_H \sim \lvert t\rvert^{-\alpha}$
Zero-field magnetization	$M \sim (-t)^{\beta}$
Zero-field isothermal susceptibility	$\chi_T \sim \lvert t\rvert^{-\gamma}$
Critical isotherm ($t = 0$)	$H \sim \lvert M\rvert^{\delta} sgn(M)$
Pair correlation function at T_c	$G(r) \sim r^{-(d-2+\eta)}$
Correlation length	$\xi \sim \lvert t\rvert^{-\nu}$

Table 1.5: Definitions of the most commonly used critical exponents for a magnetic system

1.7 Universality, Scaling and Renormalization Group Theory

Having defined the critical exponents, we need to justify why they are interesting, and indeed why they are more interesting than the critical point itself. It turns out that, whereas the critical point depends sensitively on the details of the interatomic interactions, the critical exponents are to a large degree *universal* depending only on a few fundamental parameters, consisting in the dimensionality of space, the symmetry of the order parameter and the range of the interaction. Simple systems, or numerical models appropriate for computer simulations, are used to describe the critical behavior. The results are then extended to more complex systems: by making sure that one is working in the right dimension and that the symmetry is correctly represented by a model, it can be used to obtain critical exponents for *all* the systems within its *universality class*.

Universality Class	Symmetry of Order Parameter	α	β	γ	δ	ν	η
2-d Ising	2-component scalar	0 (log)	1/8	7/4	15	1	1/4
3-d Ising	2-component scalar	0.10	0.33	1.24	4.8	0.63	0.04
3-d X-Y	2-dimensional vector	0.01	0.34	1.30	4.8	0.66	0.04
3-d Heisenberg	3-dimensional vector	-0.12	0.36	1.39	4.8	0.71	0.04
2-d Potts, $q = 3$	q-component scalar	1/3	1/9	13/9	14	5/6	4/15
$q = 4$		2/3	1/12	7/6	15	2/3	1/4

Table 1.6: Examples of universality classes with the corresponding symmetry of the order parameter and the values of the critical exponents

Striking evidence for this comes when comparing the value of the critical exponent β for phase transitions in completely different systems, with a scalar order parameter, such as the liquid-gas phase transition, magnets with uniaxial anisotropy in spin space, phase separation in the binary fluid mixture and the lattice models of ± 1 spins (Ising models); in all these cases β is the same, 1/3, and thus all four systems fall in the same *universality class* in the sense that they are described by the same scaling relations. The Ising model, however, is much simpler than the other experimental systems, and it has been used extensively in numerical simulations [21].

Some universality classes are listed in Table (1.6) with a description of the symmetry of the corresponding order parameter and the values of the critical exponents [15].

Universality means that systems differing in microscopic details (e.g. different types of interaction potentials, ion species, ... etc) exhibit identical collective behavior, or as termed by Kadanoff [22]: *"All phase transition problems can be divided into a small number of different classes depending upon the dimensionality of the system and the symmetries of the ordered state. Within each class, all phase transitions have identical behavior in the critical region, only the names of thermodynamic variables are changed".*

Not all of the critical exponents defined in the previous section are independent

Rushbrooke's law	$\alpha + 2\beta + \gamma \geq 2$
Griffiths law	$\alpha + \beta\,(1 + \delta) \geq 2$
Fisher's law	$(2 - \eta)\,\nu \geq \gamma$
Josephson's law	$d\nu \geq 2 - \alpha$

Table 1.7: Scaling laws of critical exponents

and using a number of thermodynamic arguments one can derive a series of exponent relations called *scaling laws.* Rushbrooke (1963), Griffiths (1965), Josephson (1967) and Fisher (1969) were the first to find certain inequalities between the critical exponents. By experimental evidence, it turned out later that these are in fact equalities. Table (1.7) resumes these scaling laws.

Universality in critical phenomena is described by the *Renormalization Group Theory.* The first work describing the fundamental concepts of the renormalization group approach was the paper of K. G. Wilson published in 1971 [23]. The renormalization group works by changing the length scale of a system by removing degrees of freedom, using renormalization group transformations which relate a system with correlations on the scale ξ to another system with correlations on the scale ξ/b, where the scale factor $b > 1$. Only at criticality will the properties of the system remain unaltered by the change in scale and hence the critical behavior is described by the so-called fixed points of the transformation, and this leads to the important result that the thermodynamic functions can be written in a scaling form. The equality of the critical exponents above and below the critical temperature and the relations between them then follow immediately [15, 21, 24].

We note that the ideas of *Universality, Scaling* and *Renormalization* are important concepts from which a modern understanding of critical phenomena has emerged, and H.E. Stanley has recently pointed out in his famous article [25] that: *"Scaling, Univer-*

sality and Renormalization are the three pillars of the current understanding of modern critical phenomena".

1.8 QCD phase transition and the Hagedorn temperature

Today, we think that we arrived at a deep level of structure of matter. All matter in the universe is constructed from Quarks and Leptons: the Quark-Lepton Level. These fundamental particles are spin $\frac{1}{2}$: "fermions" and are classified into three "generations" (or families) and interact through the exchange of gauge bosons. Both quarks and leptons are structureless at the smallest distances currently probed by the highest energy accelerators (current limits of resolution or present observational limit $\sim 10^{-21}m = 10^{-6}fm$ [26]).

If we heat and/or compress very highly a strongly interacting (hadronic) matter, we arrive to such extreme conditions which do not permit the hadrons to survive, and above a certain high temperature T_c and/or high density n_c, the dissolution of the hadronic matter into its components can occur, and a weakly interacting system of nearly free quarks and gluons can be created. Since quarks and gluons play similar roles in Quantum Chromo-Dynamics (QCD) than the electrons and photons in Quantum Electro-Dynamics (QED), this phase is generally known as the Quark Gluon Plasma (QGP), Partonic Plasma or Non-Abelian Plasma. In this naive picture, the phase diagram of QCD contains two important regions:

- A Hadronic Gas (HG) phase at low temperature (density).
- A QGP phase at high temperature (density).

The qualitative differences between these two phases lead to speculate the existence of a phase transition connecting them, commonly called the QCD Deconfinement Phase Transition (DPT), which is as old as the quark structure of matter [27, 28, 29, 30].

The nature and the character of this QCD DPT are still much debated questions. Its existence, however, has been partly supported by Lattice QCD calculations and the Cosmological Standard Model predictions. Experimentally, the only way to study this QCD phase transition is to try to recreate, in ultra-relativistic heavy ion collisions, conditions similar to those which occurred in the early times of the universe ($\sim 10^{-6}s$), immediately after the big bang. To understand the physics of this QCD DPT, numerous studies have been performed using phenomenological approaches to the two-phase nature of strongly interacting matter; the "Statistical Bootstrap Model" (SBM) of Hagedorn is one of those [31, 32]. It is a statistical model based on the observation that hadrons not only form bound and resonance states but also decay statistically into such states if they are heavy enough. This leads to the concept of a sequence of heavier and heavier bound and resonance states, each being a possible constituent of a still heavier resonance, while at the same time being itself composed of lighter ones. We call these states "clusters" or "fireballs". The thermodynamical study of nuclei collisions shows that when the impact energy gets very high, the temperature in the collision, estimated from the energy distribution of the emitted fragments, does not increase as fast as the model suggests. The temperature seems to approach some kind of plateau as the collision energy grows. This is due to the fact that the energy in the collision is high enough to convert into mass, and then higher-mass hadrons are created: the temperature in the collision remains the same until the most massive hadron has been created, then it starts to increase again.

The same situation occurs during the liquid-vapor transition in water: the temperature of boiling water does not change during the phase transition when water enters its vapor phase. Hagedorn suggested that this limiting temperature, of the order of pion mass, characterizes the limit of existence of hadronic matter.

Several estimates of this temperature from the SBM have been given, and here are some of them [32]:

- The Frautschi-Yellin bootstrap equation (BE) yields with pions only:

$$T_0 \approx 0.145 GeV$$

- If K and N were added to the input: $T_0 \approx 0.135 GeV$

- Hamer and Frautschi solve their BE by numerical iteration and read off:

$$T_0 \approx 0.140 GeV$$

- Nahm derives a sum rule from which he found, under different assumptions:

$$T_0 \approx 0.154 GeV$$

$$\text{or } T_0 \approx 0.142 GeV$$

Actually, this singular temperature is interpreted as the temperature where (for chemical potential $\mu = 0$) the phase transition from hadronic matter to quark-gluon plasma occurs.

Another widely used model describing the QCD phase transition is the thermodynamic approach with two-phase matter equations of state, which will be used in the present work, from chapter 3 on.

1.9 Lattice QCD

In 1974, Wilson proposed a formulation of quantum chromodynamics (QCD) on a discrete space-time lattice [33]. A few years later, Creutz demonstrated that this formulation was a promising basis for the successful numerical simulation of the theory [34]. The simulation method is the most promising currently available method for deducing nonperturbative characteristics of QCD at finite temperature and/or density [35].

In the past several years, considerable progress has been made and lattice simulations continue providing results on the equation of state of QCD [36, 37, 38, 39], the transition temperature [40, 41], the order of the deconfinement phase transition [37, 40, 42, 43], as well as the QCD phase diagram [40, 44, 45]. It has been shown that the nature of this transition depends strongly on the number of colors (N_c), the number of flavors (N_f) and the current quark masses as revealed by several lattice QCD calculations (see for example [46, 47, 48, 49, 50, 51, 52, 53, 54, 55, 56, 57, 58, 59, 60]. For infinite or very large quark masses, the transition is a 1st order deconfining transition. In the opposite case of zero quark masses, one may have a 2nd order chiral phase transition for two flavors or a 1st order chiral phase transition for three flavors. For intermediate masses, the transition is just a rapid crossover, meaning that thermodynamic quantities change very rapidly in a narrow temperature interval [61].

Chapter 2

Phase Transitions in Finite-Size Systems

2.1 Introduction

Phase transitions in statistical physics are known to be infinitely sharp only in the thermodynamic limit, where the volume V and the number of particles N go to infinity, while the density $\rho = \frac{N}{V}$ remains constant. Only in this limit is the thermodynamical potential or any of its derivatives singular at the critical point. However, real systems and systems we simulate are finite.

In general, finite size effects lead to a mixed phase system and a rounding of the transition, rendering the order of the transition difficult to infer. The main care is then how to sign a possible phase transition in a finite system. It turns out that we can extract the true critical behavior of infinite systems from calculations on finite systems, by studying how some characteristic thermodynamical quantities vary with the size of the system, namely by a *Finite Size Scaling* (FSS) analysis. Studies in statisti-

cal physics have shown that despite the apparent diversity in the underlying structure of systems undergoing phase transitions, these latter take place with some *universal* global behavior, depending only on the range of interaction of the forces at play and the dimensionality of the problem. This means the singular behavior of some characteristic observables near criticality is identical for many systems when appropriately scaled. This *universality* allows the put of all the physical systems undergoing a phase transition in a certain number of universality classes. The systems in a given universality class display the same critical behavior, meaning that certain dimensionless quantities have the same values for all these systems. *Critical exponents* are an example of these universal quantities. The determination of critical exponents has long been one of the main interests for both analytical calculations and numerical simulations.

This chapter is mainly an overview of phase transitions in finite size systems. The finite size effects are examined and the finite size scaling analysis permitting the determination of the scaling critical exponents is reviewed for both first and second order phase transitions.

2.2 Thermodynamic Limit

In statistical mechanics, the existence of phase transitions is associated with singularities of the thermodynamic potential in some region of the thermodynamic space. These singularities occur only in the thermodynamic limit, where the volume V and particle number N go to infinity, with a constant density $\rho = \frac{N}{V}$. This fact could be understood by analyzing the partition function which contains all of the essential information about the system under consideration, and whose general form for a classical

system is:

$$Z = \sum_{all\ \ states} e^{-\beta\mathcal{H}}, \tag{2.1}$$

where $\mathcal{H}$ is the Hamiltonian of the system, $\beta = \frac{1}{T}$ with the units chosen as: $k_B = \hbar = c = 1$. The sum in eq. (2.1) is over all possible states of the system and thus depends upon the size of the system and the number of degrees of freedom for each particle. For a finite system, the partition function is a finite sum of analytical terms, and therefore it is itself an analytical function. It is necessary to take an infinite number of terms to obtain a singularity, and this has been demonstrated through the work of Lee and Yang in [17].

Thus, in a finite system no singularity occurs and, strictly speaking, no phase transition occurs. The question of why a finite system can apparently describe phase transitions and the relation of this phenomenon with true phase transitions in infinite systems is the main subject of the Finite Size Scaling (FSS) theory [2, 62, 63, 64, 65, 66]. Finite Size Scaling is not only a formal way to understand the asymptotic behavior of a system when the size goes to infinity. In fact, the theory gives us numerical methods capable of obtaining accurate results for infinite systems only by studying very small systems.

2.3 Finite Size Effects and Useful Thermodynamic $x-$Response Functions

In the thermodynamic limit and at criticality, the phase transition is signaled by a divergence (infinite singularity) manifested by some thermodynamic function $F(x, \infty)$. This singularity is according to our classification in chapter 1 given by the $\boldsymbol{\delta}(\tilde{x})-$function

for a discontinuous phase transition (d-PT), while for a continuous phase transition (c-PT), the singularity has the form of a power-law $\tilde{x}^{\upsilon}-$function. Now, if the volume is finite at least in one dimension with a characteristic size $L = V^{1/d}$, the singularity is smeared out into a peak with finite mathematical properties, and three effects can be observed [3, 62, 67, 68]:

1. **The rounding effect of the maximum of the infinite singularity**

   The Infinite height of the $x_c(\infty)$-singularity ($F(x_c(\infty), \infty) = \infty$) becomes finite ($F(x_c(L), L) = finite$)

2. **The shifting effect of the transition point position**

   The position of the $x_c(\infty)$-singularity is shifted to $x_c(L)$

3. **The widening of the transition region around the transition point**

   The $x_c(\infty)$-singularity acquires a finite width ($\delta x(L) = finite$) around the $x_c(L)$-maximum.

The most important feature in a finite volume is then the localization of the finite size transition point: $x_c(L)$. If we analyze the finite peak of $F(x, L)$ when approaching the thermodynamic limit, we see that it tends to the real initial singularity. It is then logical to say that the location of the maximum of the rounded peak of $F(x, L)$ determines the finite-size transition point $x_c(L)$, i. e.,

$$\left[\frac{\partial\langle F\,(x, L)\rangle}{\partial x}\right]_{x=x_c(L)} = 0\ . \tag{2.2}$$

For each of the FSE described previously, we may associate a scaling critical exponent according to the scaling law $\sim L^{\sigma}$. The value of the critical exponent σ may

certainly depend enormously on the kind of singularity occurring in the thermodynamic limit, and differ according to the phase transitions class, i. e., $\sigma(\text{d-PT}) \neq \sigma(\text{c-PT})$. The principal reason is the dependence of $\sigma(\text{c-PT})$ on the critical exponent υ which does not exist in the case of a d-PT [69]. Thus, we can say that the value of the scaling critical exponent σ can give an indication on the order of a phase transition and may be used as a criterion for its determination.

Now, we define the most useful two thermodynamical functions for the study of FSE on the more commonly encountered $x-$ driven phase transitions, namely the first-order phase transition and the second-order phase transition, and for the derivation of the associated scaling critical exponents. These two $x-$ response functions are:

1. The $x-$ susceptibility defined to be the first derivative of the order parameter with respect to the $x-$ variable, i. e.,

$$\chi(x, L) = \frac{\partial \langle \mathcal{O}(x, L) \rangle}{\partial x}, \tag{2.3}$$

2. The $x-$ specific heat density defined to be the first derivative of the energy density $\varepsilon(x, L)$ of the system with respect to the $x-$ variable, i. e.,

$$c(x, L) = \frac{\partial \langle \varepsilon(x, L) \rangle}{\partial x}. \tag{2.4}$$

A FSS analysis of the scaling behavior of the properties describing $\chi(x, L)$ and $c(x, L)$, namely of:

- **The height of the x-susceptibility maximum** $|\chi_x|^{\max}(L)$
- **The height of the x-specific heat maximum** $c_x^{\max}(L)$

- **The shift of the pseudo-critical point from the true critical point**: $\tau_x(L) = x_c(L) - x_c(\infty)$
- **The width of the transition region** $\delta x(L)$ over which the singularities occurring in $\chi(x, L)$ and $c(x, L)$ are rounded,

is used to study quantitatively the volume dependence of these finite size effects, and to recover the scaling critical exponents characterizing the phase transition in question.

2.4 Finite Size Scaling

The appreciable rounding of the critical point singularities induced by finite size effects render it difficult to infer the order of a phase transition. Fortunately, there are characteristic signatures in a finite volume which anticipate the behavior in the thermodynamic limit. A careful analysis of these signatures allows to determine the order of the transition, by performing measurements as function of a varying volume.

In the following, we discuss the finite size scaling behavior of singularities in thermodynamic functions for both $1^{\mathbf{st}}$-Order and 2^{nd}-Order phase transitions.

2.4.1 Finite-size scaling at $2^{\mathbf{nd}}$-Order phase transitions

Let us consider a thermodynamical function $F(\tilde{x}, \infty)$ which admits a critical singularity in the infinite volume limit (the susceptibility $\chi(\tilde{x}, V)$ or the specific heat $c(\tilde{x}, V)$), characterized by an index μ:

$$F(\tilde{x}, \infty) \sim A_F \ |\tilde{x}|^{-\mu} \quad . \tag{2.5}$$

For a system which is finite at least in one dimension with a characteristic size $L = V^{1/d}$, this function is $F(\tilde{x}, L)$. For large L and small $\tilde{x}$, the property of **Finite Size Scaling** means that $F(\tilde{x}, L)$ has the asymptotic form:

$$F(\tilde{x}, L) = |\tilde{x}|^{-\mu} f(L/\xi(\tilde{x}, \infty)), \tag{2.6}$$

where $\xi(\tilde{x}, \infty) \sim \xi_0 |\tilde{x}|^{-\nu}$ is the correlation length in the infinite volume limit.

We are interested in the limit $x \to x_c$ at fixed $L < \infty$, i. e., $\dfrac{L}{\xi(\tilde{x} \to 0, \infty)} \to 0$, at which $F(\tilde{x}, L)$ should be finite. Hence, the singularity of $F(\tilde{x}, \infty)$ has to be compensated by the scaling function $f(L/\xi(\tilde{x}, \infty))$ which may behave as:

$$f(L/\xi(\tilde{x}, \infty)) \sim (\frac{L}{\xi(\tilde{x}, \infty)})^{\mu/\nu} \qquad \text{for} \quad \frac{L}{\xi(\tilde{x}, \infty)} \to 0, \tag{2.7}$$

where $\xi(\tilde{x}, \infty) \sim |\tilde{x}|^{-\nu}$ for $\tilde{x} \to 0$. It follows then [70]:

$$F(x_c, L) = F(\tilde{x} = 0, L) \sim L^{\mu/\nu} \quad . \tag{2.8}$$

The last relation (2.8) predicts for instance for the susceptibility:

$$\chi(x_c, L) \sim L^{\gamma/\nu} \quad , \tag{2.9}$$

and for the specific heat:

$$c(x_c, L) \sim L^{\alpha/\nu} \quad . \tag{2.10}$$

For the width of the transition region $\delta x\,(L)$ and the shift of the transition point $\tau_x\,(L)$ which vanish at the infinite volume limit, their scaling behavior is characterized by the same critical index $1/\nu$, according to:

$$\delta x\,(L) \sim L^{-1/\nu}, \quad \tau_x\,(L) \sim L^{-1/\nu}\ , \tag{2.11}$$

while the scaling behavior of the correlation length in a finite volume is stated as [70]:

$$\xi(\tilde{x}, L) = \xi(\tilde{x}, \infty) f_\xi(L/\xi(\tilde{x}, \infty))\ . \tag{2.12}$$

2.4.2 Finite-size scaling at $1^{\mathbf{st}}$-Order phase transitions

Finally, we turn to finite-size scaling analysis at first-order phase transitions. In an infinite system, a $1^{\mathbf{st}}$-Order phase transition is characterized by delta function singularities in the second derivatives of the thermodynamical potential at the critical point $x_c\,(\infty)$. In finite systems, of course, these delta function singularities are rounded off into finite peaks. The finite-size scaling analysis for $1^{\mathbf{st}}$-Order phase transitions is more difficult than for 2^{nd}-Order phase transitions because $\dfrac{\xi(\tilde{x},\infty)}{L}$ is no longer a sensible scaling variable as in eq. (2.7) since the correlation length for a $1^{\mathbf{st}}$-Order phase transition stays finite even in the infinite volume limit as $x \to x_c$ [70]. Thus, since there is no diverging characteristic length to which the linear dimension could be compared at $1^{\mathbf{st}}$-Order phase transition, it is simply the volume L^d that controls the size effects.

The goal of the finite size scaling analysis for $1^{\mathbf{st}}$-Order phase transitions is to predict the rounding and shifting of $\delta-$function singularities in the second derivatives of a thermodynamical potential due to the finite volume, e.g., in the specific heat due to a latent heat, or in the susceptibility due to a jump in the order parameter (see [2, 3, 64, 71, 72]).

We plot in Fig. (2.1) a diagrammatic behavior of the susceptibility $\chi(L,x)$, the specific heat $c(L,x)$ as well as the $x-$derivative of the susceptibility $[\partial\chi(L,T)/\partial x]$ as function of x, and show the characteristic maxima of the rounded peaks $|\chi_x|^{\max}(L)$ and $c_x^{\max}(L)$, the width of the region over which the transition is rounded off $\delta x(L)$, and the shift of the transition point $x_c(L) - x_c(\infty)$, which scale with the volume according

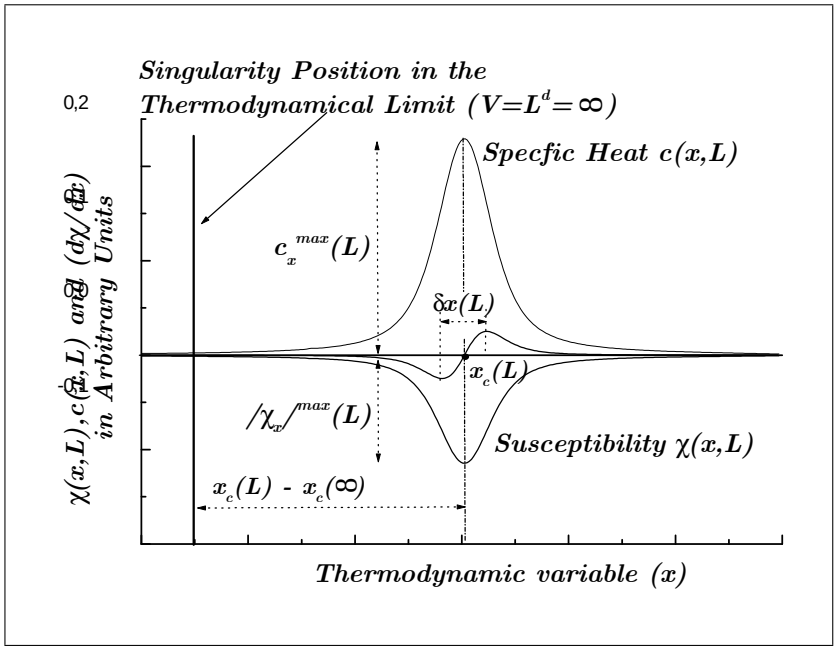

Figure 2.1: Behavior of the susceptibility $\chi(x,L)$, its first derivative $\frac{\partial \chi}{\partial x}$ and specific heat $c(x,L)$ versus the thermodynamic $x-$variable driving the transition, at the transition point x_c.

to:

$$\begin{cases} \delta x(L) \sim L^{-d\ \theta} = V^{-\theta} \\ (x_c(L) - x_c(\infty)) \sim L^{-d\ \lambda} = V^{-\lambda} \\ |\chi_x|^{\max}(L) \sim L^{d\ \gamma} = V^{\gamma} \\ C_x^{\max}(L) \sim L^{d\ \alpha} = V^{\alpha}\ . \end{cases} \tag{2.13}$$

It has been shown in the FSS theory [3, 64, 66, 67, 71] that in this case, the scaling exponents θ, λ, α and γ are all equal to unity, and it is only the dimensionality which controls the finite size effects.

As an example, we shall report on in the following the work in [3] to recover the scaling exponents for a first order phase transition. Using thermodynamic fluctuation

theory, finite-size effects at first order phase transitions have been worked out in Ising models below T_c, to discuss the rounding of the magnetization jump in the Ising ferromagnet as the field H is varied. In an infinite system, the magnetization jumps from $-M_{sp}$ as $H \to 0^+$ to $+M_{sp}$ reached for $H \to 0^-$. In a system with all linear dimensions L finite, however, no singularity can occur and the variation of the magnetization $\langle S \rangle_L$ with field is perfectly smooth. Rather than the infinitely steep variation of $\langle S \rangle_L$ with H from $H = 0^+$ to $H = 0^-$ occurring for $L \to \infty$, $\langle S \rangle_L$ has a large but finite slope of order $\dfrac{M_L^2 L^d}{kT}$, for a finite region of fields $-\dfrac{M_L L^d}{kT} \lesssim H \lesssim \dfrac{M_L L^d}{kT}$. Here $\pm M_L$ are the values of the magnetization where the probability distribution $P_L(s)$ at zero field is maximal, and d is the system's dimensionality.

The probability distribution of the magnetization of an Ising system below T_c at zero field can be approximated by two Gaussian curves, one centered on $-M$ and one on $+M$, as:

$$P_L(s) = \frac{1}{2} \frac{L^{d/2}}{\left(2\pi k T \chi_{(L)}\right)^{1/2}} \left\{ \exp\left[-\frac{(s - M_L)^2 L^d}{2kT\chi_{(L)}} \right] + \exp\left[-\frac{(s + M_L)^2 L^d}{2kT\chi_{(L)}} \right] \right\} . \quad (2.14)$$

The generalization to nonzero field H then simply is:

$$P_L(s) = A \left\{ \exp\left[-\frac{\left((s - M_{sp})^2 - 2\chi s H\right) L^d}{2kT\chi_{(L)}} \right] + \exp\left[-\frac{\left((s + M_L)^2 - 2\chi s H\right) L^d}{2kT\chi_{(L)}} \right] \right\} , \quad (2.15)$$

with A a normalization constant which can be written as:

$$A = \frac{1}{2} \frac{L^{d/2}}{\left(2\pi k T \chi_{(L)}\right)^{1/2}} \exp\left[-\frac{\chi H^{\,2} L^d}{2kT} \right] / \cosh\left[\frac{H M_{sp} L^d}{kT} \right] . \quad (2.16)$$

Eq. (2.15) can then be rewritten as:

$$\begin{aligned} P_L(s) \;=\; & \frac{1}{2} L^d \frac{\left(2\pi k T \chi_{(L)}\right)^{-1/2}}{\cosh\left[H M_{sp} L^d / kT\right]} \left\{ \exp\left[\frac{H M_{sp} L^d}{kT} \right] \exp\left[-\frac{(s - M_{sp} - \chi H)^2 L^d}{2kT\chi_{(L)}} \right] \right. \\ & \left. + \exp\left[\frac{H M_{sp} L^d}{kT} \right] \exp\left[-\frac{(s + M_L - \chi H)^2 L^d}{2kT\chi_{(L)}} \right] \right\} . \quad (2.17) \end{aligned}$$

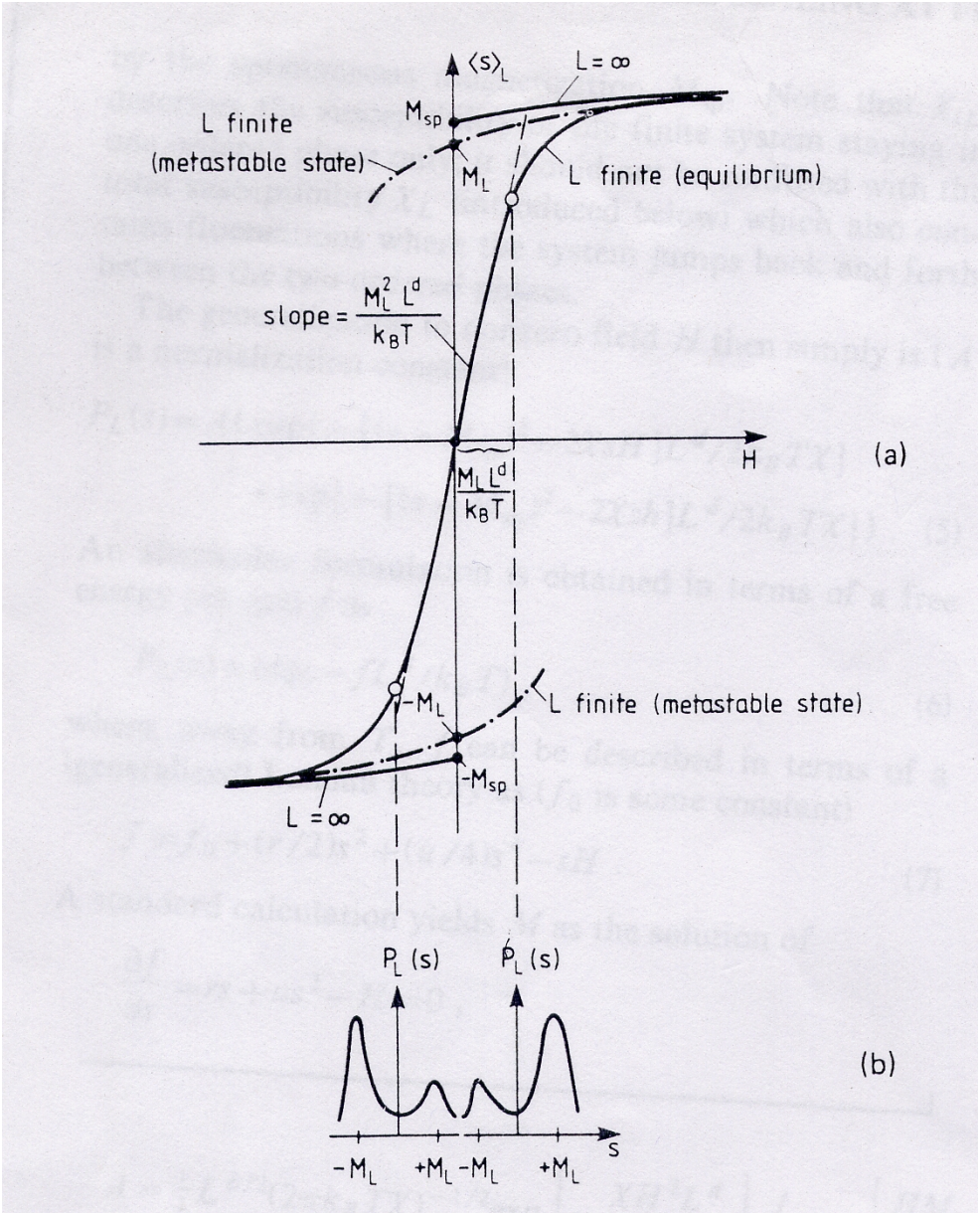

Figure 2.2: (a) Variation of magnetization $\langle s \rangle_L$ in a finite Ising ferromagnet plotted vs magnetic field H, as observed in thermal equilibrium (full curve) and in a Monte Carlo simulation with sufficiently short observation time where metastable branches occur (dash-dotted). The behavior of the infinite system is also indicated (schematized). M_{sp} is the spontaneous magnetization of the infinte system. M_L is the most probable value of the magnetization in the finite system at $T < T_c$. (b) Schematic probability distribution of the magnetization for two cases (open circles in (a)) where the magnetization is in between [3].

Thus, $P_L(s)$ still is a superposition of two Gaussians, now centered around the shifted magnetization $\pm M_{sp} + \chi H$.

From eq. (2.17), it is now easy to obtain the moments $\langle s^k \rangle_L$ of interest. The first moment $\langle s \rangle_L$ giving the magnetization is then:

$$\langle s \rangle_L = \chi H + M_{sp} \tanh \left[\frac{H M_{sp} L^d}{kT} \right], \tag{2.18}$$

and we conclude that for $\dfrac{H M_{sp} L^d}{kT} \gg 1$ we simply have the bulk behavior:

$$\langle s \rangle_L = \chi H + M_{sp}, \tag{2.19}$$

while in the limit $\dfrac{H M_{sp} L^d}{kT} \ll 1$, we have:

$$\langle s \rangle_L = \chi H + \frac{H M_{sp}^{\ 2} L^d}{kT}. \tag{2.20}$$

The width over which the transition is rounded is of the order of:

$$\Delta H_{round} \approx \frac{kT}{M_{sp} L^d}, \tag{2.21}$$

since, as can be seen from eq. (2.18), the field H has to exceed this value to find the behavior characteristic of the infinite system.

The susceptibility of the finite system χ_L becomes:

$$\chi_L = \left(\frac{\partial \langle s \rangle_L}{\partial H}\right)_T = \chi + \frac{M_{sp}^{\ 2} L^d}{kT \ \cosh^2 \left[\frac{H M_{sp} L^d}{kT} \right]}, \tag{2.22}$$

which shows that instead of the $\delta-$function singularity at $H = 0$, we now have a smooth peak of height proportional to L^d. Also, it is easy to show that:

$$\langle s^2 \rangle_L = M_{sp}^{\ 2} + \chi^2 H^2 + \frac{kT\chi}{L^d} + 2 M_{sp} \chi H \ \tanh \left[\frac{H M_{sp} L^d}{kT} \right], \tag{2.23}$$

and hence the fluctuation relation:

$$\langle s^2 \rangle_L - \langle s \rangle_L^2 = \frac{kT\chi_L}{L^d}, \tag{2.24}$$

holds as usual. Thus, the only scaling power of L which enters in the above relations of $\langle s \rangle_L$, χ_L, etc. comes via the volume L^d of the system. Hence, it is only the dimensionality of the system which controls the finite size effects.

In the following, Table (2.1) resumes the scaling behavior at the limit of an infinite volume and in the vicinity of the transition point for each of the previous four quantities of eq. (2.13), and shows how to relate the finite size effects on the singularities of thermodynamic quantities close to both $1^{\mathbf{st}}$-order and $2^{\mathbf{nd}}$-order phase transitions, to the critical exponents of the infinite system.

The difference between the scaling critical exponents for $1^{\mathbf{st}}$-Order and 2^{nd}-Order phase transitions allows to distinguish between the two classes, since for a $1^{\mathbf{st}}$-Order phase transition $\gamma = \alpha = \lambda = \theta = 1$ and for a 2^{nd}-Order phase transition γ, α and ν differ from 1. This is also revealed by the results found for the scaling critical exponents in theoretical, numerical and experimental studies, hence the use of the critical exponents as a criterion for the determination of the order of a phase transition [47, 48, 49, 50, 70, 73, 74].

2.5 Localization of the transition point in a finite volume

In addition to the two ways cited in section (2.3) for determining the transition point in a finite volume $x_c(L)$, from the localization of the extrema of the susceptibility $\chi(x, L)$

	1st-Order PT		**2nd-Order PT**	
	Infinite System (TL)	Finite-Size System	Infinite System (TL)	Finite-Size System
$\lvert\chi_x\rvert^{\max}(V)$	$\delta(\tilde{x})$	$L^{d\ \gamma}$	$\tilde{x}^{-\gamma}$	$L^{\gamma/\nu}$
$c_x^{\max}(V)$	$\delta(\tilde{x})$	$L^{d\ \alpha}$	$\tilde{x}^{-\alpha}$	$L^{\alpha/\nu}$
$\tau_x(V)$	★	$L^{-d\ \lambda}$	★	$L^{-1/\nu}$
$\delta x\,(V)$	★	$L^{-d\ \theta}$	★	$L^{-1/\nu}$

Table 2.1: Scaling behavior of characteristic quantities for 1st-order phase transition and 2nd-order phase transition in both infinite and finite systems.

and specific heat $c(x, L)$, another quantity has been proposed in [3, 66, 75] which is the fourth order cumulant of the order parameter, defined as:

$$B_4(L) = 1 - \frac{\langle \mathcal{O}(L) \rangle^4}{3\ \langle \mathcal{O}^2(L) \rangle^2}\ , \tag{2.25}$$

and which presents a minimum value at an effective transition point $x_c(L)$ whose shift from the true transition point $x_c(\infty)$ is of order L^{-d} for a first order transition. This cumulant is a finite size scaling function [3, 66, 67, 68, 76], and is widely used to indicate the order of the transition in a finite volume.

Other cumulants are also expected to give information on the transition point in a finite volume, and some of them (the second and third order ones) will be examined later in this work (chapter 4) to determine the effective transition temperature.

The speed of sound (squared) defined by: $c_s^2 = \dfrac{dP}{d\varepsilon}$, P being the pressure and ε the energy density, is also used to localize the transition point, since for a first order phase transition, occurring at the thermodynamic limit, c_s^2 has a vanishing minimum at the transition point $x_c(\infty)$. In a finite volume, c_s^2 decreases in the transition region and has a minimum at the effective transition point $x_c(L)$.

Chapter 3

Finite-Size Effects for the Deconfinement Phase Transition

3.1 Introduction and Motivation

If ever the QGP phase is created in ultra-relativistic heavy ion collisions, the volume in which its eventual formation may take place would certainly be finite. Naively, the formation of a quark-gluon plasma (QGP) in a relativistic heavy ion collision is generally assumed to take place in a reaction zone having a finite volume V, about $1\,fermi$ of width and a transverse area of colliding nuclei $\sim A^{2/3}$, which gives: $V \simeq A^{2/3} fm^3$. Since the AGS and SPS data are available, then the use of the Hanbury Brown Twiss (HBT) interferometry method to estimate the possible sizes of the QGP gives the results resumed in Table (3.1) (for the RHIC and LHC energies, simple entropy arguments have been used to predict the QGP sizes [77]) :

Also, the study of the phase transition from HG to QGP with lattice QCD calculations is necessarily performed in finite lattices [78]. In lattice QCD and if we consider

Accelerator	**AGS-SPS**	**RHIC**	**LHC**
QGP Volume (fm^3)	$\sim (34 - 268)$	$\sim (268 - 2144)$	$\sim (905 - 5575)$

Table 3.1: QGP volumes realised at AGS-SPS and RHIC and expected at LHC.

References	[79]	[80]	[81]	[82]	[83]	[78]
QCD Lattice Volume $V_{\max}$ (fm^3)	$\lesssim 40$	~ 7	~ 8	~ 21	~ 37	~ 14

Table 3.2: Values of some lattice volumes used in lattice-QCD calculations

a 4-dimensional lattice, of lattice spacing a, on which we want to perform Monte-carlo simulations of QCD, the lattice sizes are $T \times L \times L \times L$.

Effects of the finite volume are certainly important, since statistical fluctuations in a finite volume are considerable and may hinder a sharp transition between the two phases. Indeed, phase transitions are known to be infinitely sharp only in the thermodynamic limit. In general, finite size effects lead to a mixed phase system, a rounding of the transition and a broadened transition region.

This chapter is devoted to the study of a finite system undergoing a deconfinement phase transition from a hadronic gas phase to a QGP. The finite size effects are studied within a simple thermodynamic model used in [4], based on the assumption of the co-existence of confined and deconfined phases in a finite volume, and using the equations of state of the two phases. For the HG phase, we consider the partition function of a pionic gas. For the QGP phase, we first consider the partition function of a free gas of quarks and gluons derived simply within the bag model.

After this, to account for the 'color neutrality' of the observed free particles, and then of the total QGP, we require that all physical states be color-singlet with respect to the SU(3) color gauge group. Hence, we include the exact color-singletness con-

dition in the calculation of the QGP partition function using the Group Theoretical Projection Technique [6]. This color-singlet partition function can not be exactly calculated and is usually calculated within the saddle point and Gaussian approximations in the limit $VT^3 >> 1$ [7, 8]. It turns out that the use of the such obtained partition function, within the phase coexistence model, has as a consequence the absence of the deconfinement phase transition. We show that this is due to the fact that the approximations used for the calculation of the color-singlet partition function break down at $VT^3 << 1$, and this limit is attained using the phase coexistence model, since the fractional volume V_{QGP} occupied by the QGP is allowed to take small and even zero values.

In view to analyze the finite-size effects in such a model, we first proposed in [13, 14] the calculation of an adequate color-singlet partition function expanded in a power series of the QGP volume fraction, using some approximations but avoiding the problem arising at $VT^3 << 1$. The color-singlet partition function derived in this way allowed us to accurately calculate physical quantities describing well the deconfinement phase transition at finite volumes, and to probe the behavior of the phase transition at criticality, for both temperature-driven and density-driven deconfinement phase transition. This part of the work will not be exposed in this thesis.

After this, we proceeded in a different way for calculating the mean values of physical quantities numerically and without any approximation, by including the exact definition of the color-singlet partition function within the phase coexistence model, without explicitly calculating this latter [84]. The effects of finiteness of the system size are then studied by examining the behavior of several physical quantities with varying volume. This is the main object of the present chapter.

3.2 The Deconfinement Phase Transition in a Finite Volume

3.2.1 The Deconfinement Phase Transition within the Phase Coexistence Model

To study the QCD deconfinement phase transition in a finite volume, we consider a simple phase coexistence model used in [4], in which the mixed HG-QGP phase system has a finite volume: $V = V_{HG} + V_{QGP}$. The parameter $\mathfrak{h}$ representing the fraction of volume occupied by the HG: $V_{HG} = \mathfrak{h}V$, is then defined. Thus, the value: $\mathfrak{h} = 1$ corresponds to a total HG phase and when $\mathfrak{h} = 0$, the system is completely in the QGP phase. Assuming non-interacting phases (separability of the energy spectra of the two phases), the total partition function of the system can be approximately written as:

$$Z\left(\mathfrak{h},T,\mu,V\right) = Z_{QGP}\left(\mathfrak{h},T,\mu,V\right) Z_{HG}\left(\mathfrak{h},T,\mu,V\right), \tag{3.1}$$

and the probability to find the system in the state $\mathfrak{h}$, as defined in [4], is then given by:

$$p\left(\mathfrak{h},T,\mu,V\right) = \frac{Z\left(\mathfrak{h},T,\mu,V\right)}{\int\limits_0^1 Z\left(\mathfrak{h},T,\mu,V\right) d\mathfrak{h}}. \tag{3.2}$$

The mean value of any thermodynamic quantity $\mathcal{A}(T,\mu,V)$ of the system can then be calculated by:

$$\begin{aligned} \left\langle \mathcal{A}(T,\mu,V) \right\rangle &= \int\limits_0^1 \mathcal{A}\left(\mathfrak{h},T,\mu,V\right) p\left(\mathfrak{h},T,\mu,V\right) d\mathfrak{h} \\ &= \frac{\int\limits_0^1 \mathcal{A}\left(\mathfrak{h},T,\mu,V\right) Z\left(\mathfrak{h},T,\mu,V\right) d\mathfrak{h}}{\int\limits_0^1 Z\left(\mathfrak{h},T,\mu,V\right) d\mathfrak{h}}, \end{aligned} \tag{3.3}$$

where $\mathcal{A}(\mathfrak{h},T,\mu,V)$ is the total thermodynamic quantity in the state $\mathfrak{h}$, given in the case of an extensive quantity by:

$$\mathcal{A}(\mathfrak{h},T,\mu,V) = \mathcal{A}_{HG}(T,\mu,\mathfrak{h}V) + \mathcal{A}_{QGP}(T,\mu,(1-\mathfrak{h})\,V), \tag{3.4}$$

and in the case of an intensive quantity, by:

$$\mathcal{A}(\mathfrak{h},T,\mu,V) = \mathfrak{h}\mathcal{A}_{HG}(T,\mu,\mathfrak{h}V) + (1-\mathfrak{h})\mathcal{A}_{QGP}(T,\mu,(1-\mathfrak{h})\,V), \tag{3.5}$$

with $\mathcal{A}_{QGP}$ and $\mathcal{A}_{HG}$ the thermodynamic quantities relative to the individual QGP and HG phases, respectively.

Let us note that the coexistence of two phases in a finite system undergoing a phase transition taken alone seems not to be sufficient for anticipating the first order nature of the phase transition when approaching the thermodynamic limit. A similar confusion can arise in the case of a correlation length scaling with the volume and suggesting a second order nature of the transition in the thermodynamic limit. This subtle situation has been noticed and clarified in several works [46, 70, 85, 86, 87, 88, 89, 90, 91, 92, 93, 94, 95, 96]. Then, for a firm determination of the order of a phase transition in a finite system, a full and detailed finite size scaling analysis of different response functions simultaneously, yielding various scaling critical exponents, seems to be necessary. This is not all in our case, since other basic parameters of QCD like the number of flavors and the current quark masses have a strong influence on how the phase transition occurs. A clear sensitivity of the order of the QCD deconfinement phase transition to these parameters has been revealed by several lattice QCD calculations (see for example [46]-[60]).

The partition functions of both HG and QGP phases are calculated, and their final expressions are given in the following. For a pionic gas, the partition function is simply

given by:

$$Z_{HG}\left(T, V_{HG}\right) = e^{\frac{\pi^2}{30}T^3 V_{HG}}, \tag{3.6}$$

and for a QGP consisting of gluons and two flavors of massless quarks (up, down), with a chemical potential μ, within the bag model [5], the partition function is given by [97]:

$$Z_{QGP}(T, \mu, V_{QGP}) = \exp\left(\left(\frac{37\pi^2}{90}T^3 + \mu^2 T + \frac{1}{2\pi^2}\frac{\mu^4}{T} - \frac{B}{T}\right)V_{QGP}\right), \tag{3.7}$$

where B is the bag constant accounting for the real vacuum pressure exerted on the perturbative vacuum. Let us note that taking the same chemical potential for quarks, i.e., $\mu_u = \mu_d = \mu$, is just an approximation for simplification, and is usually used [98]. The chemical potential depends on several parameter as the bath temperature and the particle masses, since it determines the energy required to add/remove a particle at fixed pressure, energy and entropy [99].

The pressure of the QGP can then be derived directly as:

$$P_{QGP} = \frac{37\pi^2}{90}T^4 + \mu^2 T^2 + \frac{1}{2\pi^2}\mu^4 - B. \tag{3.8}$$

and that of the hadronic matter is given by:

$$P_{HG} = \frac{\pi^2}{30}T^4. \tag{3.9}$$

From the Gibbs criteria, the two matter phases are in equilibrium when the temperature, the chemical potential and the pressure of both of them are equal [100]. The phase transition parameters in our simple model come then from setting:

$$P_{HG}\left(\mu_c, T_c\right) = P_{QGP}\left(\mu_c, T_c\right), \tag{3.10}$$

which gives the following expression relating between T_c and μ_c:

$$\frac{17\pi^2}{45}T_c^4 + \mu_c^2 T_c^2 + \frac{1}{2\pi^2}\mu_c^4 = B. \tag{3.11}$$

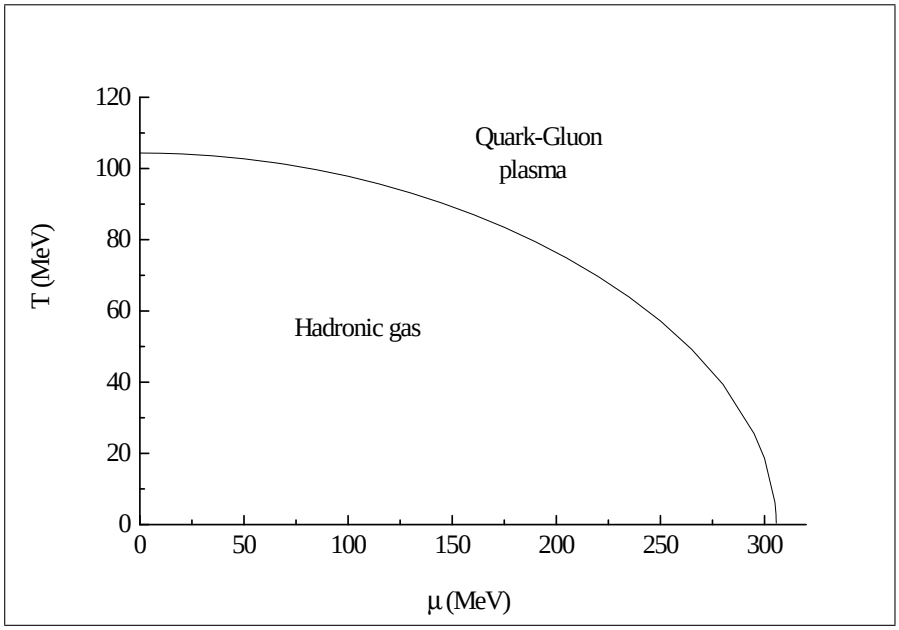

Figure 3.1: Phase diagram in the $\mu - T$ plane.

Fig. (3.1) shows the phase diagram in the $\mu - T$ plane [101], separating between hadronic and QGP phases, and giving at each point the transition parameters (μ_c, T_c) for two flavors ($N_f = 2$), with the common value of the bag constant $B^{1/4} = 145MeV$.

The extreme case $\mu = 0$ could be attained in heavy-ion collisions at high energy (i. e., at high temperature), and the critical temperature evaluated in this case is:

$$T_c = \frac{B^{1/4}}{\left(\frac{17\pi^2}{45}\right)^{\frac{1}{4}}} , \tag{3.12}$$

so the QGP is favored at high temperature ($T > T_c$), and the hadronic phase is favored at low temperature ($T < T_c$) .

The second extreme case $T = 0$ could be reached in the core of some neutron stars

where the density is high, and the critical chemical potential is then given by:

$$\mu_c = \frac{B^{1/4}}{\left[\frac{1}{2\pi^2}\right]^{\frac{1}{4}}}, \tag{3.13}$$

so the QGP is favored at large baryon density, i. e., large chemical potential ($\mu > \mu_c$), and the hadronic phase is favored at low baryon density ($\mu < \mu_c$).

3.2.2 Finite Size Rounding of the Deconfinement Phase Transition

As it is known, the deconfined quark matter state can be obtained at extreme conditions of temperature and/or density, i. e., either by raising temperature or chemical potential. The deconfinement phase transition is then temperature-driven or density-driven. We'll study in the following the FSE for a temperature driven deconfinement phase transition, at a vanishing chemical potential ($\mu = 0$), and for a density driven deconfinement phase transition at a fixed temperature ($T = 100MeV$), using the common value $B^{1/4} = 145MeV$ for the bag constant. To study these effects of volume finiteness, we'll examine the behavior of some thermodynamic quantities with temperature and chemical potential for varying volume. The main quantities of interest are the order parameter, which is simply in this case the mean value of the hadronic volume fraction, the entropy density and the energy density. The mean values of these latter, i. e., $\langle s(T,\mu,V)\rangle$ and $\langle \varepsilon(T,\mu,V)\rangle$ are related to the order parameter $\langle \mathfrak{h}(T,\mu,V)\rangle$ by the expressions:

$$\begin{aligned} \langle s(T,\mu,V)\rangle &= \mathfrak{s}_{QGP} + (\mathfrak{s}_{HG} - \mathfrak{s}_{QGP})\ \langle \mathfrak{h}(T,\mu,V)\rangle \\ \langle \varepsilon(T,\mu,V)\rangle &= \mathfrak{e}_{QGP} + (\mathfrak{e}_{HG} - \mathfrak{e}_{QGP})\ \langle \mathfrak{h}(T,\mu,V)\rangle, \end{aligned} \tag{3.14}$$

where:

$$\langle \mathfrak{h}\,(T,\mu,V)\rangle = \frac{\left(-\frac{1}{T}(f_{HG}-f_{QGP})V-1\right)e^{-\frac{1}{T}(f_{HG}-f_{QGP})V}+1}{-\frac{1}{T}(f_{HG}-f_{QGP})V\left(e^{-\frac{1}{T}(f_{HG}-f_{QGP})V}-1\right)}, \tag{3.15}$$

with:

$$\begin{cases} f_{QGP} = -\frac{37\pi^2}{90}T^4 - \mu^2T^2 - \frac{1}{2\pi^2}\mu^4 + B;\ f_{HG} = -\frac{\pi^2}{30}T^4 \\ \mathfrak{s}_{QGP} = \frac{74\pi^2}{45}T^3 + 2\mu^2T;\ \mathfrak{s}_{HG} = \frac{2\pi^2}{15}T^3 \\ \mathfrak{e}_{QGP} = B + \frac{37\pi^2}{30}T^4 + \mu^2T^2 - \frac{\mu^4}{2\pi^2};\ \mathfrak{e}_{HG} = \frac{\pi^2}{10}T^4. \end{cases} \tag{3.16}$$

Fig. (3.2) shows the three-dimensional plots of the order parameter, energy density $\langle \varepsilon\,(T,V)\rangle$ and entropy density $\langle s\,(T,V)\rangle$, vs temperature and system volume, at a vanishing chemical potential ($\mu = 0$), with $B^{1/4} = 145MeV$ for the bag constant, and Fig. (3.3) illustrates those of the normalized energy density $\frac{\langle \varepsilon\,(T,V)\rangle}{T^4}$ and entropy density $\frac{\langle s\,(T,V)\rangle}{T^3}$. The first-order character of the transition is showed by the step-like rise or sharp discontinuity of each of the order parameter, as well as the normalized energy and entropy densities, when approaching the thermodynamic limit, at a transition temperature $T_c\,(\infty) \simeq 104.35MeV$, which reflects the existence of a latent heat accompanying the phase transition. The quantities $\frac{\langle \varepsilon\rangle}{T^4}$ and $\frac{\langle s\rangle}{T^3}$ are traditionally interpreted as a measure of the number of effective degrees of freedom [102]; the temperature increase causes then a "melting" of the constituent degrees of freedom "frozen" in the hadronic state, making the energy and entropy densities attain their plasma values. In small systems, the phase transition is rounded since the probability of presence of the QGP phase below T_c, and of the hadron phase above T_c are finite because of the considerable thermodynamical fluctuations. The transition region around the transition temperature $T_c\,(\infty)$ is then broadened, acquiring a bigger width $\delta T(V)$, smaller is the volume.

Similarly, Fig. (3.4) shows the variations of the order parameter, the energy and

entropy densities with chemical potential and system volume, at the temperature $T = 100MeV$. The first-order character of the transition can, also in this case, clearly be seen from the sharp discontinuity of the three quantities at a transition chemical potential $\mu_c(\infty) \simeq 81.8MeV$, at the large volume limit. In small systems, the transition is perfectly smooth over a broadened region of chemical potential of width $\delta\mu(V)$. Let us note that in the QGP phase at $\mu > \mu_c(V)$, the energy and entropy densities grow with chemical potential like in Fig. (3.2) with temperature, but in this case it is no more possible to normalize in view to obtain the number of degrees of freedom because of the existence of both chemical potential and temperature in the expressions.

3.3 The QCD Deconfinement Phase Transition in a Finite Volume Including the Color-Singletness Requirement

3.3.1 The Color-Singlet Partition Function of the QGP

For the QGP phase, we consider a free gas of quarks and gluons with the exact color-singletness requirement. To implement the color-singletness constraint into the quantum statistical description of the system, we use the group theoretical projection technique formulated by Turko and Redlich [6], as done in several works [7, 8, 103, 104, 105, 106, 107, 108, 109, 110, 111, 112, 113]. The projected partition function for a system of quarks, antiquarks and gluons in a volume V, at temperature T and quark chemical potential μ is given by:

$$Z_j(T,\mu,V) = Tr(\widehat{\mathcal{P}}_j e^{-\beta\widehat{H}}), \tag{3.17}$$

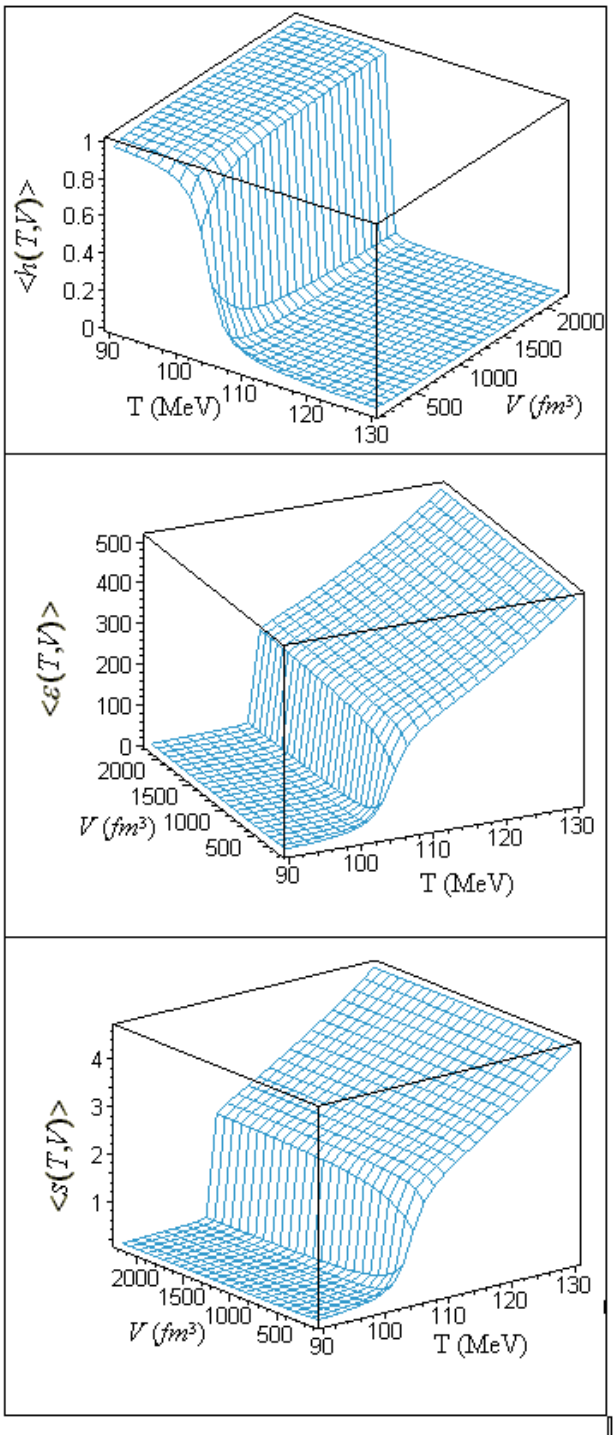

Figure 3.2: Mean values of (top) the order parameter, (middle) the energy density and (bottom) the entropy density as functions of temperature T and system size V, at $\mu = 0$.

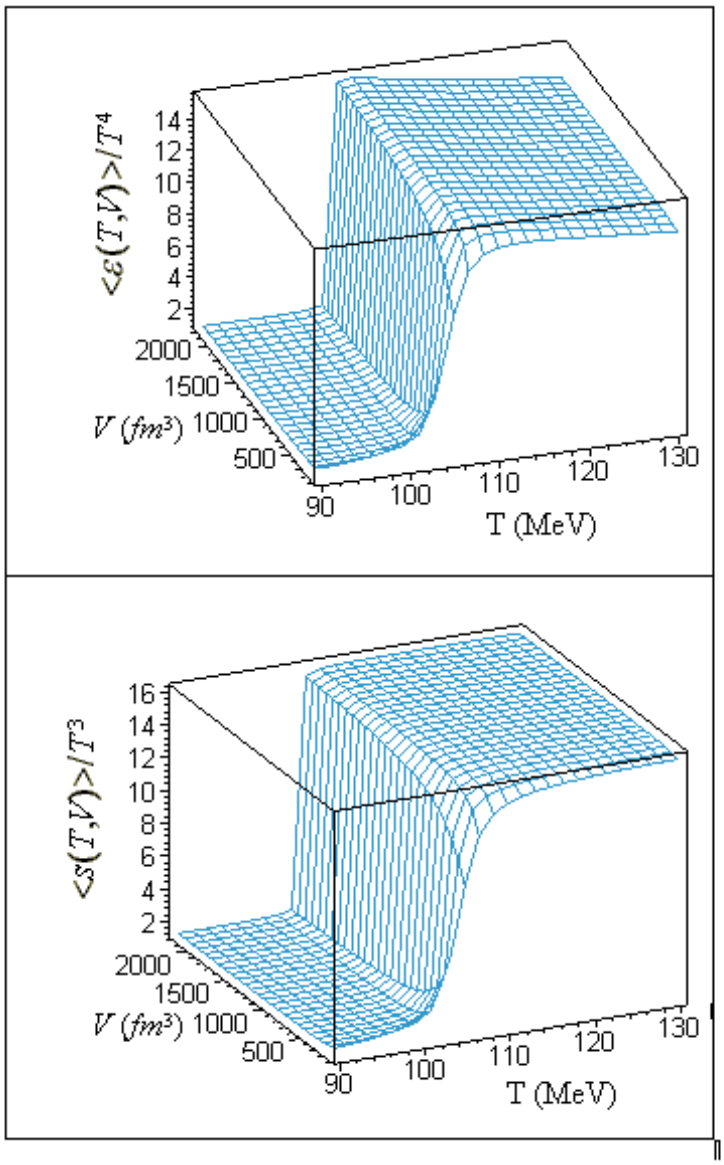

Figure 3.3: Mean values of (top) the energy density normalized by T^4 and (bottom) the entropy density normalized by T^3as functions of temperature T and system size V, at $\mu = 0$.

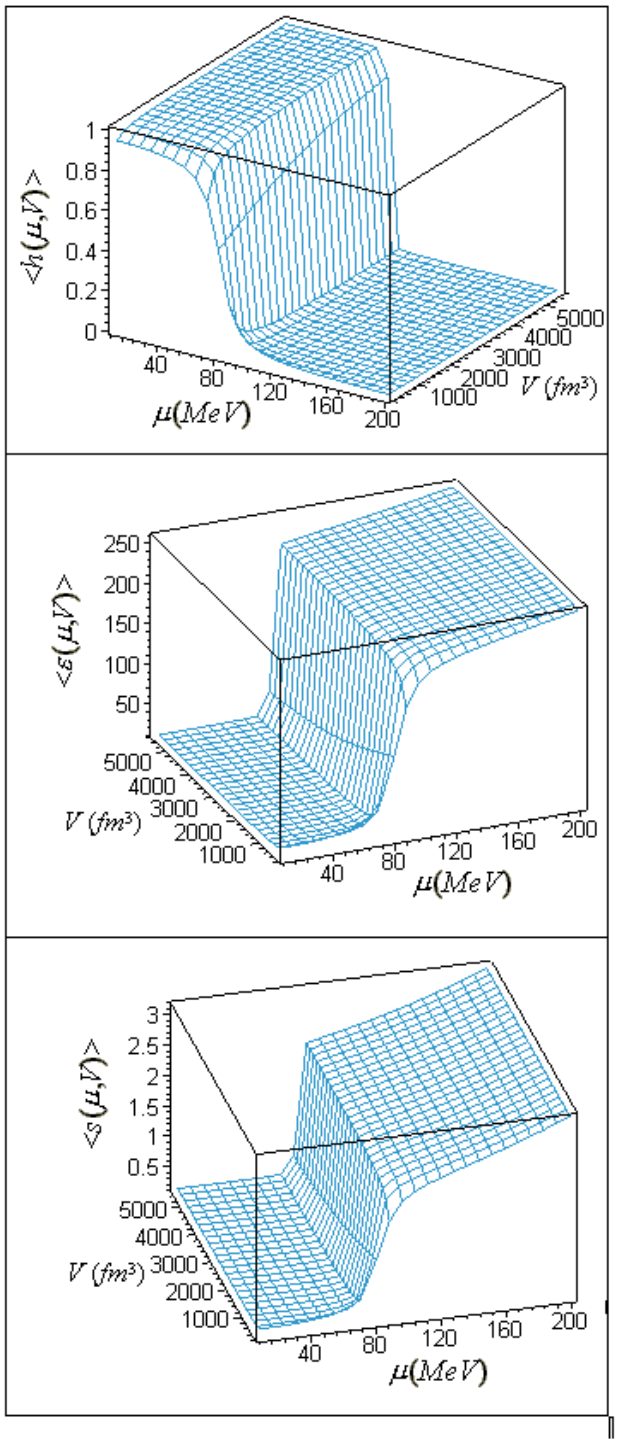

Figure 3.4: Mean values of (top) the order parameter, (middle) the energy density and (bottom) the entropy density as functions of chemical potential μ and system size V, at the temperature $T = 100MeV$.

where: $\beta = \frac{1}{T}$ with the units chosen as: $k_B = \hbar = c = 1$, $\widehat{H}$ is the Hamiltonian of the system and $\widehat{\mathcal{P}}_j$ is a projection operator for a symmetry group $\mathcal{G}$ (compact Lie group) having a unitary representation $\widehat{U}(g)$ in a Hilbert space $\mathcal{H}$,

$$\widehat{\mathcal{P}}_j = d_j \int_{\mathcal{G}} d\mu(g) \chi_j^*(g) \widehat{U}(g), \tag{3.18}$$

$d\mu(g)$ being the normalized Haar measure in $\mathcal{G}$, d_j the dimension and $\chi_j^*(g)$ the character of the irreducible representation "j" of $\mathcal{G}$.

For $SU(3)$ color-singlet configuration, $d_j = 1$, $\chi_j = 1$, and the explicit form of the Haar measure is:

$$\int_{SU(N_c)} d\mu(g) = \frac{1}{N_c!} \left(\prod_{c=1}^{N_c-1} \int_{-\pi}^{+\pi} \frac{d\theta_c}{2\pi} \right) \left[\prod_{i<k}^{N_c} \left(2 \sin \frac{\theta_i - \theta_k}{2} \right)^2 \right], \tag{3.19}$$

θ_l being a class parameter obeying the periodicity condition $\sum_{l=1}^{N_c} \theta_l = 0 \pmod{2\pi}$ and insuring that the group element is $SU(N_c)$. Hence, eq. (3.17) becomes:

$$Z_c(T, \mu, V) = \int_{SU(3)} d\mu(g) \mathcal{T}r(\widehat{U}(g) e^{-\beta \widehat{H}}). \tag{3.20}$$

The Hilbert space $\mathcal{H}$ of the composite system has the structure of a tensor product of their individual Fock spaces as:

$$\mathcal{H} = \mathcal{H}_q \otimes \mathcal{H}_{\overline{q}} \otimes \mathcal{H}_{\mathbf{g}}, \tag{3.21}$$

where the subscripts q, $\overline{q}$ and $\mathbf{g}$ denote respectively the quark, antiquark and gluon. The trace involved in eq. (3.20) decomposes then into the product of 3 traces as:

$$Z_c(T, \mu, V) = \int_{SU(3)} d\mu(g) \mathcal{T}r(\widehat{U_q}(g) e^{-\beta \widehat{H}_q}) \mathcal{T}r(\widehat{U_{\overline{q}}}(g) e^{-\beta \widehat{H_{\overline{q}}}}) \mathcal{T}r(\widehat{U_{\mathbf{g}}}(g) e^{-\beta \widehat{H_{\mathbf{g}}}}). \tag{3.22}$$

Now, the trace operations may be performed, and one can then write Z_c as:

$$Z_c(T,\mu,V) = \int\limits_{SU(3)} d\mu(g)\widetilde{Z}_{quark}\widetilde{Z}_{glue}, \tag{3.23}$$

with the quark and gluon contributions individually given by:

$$\begin{aligned}\widetilde{Z}_{quark} &= \prod_{q=r,g,b}\prod_{\alpha}\left[1+e^{-\beta(\epsilon_q^\alpha-\mu_q)+i\theta_q}\right]\left[1+e^{-\beta(\epsilon_{\overline{q}}^\alpha-\mu_{\overline{q}})-i\theta_q}\right] \\ &= \prod_{q=r,g,b}\prod_{\alpha}\left[1+e^{-\beta(\epsilon^\alpha-\mu)+i\theta_q}\right]\left[1+e^{-\beta(\epsilon^\alpha+\mu)-i\theta_q}\right], \end{aligned}\tag{3.24}$$

where ϵ^α are single-particle energies, the explicit expressions of the angles θ_q ($q = r,\ b,\ g$) in $SU(3)$ are:

$$\theta_r = \frac{\varphi}{2}+\frac{\psi}{3},\ \ \theta_g = -\frac{\varphi}{2}+\frac{\psi}{3},\ \ \theta_b = -\frac{2\psi}{3}, \tag{3.25}$$

and in the second factor arising from the antiquarks, we have replaced: $\epsilon_{\overline{q}}^\alpha = \epsilon_q^\alpha = \epsilon^\alpha$ and $\mu_{\overline{q}} = -\mu_q = -\mu$; and:

$$\widetilde{Z}_{glue} = \prod_{\mathbf{g}=1,2,3,4}\prod_{\alpha}\left[1-e^{-\beta\epsilon_\alpha+i\theta_{\mathbf{g}}}\right]^{-1}\left[1-e^{-\beta\epsilon_\alpha-i\theta_{\mathbf{g}}}\right]^{-1}, \tag{3.26}$$

with the angles $\theta_{\mathbf{g}}$ ($\mathbf{g} = 1, ...4$) being:

$$\theta_1 = \theta_r-\theta_g,\ \ \theta_2 = \theta_g-\theta_b,\ \ \theta_3 = \theta_b-\theta_r,\ \ \theta_4 = 0. \tag{3.27}$$

In the continuum approximation for the single-particle energy levels, one can replace $\sum\limits_\alpha$ by $\int\rho(\epsilon)d\epsilon$ where: $\rho(\epsilon) = d_{Q/g}\frac{V}{2\pi^2}\epsilon^2$ is the single-particle density of states, $d_{Q/G}$ is the spin-isospin degeneracy factor for quarks or gluons, with $d_Q = 2N_f$ and $d_G = 2$. After integration, the quark contribution is given by:

$$\widetilde{Z}_{Quark}\left(T,V,\mu;\varphi,\psi\right) = \exp\left[\frac{\pi^2}{12}T^3Vd_Q\sum_{q=r,g,b}\left(\frac{7}{30}-\left(\frac{\theta_q-i(\frac{\mu}{T})}{\pi}\right)^2+\frac{1}{2}\left(\frac{\theta_q-i(\frac{\mu}{T})}{\pi}\right)^4\right)\right], \tag{3.28}$$

and the gluon contribution by:

$$\widetilde{Z}_{Gluon}\left(T,V;\varphi,\psi\right)=\exp\left[\frac{\pi^2}{12}T^3Vd_G\sum_{\mathbf{g}=1}^{4}\left(-\frac{7}{30}+\left(\frac{\theta_{\mathbf{g}}-\pi}{\pi}\right)^2-\frac{1}{2}\left(\frac{\theta_{\mathbf{g}}-\pi}{\pi}\right)^4\right)\right]. \tag{3.29}$$

Thus, the partition function for a color-singlet quark-gluon plasma can be written as [7, 8]:

$$Z(T,V,\mu)=\frac{8}{3\pi^2}e^{-\frac{BV}{T}}\int_{-\pi}^{+\pi}\int_{-\pi}^{+\pi}d\left(\frac{\varphi}{2}\right)d\left(\frac{\psi}{3}\right)M(\varphi,\psi)\widetilde{Z}(T,V,\mu;\varphi,\psi), \tag{3.30}$$

where $M(\varphi,\psi)$ is explicitly given by:

$$M(\varphi,\psi)=\left(\sin\left(\frac{1}{2}(\psi+\frac{\varphi}{2})\right)\sin(\frac{\varphi}{2})\sin\left(\frac{1}{2}(\psi-\frac{\varphi}{2})\right)\right)^2, \tag{3.31}$$

B being the bag constant.

Let us write $\widetilde{Z}$ on the form:

$$\widetilde{Z}\left(T,V,\mu;\varphi,\psi\right)=e^{VT^3g(\varphi,\psi,\frac{\mu}{T})}, \tag{3.32}$$

with:

$$\begin{aligned}g(\varphi,\psi,\frac{\mu}{T}) &= \frac{\pi^2}{12}(\frac{21}{30}d_Q+\frac{16}{15}d_G)+\frac{\pi^2}{12}\frac{d_Q}{2}\sum_{q=r,b,g}\left\{-1+\left(\frac{\left(\theta_q-i(\frac{\mu}{T})\right)^2}{\pi^2}-1\right)^2\right\}\\ &\quad -\frac{\pi^2}{12}\frac{d_G}{2}\sum_{\mathbf{g}=1}^{4}\left(\frac{(\theta_{\mathbf{g}}-\pi)^2}{\pi^2}-1\right)^2,\end{aligned} \tag{3.33}$$

then eq. (3.30) becomes:

$$Z(T,V,\mu)=\frac{8}{3\pi^2}e^{-\frac{BV}{T}}\int_{-\pi}^{+\pi}\int_{-\pi}^{+\pi}d\left(\frac{\varphi}{2}\right)d\left(\frac{\psi}{3}\right)M(\varphi,\psi)e^{VT^3g(\varphi,\psi,\frac{\mu}{T})}. \tag{3.34}$$

3.3.2 Calculation of the Color-Singlet Partition Function of the QGP, within the Saddle Point Approximation

The analytic calculation of the color-singlet partition function of the QGP in eq. (3.34) being not possible to be effectuated exactly, an approximated calculus is usually carried

out using the saddle point approximation as in [8, 9, 10]. Let's derive in the following such an approximate color-singlet partition function at zero chemical potential ($\mu = 0$).

In this case, we have:

$$\begin{aligned} g_{\mu=0}(\varphi,\psi) &= \frac{\pi^2}{12}(\frac{21}{30}d_Q + \frac{16}{15}d_G) + \frac{\pi^2}{12}\frac{d_Q}{2}\sum_{q=r,b,g}\left(\left(\frac{\alpha_q^2}{\pi^2}-1\right)^2-1\right) \\ &\quad -\frac{\pi^2}{12}\frac{d_G}{2}\sum_{\mathbf{g}=1}^{4}\left(\frac{(\alpha_{\mathbf{g}}-\pi)^2}{\pi^2}-1\right)^2, \end{aligned} \tag{3.35}$$

and then the color-singlet partition function for a quark-gluon plasma contained in a volume V_{QGP} becomes:

$$Z(T,V_{QGP}) = \frac{8}{3\pi^2}e^{-\frac{BV_{QGP}}{T}}\int_{-\pi}^{+\pi}\int_{-\pi}^{+\pi} d\left(\frac{\varphi}{2}\right) d\left(\frac{\psi}{3}\right) M(\varphi,\psi)\exp\left(V_{QGP}T^3 g_{\mu=0}(\varphi,\psi)\right). \tag{3.36}$$

The integral in (3.36) can be evaluated by a saddle point approximation around the maximum of the integrand at $(\varphi,\psi) = (0,0)$. For that purpose, we expand the weight function M to leading order in the angular variables, and expand the argument of the exponential to second order in φ and ψ (gaussian approximation). The measure function has then the following form:

$$M(\varphi,\psi) \approx M^{(0,0)}(\varphi,\psi) = \frac{1}{64}\varphi^2\left(\psi^2 - \frac{\varphi^2}{4}\right)^2, \tag{3.37}$$

and $g_{\mu=0}(\varphi,\psi)$ becomes for two flavors ($N_f = 2$) (up and down quarks):

$$g_{\mu=0}(\varphi,\psi) \approx g_{\mu=0}^{(0,0)}(\varphi,\psi) = S_0 - \frac{2}{3}\left(\varphi^2 + \frac{4}{3}\psi^2\right), \tag{3.38}$$

with:

$$S_0 = \frac{\pi^2}{12}(\frac{7N_f}{5} + \frac{32}{15}). \tag{3.39}$$

Therefore, we have integrals like:

$$\int_0^a e^{-\alpha x^2}dx \approx \int_0^\infty e^{-\alpha x^2}dx = \sqrt{\pi/\alpha}, \tag{3.40}$$

with $\alpha \gg 1$.

From all these considerations, the partition function can then be rewritten as:

$$Z(T, V_{QGP}) = \frac{8}{3\pi^2} e^{-\frac{BV_{QGP}}{T}} \int_{-\infty}^{+\infty} \int_{-\infty}^{+\infty} d\left(\frac{\varphi}{2}\right) d\left(\frac{\psi}{3}\right) M^{(0,0)}(\varphi, \psi) \exp\left(g_{\mu=0}^{(0,0)}(\varphi, \psi) V_{QGP} T^3\right), \tag{3.41}$$

which gives after calculation:

$$Z(T, V_{QGP}) = \frac{A_0 e^{\left(S_0 T^3 - \frac{B}{T}\right) V_{QGP}}}{\left(V_{QGP} T^3\right)^4}, \tag{3.42}$$

where:

$$A_0 = \frac{27\sqrt{3}}{8192\pi}. \tag{3.43}$$

We mention here a similar result obtained in [9] given for a zero baryon density as:

$$Z_{QGP}(T, V_{QGP}) = A\, C^{-4} u^{-3/2} \frac{\exp\left(\frac{1}{3} u V_{QGP} T^3\right)}{\left(V_{QGP} T^3\right)^{13/2}} \exp(-\frac{B V_{QGP}}{T}), \tag{3.44}$$

with:

$$\begin{cases} A = \dfrac{3\sqrt{2\pi}}{4} \\ C = 2 + \dfrac{N_f}{3} \\ u = \left(\dfrac{8}{15} + \dfrac{7N_f}{20}\right) \pi^2. \end{cases} \tag{3.45}$$

3.3.3 Problem with the Use of the Color-Singlet Partition Function Derived within the Saddle Point Approximation, in the Phase Coexistence Model

Let us incorporate such an approximate partition function, eqs. (3.42-43), for the QGP in the phase coexistence model. The order parameter can then be expressed as:

$$\langle \mathfrak{h}(T, V) \rangle = 1 - \left(\int_0^1 \mathfrak{q}^{-3} e^{K\mathfrak{q}} d\mathfrak{q} \; / \; \int_0^1 \mathfrak{q}^{-4} e^{K\mathfrak{q}} d\mathfrak{q} \right), \tag{3.46}$$

where $\mathfrak{q}$ is the QGP volume fraction defined as: $\mathfrak{q} = 1 - \mathfrak{h}$, and: $K = \left(S_0 - \frac{\pi^2}{30}\right) T^3 V - \frac{BV}{T}$.

By expanding the exponential $e^{K\mathfrak{q}}$, and taking the limit $\mathfrak{q}_0$ for $\mathfrak{q}$ instead of 0 in the integral above (i.e., $\mathfrak{h} \longrightarrow \mathfrak{h}_0$), we obtain the following expression for the mean value of the hadronic volume fraction:

$$\langle \mathfrak{h}(T,V) \rangle = 1 - \mathfrak{q}_0 \left(\sum_{p=0}^{\infty} \frac{K^p}{p!\,(p-2)} \left(\mathfrak{q}_0^p - \mathfrak{q}_0^2\right) / \sum_{p=0}^{\infty} \frac{K^p}{p!\,(p-3)} \left(\mathfrak{q}_0^p - \mathfrak{q}_0^3\right) \right). \tag{3.47}$$

We can easily show that for $\mathfrak{q}_0 \longrightarrow 0$ (i. e., $\mathfrak{h}_0 \longrightarrow 1$), the mean value of the hadronic volume fraction is equal to 1 for all values of temperature and volume [12].

Hence, the use of the obtained approximate total partition function $Z(\mathfrak{h})$ in the definition (3.3), has as a consequence the absence of the deconfinement phase transition. This is due to the fact that the saddle point approximation, used for the calculation of the color-singlet partition function, breaks down at $V_{QGP}T^3 << 1$. We propose in the following, first, a new method for calculating an exact color-singlet partition function with the unique disadvantage of necessitating very long times for numerical calculations.

3.3.4 Remedy to the problem

To remedy to the problem exposed above in a first step, we have tried to do the expansion of the exponential $e^{V_{QGP}T^3 g(\varphi,\psi,\frac{\mu}{T})}$ as:

$$e^{V_{QGP}T^3 g(\varphi,\psi,\frac{\mu}{T})} = \sum_{j=0}^{\infty} \frac{(V_{QGP}T^3)^j}{j!} \left(g(\varphi,\psi,\frac{\mu}{T}) \right)^j, \tag{3.48}$$

then (3.34) becomes:

$$Z_{QGP}(T,\mu,V_{QGP}) = \frac{8}{3\pi^2} \int_{-\pi}^{+\pi} \int_{-\pi}^{+\pi} d(\varphi/2) d(\psi/3) M(\varphi,\psi) \sum_{j=0}^{\infty} \frac{(V_{QGP}T^3)^j}{j!} \left(g(\varphi,\psi,\frac{\mu}{T}) \right)^j, \tag{3.49}$$

and by putting:

$$\alpha_j = \frac{4}{9\pi^2}\int_{-\pi}^{+\pi}\int_{-\pi}^{+\pi} d\varphi d\psi M(\varphi,\psi)\frac{\left(g(\varphi,\psi,\frac{\mu}{T})\right)^j}{j!}, \tag{3.50}$$

the partition function becomes:

$$Z_{QGP}(T,\mu,V_{QGP}) = \sum_{j=0}^{\infty}\alpha_j(V_{QGP}T^3)^j = \sum_{j=0}^{\infty}\alpha_j z^j, \tag{3.51}$$

where: $z = V_{QGP}T^3$. It can be seen that the series (3.51) giving the color-singlet partition function is convergent and causes no more problems at $z \to 0$ since for $V_{QGP}T^3 = 0$, $Z\left(V_{QGP}T^3 = 0\right) = \alpha_0$. It can then be incorporated in the phase coexistence model to probe the critical behavior of thermodynamic quantities characterizing the system which undergoes a deconfinement phase transition. Because of numerical difficulties, it was not possible for us to illustrate this exact calculus at the present time. Indeed, the integral coefficients α_j have been calculated to high ranks ($j = 175$) using a numerical integration program with fortran, and the series giving Z_{QGP} has been calculated for values of T and V_{QGP} such that $V_{QGP}T^3 \leq 5$; for example, for $V_{QGP}T^3 = 2$ the value of Z_{QGP} is stable at $j \approx 110$. But it turned out that for large volumes and/or temperatures, the rank j at which the convergence of Z_{QGP} is attained is very high, and since the values of the coefficients α_j are largely increasing and due to the insufficient precision offered by fortran, the convergence of Z_{QGP} couldn't be attained.

After this, we have tried to use Mathematica 4.0 for the numerical calculation of α_j, since this software can insure much more precision but it turned out that the time of calculus at ranks $j \gtrsim 13$ begins to become too long, rendering the use of such a method practically a waste of time.

In order to get a first understanding of the deconfinement phase transition in a

finite volume, we have proceeded, in a second step of the work, by effectuating some approximations to derive a suitable color-singlet partition function, which allowed us to accurately calculate physical quantities describing well the deconfinement phase transition at finite volumes. This part of the work can be found in [13, 14].

A more rigorous calculus then followed, where the color-singlet partition function of the QGP has not been calculated explicitly, but has just been used with its exact expression (3.34) in order to calculate mean values of physical quantities of the system using the definition (3.3) [84]. Details are given in the following.

3.4 Finite-Size Effects with the Exact Color-Singlet Partition Function within the L_{mn} *Method*

In the following, we'll derive the mean values of the order parameter, and then of other thermodynamic quantities, directly from the definition (3.3) of the mean value of any physical quantity within the phase coexistence model, using the exact definition (3.34) of the QGP color-singlet partition function. The exact total partition function given by:

$$Z\left(\mathfrak{q}\right)=\frac{4}{9\pi^{2}}e^{\frac{\pi^{2}}{30}VT^{3}}\int_{-\pi}^{+\pi}\int_{-\pi}^{+\pi}d\varphi d\psi M(\varphi,\psi)e^{\mathfrak{q}VT^{3}\left(g(\varphi,\psi,\frac{\mu}{T})-\frac{\pi^{2}}{30}-\frac{B}{T^{4}}\right)}, \tag{3.52}$$

will not be calculated itself exactly, but the integration on $\mathfrak{q}$ in the calculation of the mean values using this exact partition function will first be effectuated, then the integrations on φ and ψ will be done at last [84].

Let's first illustrate the variations of the probability density $p(\mathfrak{h})=\frac{Z(\mathfrak{h})}{\int_{0}^{1}Z(\mathfrak{h})d\mathfrak{h}}$ with the hadron fraction $\mathfrak{h}$, for various system volumes, at the temperature $T=105MeV$

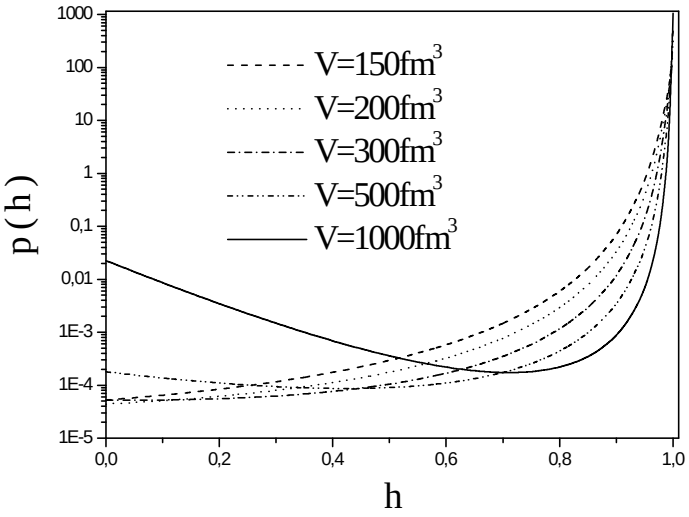

Figure 3.5: Probability density as a function of the hadron fraction for different system volumes, at the temperature $T = 105MeV$.

(Fig. (3.5)). The probability density exhibits a "two hump" structure at the extremal values of the hadron fraction $\mathfrak{h}$, more accentuated for big volumes. This structure indicates the dominance of one phase in the mixed phase system. It has been shown in [3] that such a structure is expected in the case of first order phase transitions.

The probability distribution at a fixed value of $\mathfrak{h}$ is also plotted versus temperature at different volumes in Fig. (3.6), which shows that the probability at fixed $\mathfrak{h}$ and V is peaked at a certain temperature tending to the true transition temperature $T_c(\infty)$ with increasing volume, at which it is maximal. This temperature is shifted to bigger values for small volumes. It can also be noted that the probability distribution looks to be symmetric for $\mathfrak{h} = 0.5$, while for $\mathfrak{h} = 0.1$ and $\mathfrak{h} = 0.9$ it is not symmetric. The tail of the distribution is heavier on the right for $\mathfrak{h} = 0.1$ and heavier on the left for $\mathfrak{h} = 0.9$. This is easily understandable, since at $\mathfrak{h} = 0.1$ it is the QGP which is dominant and

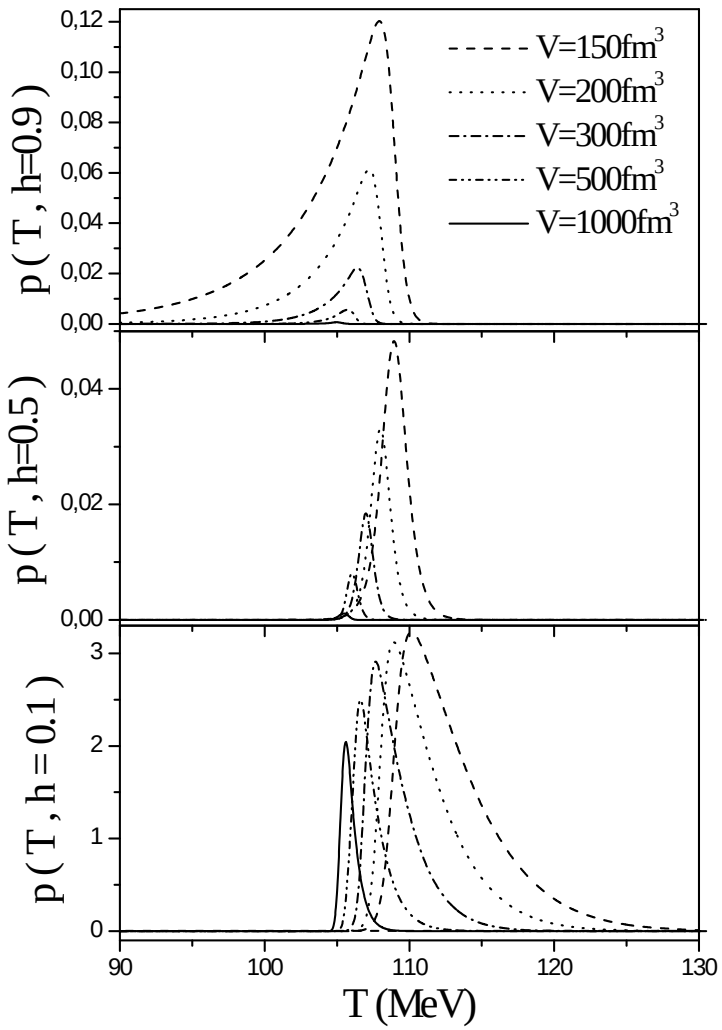

Figure 3.6: Variations of the probability of finding the system (of volume V) in a state (bottom) $\mathfrak{h}$ =0.1, (middle) $\mathfrak{h}$ =0.5, and (top) $\mathfrak{h}$ =0.9 with temperature T, for different system volumes.

this occurs above the transition temperature, and at $\mathfrak{h} = 0.9$ it is the hadronic gas phase which is dominant and this occurs below the transition temperature.

3.4.1 Order Parameter, Energy and Entropy Densities

Like in the case without including the color-singletness requirement, let's calculate now the order parameter at zero chemical potential ($\mu = 0$), using the total partition function (3.52). Its expression is in this case:

$$< \mathfrak{h}(T,V) >^{*} = 1 - \frac{\int_{-\pi}^{+\pi}\int_{-\pi}^{+\pi} d\varphi d\psi M(\varphi,\psi) \int_{0}^{1} \mathfrak{q} e^{\mathfrak{q}\ \mathfrak{R}(\varphi,\psi;T,V)} d\mathfrak{q}}{\int_{-\pi}^{+\pi}\int_{-\pi}^{+\pi} d\varphi d\psi M(\varphi,\psi) \int_{0}^{1} e^{\mathfrak{q}\ \mathfrak{R}(\varphi,\psi;T,V)} d\mathfrak{q}}, \tag{3.53}$$

with:

$$\mathfrak{R}\left(\varphi,\psi;T,V\right) = \left(g_{\mu=0}(\varphi,\psi) - \frac{\pi^2}{30} - \frac{B}{T^4}\right) VT^3. \tag{3.54}$$

After effectuation of the integrations on $\mathfrak{q}$, the order parameter can be written on the form:

$$< \mathfrak{h}(T,V) >^{*} = \frac{L_{01}\left(0\right) + L_{02}\left(0\right) - L_{02}\left(1\right)}{L_{01}\left(0\right) - L_{01}\left(1\right)}, \tag{3.55}$$

where the general form of the integrals on φ and ψ appearing in this expression is:

$$L_{mn}\left(\mathfrak{q}\right) = \int_{-\pi}^{+\pi}\int_{-\pi}^{+\pi} d\varphi d\psi M(\varphi,\psi)(g_{\mu=0}(\varphi,\psi))^m \frac{e^{\mathfrak{q}\ \mathfrak{R}(\varphi,\psi;T,V)}}{\left(\mathfrak{R}\left(\varphi,\psi;T,V\right)\right)^n}. \tag{3.56}$$

The integrals L_{mn} represent in themselves state functions, and they have been chosen in a judicious way so that all thermodynamic quantities can, in one way or the other, be written as function of these L_{mn}'s. They can be calculated numerically at each temperature T and volume V, and the mean values of physical quantities can therefore be illustrated on the hole range of temperature for varying volume. Fig. (3.7) illustrates the variations of some L_{mn}'s with temperature at fixed volume.

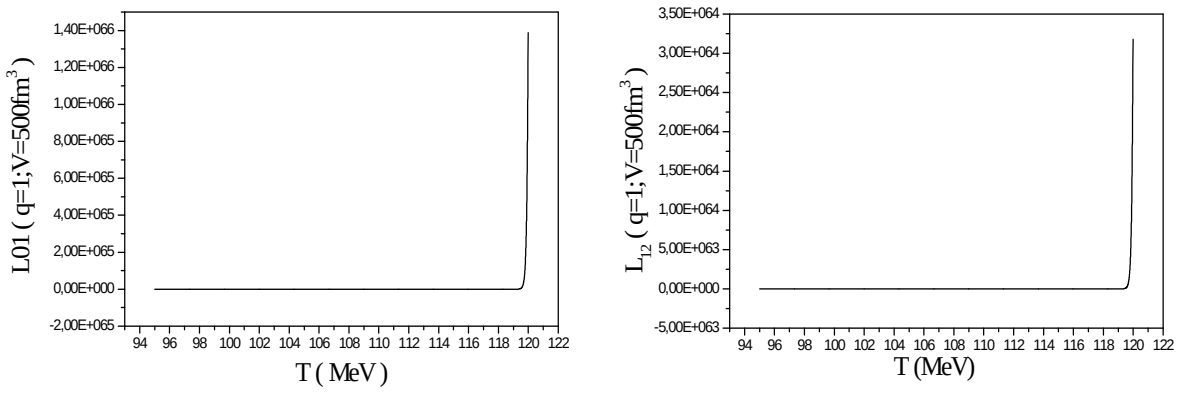

Figure 3.7: Variations of $L_{01}\,(\mathfrak{q}=1)$ and $L_{12}\,(\mathfrak{q}=1)$ with temperature at the volume $V = 500 fm^3$.

The mean value of the energy density is also calculated in the same way, and is found to be related to $<\mathfrak{h}(T,V)>^*$ by the expression:

$$<\varepsilon(T,V)>^* = B-(B-e_{HG})<\mathfrak{h}(T,V)>^* -3T^4\,\frac{L_{12}\,(0)+L_{11}\,(1)-L_{12}\,(1)}{L_{01}\,(0)-L_{01}\,(1)}. \quad (3.57)$$

Let us note that we have used "Mathematica 4.0" to evaluate the integrals L_{mn} numerically, and then the mean values of the order parameter and energy density. The evaluation of the order parameter at a given temperature and volume takes an approximate time of about 13 minutes, and that of $<\varepsilon(T,V)>^*$ about 25 minutes, on a (PentiumIII, 500MHz). For the illustration of both $<\mathfrak{h}(T,V)>^*$ and $<\varepsilon(T,V)>^*$, the calculations are done on an interval of temperature $(95-120 MeV)$ with a temperature step $(dT = 0.1 MeV)$ and are repeated for various volumes.

The entropy can be obtained from the thermodynamic relation: $s = \frac{1}{T}(\varepsilon - f)$, knowing the free energy $F = fV$, which is defined as: $F = -T\ln Z$. The mean value

of this latter involves then an integral $\int_0^1 d\mathfrak{h} Z(\mathfrak{h}) \ln Z(\mathfrak{h})$ as given by the expression:

$$\begin{aligned}\langle F(T,V)\rangle^* &= -T\left[\ln(\frac{4}{9\pi^2}) + \frac{\pi^2}{30}VT^3\right. \\ &\left. + \frac{\int_0^1 d\mathfrak{q}\left(\int_{-\pi}^{+\pi}\int_{-\pi}^{+\pi} d\varphi d\psi M(\varphi,\psi) e^{\mathfrak{q}\ \mathfrak{R}(\varphi,\psi;T,V)}\right)\ln\left(\int_{-\pi}^{+\pi}\int_{-\pi}^{+\pi} d\varphi d\psi M(\varphi,\psi) e^{\mathfrak{q}\ \mathfrak{R}(\varphi,\psi;T,V)}\right)}{\int_0^1 d\mathfrak{q}\int_{-\pi}^{+\pi}\int_{-\pi}^{+\pi} d\varphi d\psi M(\varphi,\psi) e^{\mathfrak{q}\ \mathfrak{R}(\varphi,\psi;T,V)}}\right] \end{aligned} \quad (3.58)$$

and can not be evaluated as $< \mathfrak{h}(T,V) >^*$ and $< \varepsilon(T,V) >^*$ simply with the L_{mn}'s. Hence, it is evaluated with a numerical integration of the numerator in the last term of eq. (3.58).

The entropy density can also be obtained from the definitions of the specific heat at constant V (see section 1.2): $C_V = \left(\frac{\partial U}{\partial T}\right)_V = T\left(\frac{\partial S}{\partial T}\right)_V$. We have then the specific heat density related to both energy and entropy densities as:

$$c = \left(\frac{\partial \langle\varepsilon\rangle^*}{\partial T}\right)_V = T\left(\frac{\partial \langle s\rangle^*}{\partial T}\right)_V. \quad (3.59)$$

Hence, the entropy density can be obtained from:

$$\langle s(T,V)\rangle^* = \int \frac{1}{T}\left(\frac{\partial \langle\varepsilon\rangle^*}{\partial T}\right) dT = \int \frac{c(T,V)}{T}\ dT, \quad (3.60)$$

by the mean of a numerical integration of the specific heat density, whose expression after differentiation of the energy density in (3.57) with respect to temperature, is given

by:

$$\begin{aligned} c(T,V) &= \frac{2\pi^2}{5}T^3\left\langle \mathfrak{h}(T,V)\right\rangle^* + \left(\frac{\pi^2}{10}T^4 - B\right)\chi(T,V) + 12T^3\frac{\left(L_{11}\left(1\right) - L_{12}\left(1\right) + L_{12}\left(0\right)\right)}{L_{01}\left(1\right) - L_{01}\left(0\right)} \\ &+3T^6V\left[\frac{1}{L_{01}\left(1\right) - L_{01}\left(0\right)}\left(3(L_{21}\left(1\right) - 2L_{22}\left(1\right) + 2L_{23}\left(1\right) - 2L_{23}\left(0\right)\right)\right. \\ &\left.-(\frac{B}{T^4} - \frac{\pi^2}{10})(L_{11}\left(1\right) - 2L_{12}\left(1\right) + 2L_{13}\left(1\right) - 2L_{13}\left(0\right))\right) \\ &-\frac{L_{11}\left(1\right) - L_{12}\left(1\right) + L_{12}\left(0\right)}{\left(L_{01}\left(1\right) - L_{01}\left(0\right)\right)^2}\left(3(L_{11}\left(1\right) - L_{12}\left(1\right) + L_{12}\left(0\right)\right) \\ &\left.+(\frac{B}{T^4} - \frac{\pi^2}{10})(L_{01}\left(1\right) - L_{02}\left(1\right) + L_{02}\left(0\right))\right)\Bigg], \end{aligned} \tag{3.61}$$

with:

$$\begin{aligned} \chi\left(T,V\right) &= T^2V\left[\frac{1}{L_{01}\left(0\right) - L_{01}\left(1\right)}\left(-3(L_{12}\left(0\right) + 2L_{13}\left(0\right) + L_{12}\left(1\right) - 2L_{13}\left(1\right)\right)\right. \\ &\left.-(\frac{B}{T^4} - \frac{\pi^2}{10})(L_{02}\left(0\right) + 2L_{03}\left(0\right) + L_{02}\left(1\right) - 2L_{03}\left(1\right))\right) \\ &+\frac{L_{01}\left(0\right) + L_{02}\left(0\right) - L_{02}\left(1\right)}{\left(L_{01}\left(0\right) - L_{01}\left(1\right)\right)^2}\left(3(L_{11}\left(1\right) - L_{12}\left(1\right) + L_{12}\left(0\right)\right) \\ &\left.+(\frac{B}{T^4} - \frac{\pi^2}{10})(L_{01}\left(1\right) - L_{02}\left(1\right) + L_{02}\left(0\right))\right)\Bigg]. \end{aligned} \tag{3.62}$$

Our results for the variations of each of the order parameter, the energy density normalized by T^4 and the entropy density normalized by T^3, with temperature at different system sizes are presented in the plots on Fig. (3.8). A pronounced size dependence of these quantities can be noted over almost the entire temperature range. The main and striking difference, comparatively with Fig. (3.2), is the shift of the transition temperature to higher values for small sizes. This is due to the effect of the color-singletness requirement which was found to lead to a gradual freezing of the effective number of degrees of freedom in the QGP [7]. In a finite volume, the pressure at a given temperature has a lower value and the equilibrium between the two phases according to the Gibbs criterion is then reached at temperatures greater than $T_c\left(\infty\right)$.

This freezing in the QGP degrees of freedom can more clearly be seen on Fig. (3.9) where we compare the normalized energy density $\frac{\langle \varepsilon (T,V) \rangle}{T^4}$, representing the effective number of degrees of freedom as yet mentioned, with (dashed line) and without (solid line) color-singletness requirement at the volume $V = 150 fm^3$ for example. It can also be noted that the smearing due to the fluctuations including the color-singletness is less pronounced than in the case without color-singletness, maybe because of the reduction of the QGP degrees of freedom.

Let's note that as it was the case in Fig. (3.3), the variations of the normalized energy and entropy densities, including color singletness are not exactly the same,. This can better be seen in Fig. (3.10) where the normalized energy density vs temperature at different volumes is illustrated more clearly. The difference from the normalized entropy density, which can be approximated by a step function, can easily be observed.

3.4.2 Susceptibility and Specific Heat Density

It is also worth to illustrate two additional thermal response functions relevant to this case, which are the specific heat density $c(T,V) = \frac{\partial \langle \varepsilon(T,V) \rangle^*}{\partial T}$ and susceptibility $\chi(T,V) = \frac{\partial \langle \mathfrak{h}(T,V) \rangle^*}{\partial T}$, obtained by differentiating the energy density in (3.57) and the order parameter in (3.55-56) with respect to temperature. Their expressions have been obtained in (3.61) and (3.62) respectively.

In the following, the variations of the thermal susceptibility and specific heat density with temperature are illustrated on Figs. (3.11) and (3.12) respectively, for various sizes. It can clearly be seen that the delta function singularity of both quantities occurring in the thermodynamical limit is smeared, in a finite volume, into a finite peak of width $\delta T(V)$. This result is expected, since the derivative of the step function

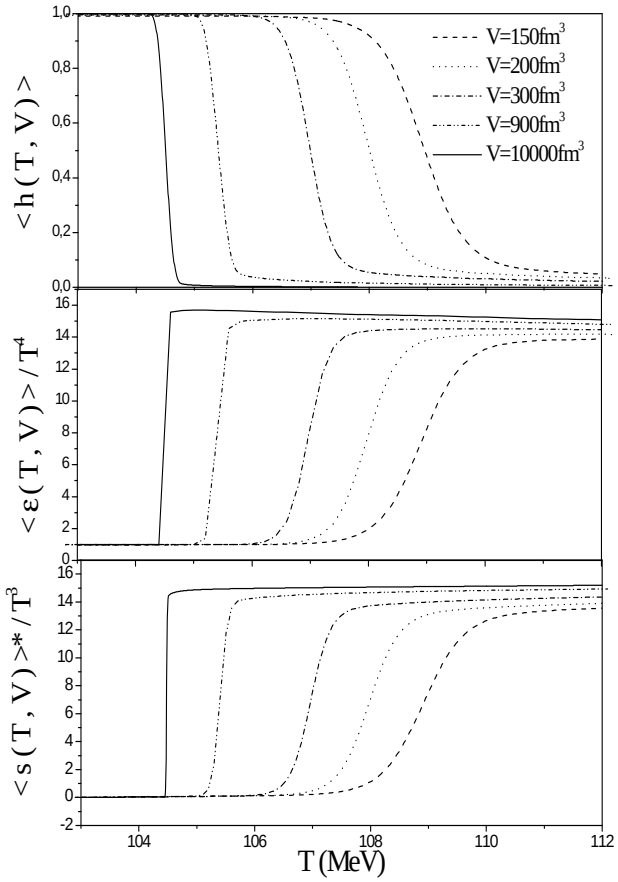

Figure 3.8: Temperature variation of the order parameter (bottom), the energy density normalized by T^4 (middle) and the entropy density normalized by T^3 (top) at $\mu = 0$, for different system volumes.

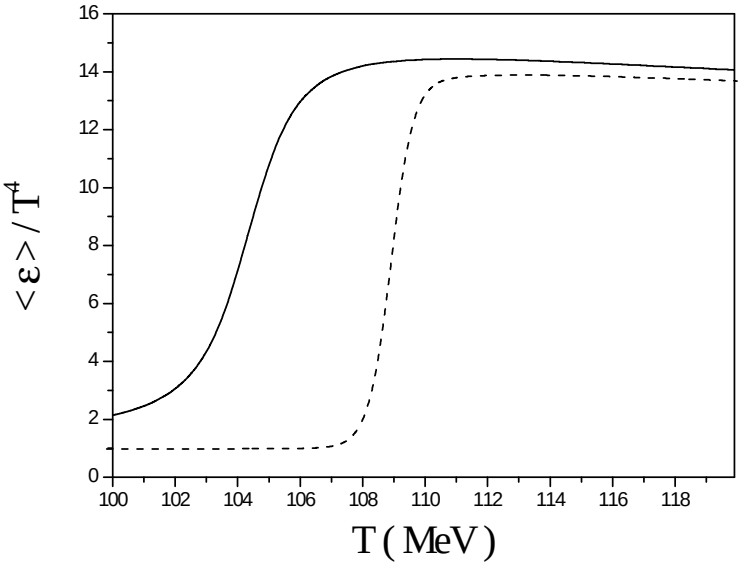

Figure 3.9: Normalized energy density $\frac{\langle \varepsilon(T,V)\rangle}{T^4}$, versus temperature, with (dashed line) and without (solid line) color-singletness requirement at the volume $V = 150 fm^3$.

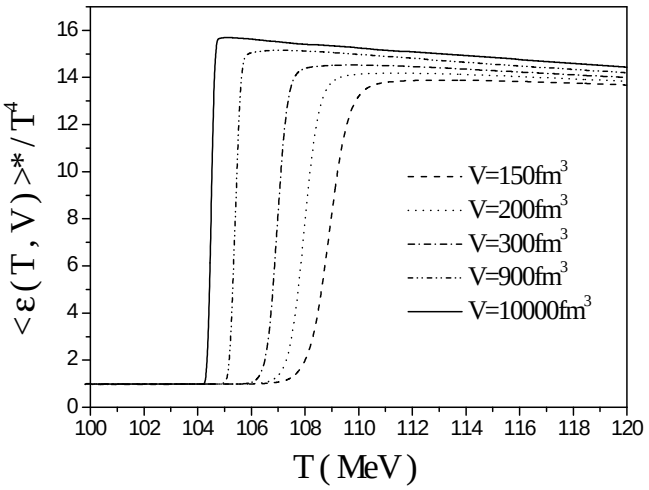

Figure 3.10: Normalized energy density $\frac{\langle \varepsilon(T,V)\rangle *}{T^4}$ with the color-singletness requirement versus temperature at various volumes.

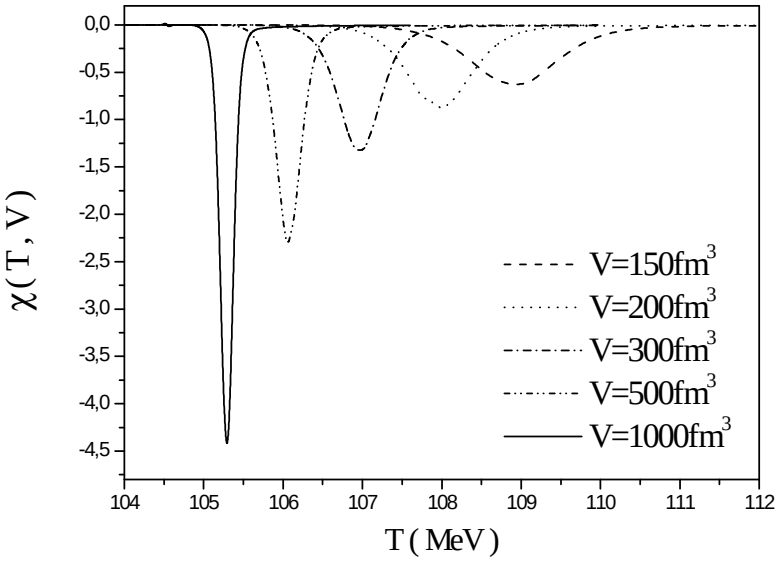

Figure 3.11: Plot of the susceptibility $\chi\,(T,V)$ versus temperature for different system volumes.

is a delta function, as well known. The rounding of each of $\langle \mathfrak{h}\,(T,V)\rangle^*$ and $\langle \varepsilon(T,V)\rangle^*$ manifests then at the level of their first derivatives as a smearing of the delta function. For decreasing volume, the width of the peaks gets larger while their heights, noted $\mid \chi_T \mid^{\max}(V)$ and $c_T^{\max}(V)$, decrease, occurring at effective transition temperatures $T_c(V)$ shifted away from the true transition temperature $T_c\,(\infty)$.

3.4.3 Pressure and Sound Velocity

In what follows, let's examine the behavior of the pressure for the system undergoing a deconfinement phase transition. Its mean value can be determined, and is simply in this case related to both energy density and order parameter by:

$$\langle P(T,V)\rangle^* = \frac{1}{3}\left(\langle \varepsilon(T,V)\rangle^* - 4\ B\ \left(1 - \langle \mathfrak{h}(T,V)\rangle^*\right)\right). \tag{3.63}$$

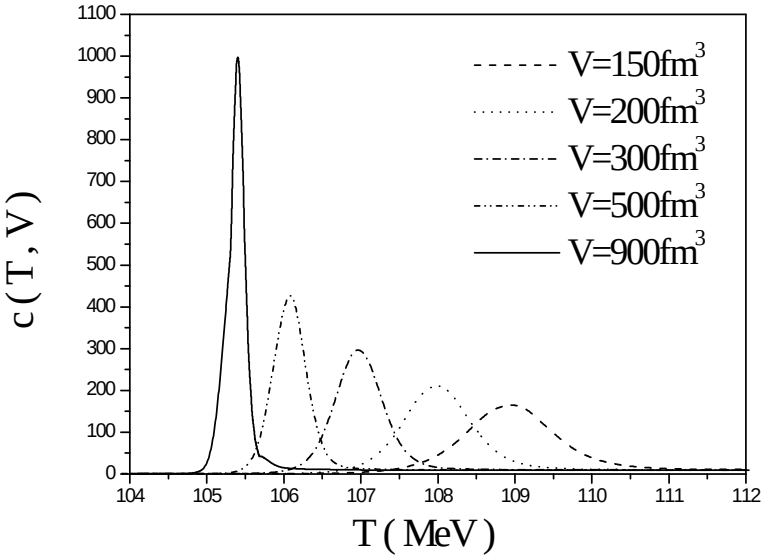

Figure 3.12: Plot of the specific heat density $c\,(T, V)$ versus temperature for different system volumes.

An other quantity, determined by the pressure gradient dP for a given gradient in the energy density $d\varepsilon$, is the sound velocity squared, defined as [114]:

$$c_s^2 = \left(\frac{\mathfrak{v}_s}{c}\right)^2 = \frac{dP}{d\varepsilon}, \tag{3.64}$$

which is the most relevant measure of the system's tendency to expand [115]. After a straightforward calculation, c_s^2 can be related to both thermal susceptibility $\chi(T,V)$ and specific heat density $c(T,V)$, by the relation:

$$c_s^2 = \frac{1}{3}\left(1 + 4B\frac{\chi}{c}\right). \tag{3.65}$$

Fig. (3.13) illustrates the variations of the pressure normalized by T^4 with temperature for different volumes, and it can clearly be seen that below the transition temperature, the pressure is constant with the Stefan-Boltzmann value for a hadronic gas, then it abruptly increases around $T_c(V)$ and continues increasing, rather slowly this time.

The velocity of sound squared is plotted on Fig. (3.14) as a function of temperature, for different sizes, and it is obvious from the curves that for temperatures well below and/or above a transition temperature, it approaches the value for an ultra-relativistic ideal gas $c_s^2 = \frac{1}{3}$. In a finite volume, c_s decreases in the transition region, and has a minimum at the effective transition temperature $T_c(V)$. For a first order phase transition, occurring at the thermodynamic limit, this minimum is zero at $T_c(\infty)$.

It is more common and useful to plot thermodynamic quantities as a function of the energy density $\langle\varepsilon\rangle^*$, especially in hydrodynamics, as in [115, 116, 117]. The graph of the pressure $\langle P\rangle^*$ vs $\langle\varepsilon\rangle^*$ in Fig. (3.15-top) shows that for large volumes, $\langle P\rangle^*$ increases with increasing energy density below a value ε_{HG} and above ε_{QGP}. On a range of energy density $\varepsilon_{HG} \leq \varepsilon \leq \varepsilon_{QGP}$, the pressure remains constant meaning that

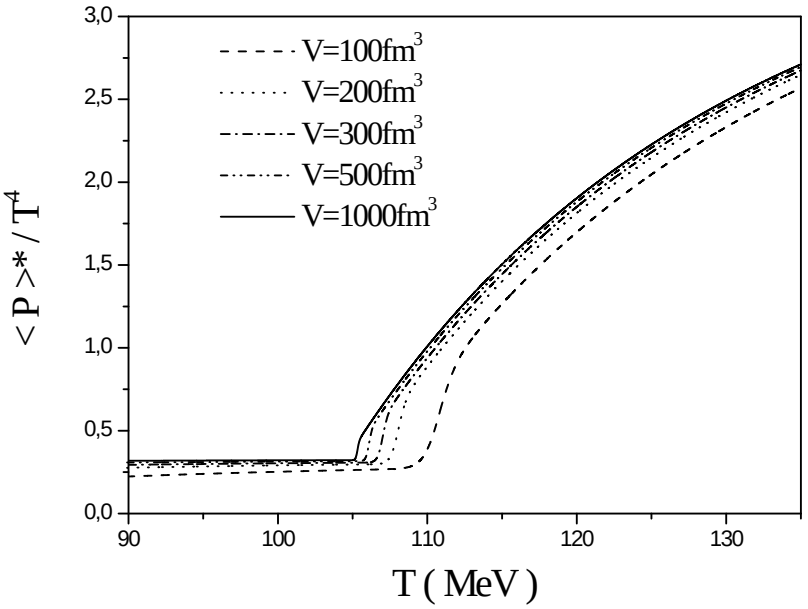

Figure 3.13: Plot of the normalized pressure $\frac{\langle P \rangle^*}{T^4}$ versus temperature for different system volumes.

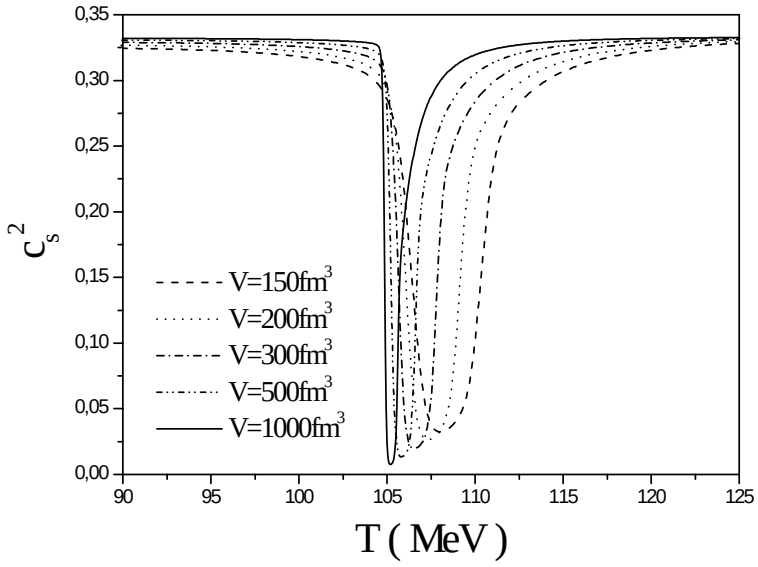

Figure 3.14: Velocity of sound squared c_s^2 as a function of temperature at different system volumes.

the system does not perform mechanical work. This region is referred to as the *soft region* of the equation of state [115, 116, 117, 118]. For small systems, it can clearly be seen that the pressure increases continuously with increasing energy density. The notions of *soft region* and *softest point* can better be seen by illustrating the ratio $\frac{\langle P\rangle^*}{\langle\varepsilon\rangle^*}$ as a function of $\langle\varepsilon\rangle^*$. The minimum of this latter occurs at the point $\langle\varepsilon\rangle^* = \varepsilon_{QGP}$ which is called the *softest point* of the equation of state. Fig. (3.15-middle) shows that for large volumes, the ratio $\frac{\langle P\rangle^*}{\langle\varepsilon\rangle^*} = \frac{1}{3} = c_s^2$ in the hadronic phase, then it starts to decrease at ε_{HG}, since $\langle P\rangle^*$ is constant in the mixed phase while $\langle\varepsilon\rangle^*$ increases. At the softest point ε_{QGP}, $\frac{\langle P\rangle^*}{\langle\varepsilon\rangle^*}$ takes its minimum value then resumes increasing in the QGP phase ($\langle\varepsilon\rangle^* \geq \varepsilon_{QGP}$) to reach again the asymptotic value $\frac{1}{3}$ for $\langle\varepsilon\rangle^* \to \infty$. For small volumes, the minimum of $\frac{\langle P\rangle^*}{\langle\varepsilon\rangle^*}$ increases and the softening of the equation of state is less pronounced.

Fig. (3.15-bottom) illustrates the variations of the speed of sound squared with the energy density for different system volumes, and shows that for big volumes, the speed of sound takes the value for an ultra-relativistic ideal gas $c_s^2 = \frac{1}{3}$ at $\langle\varepsilon\rangle^* \leq \varepsilon_{HG}$ and $\langle\varepsilon\rangle^* \geq \varepsilon_{QGP}$. On a range of energy density between ε_{HG} and ε_{QGP}, i.e., in the mixed phase, the speed of sound is nearly vanishing, reflecting the first order character of the transition. It has been interpreted in [115, 116, 117, 118] that mixed phase matter does not expand at all on account of its internal pressure, even if there are strong gradients in the energy density, and this has, in turn, the consequence that it does not perform mechanical work and therefore cools less rapidly. Thus, the expansion of the system is delayed and its lifetime is considerably prolonged. For small systems, the sound velocity is damped in a larger domain of energy density and does not vanish, since pressure gradients are finite, but they are still smaller than for an ideal gas equation

of state, and therefore the tendency of the system to expand is also reduced.

3.4.4 Second Derivative of the Order Parameter

The second derivative of the order parameter $\frac{\partial^2}{\partial T^2}\langle \mathfrak{h}\,(T,V)\rangle^*$ is also worth to be studied. Its expression is given by:

$$
\begin{aligned}
\frac{\partial^2}{\partial T^2}\langle \mathfrak{h}\,(T,V)\rangle^* \;=\; & \frac{2\chi}{T} + \frac{\left(T^2V\right)^2}{L_{01}(0)-L_{01}(1)}\left[18L_{23}(0)+54L_{24}(0)-9L_{22}(1)+36L_{23}(1)\right. \\
& -54L_{24}(1)+\left(\tfrac{B}{T^4}-\tfrac{\pi^2}{10}\right)\left(12L_{13}(0)+36L_{14}(0)-6L_{12}(1)+24L_{13}(1)-36L_{14}(1)\right) \\
& \left.+\left(\tfrac{B}{T^4}-\tfrac{\pi^2}{10}\right)^2\left(2L_{03}(0)+6L_{04}(0)-L_{02}(1)+4L_{03}(1)-6L_{04}(1)\right)\right] \\
& + \frac{4BV}{T^3}\,\frac{L_{02}(0)+2L_{03}(0)+L_{02}(1)-2L_{03}(1)}{L_{01}(0)-L_{01}(1)} \\
& + \frac{\left(T^2V\right)^2}{\left(L_{01}(0)-L_{01}(1)\right)^2}\left[\left(-3L_{12}(0)-3L_{11}(1)+3L_{12}(1)+\left(\tfrac{B}{T^4}-\tfrac{\pi^2}{10}\right)\left(-L_{02}(0)-L_{01}(1)\right.\right.\right. \\
& \left.\left.+L_{02}(1)\right)\right)\left(3L_{12}(0)+6L_{13}(0)+3L_{12}(1)-6L_{13}(1)+\left(\tfrac{B}{T^4}-\tfrac{\pi^2}{10}\right)\left(L_{02}(0)+2L_{03}(0)\right.\right. \\
& \left.\left.+L_{02}(1)-2L_{03}(1)\right)\right)+\left(L_{01}(0)+L_{02}(0)-L_{02}(1)\right)\left(9L_{21}(1)-18L_{22}(1)+18L_{23}(1)\right. \\
& -18L_{23}(0)+\left(\tfrac{B}{T^4}-\tfrac{\pi^2}{10}\right)\left(6L_{11}(1)-12L_{12}(1)+12L_{13}(1)-12L_{13}(0)\right) \\
& \left.+\left(\tfrac{B}{T^4}-\tfrac{\pi^2}{10}\right)^2\left(L_{01}(1)-2L_{02}(1)+2L_{03}(1)-2L_{03}(0)\right)-\tfrac{4B}{T^{\,7}V}\left(L_{01}(1)-L_{02}(1)+L_{02}(0)\right)\right) \\
& +\left(3L_{11}(1)-3L_{12}(1)+3L_{12}(0)+\left(\tfrac{B}{T^4}-\tfrac{\pi^2}{10}\right)\left(L_{01}(1)-L_{02}(1)+L_{02}(0)\right)\right) \\
& \times\left(6L_{13}(1)-3L_{12}(1)-3L_{12}(0)-6L_{13}(0)+\left(\tfrac{B}{T^4}-\tfrac{\pi^2}{10}\right)\left(2L_{03}(1)-L_{02}(1)-L_{02}(0)\right.\right. \\
& \left.\left.-2L_{03}(0)\right)\right)]+\frac{2\left(T^2V\right)^2}{\left(L_{01}(0)-L_{01}(1)\right)^3}\left(L_{01}(0)+L_{02}(0)-L_{02}(1)\right) \\
& \times\left(3L_{12}(0)+3L_{11}(1)-3L_{12}(1)+\left(\tfrac{B}{T^4}-\tfrac{\pi^2}{10}\right)\left(L_{02}(0)+L_{01}(1)-L_{02}(1)\right)\right)^2, \qquad (3.66)
\end{aligned}
$$

and its variations with temperature for various system sizes are illustrated in Fig. (3.16). It can be seen that this quantity takes its extrema at two temperatures $T_1(V)$

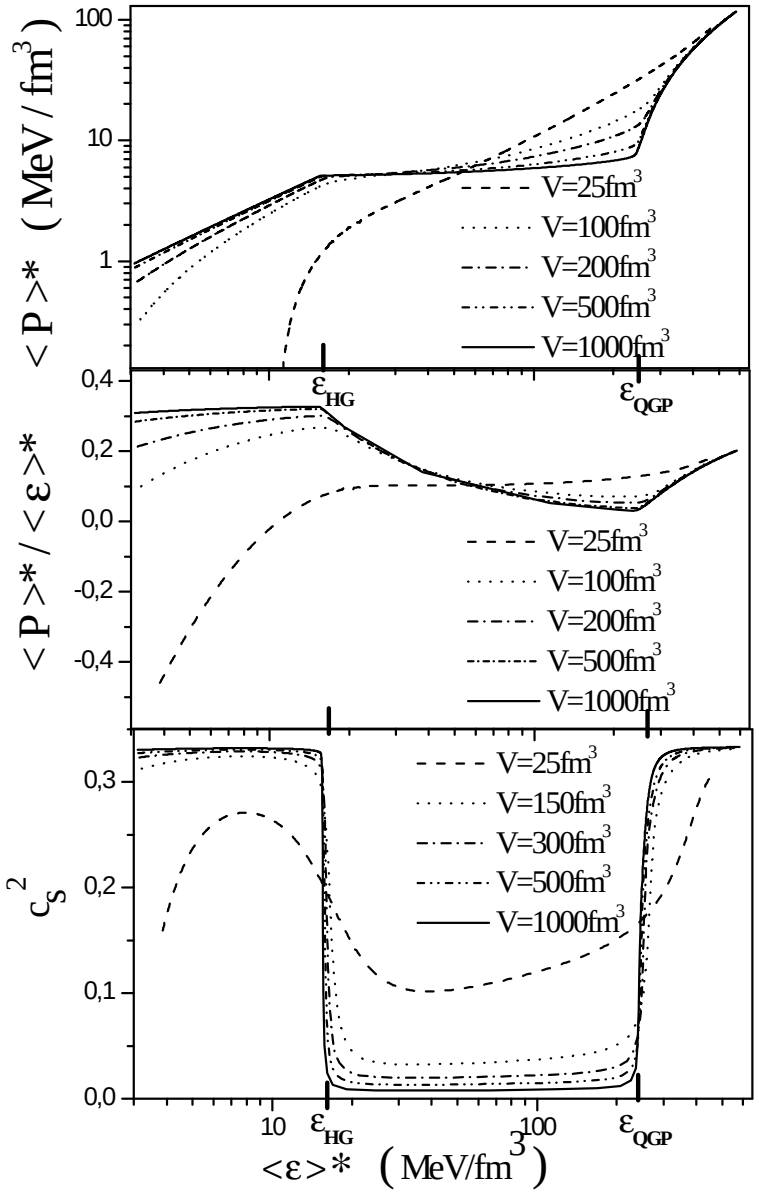

Figure 3.15: (Top) Pressure, (middle) Pressure over energy density and (bottom) Sound velocity vs energy density, for different volumes of the system.

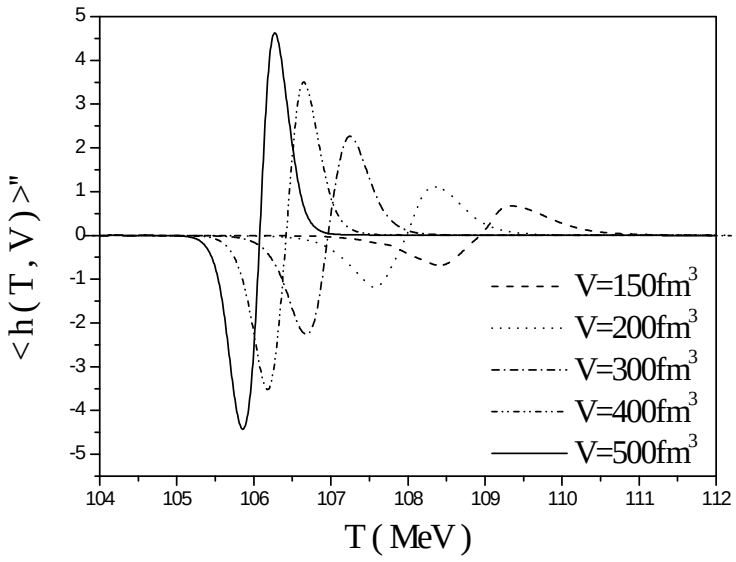

Figure 3.16: Plot of the second derivative of the order parameter, $\langle \mathfrak{h}\,(T,V)\rangle'' = \partial^2\langle \mathfrak{h}\,(T,V)\rangle/\partial T^2$, versus temperature for different system volumes.

and $T_2(V)$, so that the gap $T_2(V) - T_1(V)$, which represents the broadening of the transition region $\delta T(V)$, decreases with increasing volume.

Thus, from the illustration of all these response functions for the studied deconfinement phase transition, the three effects of finiteness of the volume evoked in section (2.3) have been recovered. A finite size scaling analysis will then be carried out in the next chapter to determine the corresponding scaling behavior and determine the relevant scaling critical exponents.

Chapter 4

Numerical Determination of the Scaling Critical Exponents for the Deconfinement Phase Transition

4.1 Introduction

In the precedent chapter, we have seen that finite-size effects have led to a rounding of the deconfinement phase transition over a range of temperature $\delta T(V)$, around a transition temperature $T_c(V)$. This effective transition temperature is shifted relative to the true one $T_c(\infty)$ in such a way that the shift $T_c(V) - T_c(\infty)$ increases for small volumes. This smearing makes the order of the transition difficult to infer. It turns out that the analysis of some known characteristic signatures as functions of varying volume allows one to go up to the order of the transition.

In finite systems, the shift of the effective transition temperature $T_c(V)$ relative to the true one $T_c(\infty)$, the width $\delta T(V)$ of the critical region over which the transition

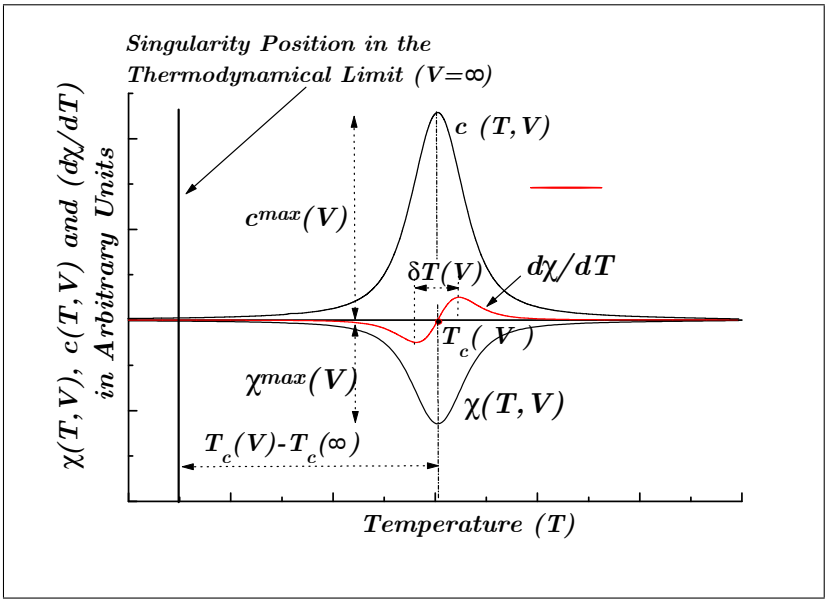

Figure 4.1: Illustration of the finite size behavior of the susceptibility $\chi(T,V)$, the specific heat density $c(T,V)$ and the second derivative of the order parameter $\partial\chi/\partial T$.

is smeared out and the maxima of the rounded peaks of the thermal susceptibility $\chi(T,V) = \dfrac{\partial\langle \mathfrak{h}(T,V)\rangle^*}{\partial T}$ and specific heat density $c(T,V) = \dfrac{\partial\langle \varepsilon(T,V)\rangle^*}{\partial T}$, which are illustrated on Fig. (4.1), are expected to behave like powers of the volume V, respectively, as:

$$\begin{cases} \tau_T(V) = T_c(V) - T_c(\infty) \sim V^{-\lambda_T} \\ \delta T(V) \sim V^{-\theta_T} \\ |\chi_T|^{\max}(V) \sim V^{\gamma_T} \\ c_T^{\max}(V) \sim V^{\alpha_T} \ , \end{cases} \tag{4.1}$$

where the scaling critical exponents λ_T, θ_T, γ_T and α_T characterize their dependence on the volume in a d-space, and are expected to be all equal to unity [2, 3, 66, 67], i.e., $\lambda_T = \theta_T = \gamma_T = \alpha_T = 1$.

These results have been recovered in our work [119] where an analytic determination

of the scaling critical exponents relevant to a thermally driven deconfinement phase transition has been carried out.

In the following, we shall determine numerically these scaling critical exponents. For this purpose, a FSS analysis of characteristic quantities for a system which undergoes a thermal deconfinement phase transition, from a pionic gas to a QGP consisting of two massless quarks at zero chemical potential, may be used.

4.2 Numerical Determination of the Critical Exponents for the Thermal Deconfinement Phase Transition with the Exact Color-Singlet Partition Function

In the following, we use a FSS analysis to recover the scaling exponents θ_T, λ_T, α_T and γ_T for the thermally driven deconfinement phase transition. For this purpose, we proceed by studying the thermal susceptibility and specific heat density. We examine the behavior of their maxima, their rounding as well as the shift of the effective transition temperature with varying volume. Let's note that the determination of the location of the maxima of the finite size peaks as well as their heights is done in a numerical way, and this yields a systematic error, which is estimated and given for the determined scaling exponents.

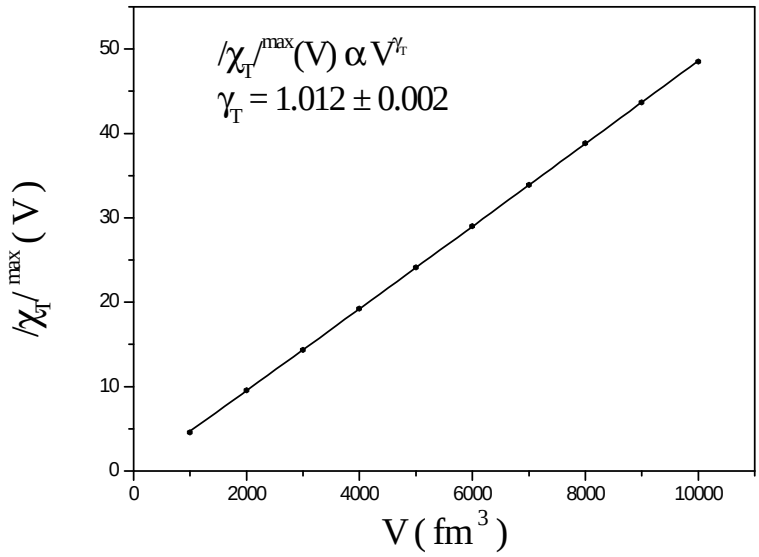

Figure 4.2: Linear fit of the results for the maxima of the susceptibility vs volume.

4.2.1 The susceptibility critical exponent

Fig. (4.2) illustrates the plot of the maxima of the thermal susceptibility peaks, $\mid \chi_T \mid^{\max}(V)$ versus volume. The linearity of the data with V can clearly be noted. A numerical parametrization with the power-law form: $\mid \chi_T \mid^{\max}(V) \sim V^{\gamma_T}$, gives the value of the susceptibility critical exponent: $\gamma_T = 1.012 \pm 0.002$.

4.2.2 The specific heat critical exponent

As in the precedent case, the data of the maxima of the specific heat $c_T^{\max}(V)$ are plotted in Fig. (4.3), and are fitted to the power-law form: $c_T^{\max}(V) \sim V^{\alpha_T}$. The obtained specific heat critical exponent is: $\alpha_T = 1.0075 \pm 0.0007$.

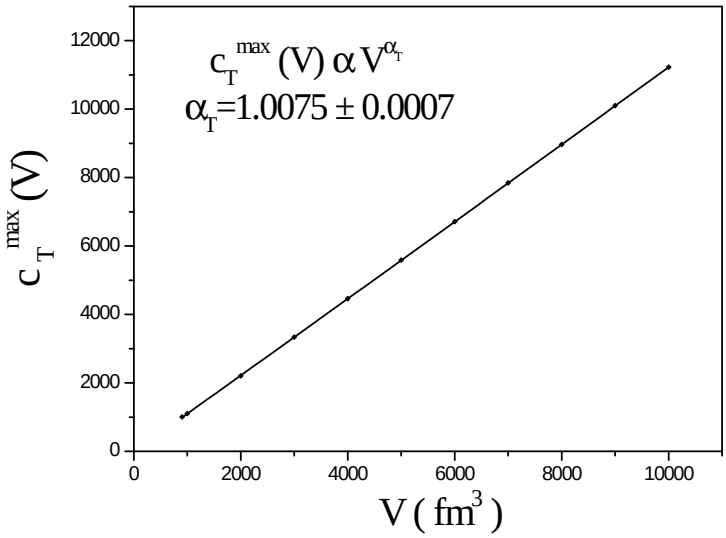

Figure 4.3: Variations of the maxima of the specific heat density with the volume.

4.2.3 The smearing critical exponent

The width of the transition region can be defined by the gap: $\delta T(V) = T_2(V) - T_1(V)$ with $T_1(V)$ and $T_2(V)$ the temperatures at which the second derivative of the order parameter reaches its extrema, or in other terms the temperatures at which the third derivative of the order parameter vanishes, i. e., $\frac{\partial^3}{\partial T^3}\langle \mathfrak{h}\,(T,V)\rangle^*\Big|_{T_1(V),T_2(V)} = 0$. To localize $T_1(V)$ and $T_2(V)$, we'll then search for the locations of the extrema of $\frac{\partial^2}{\partial T^2}\langle \mathfrak{h}\,(T,V)\rangle^*$, whose expression was given in (3.66).

The results for the widths $\delta T\,(V)$, plotted in Fig. (4.4) vs the inverse of the volume, were fitted to the power law form: $\delta T\,(V) \sim V^{-\theta_T}$, and the obtained smearing critical exponent is: $\theta_T = 1.03 \pm 0.02$.

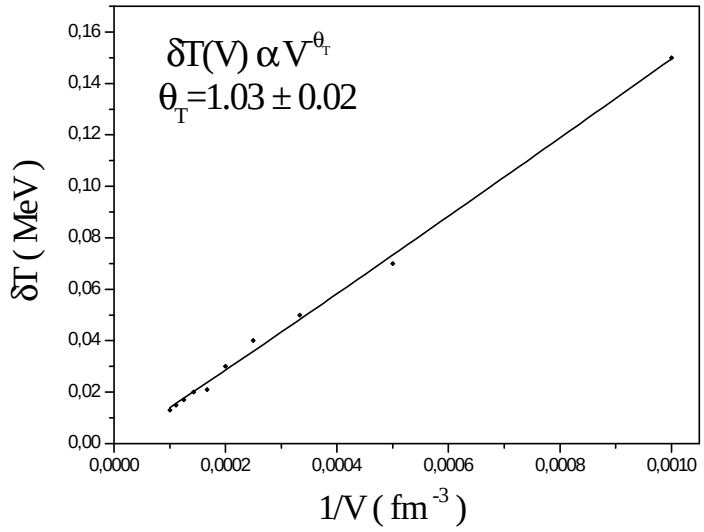

Figure 4.4: Data of the width of the temperature region over which the transition is smeared, fitted to a power-law of the inverse volume.

4.2.4 The shift critical exponent

For the study of the shift of the transition temperature $\tau_T(V) = T_c(V) - T_c(\infty)$, we need to locate the effective transition temperature in a finite volume $T_c(V)$. A way to define $T_c(V)$ is to locate the maxima of the rounded peaks of the susceptibility and the specific heat, shifted away from the true transition temperature $T_c(\infty)$.

Results of the shift of the transition temperature obtained in this way are plotted in Fig. (4.5) versus inverse volume. The shift critical exponent obtained from a fit to the form: $\tau_T(V) \sim V^{-\lambda}$, is : $\lambda = 0.876 \pm 0.041$. Such a value $\neq 1$ suggests the contribution of non-leading terms in the expression of the volume variation of the shift. Different forms of the fit of $\tau_T(V)$ including additional terms with higher powers of V^{-1}, such as $A_1 V^{-\lambda} + A_2 V^{-2}$, and $A_1 V^{-\lambda} + A_2 V^{-2} + A_3 V^{-3}$, have been tested, and the obtained results show that effectively, the shift critical exponent λ increases from the value 0.876

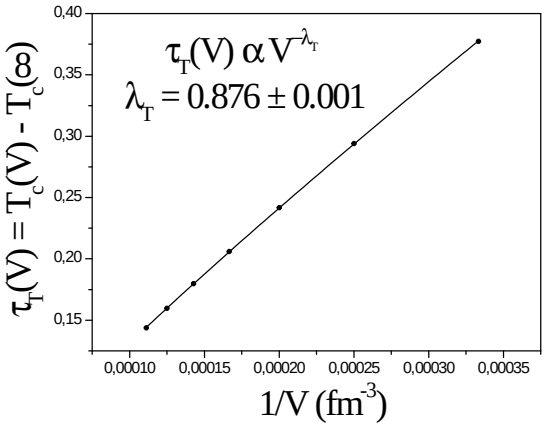

Figure 4.5: Plot of the shift of the transition temperature (from the maxima of $\chi(T,V)$ and $c(T,V)$) vs inversed volume.

and tends to 1, with a better $\boldsymbol{\chi}^2$. Other forms have been tested, where the value of the shift exponent has been fixed to 1, and finite-size correction terms have been included. In this case also, we note that we obtain a better $\boldsymbol{\chi}^2$ value with the presence of the non-leading terms.

The effective transition temperature can also be obtained from the minimum of the velocity of sound, as explained in subsection (3.5.3). Data of the locations of the minima of the sound velocity at different volumes $T_c^{(c_s^{2\ (\min)})}(V)$ are collected, and their shifts away from the true transition temperature $T_c(\infty)$ are plotted vs inversed volume in Fig. (4.6). A fit of this shift to the form: $\tau_T^{(c_s^{2\ (\min)})}(V) = T_c^{(c_s^{2\ (\min)})}(V) - T_c(\infty) \sim V^{-\lambda'_T}$, gives the shift critical exponent : $\lambda'_T = 0.841 \pm 0.004$. Such a value suggests, in turn, the contribution of non-leading terms to the expression of the shift as a function of the volume.

Other ways for defining the transition temperature are investigated and the details are given in the two next subsections.

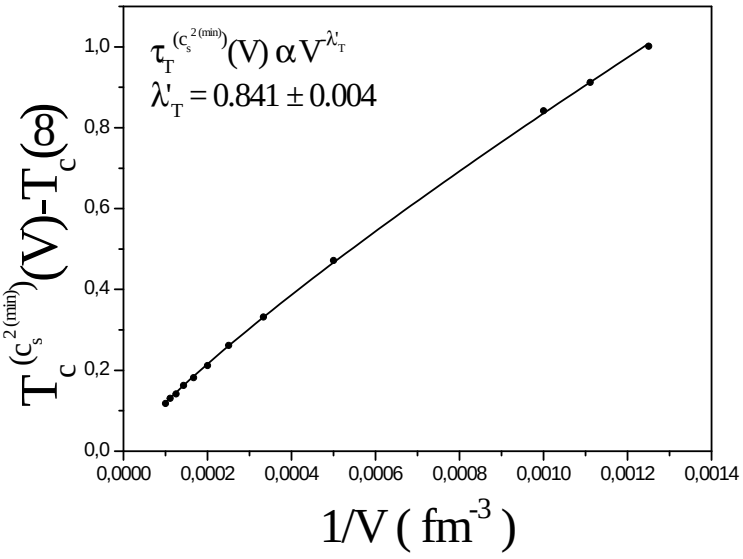

Figure 4.6: Plot of the shift of the transition temperature, from the minima of the sound velocity c_s^2, vs inversed volume.

4.2.5 Parametrization of the Order Parameter and the Susceptibility

Within the model used in this work, the order parameter in the limit of infinite volume being equal to 1 below the transition temperature and zero above it, it can then be expressed in a simple way using the Heaviside step-function Θ as:

$$\langle \mathfrak{h}\,(T, V \longrightarrow \infty)\rangle = 1 - \Theta\,(T - T_c\,(\infty))\,. \tag{4.2}$$

Such a parametrization has been used first in [120], for a similar case of a system of coexisting hadronic matter and QGP phases, then in other works as [121]. Using one of the known mathematical representations of the smoothed step function $\Theta\,(T - T_c)$,

the order parameter may then be expressed as:

$$\langle \mathfrak{h}\,(T,V)\rangle = \frac{1}{2}\left(1-\tanh\left(\frac{T-T_c\,(V)}{\Gamma_T\,(V)}\right)\right), \tag{4.3}$$

where $T_c\,(V)$ is the effective transition temperature and $\Gamma_T\,(V)$ the half-width of the rounded transition region, which leads to the susceptibility expression :

$$\chi\,(T,V) = \frac{-1}{2\Gamma_T\,(V)\ \ \cosh^2\left(\frac{T-T_c(V)}{\Gamma_T(V)}\right)}. \tag{4.4}$$

The parametrization choice (4.3) is the most accepted physically, and it can be understood phenomenologically in the context of the Double Gaussian Peaks model where the obtained expressions of the order parameter and the susceptibility are very similar to (4.3) and (4.4) [3, 70, 122].

An illustration of such parametrizations of the order parameter at the volume $V = 4000fm^3$, and the susceptibility at the volume $V = 900fm^3$ are presented in Figs. (4.7-left) and (4.7-right) respectively, and the parameters $T_c\,(V)$ and $\Gamma_T\,(V)$ obtained from each fit are given.

The results for the width of the transition region and the shift of the transition temperature from the parametrizations of the order parameter and the susceptibility are fitted to power law forms: ${\tau_T}^{fit(1)}(V) \sim V^{-\lambda_1}$, ${\tau_T}^{fit(2)}(V) \sim V^{-\lambda_2}$, $\delta T^{\,fit(1)}\,(V) \sim V^{-\theta_1}$ and $\delta T^{\,fit(2)}\,(V) \sim V^{-\theta_2}$ which give the scaling critical exponents: $\lambda_1 = 0.830 \pm 0.013$, $\lambda_2 = 0.857 \pm 0.006$, $\theta_1 = 0.990 \pm 0.015$ and $\theta_2 = 1.032 \pm 0.003$.

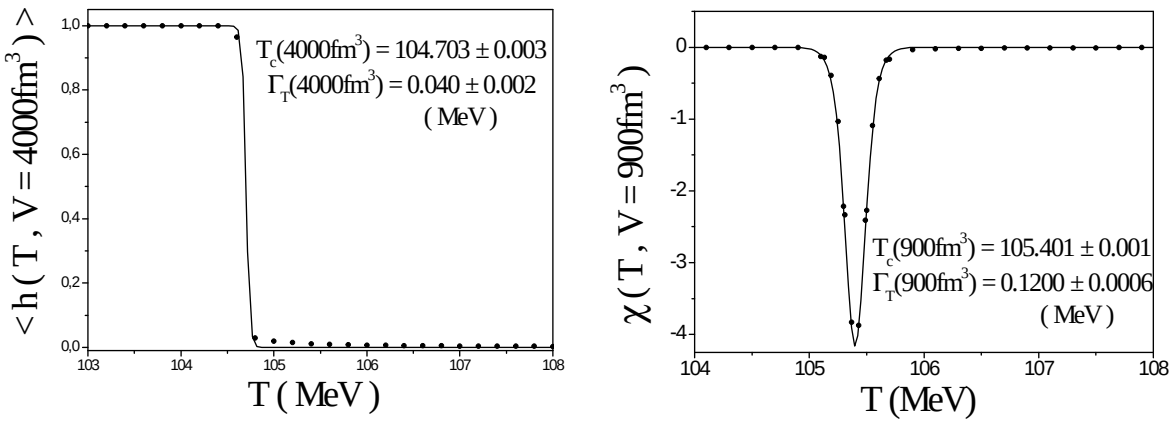

Figure 4.7: Parametrization of the order parameter to the form (4.3) at the volume $V = 4000 fm^3$, and of the susceptibility to the form (4.4) at the volume $V = 900 fm^3$.

4.2.6 Shift of the transition temperature and width of the transition region from cumulants

A way for locating $T_c\,(V)$ is to consider the fourth order cumulant:

$$B_4\,(T,V) = 1 - \frac{\langle \mathfrak{h}\,(T,V)\rangle^{*4}}{3\,\langle \mathfrak{h}^2\,(T,V)\rangle^{*2}}, \tag{4.5}$$

introduced by Binder [75, 3], and which is known to present a minimum at an effective transition temperature whose shift from the true transition temperature $T_c(\infty)$ is of order V^{-1} for a first order transition. This cumulant is a finite size scaling function [3, 66, 67, 68, 76], and is widely used to indicate the order of the transition in a finite volume.

The expression of $B_4\,(T,V)$ as function of the integral terms, for this case of the

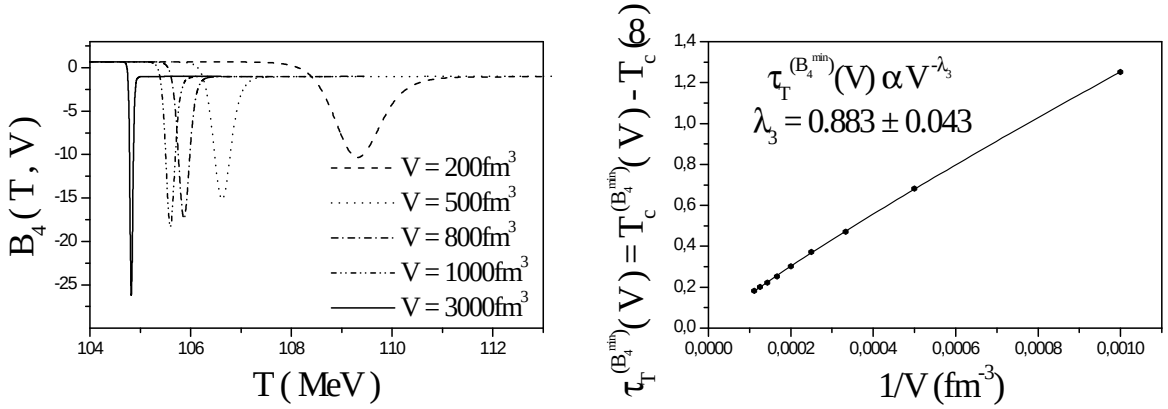

Figure 4.8: (Left) Binder Cumulant B_4 vs temperature at different system volumes. (Right) Shift of the transition temperature obtained from the minimum of the Binder cumulant vs inversed volume.

deconfinement transition, is after calculation:

$$B_4(T,V) = 1 - \frac{(L_{01}(1) - L_{01}(0))}{3\ (2L_{03}(1) - 2L_{03}(0) - 2L_{02}(0) - L_{01}(0))^2} \times (24\,(L_{05}(1) - L_{05}(0) - L_{04}(0)) - 12L_{03}(0) - 4L_{02}(0) - L_{01}(0)) \quad (4.6)$$

Fig. (4.8-left) illustrates the variations of the Binder cumulant with temperature for various volumes, and shows that the locations of the minima in finite sizes $T_{\min}(V)$ are shifted to higher values from $T_c(\infty)$. Data of the shift of the transition temperature obtained in this way are plotted in Fig. (4.8-right) versus inversed volume, and the scaling shift critical exponent obtained from a fit to the form: $\tau_T^{(B_4^{\min})}(V) = T_c^{(B_4^{\min})}(V) - T_c(\infty) \sim V^{-\lambda_3}$, is: $\lambda_3 = 0.883 \pm 0.043$. In this case also, non-leading terms appear in the expression of $\tau_T^{(B_4^{\min})}(V)$.

We can also calculate the Binder cumulant defined from the 4^{th} normalized central moment as:

$$B_4'(T,V) = 1 - \frac{\langle(\mathfrak{h} - \langle\mathfrak{h}\rangle^*)^4\rangle^*}{3\ \langle(\mathfrak{h} - \langle\mathfrak{h}\rangle^*)^2\rangle^{*2}}, \quad (4.7)$$

which is directly related to the kurtosis $K(T,V)$, which will be defined in the following, by:

$$B_4'(T,V) = \frac{-K(T,V)}{3} \ . \tag{4.8}$$

The locations of the extrema of both $B_4'(T,V)$ and $K(T,V)$ are then the same.

In the same context, we have thought to examine the second and third cumulants for the case of the probability distribution $p(\mathfrak{h})$ used in the present work. For this purpose, let's first begin with some definitions.

Definitions of the Moments

The n^{th} moment of a function $f(x)$ of a variable x about a value x_0 is mathematically defined by:

$$\mathcal{M}_n = \int_0^1 (x - x_0)^n f(x) dx \ \ . \tag{4.9}$$

The moments about zero are usually referred to simply as the *moments* of a function. Usually, the function will be a probability density function. The n^{th} moment (about zero) of a probability density function $f(x)$ is the *expected value* of x^n. The moments about its mean $\mathcal{M}$ are called *central moments*; these describe the shape of the function, independently of translation.

Significance of the Moments

The first moment about zero, if it exists, is the *expectation* of x, i.e., the *mean* of the probability distribution of x, designated $\mathcal{M}$. In higher orders, the central moments are more interesting than the moments about zero.

The n^{th} central moment of the probability distribution of a random variable x is

then given by:

$$\mathcal{M}_n = \langle (x - \mathcal{M})^n \rangle = \langle (x - \langle x \rangle)^n \rangle. \tag{4.10}$$

The first central moment is thus 0; the second central moment is the *variance* σ^2, the square root of which is the *standard deviation* σ defined as:

$$\sigma = \left(\langle (x - \langle x \rangle)^2 \rangle \right)^{1/2}. \tag{4.11}$$

The normalized n^{th} central moment is the n^{th} central moment divided by σ^n. These normalized central moments are dimensionless quantities, which represent the distribution independently of any linear change of scale.

The third central moment is a measure of symmetry, or more precisely, the lack of symmetry. A distribution, or data set, is symmetric if it looks the same to the left and right of the center point. The 3^{rd} central moment for a normal distribution is zero, and any symmetric distribution will have a third central moment, if defined, near zero. The normalized 3^{rd} central moment is called the *skewness* Σ :

$$\Sigma = \frac{\langle (x - \langle x \rangle)^3 \rangle}{\sigma^3}. \tag{4.12}$$

A distribution that is skewed to the left (the tail of the distribution is heavier on the left) will have a negative skewness. A distribution that is skewed to the right (the tail of the distribution is heavier on the right) will have a positive skewness.

The fourth central moment is a measure of whether the distribution is peaked or flat relative to a normal distribution. Since it is the expectation of a fourth power, the fourth central moment, where defined, is always positive. The fourth central moment of a normal distribution is $3\sigma^4$.

The *Kurtosis* is defined to be the normalized 4^{th} central moment minus 3:

$$K = \frac{\langle (x - \langle x \rangle)^4 \rangle}{\sigma^4} - 3, \tag{4.13}$$

so that the standard normal distribution has a kurtosis of zero. Positive kurtosis indicates a "peaked" distribution and negative kurtosis indicates a "flat" distribution. That is, distributions or data sets with high kurtosis tend to have a distinct peak near the mean, decline rather rapidly, and have heavy tails. Data sets with low kurtosis tend to have a flat top near the mean rather than a sharp peak

Cumulants

The first moment and the second and third unnormalized central moments are linear in the sense that if x and y are independent random variables, then:

$$\mathcal{M}_1(x+y) = \mathcal{M}_1(x) + \mathcal{M}_1(y) \ , \tag{4.14}$$

and:

$$\mathcal{M}_2(x+y) = \mathcal{M}_2(x) + \mathcal{M}_2(y) \ , \tag{4.15}$$

and:

$$\mathcal{M}_3(x+y) = \mathcal{M}_3(x) + \mathcal{M}_3(y) \ . \tag{4.16}$$

This is true because these moments are the first three cumulants; the fourth cumulant is the kurtosis times σ^4.

The four first cumulants for the probability density $p(\mathfrak{h})$

For this case of probability distribution $p(\mathfrak{h})$, the first cumulant is the order parameter $\langle\mathfrak{h}\rangle^*$, the second is the variance given by:

$$\sigma^2\left(T,V\right) = \langle(\mathfrak{h} - \langle\mathfrak{h}\rangle^*)^2\rangle^* = \langle\mathfrak{h}^2\rangle^* - \langle\mathfrak{h}\rangle^{*2}, \tag{4.17}$$

which is expressed by mean of the L_{mn}'s as:

$$\begin{aligned}\sigma^2(T,V) &= \frac{1}{\left(L_{01}(1)-L_{01}(0)\right)^2}\left[\left(2L_{03}(1)-2L_{03}(0)-2L_{02}(0)-L_{01}(0)\right)\right.\\ &\left.\times\left(L_{01}(1)-L_{01}(0)\right)-\left(L_{01}(0)+L_{02}(0)-L_{02}(1)\right)^2\right]. \qquad (4.18)\end{aligned}$$

The third cumulant is the skewness times σ^3, with the skewness given by:

$$\Sigma(T,V)=\frac{\langle(\mathfrak{h}-\langle\mathfrak{h}\rangle^*)^3\rangle^*}{\sigma^3}=\frac{\langle\mathfrak{h}^3\rangle^*-3\langle\mathfrak{h}\rangle^*\langle\mathfrak{h}^2\rangle^*+2\langle\mathfrak{h}\rangle^{*3}}{\left(\langle\mathfrak{h}^2\rangle^*-\langle\mathfrak{h}\rangle^{*2}\right)^{3/2}}, \qquad (4.19)$$

which can be written as function of the L_{mn}'s as:

$$\begin{aligned}\Sigma(T,V) &= \left[\left(L_{01}(1)-L_{01}(0)\right)^2\left(6L_{04}(1)-6L_{04}(0)-6L_{03}(0)-3L_{02}(0)-L_{01}(0)\right)\right.\\ &+3\left(L_{01}(1)-L_{01}(0)\right)\left(L_{01}(0)+L_{02}(0)-L_{02}(1)\right)\left(2L_{03}(1)-2L_{03}(0)-2L_{02}(0)-L_{01}(0)\right)\\ &\left.-2\left(L_{01}(0)+L_{02}(0)-L_{02}(1)\right)^3\right]/\left[\left(2L_{03}(1)-2L_{03}(0)-2L_{02}(0)-L_{01}(0)\right)\right.\\ &\left.\times\left(L_{01}(1)-L_{01}(0)\right)-\left(L_{01}(0)+L_{02}(0)-L_{02}(1)\right)^2\right]^{3/2}. \qquad (4.20)\end{aligned}$$

The fourth cumulant is the kurtosis times σ^4, where the kurtosis is given by:

$$K(T,V)=\frac{\langle(\mathfrak{h}-\langle\mathfrak{h}\rangle^*)^4\rangle^*}{\sigma^4}-3=\frac{\langle\mathfrak{h}^4\rangle^*-4\langle\mathfrak{h}\rangle^*\langle\mathfrak{h}^3\rangle^*+6\langle\mathfrak{h}\rangle^{*2}\langle\mathfrak{h}^2\rangle^*-3\langle\mathfrak{h}\rangle^{*4}}{\left(\langle\mathfrak{h}^2\rangle^*-\langle\mathfrak{h}\rangle^{*2}\right)^2}-3, \qquad (4.21)$$

whose expression with the L_{mn}'s is:

$$\begin{aligned}K(T,V) &= \left\{\left[\left(L_{01}(1)-L_{01}(0)\right)^3\left(24L_{05}(1)-24L_{05}(0)-24L_{04}(0)-12L_{03}(0)\right)\right.\right.\\ &-4L_{02}(0)-L_{01}(0))+4\left(L_{01}(1)-L_{01}(0)\right)^2\left(L_{01}(0)+L_{02}(0)-L_{02}(1)\right)\\ &\times\left(6L_{04}(1)-6L_{04}(0)-6L_{03}(0)-3L_{02}(0)-L_{01}(0)\right)-3\left(L_{01}(0)+L_{02}(0)-L_{02}(1)\right)^4\Big]\\ &/\left[\left(2L_{03}(1)-2L_{03}(0)-2L_{02}(0)-L_{01}(0)\right)\left(L_{01}(1)-L_{01}(0)\right)\right.\\ &\left.\left.-\left(L_{01}(0)+L_{02}(0)-L_{02}(1)\right)^2\right]^2\right\}-3\,. \qquad (4.22)\end{aligned}$$

with:

$$\langle \mathfrak{h}^2 \rangle^* = \frac{2L_{03}(1) - 2L_{03}(0) - 2L_{02}(0) - L_{01}(0)}{L_{01}(1) - L_{01}(0)}, \tag{4.23}$$

$$\langle \mathfrak{h}^3 \rangle^* = \frac{6L_{04}(1) - 6L_{04}(0) - 6L_{03}(0) - 3L_{02}(0) - L_{01}(0)}{L_{01}(1) - L_{01}(0)}, \tag{4.24}$$

$$\langle \mathfrak{h}^4 \rangle^* = \frac{24L_{05}(1) - 24L_{05}(0) - 24L_{04}(0) - 12L_{03}(0) - 4L_{02}(0) - L_{01}(0)}{L_{01}(1) - L_{01}(0)}. \tag{4.25}$$

As it can clearly be observed on Fig. (4.9), the plots of the variance versus temperature for different system volumes look like bell functions, with the peaks broadened, smaller is the volume. These peaks are located at temperatures $T^{(\sigma^{2^{\max}})}(V)$, seemingly tending to $T_c(\infty)$ with increasing volume.

Similarly, Fig. (4.10) illustrates the variations of skewness with temperature at different sizes. The curves of skewness show that this latter vanishes at a temperature $T_c^{(\Sigma=0)}$, being negative for $T < T_c^{(\Sigma=0)}$ and positive for $T > T_c^{(\Sigma=0)}$, and the probability distribution seems then to be skewed to the left for $T < T_c^{(\Sigma=0)}$, and skewed to the right for $T > T_c^{(\Sigma=0)}$. The temperature at which skewness vanishes is expected to represent the transition temperature, and tends apparently to $T_c(\infty)$ with increasing volume, while the temperature gap between the two maxima is expected to give the width of the transition region.

Finally, the plots of kurtosis versus temperature are represented on Fig. (4.11), as usual at different sizes, but because of the high values taken by the kurtosis at large volumes, information on a part of the temperature range is lost. To see the detailed kurtosis, an individual plot at the volume $V = 300fm^3$ is illustrated on Fig. (4.12), which shows that kurtosis is positively peaked around a temperature $T_c^{(K^{\max_1})}(V)$ attaining high values, vanishes then takes negative values on a narrow interval of temperatures with a minimum at a temperature $T_c^{(K^{\min})}(V)$ and vanishes again, then takes positive

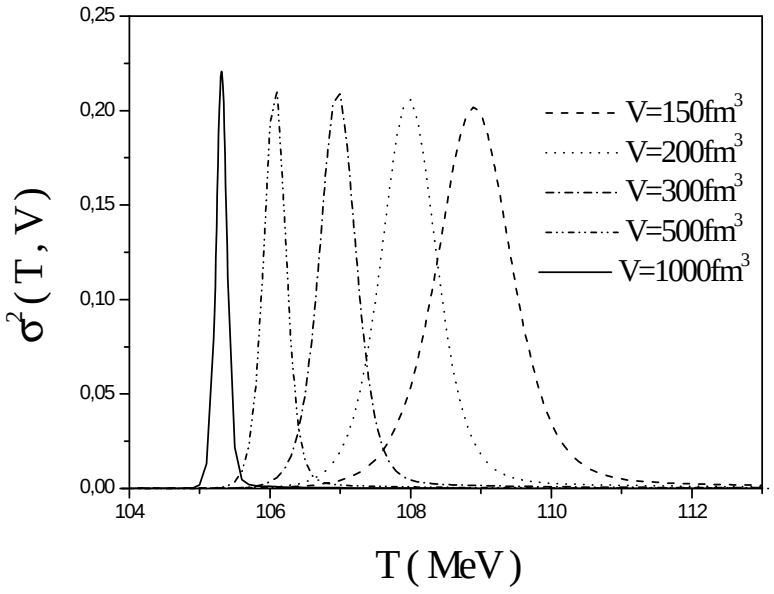

Figure 4.9: Variance vs Temperature at different system volumes.

but low values with a peak around a temperature $T_c^{(K^{\max_2})}(V)$. In this case, we expect the transition temperature to occur at the minimum of kurtosis.

To verify the validity of the assumptions that the transition temperatures can be defined at the maximum of the variance, at vanishing skewness and at the minimum of kurtosis, we plot the variations of the shifts of the such obtained transition temperatures, relative to $T_c(\infty)$, with inversed volume and fit to a power law, like in eq. (4.1). The numerical values of the shift critical exponents obtained in this way are:

$$\begin{aligned}
\tau_T^{(Var)}(V) &= T^{(\sigma^{2^{\max}})}(V) - T_c(\infty) \sim V^{-\lambda_4}, \quad \lambda_4 = 0.861 \pm 0.002, \\
\tau_T^{(Skew)}(V) &= T^{(\Sigma=0)}(V) - T_c(\infty) \sim V^{-\lambda_5}, \quad \lambda_5 = 0.862 \pm 0.002, \\
\tau_T^{(Kurt)}(V) &= T^{(K^{\min})}(V) - T_c(\infty) \sim V^{-\lambda_6}, \quad \lambda_6 = 0.861 \pm 0.002,
\end{aligned} \tag{4.26}$$

and are very close to the values of the shift critical exponent previously obtained

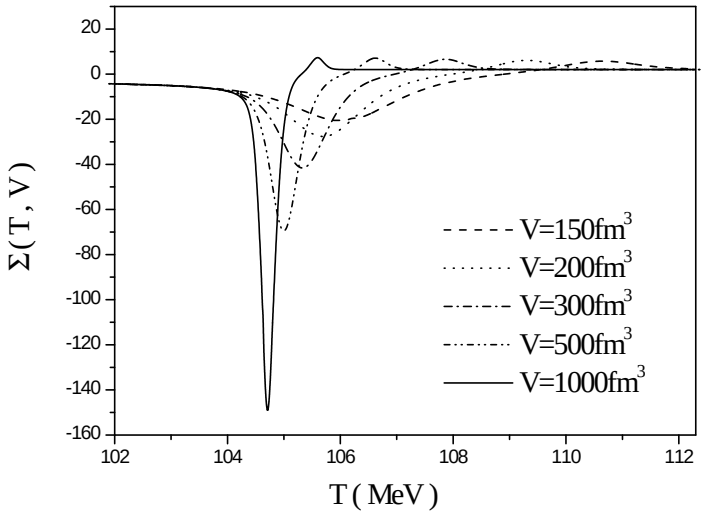

Figure 4.10: Skewness vs Temperature at different system volumes.

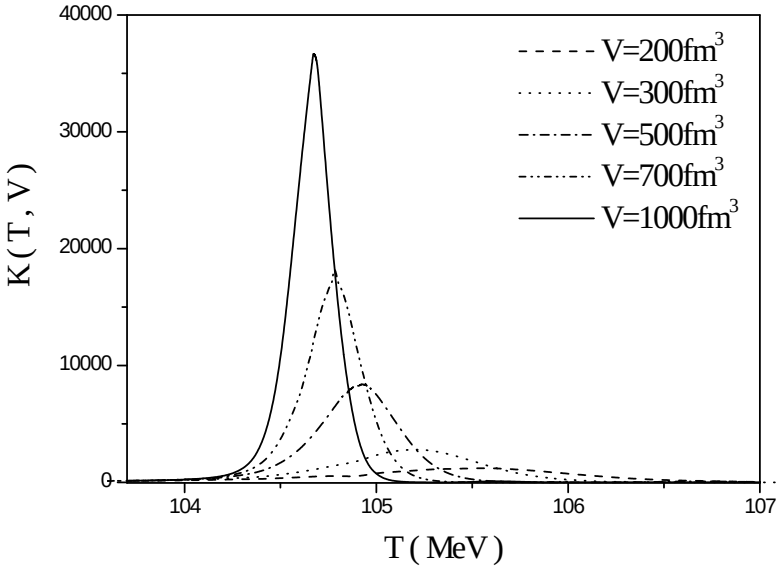

Figure 4.11: Kurtosis vs Temperature at different system volumes.

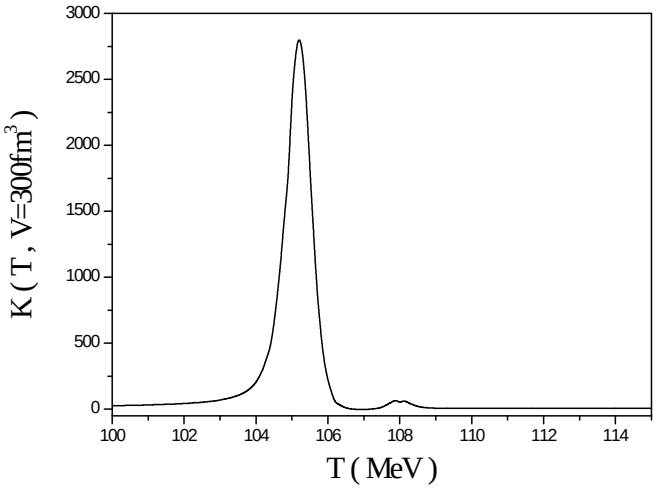

Figure 4.12: Kurtosis vs Temperature at the volume $V = 300fm^3$.

(subsections 4.2.4 to 4.2.6), and which are $\neq 1$ suggesting the contribution of non-leading terms in the expression of the volume variation of the shift, as yet mentioned.

For the width of the transition region, data are obtained from skewness as the gap in temperature between the two extrema, and are fitted to power laws of the inversed volume. The smearing critical exponent obtained in this case is:

$$\delta T^{(Skew)}(V) \sim V^{-\theta'_T}; \quad \theta'_T = 0.903 \pm 0.011 \ . \tag{4.27}$$

For more accuracy, we'll search in the next section for the correlation between the such obtained shifts and the shift of the transition temperature obtained from the value 0.5 of the order parameter, or equivalently from the peaks of the susceptibility. A linear relation between the two, with a slope equal to 1 will indicate whether the transition temperature is effectively that determined from each cumulant.

Cumulant	Value of a	Value of b
Variance maximum $c^{(\sigma^2_{\max})}$	0.0019 ± 0.0098	0.971 ± 0.024
Vanishing skewness ($\Sigma = 0$)	0.000593 ± 0.000078	0.9941 ± 0.0002
First kurtosis maximum	0.00152 ± 0.00344	0.3331 ± 0.0008
Kurtosis minimum	0.00105 ± 0.00027	0.99150 ± 0.00067
Second kurtosis maximum	-0.00569 ± 0.00105	1.30045 ± 0.00259
Binder cumulant minimum	-0.0117 ± 0.0018	1.0008 ± 0.0002

Table 4.1: Numerical values of the fit parameters a and b, with the formula (4.28).

4.3 Correlation between the cumulants and the susceptibility

In the following, we shall examine the correlation between the temperatures at the locations of the different cumulant peaks and the transition temperatures obtained from the maxima of the peaks of the thermal susceptibility $\mid \chi_T \mid^{\max}$. For this, we plot the shift $T_c^{(Cum)}(V) - T_c(\infty)$ with $T_c^{(Cum)}(V)$ obtained from the peaks of each of the dispersion σ^2 and the kurtosis K, versus $T_c^{(|\chi_T|^{\max})}(V) - T_c(\infty)$. For the skewness Σ, $T_c^{(Cum)}(V)$ is obtained at the vanishing value $\Sigma(V) = 0$.

The different plots are illustrated on Figs. (4-13) to (4.17), and the linearity of the variations can clearly be observed. Fits with the linear forms:

$$T_c^{(Cum)}(V) - T_c(\infty) = a + b(T_c^{(|\chi_T|^{\max})}(V) - T_c(\infty)) \ , \tag{4.28}$$

give the values of the fit parameters a and b presented in Table 4.1.

Results of these fits show exact linear variations of the shifts of the transition temperatures from cumulants with the shifts of the transition temperatures from the susceptibility maxima, except for the kurtosis maxima, indicating that the most appropriate way for defining the transition temperature from kurtosis is at the location of its minimum, while its definition from the maximum of the variance and the vanishing

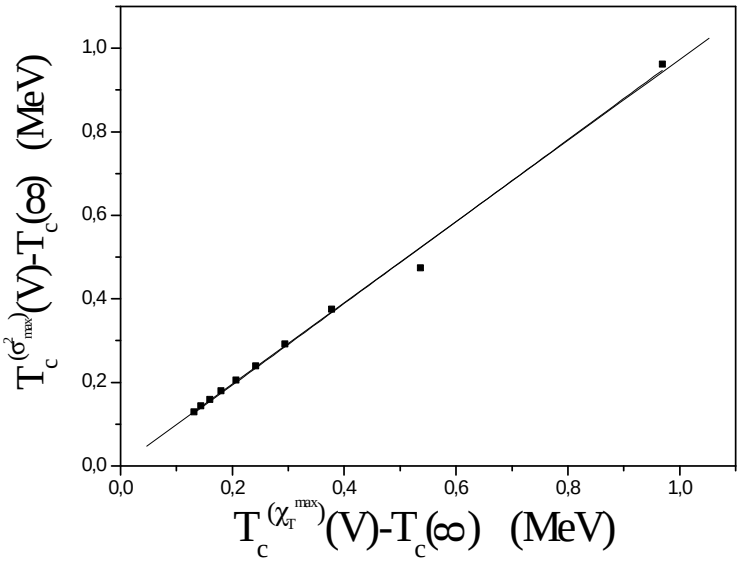

Figure 4.13: Linear fit of the data of the shift of the transition temperature defined as the location of the variance maximum vs the shift of the transition temperature obtained from $\mid \chi_T \mid^{\max}$.

skewness are well justified and can be adopted.

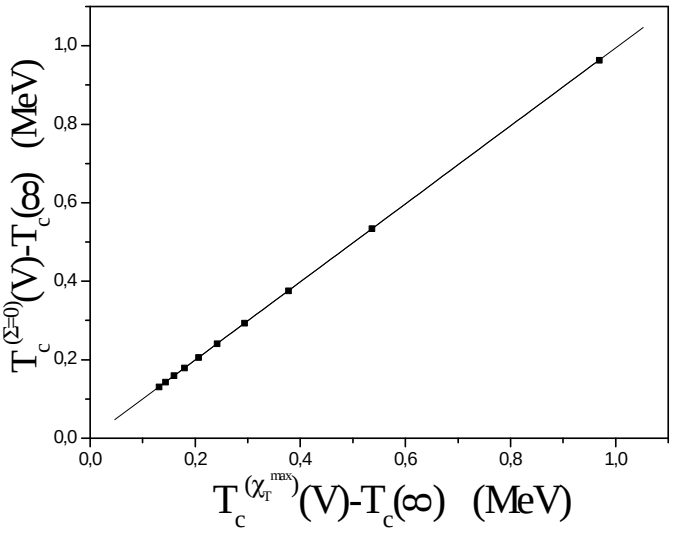

Figure 4.14: Linear fit of the data of the shift of the transition temperature defined at a vanishing skewness vs the shift of the transition temperature obtained from $\mid \chi_T \mid^{\max}$.

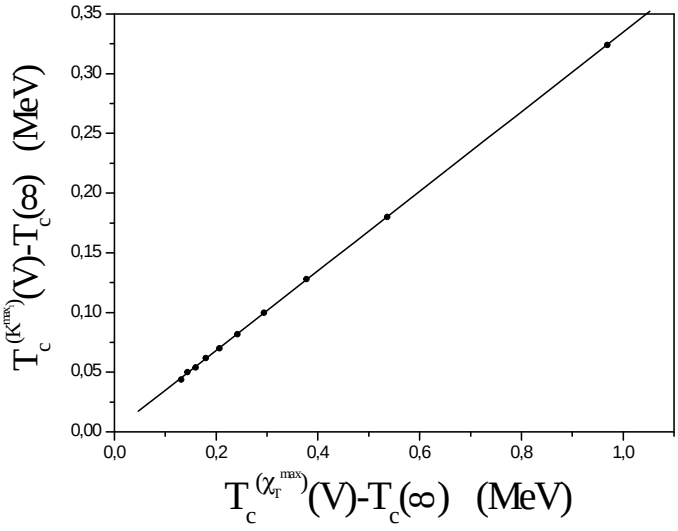

Figure 4.15: Linear fit of the data of the shift of the transition temperature defined at the first maximum of kurtosis vs the shift of the transition temperature obtained from $\mid \chi_T \mid^{\max}$.

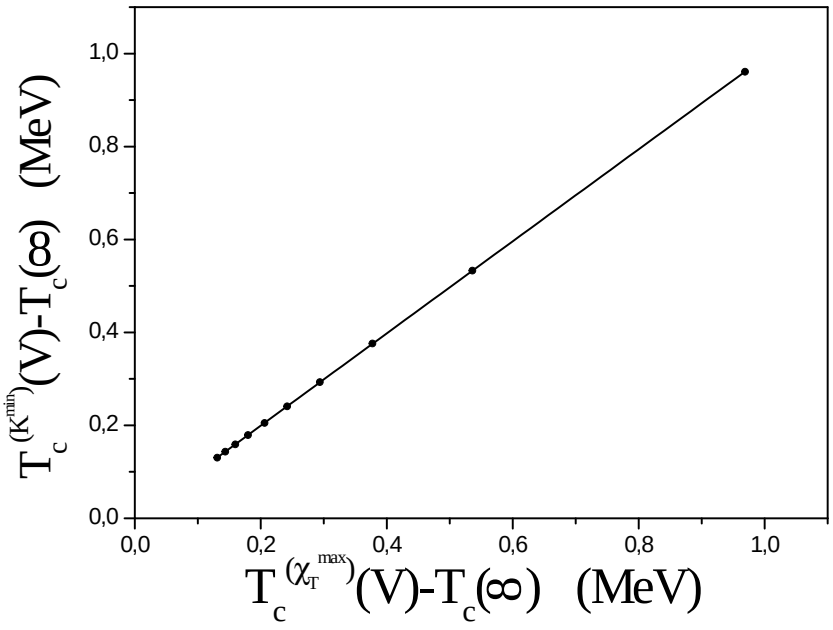

Figure 4.16: Linear fit of the data of the shift of the transition temperature defined at the minimum of kurtosis vs the shift of the transition temperature obtained from $\mid \chi_T \mid^{\max}$.

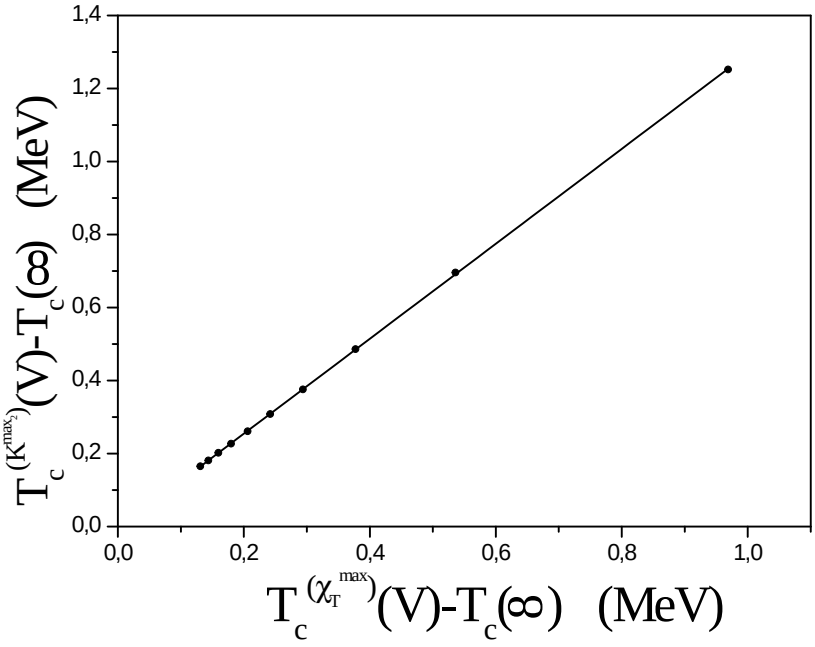

Figure 4.17: Linear fit of the data of the shift of the transition temperature defined at the second maximum of kurtosis vs the shift of the transition temperature obtained from $\mid \chi_T \mid^{\max}$.

Chapter 5

Finite-Size Effects and Scaling of the Deconfinement Phase Transition within the Excluded Volume Effects

5.1 Introduction

So far in this work, hadrons have been considered as point particles, and the considered finite size effects were those due to the finiteness of the system undergoing a phase transition, additionally to those induced by the color-singletness requirement. But, since hadrons are composed of quarks, they are extended particles and have finite volumes.

In the present chapter, such excluded volume effects are considered within the

phase coexistence model, using the color-singlet partition function for the QGP. Their effects on the studied deconfinement phase transition are then examined by probing the behavior of some physical quantities, as in the two previous chapters. It has been shown in [123] that "*dense nuclear matter can go through a second order phase transition into a QGP when the finite extensions of hadronic constituents are taken into account*".

5.2 The role of the finite volume of particles and their interactions: Hagedorn correction

The Hagedorn model described in section (1.8) represents a nonperturbative, analytically soluble model of a strongly interacting many-particle system. It predicts either the existence of a limiting temperature or a phase transition at high energy density. If the latter is true, the new phase cannot be treated in the framework of this model. Much progress has also been achieved in the mathematical understanding of the bootstrap constraint, mostly due to its reformulation in a relativistically covariant way. An excellent review of these results can be found in [124]. There were, however, two important questions to be answered. First, why can the fireball be treated as an ideal gas of hadron resonances? Second, how to take into account the finite proper volumes of the hadrons in the fireball? As to the first question, it has been argued that the rest masses of the observed hadron resonances arise as a result of strong interaction and with the inclusion of the total mass spectrum, the interaction (more precisely, its attractive part) is entirely taken into account [125]. According to this point of view, the observed hadron resonances are considered as quasiparticles among which only some residual interaction can be imagined, and which is neglected.

The second problem has been addressed by differentiating between the volume V_{ext} of the gas and the volume V available for the particles [126, 127];

$$V = V_{ext} - \sum_{i=1}^{N_p} V_i \tag{5.1}$$

where V_i are the proper volumes of the resonances. From the consistent, relativistically covariant treatment, it follows that the proper volume of the resonances must be proportional to their mass, $V_i = \frac{m_i}{4B}$. This is precisely the relation derived in the MIT bag model. Therefore, the constant B can be identified with the bag constant. The particles occupy an available volume,

$$V = V_{ext} - \frac{E}{4B} \tag{5.2}$$

depending on their energy. Thus, V is the volume in which the particles move as if they were pointlike, while in reality they have finite proper volumes and move in V_{ext}.

Treating the hadrons as extended particles leads to important consequences in the thermodynamical behavior of the gas. If the gas of hadron resonances is a real gas with some repulsion among the particles represented by the impenetrability of their proper volumes, then there is no limiting temperature, but the gas undergoes a phase transition and the energy density becomes too large. We can explain what happens as follows: The thermodynamical problem can be solved at first for a gas of fictitious point particles enclosed in the available volume V and one gets the corresponding equations of state. Then one can express the energy density of the real gas through the energy density of the gas of fictitious particles by means of the formula:

$$\frac{E}{V_{ext}} = \frac{(E/V)}{1 + \frac{(E/V)}{4B}} \ . \tag{5.3}$$

Even if the energy density (E/V) of the gas of fictitious point particles diverges in the limit $T \to T_c$, the energy density of the real gas remains constant and tends to the energy density of the hadronic bag, $(E/V_{ext}) \to 4B$.

In order to take into account the repulsive interactions between hadrons, all thermodynamical quantities in the hadronic phase may be corrected by the Hagedorn factor [126, 99]:

$$\eta_{Hag} = \frac{1}{1 + \frac{\varepsilon_{HG}}{4B}}, \tag{5.4}$$

where $\varepsilon_{HG}(T, V)$ is the energy density of the hadronic matter. The corrected thermodynamical quantities of the hadronic gas phase are then written as:

$$A_{HG\ cor}(T, V) = \eta_{Hag}\, A_{HG}(T, V). \tag{5.5}$$

5.3 Finite Size Rounding of the Deconfinement Phase Transition within the Excluded Volume Effects

Taking the excluded volume effects into account, the phase transition between the hadronic and QGP phases then occurs when:

$$P_{HG\ cor}\ (\mu_c, T_c) = P_{QGP}\ (\mu_c, T_c)\,, \tag{5.6}$$

with:

$$P_{QGP} = \frac{37\pi^2}{90} T^4 + \mu^2 T^2 + \frac{1}{2\pi^2}\mu^4 - B, \tag{5.7}$$

and:

$$P_{HG\ cor} = \eta_{Hag} \frac{\pi^2}{30} T^4. \tag{5.8}$$

Thus, the relation between T_c and μ_c is:

$$\frac{127}{12}T_c^4+\frac{37\pi^2}{120}\frac{T_c^8}{B}+\frac{30}{\pi^2}\mu_c^2T_c^2+\frac{3}{4}\frac{\mu_c^2T_c^6}{B}+\frac{15}{\pi^4}\mu_c^4+\frac{3}{8\pi^2}\frac{\mu_c^4T_c^4}{B}-\frac{30}{\pi^2}B=0. \tag{5.9}$$

The phase diagram in the $\mu-T$ plane, separating between hadronic and QGP phases, and giving at each point the transition parameters (μ_c, T_c) for two flavors $(N_f=2)$, with the common value of the bag constant $B^{1/4}=145MeV$, can also be illustrated in this case when the volume of the hadrons is considered. The extreme values of the transition parameters at $\mu=0$ and $T=0$ are: $T_c'(\mu=0;V=\infty)=104.21MeV$; $\mu_c'(T=0;V=\infty)=305.63MeV$.

We'll study in the following the FSE for a temperature driven deconfinement phase transition, at a vanishing chemical potential $(\mu=0)$, and for a density driven deconfinement phase transition at a fixed temperature $(T=100MeV)$, taking into account these excluded volume effects. For this purpose, we'll examine, like in chapter 3, the behavior of the order parameter, the entropy and energy densities with temperature and chemical potential for varying volume, when the volume of the hadrons is considered.

The corrected mean values of the energy and entropy densities are then related to the corrected order parameter by:

$$\begin{aligned}\langle s\left(T,\mu,V\right)\rangle_{cor} &= \mathfrak{s}_{QGP}+\left(\mathfrak{s}_{HG\ cor}-\mathfrak{s}_{QGP}\right)\ \langle\mathfrak{h}\left(T,\mu,V\right)\rangle_{cor}\\ \langle\varepsilon\left(T,\mu,V\right)\rangle_{cor} &= \mathfrak{e}_{QGP}+\left(\mathfrak{e}_{HG\ cor}-\mathfrak{e}_{QGP}\right)\ \langle\mathfrak{h}\left(T,\mu,V\right)\rangle_{cor},\end{aligned} \tag{5.10}$$

where:

$$\langle\mathfrak{h}\left(T,\mu,V\right)\rangle_{cor}=\frac{\left(-\frac{1}{T}(f_{HG\ cor}-f_{QGP})V-1\right)e^{-\frac{1}{T}(f_{HG\ cor}-f_{QGP})V}+1}{-\frac{1}{T}(f_{HG\ cor}-f_{QGP})V\left(e^{-\frac{1}{T}(f_{HG\ cor}-f_{QGP})V}-1\right)}. \tag{5.11}$$

In Fig. (5.1), we compare the order parameters without and with the Hagedorn correction, for two volumes, $V=150fm^3$ and $V=1000fm^3$, and for more clearness let's rather illustrate the variations of the relative difference between the order

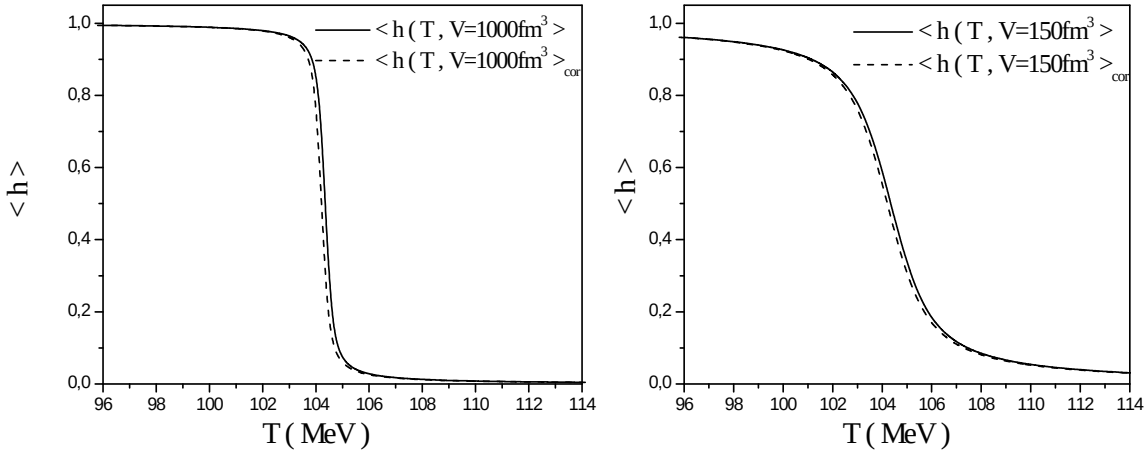

Figure 5.1: Order parameter versus temperature without (solid line) and with (dashed line) the Hagedorn correction, for the volumes, (left) $V = 1000fm^3$ and (right) $V = 150fm^3$.

parameters with and without the hagedorn correction $\frac{\langle h\rangle - \langle h\rangle_{cor}}{\langle h\rangle_{cor}}$, with temperature at different volumes in Fig. (5.2). We can notice that the difference is mostly notable in a temperature region around a temperature at which it is maximal, and which tends to $T_c(\infty)$ with increasing volume. This relative difference is more and more appreciable for big volumes, meaning that the transition region is the more sensitive to the extended volume correction

The three-dimensional plots of the corrected order parameter, entropy density scaled by T^3, $\frac{\langle s(T,V)\rangle_{cor}}{T^3}$, and energy density scaled by T^4, $\frac{\langle \varepsilon(T,V)\rangle_{cor}}{T^4}$ are illustrated, respectively, in the top, middle and bottom of Fig. (5.3). Like for the non-corrected quantities in Figs. (3.2), these plots exhibit a discontinuity at a critical temperature $T_c'(\infty) \simeq 104.21MeV$ for big volumes ($V \geq 1000fm^3$), indicating a first-order phase transition, while rounded curves are obtained when the volume decreases.

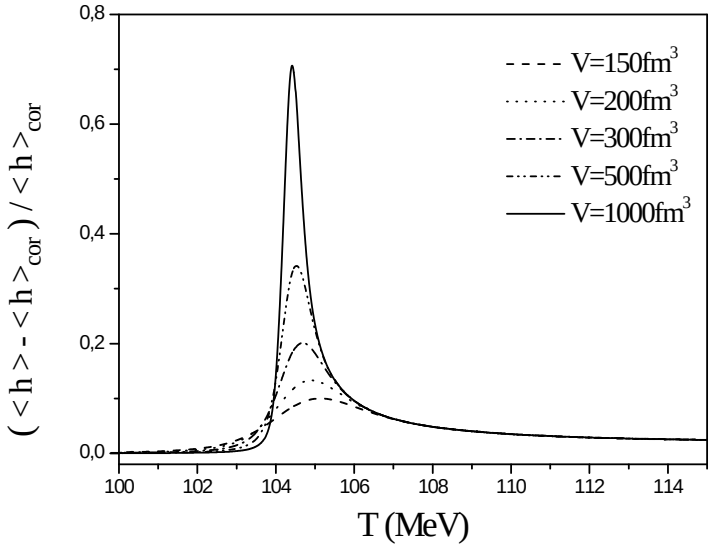

Figure 5.2: Relative difference $\frac{\langle h\rangle - \langle h\rangle_{cor}}{\langle h\rangle_{cor}}$ versus temperature for different volumes.

Similarly, Fig. (5.4) shows the variations of the corrected order parameter, normalized energy and entropy densities with chemical potential and system volume, at the temperature $T = 100MeV$. The first-order character of the transition can, also in this case, clearly be seen from the sharp discontinuity of the three quantities at a transition chemical potential $\mu_c'(\infty) \simeq 80.81MeV$, at the large volume limit. In small systems, the transition is perfectly smooth over a broadened region of chemical potential.

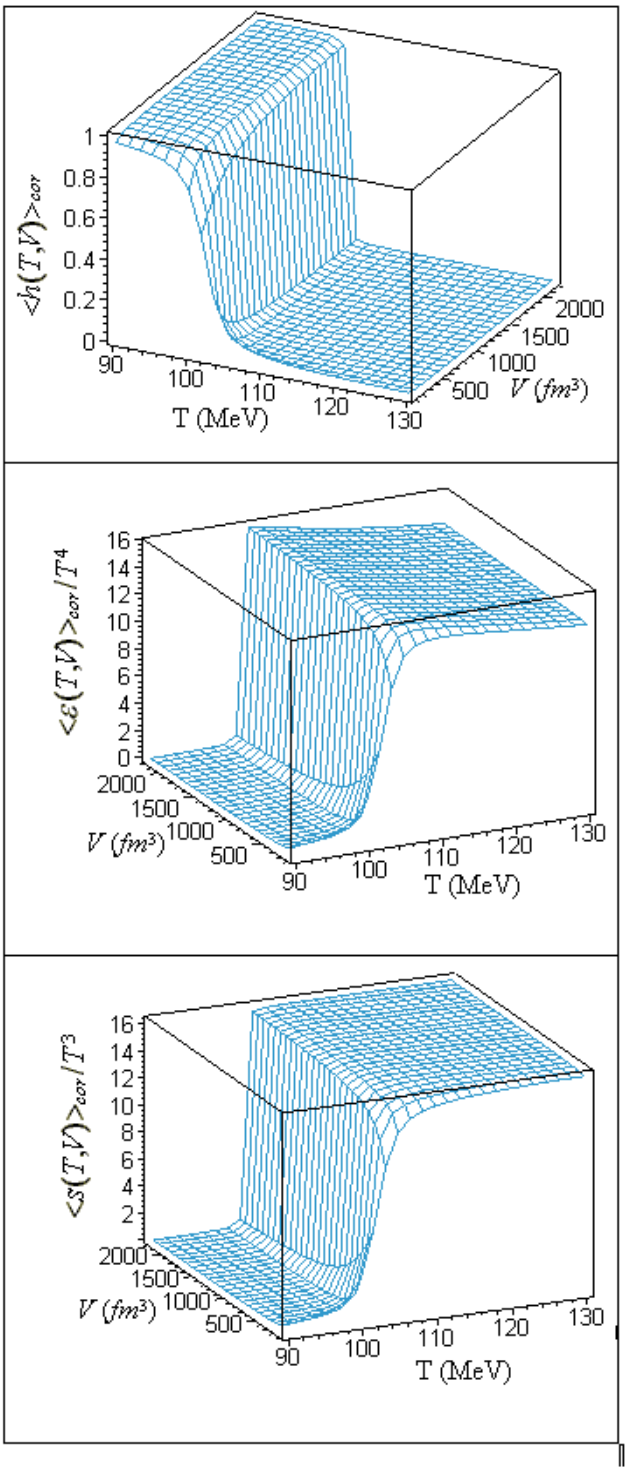

Figure 5.3: Three-dimensional plots of the corrected (top) order parameter, (middle) entropy density scaled by T^3, and (bottom) energy density scaled by T^4, with temperature and volume, at $\mu = 0$.

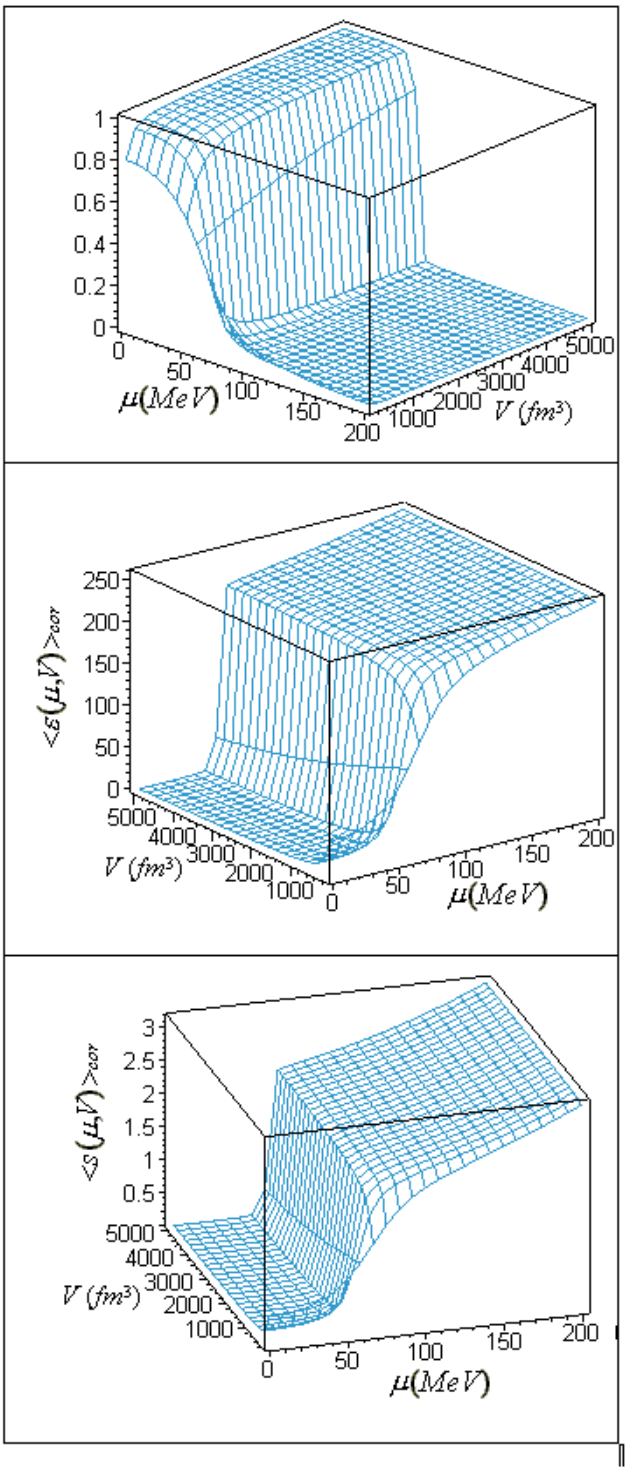

Figure 5.4: Three-dimensional plots of the corrected (top) order parameter, (middle) entropy density and (bottom) energy density with chemical potential and volume, at the temperature $T = 100MeV$.

5.4 Finite-Size Effects with the Exact Color-Singlet Partition Function and the Excluded Volume Correction

Hereafter, we shall consider the excluded volume correction for hadrons, as well as the color-singletness condition for the QGP phase within the phase coexistence model. The effects on the thermal deconfinement phase transition are then investigated by illustrating, first, each of the order parameter, energy and entropy densities calculated in this case.

The corrected mean value of the order parameter at zero chemical potential ($\mu = 0$) is calculated from the expression:

$$< \mathfrak{h}(T,V) >^{*}_{cor} = 1 - \frac{\int_{-\pi}^{+\pi}\int_{-\pi}^{+\pi} d\varphi d\psi M(\varphi,\psi) \int\limits_{0}^{1} \mathfrak{q} e^{\mathfrak{q}\mathsf{R}_{cor}(\varphi,\psi;T,V)} d\mathfrak{q}}{\int_{-\pi}^{+\pi}\int_{-\pi}^{+\pi} d\varphi d\psi M(\varphi,\psi) \int\limits_{0}^{1} e^{\mathfrak{q}\mathsf{R}_{cor}(\varphi,\psi;T,V)} d\mathfrak{q}}, \tag{5.12}$$

with:

$$\mathfrak{R}_{cor}\left(\varphi,\psi;T,V\right) = \left(g_{\mu=0}(\varphi,\psi) - \eta_{Hag}\,\frac{\pi^2}{30} - \frac{B}{T^4}\right) VT^3. \tag{5.13}$$

After effectuation of the integrations on $\mathfrak{q}$, the order parameter can be written on the form:

$$< \mathfrak{h}(T,V) >^{*}_{cor} = \frac{L_{01\ cor}\left(0\right) + L_{02\ cor}\left(0\right) - L_{12\ cor}\left(1\right)}{L_{01\ cor}\left(0\right) - L_{11\ cor}\left(1\right)}, \tag{5.14}$$

where the general form of the corrected integral coefficients appearing in this expression is:

$$L_{mn\ cor}\left(\mathfrak{q}\right) = \int_{-\pi}^{+\pi}\int_{-\pi}^{+\pi} d\varphi d\psi M(\varphi,\psi)(g_{\mu=0}(\varphi,\psi))^{m} \frac{\left(e^{\mathsf{R}_{cor}(\varphi,\psi;T,V)}\right)^{n}}{\mathfrak{R}_{cor}\left(\varphi,\psi;T,V\right)}. \tag{5.15}$$

The corrected mean value of the energy density is then related to $< \mathfrak{h}(T,V) >^*_{cor}$ by the expression:

$$< \varepsilon(T,V) >^*_{cor} = B + \left(e_{HG}\, \eta_{Hag} \left(1 - \frac{e_{HG}\, \eta_{Hag}}{3B} \right) - B \right) < \mathfrak{h}(T,V) >^*_{cor} - 3T^4\, \frac{L_{12\ cor}(0) + L_{11\ cor}(1) - L_{12\ cor}(1)}{L_{01\ cor}(0) - L_{01\ cor}(1)} \ . \tag{5.16}$$

Also in this case, as in (3.5.1), the corrected mean value of the entropy density will be calculated numerically by integrating $\frac{1}{T}(\frac{d<\varepsilon(T,V)>^*_{cor}}{dT})$, since it can not be expressed simply by the mean of the $L_{mn\ cor}$'s.

Fig. (5.5) shows the variations of the corrected order parameter, energy density over T^4 and entropy density over T^3 with temperature for various volumes. The same behavior as in Fig. (3.8) is observed, with the shifting effect induced by the color-singletness requirement.

5.5 Scaling Critical Exponents for the Deconfinement Phase Transition with the Exact Color-Singletness Condition and the Excluded Volume Correction

In the following, we shall carry out a finite size scaling analysis in order to determine the scaling critical exponents, given in eqs. (4.1), characterizing the deconfinement phase transition, when both excluded volume effects and color-singletness requirement are taken into account. For this purpose, each of the corrected thermal susceptibility, specific heat density and second derivative of the order parameter are first derived,

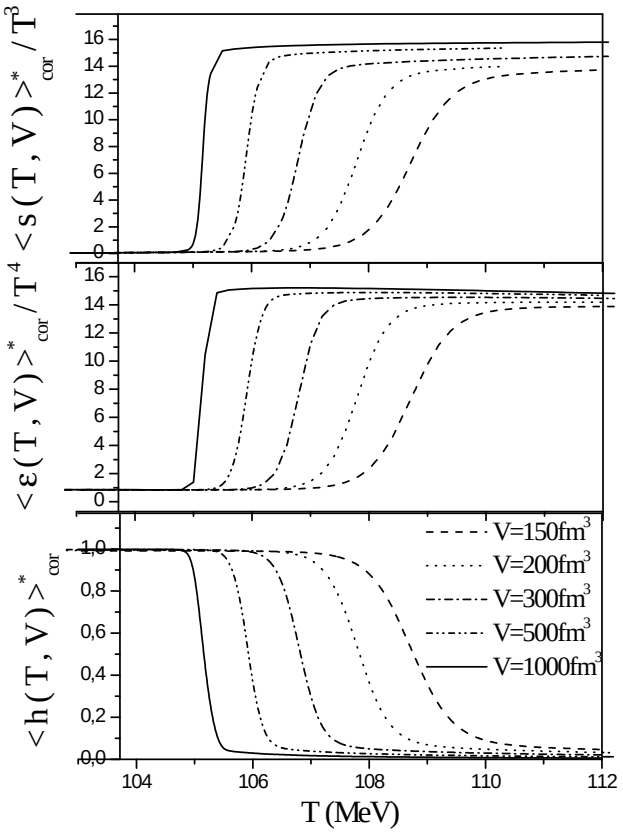

Figure 5.5: Variations of the corrected order parameter, normalized energy density $< \varepsilon(T,V) >^*_{cor} /T^4$ and normalized entropy density $< s(T,V) >^*_{cor} /T^3$ with temperature, at various volumes.

then analyzed in the transition region.

5.5.1 The susceptibility critical exponent

The obtained expression of the corrected thermal susceptibility is:

$$\begin{aligned}\chi_{cor}(T,V) &= \frac{T^2V}{L_{01}(0)-L_{01}(1)}\left[-3(L_{12\ cor}(0)+2L_{13\ cor}(0)+L_{12\ cor}(1)-2L_{13\ cor}(1))\right.\\ &\left.-(\frac{B}{T^4}-\frac{\pi^2}{10}\eta_{Hag}+\frac{\pi^4}{300}\frac{T^4}{B}\eta_{Hag}^2)(L_{02\ cor}(0)+2L_{03\ cor}(0)+L_{02\ cor}(1)-2L_{03\ cor}(1))\right]\\ &-T^2V\frac{L_{01\ cor}(0)+L_{02\ cor}(0)-L_{02\ cor}(1)}{(L_{01\ cor}(0)-L_{01\ cor}(1))^2}\left[-3(L_{12\ cor}(0)-L_{11\ cor}(1)+L_{12\ cor}(1))\right.\\ &\left.-(\frac{B}{T^4}-\frac{\pi^2}{10}\eta_{Hag}+\frac{\pi^4}{300}\frac{T^4}{B}\eta_{Hag}^2)(L_{02\ cor}(0)-L_{01\ cor}(1)+L_{02\ cor}(1))\right]\ , \qquad (5.17)\end{aligned}$$

and its variations with temperature at different volumes are represented on Fig. (5.6). Exactly the same behavior as in chapter 3 is found, and the difference between the values of the corrected and non corrected susceptibility at fixed temperature and volume is extremely small.

The data of the minima of the susceptibility at different system volumes are then extracted, and fitted to a power law of the volume: $\mid \chi_T \mid^{\max}(V) \sim V^{\gamma'_T}$, with the susceptibility scaling critical exponent: $\gamma'_T = 1.029 \pm 0.003$.

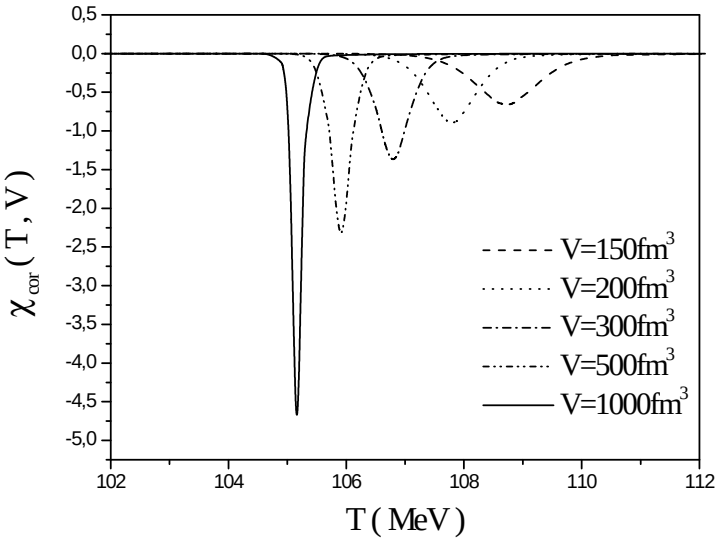

Figure 5.6: Variations of the corrected susceptibility with temperature for various volumes.

5.5.2 The specific heat critical exponent

The corrected thermal specific heat density given by:

$$
\begin{aligned}
c_{cor}\left(T,V\right) &= \left(\frac{2\pi^2}{5}\eta_{Hag}-\frac{\pi^2}{10}\eta_{Hag}^2\frac{\varepsilon_{HG}}{B}\right)T^3\ \left\langle \mathfrak{h}\left(T,V\right)\right\rangle^*_{cor} \\
&+\left(e_{HG}\ \eta_{Hag}\left(1-\frac{e_{HG}\ \eta_{Hag}}{3B}\right)-B\right)\ \chi_{cor}\left(T,V\right)+12T^3\frac{L_{11\ cor}(1)-L_{12\ cor}(1)+L_{12\ cor}(0)}{L_{11\ cor}(1)-L_{01\ cor}(0)} \\
&+\frac{3T^6V}{L_{01\ cor}(1)-L_{01\ cor}(0)}\left[-6L_{23\ cor}(0)+3L_{21\ cor}(1)-6L_{22\ cor}(1)+6L_{23\ cor}(1)\right. \\
&\left.+(\frac{B}{T^4}-\frac{\pi^2}{10}\eta_{Hag}+\frac{\pi^4}{300}\frac{T^4}{B}\eta_{Hag}^2)(-2L_{13\ cor}(0)+L_{11\ cor}(1)-2L_{12\ cor}(1)+2L_{13\ cor}(1))\right] \\
&-3T^6V\frac{L_{11\ cor}(1)-L_{12\ cor}(1)+L_{12\ cor}(0)}{\left(L_{01\ cor}(1)-L_{01\ cor}(0)\right)^2}\left[3(L_{12\ cor}(0)+L_{11\ cor}(1)-L_{12\ cor}(1))\right. \\
&\left.+(\frac{B}{T^4}-\frac{\pi^2}{10}\eta_{Hag}+\frac{\pi^4}{300}\frac{T^4}{B}\eta_{Hag}^2)(L_{02\ cor}(0)+L_{01\ cor}(1)-L_{02\ cor}(1))\right], \qquad (5.18)
\end{aligned}
$$

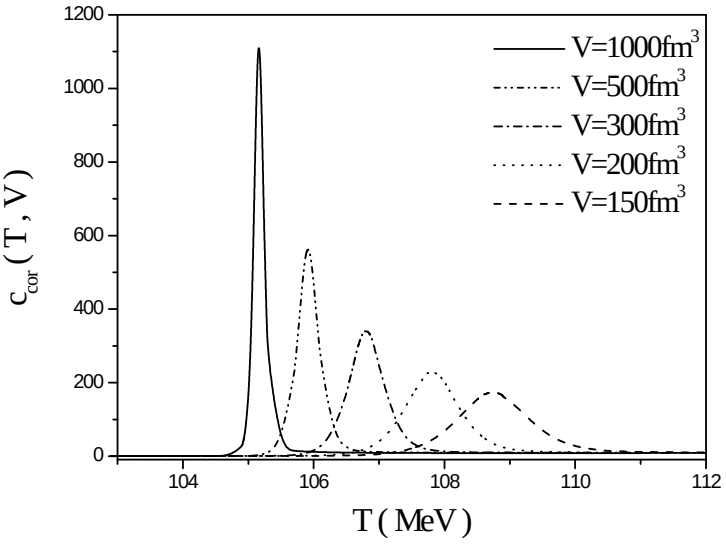

Figure 5.7: Variations of the corrected specific heat density with temperature for various volumes.

is illustrated in Fig. (5.7) versus temperature at various volumes. Here also, the same behavior as for the specific heat density in Fig. (3.12) is observed. Results of the maxima of the corrected specific heat density $c^{\max}_{T_{cor}}(V)$ are fitted to the power-law form: $c^{\max}_{T_{cor}}(V) \sim V^{\alpha'_T}$, and the obtained specific heat scaling exponent is: $\alpha'_T = 0.996 \pm 0.005$.

5.5.3 The smearing critical exponent

The width of the transition region is given by the difference: $\delta T'(V) = T'_2(V) - T'_1(V)$ with $T'_1(V)$ and $T'_2(V)$ the locations of the extrema of the corrected second derivative of the order parameter $\frac{\partial^2}{\partial T^2}\langle \mathfrak{h}(T,V)\rangle^*_{cor}$. The expression of this latter is:

$$
\begin{aligned}
\frac{\partial^2\langle\mathfrak{h}\,(T,V)\rangle^*_{cor}}{\partial T^2} &= \frac{2\chi_{cor}}{T} + \frac{\left(T^2V\right)^2}{L_{01_{cor}}(0)-L_{01_{cor}}(1)}\times \\
&[18L_{23_{cor}}(0)+54L_{24_{cor}}(0)-9L_{22_{cor}}(1)+36L_{23_{cor}}(1)-54L_{24_{cor}}(1) \\
&+\left(\tfrac{B}{T^4}-\tfrac{\pi^2}{10}\eta_{Hag}+\tfrac{\pi^4}{300}\tfrac{T^4}{B}\eta^2_{Hag}\right)(12L_{13_{cor}}(0)+36L_{14_{cor}}(0)-6L_{12_{cor}}(1)+24L_{13_{cor}}(1) \\
&-36L_{14_{cor}}(1))+\left(\tfrac{B}{T^4}-\tfrac{\pi^2}{10}\eta_{Hag}+\tfrac{\pi^4}{300}\tfrac{T^4}{B}\eta^2_{Hag}\right)^2(2L_{03_{cor}}(0)+6L_{04_{cor}}(0)-L_{02_{cor}}(1) \\
&+4L_{03_{cor}}(1)-6L_{14_{cor}}(1))-(L_{02_{cor}}(0)+2L_{03_{cor}}(0)+L_{02_{cor}}(1)-2L_{03_{cor}}(1)) \\
&\times\left(\tfrac{-4B}{T^7V}+\tfrac{7\pi^4}{300}\tfrac{T}{BV}\eta^2_{Hag}-\tfrac{\pi^6}{1500}\tfrac{T^5}{B^2V}\eta^3_{Hag}\right)]-\frac{\left(T^2V\right)^2}{\left(L_{01_{cor}}(0)-L_{01_{cor}}(1)\right)^2} \\
&\times[(3L_{12_{cor}}(0)+3L_{11_{cor}}(1)-3L_{12_{cor}}(1)+\left(\tfrac{B}{T^4}-\tfrac{\pi^2}{10}\eta_{Hag}+\eta_{Hag}+\tfrac{\pi^4}{300}\tfrac{T^4}{B}\eta^2_{Hag}\eta^2_{Hag}\right) \\
&\times(L_{02_{cor}}(0)+L_{01_{cor}}(1)-L_{02_{cor}}(1)))\,(3L_{12_{cor}}(0)+6L_{13_{cor}}(0)+3L_{12_{cor}}(1)-6L_{13_{cor}}(1) \\
&+\left(\tfrac{B}{T^4}-\tfrac{\pi^2}{10}\eta_{Hag}+\tfrac{\pi^4}{300}\tfrac{T^4}{B}\eta^2_{Hag}\right)(L_{02_{cor}}(0)+2L_{03_{cor}}(0)+L_{02_{cor}}(1)-2L_{03_{cor}}(1))\Big) \\
&+(L_{01_{cor}}(0)+L_{02_{cor}}(0)-L_{02_{cor}}(1))\,(-9L_{21_{cor}}(1)+18L_{22_{cor}}(1)-18L_{23_{cor}}(1)+18L_{23_{cor}}(0) \\
&-\left(\tfrac{B}{T^4}-\tfrac{\pi^2}{10}\eta_{Hag}+\tfrac{\pi^4}{300}\tfrac{T^4}{B}\eta^2_{Hag}\right)(6L_{11_{cor}}(1)-12L_{12_{cor}}(1)+12L_{13_{cor}}-12L_{13_{cor}}(0)) \\
&-\left(\tfrac{B}{T^4}-\tfrac{\pi^2}{10}\eta_{Hag}+\tfrac{\pi^4}{300}\tfrac{T^4}{B}\eta^2_{Hag}\right)^2(L_{11_{cor}}(1)-2L_{12_{cor}}(1)+2L_{13_{cor}}(1)-2L_{03_{cor}}(0)) \\
&-\left(\tfrac{-4B}{T^7V}+\tfrac{7\pi^4}{300}\tfrac{T}{BV}\eta^2_{Hag}-\tfrac{\pi^6}{1500}\tfrac{T^5}{B^2V}\eta^3_{Hag}\right)(L_{01}(1)-L_{02_{cor}}(1)+L_{02_{cor}}(0))\Big) \\
&-\Big(3L_{11_{cor}}(1)-3L_{12_{cor}}(1)+3L_{12_{cor}}(0)+\left(\tfrac{B}{T^4}-\tfrac{\pi^2}{10}\eta_{Hag}+\tfrac{\pi^4}{300}\tfrac{T^4}{B}\eta^2_{Hag}\right) \\
&\times(L_{01_{cor}}(1)-L_{02_{cor}}(1)+L_{02_{cor}}(0)))\,(6L_{13_{cor}}(1)-3L_{12_{cor}}(1)-3L_{12_{cor}}(0)-6L_{13_{cor}}(0) \\
&+\left(\tfrac{B}{T^4}-\tfrac{\pi^2}{10}\eta_{Hag}+\tfrac{\pi^4}{300}\tfrac{T^4}{B}\eta^2_{Hag}\right)(2L_{03_{cor}}(1)-L_{02_{cor}}(1)-L_{02_{cor}}(0)-2L_{03_{cor}}(0))\Big)\Big] \\
&+\frac{2\left(T^2V\right)^2}{\left(L_{01_{cor}}(0)-L_{01_{cor}}(1)\right)^3}\;(L_{01_{cor}}(0)+L_{02_{cor}}(0)-L_{02_{cor}}(1))\,(3L_{12_{cor}}(0)+3L_{11_{cor}}(1) \\
&-3L_{12_{cor}}(1)+\left(\tfrac{B}{T^4}-\tfrac{\pi^2}{10}\eta_{Hag}+\tfrac{\pi^4}{300}\tfrac{T^4}{B}\eta^2_{Hag}\right)(L_{02_{cor}}(0)+L_{01_{cor}}(1)-L_{02_{cor}}(1))\Big)^2\,, \qquad (5.19)
\end{aligned}
$$

and its variations with temperature at various system sizes are represented in Fig. (5.8).

The results of the width $\delta T(V)$ are fitted to the power-law form: $\delta T\,(V) \sim V^{-\theta'_T}$,

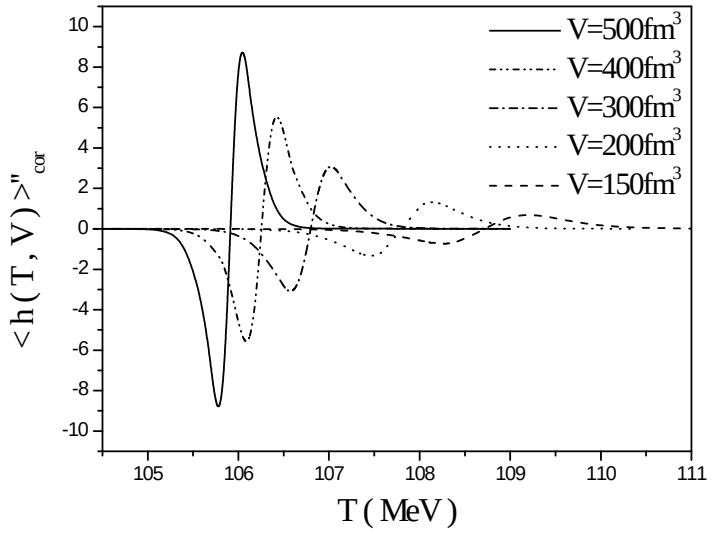

Figure 5.8: Second derivative of the corrected order parameter versus temperature at different volumes.

and the obtained value of the smearing scaling critical exponent is: $\theta'_T = 0.998 \pm 0.005$.

5.5.4 The shift critical exponent

The transition temperature can, also in this case, be obtained by several ways as in chapter 4. Extracting the data of $T_c(V)$ from the locations of the peaks of the thermal susceptibility $\mid \chi_T \mid^{\max} (V)$, and fitting them to a power-law function of the volume: $\tau_T(V) \sim V^{-\lambda'_T}$, gives the shift scaling critical exponent: $\lambda'_T = 0.812 \pm 0.003$.

The obtained results for the scaling critical exponents in this case are akin to those obtained previously in chapter 4 without the excluded volume correction. The phase transition is then still of first order, and has not been affected by the finite extention of the hadrons, as in [123].

Conclusion

The present work dealt with the study of the finite-size effects on the deconfinement phase transition, using a simple model of coexisting hadronic and QGP phases in a finite volume. Our model has shown the influence of the finiteness of the system size on the behavior of some response functions in the vicinity of the transition point. A sharp transition is observed in the thermodynamical limit, signaled by discontinuities in the order parameter, the entropy density s and the energy density ε at a transition temperature $T_c(\infty)$ for a thermally driven deconfinement phase transition (at $\mu = 0$), and at a transition chemical potential $\mu_c(\infty)$ for a density driven deconfinement phase transition (at $T = 100MeV$). In other terms, the deconfinement phase transition is labelled by a rapid rise in the effective degrees of freedom, represented by the ratios $\frac{\varepsilon}{T^4}$ and $\frac{s}{T^3}$ for a thermal deconfinement phase transition. Such a step-like rise behavior reflects a first-order phase transition. In finite volumes, the transition is rounded off and the variations of these thermodynamic quantities are perfectly smooth on the whole range of temperature. The delta function singularities appearing in the first derivatives of these discontinuous quantities, i.e., in the susceptibility $\chi = \frac{\partial \langle \mathsf{h} \rangle}{\partial T}$ and the specific heat density $c = \frac{\partial \langle \varepsilon \rangle}{\partial T}$, are then smeared out into finite peaks of widths $\delta T(V)$.

When the color-singlet character of physical states is exactly treated in the equation of state for the QGP in a finite volume, then a gradual "'freezing" of internal degrees

of freedom appears, as compared to the equation of state for infinite matter. This is reflected by a shift of the transition temperature $T_c(V)$ at which the thermal deconfinement phase transition from hadronic to QGP phases occurs, for finite systems. The maxima of the peaks of both susceptibility and specific heat density occur at effective transition temperatures $T_c\left(V\right)$ shifted away from the true transition temperature $T_c\left(\infty\right)$.

Our work has also shown that temperature and chemical potential play the same role when they drive the deconfinement phase transition. For a density driven deconfinement phase transition at a fixed temperature, the sharp transition occurring at the thermodynamic limit is smeared out in finite volumes over a range of chemical potential $\delta\mu\left(V\right)$ around the transition chemical potential $\mu_c\left(\infty\right)$, and when the color-singletness requirement is included for the QGP, the effective transition chemical potential $\mu_c\left(V\right)$ is shifted away from $\mu_c\left(\infty\right)$.

Other physical quantities can also be examined, which carry informations on the transition. Examples of such quantities are the sound velocity, rate of fluctuations and the second, third and fourth cumulants of the used probability distribution, each giving the transition temperature at some defined point. An other quantity of interest is the second derivative of the order parameter from which the width of the transition region can be obtained.

For a thermal deconfinement phase transition, finite size scaling analysis of the behavior of the maxima of the rounded peaks of the thermal susceptibility $\chi_T^{\max}\left(V\right)$ and specific heat density $c_T^{\max}\left(V\right)$, the width of the transition region $\delta T\left(V\right)$, and the shift of the effective transition temperature relative to the true one $\tau_T\left(V\right)=T_c\left(V\right)-T_c\left(\infty\right)$, shows their power-law variations with the volume characterized by the scaling critical

exponents γ, α, θ, and λ respectively. Numerical results of these scaling exponents have been determined in chapter 4, where the transition temperature has been obtained from various quantities as well from parametrizations of the order parameter and the susceptibility. These results are in good agreement with the analytical ones: $\gamma = \alpha = \theta = \lambda = 1$ obtained in our work [97], except for the shift critical exponent which slightly deflects from the analytical value 1. This may be due on one hand to the difficulty of locating accurately the peaks of the physical quantities, especially in the case of large volumes for which the peaks become very sharp, and on the other hand to the non-leading terms which contribute to the expression of the shift $\tau_T(V)$. However, a first estimate of the scaling critical exponents for the thermal deconfinement phase transition within this model has been obtained, and our result expressing the equality between all scaling exponents and the space dimensionality is a consequence of the singularity characterizing a first order phase transition and agrees very well with the predictions of the standard finite size scaling theoretical approaches to a first order phase transition [49, 50, 55, 106, 107, 108, 109] and with those obtained in a rather different and rigorous way, generalizing the finite size scaling description of a first order phase transition [110]. Also, we note a good agreement with the results of calculations using Monte Carlo methods in both lattice QCD [78, 111, 112, 113, 114] and other models in statistical physics [57, 115, 116].

A supplementary volume effect due to the finite hadron volumes has been considered in a part of this work. Wether the excluded volume effects influence the deconfinement phase transition has been examined, since it has been demonstrated that they can alter the kind of the transition. It has been shown in [100] that when the finite volume extensions of constituents in a hadronic gas are taken into account, for certain values of

the parameters of the used model, namely the QCD coupling constant α_s and the bag constant B, a smooth evolution from nuclear matter to a quark plasma phase through a second order transition becomes possible. In our model, we have found that such a correction does not affect the order of the transition.

Bibliography

[1] C. N. Yang and T. D. Lee, Phys. Rev. **87** (1952) 404; Phys. Rev. **87** (1952) 410.

[2] J. Imry, Phys. Rev. B **21** (1980) 2042.

[3] K. Binder and D. P. Landau, Phys. Rev. B **30** (1984) 1477.

[4] C. Spieles, H. Stöcker and C. Greiner, Phys. Rev. C **57** (1998) 908.

[5] A. Chodos and al., Phys. Rev. D **9** (1974) 3471; J. Cleymans, R. V. Gavai & E. Suhonen, Phys. Rep. **130** (1986) 217.

[6] K. Redlich and L. Turko, Z. Phys. C **5** (1980) 201; L.Turko, Phys. Lett. B **104** (1981) 153.

[7] H.-Th. Elze, W. Greiner and J. Rafelski , Phys. Lett. B **124** (1983) 515; Zeit. Phys. C **24** (1984) 361.

[8] H.-Th. Elze and W. Greiner, Phys. Lett. B **179** (1986) 385.

[9] A. Tounsi, J. Letessier and J. Rafelski, hep-ph/9811290.

[10] M. G. Mustafa, D. K. Srivastava and B. Sinha, Eur. Phys. J. C **5** (1998) 711; nucl-th/9712014.

[11] J. Madsen, D. M. Jensen and M. B. Christiansen, Phys. Rev. C **53** (1996) 1883.

[12] G. Yezza, Magister thesis in theoretical physics, Ecole Normale Supérieure-Kouba, Algiers (March 2002).

[13] A. Ait-El-Djoudi, M. Ladrem and G. Yezza, communication at the international conference *The Sixth Constantine High Energy Physics School*, held in Constantine-Algeria from 06 to 12 April 2002.

[14] M. Ladrem, A. Ait-El-Djoudi and G. Yezza, communication at the international conference Quark Matter 2002, held in Nantes-France from 18 to 24 July 2002.

[15] J. M. Yeomans, *Statistical Mechanics of Phase Transitions*, (Oxford University Press, 1992).

[16] J. W. Gibbs, Elementary Principles of Statistical Mechanics, The Collected Works of J. W. Gibbs, vol. II, Yale University Press, New Haven, CT, 1948.

[17] C. N. Yang and T. D. Lee, Phys. Rev. **87** (1952) 404; T. D. Lee and C. N. Yang, Phys. Rev. **87** (1952) 410.

[18] D. P. Landau & K. Binder, *A Guide to Monte Carlo Simulations in Statistical Physics,* Cambridge University Press (2000).

[19] W. Greiner, L. Neise and H. Stöcker, *Thermodynamics and Statistical Mechanics*, Springer-Verlag (1995).

[20] H. E. Stanley, *Introduction to Phase Transitions and Critical Phenomena*, Clarendon Press-Oxford (1971).

[21] V. Privman, Encycl. Appl. Phys. 23 (1998) 31.

[22] L. P. Kadanoff, in Proc. School of Physics "Enrico Fermi", Corso LI, edited by M. S. Green (Academic Press, New York, 1971).

[23] K.G. Wilson, Phys. Rev. **B4** (1971) 3174; **B4** (1971) 3184.

[24] M.E. Fisher, Rev. Mod. Phys. **46** (1974) 597; **70** (1998) 653.

[25] H. E. Stanley, Reviews of Modern Physics, Vol 71, 2, (1999) S358.

[26] http://d0server1.fnal.gov/users/gll/public/edpublic.htm .

[27] Ya. B. Zeldovitch, JETP 37 (1959) 569.

[28] Ya. B. Zeldovitch, L. B. Okun and S. B. Pikelner, Usp. Fiz. Nauk 87 (1965) 113.

[29] D. Ivanenko and D. E. Kurdgelaidze, Nuovo Cimento Lett.2 (1969) 13.

[30] N. Itoh, Progr. Theoret. Phys. 44 (1970) 291.

[31] R. Hagedorn, Nuovo Cim. Suppl. 3 (1965) 147.

[32] R. Hagedorn, Lectures given at the “Advanced NATO Workshop: Hot Hadronic matter, Theory and experiment.”, Divonne-les-Bois, France, preprint CERN-TH.7190 (1994).

[33] K. G. Wilson, Phys. Rev. **D10** (1974) 2445.

[34] M. Creutz, Phys. Rev. Lett. **43** (1979) 553; Phys. Rev. **D21** (1980) 2308.

[35] C. DeTar, hep-ph/9504325.

[36] S. Ejiri et al., hep-lat/0408046.

[37] F. Karsch, J. Phys. G31 (2005) S633, hep-lat/0412038.

[38] S. Ejiri et al., Nucl. Phys. A774 (2006) 837, hep-ph/0509361.

[39] S. Ejiri, F. Karsch,c, E. Laermann and C. Schmidt, Phys. Rev. D73 (2006) 054506, hep-lat/0512040.

[40] F. Karsch, AIP Conf. Proc. 602 (2001) 323, hep-lat/0109017.

[41] M. Cheng et al., Phys. Rev. D74 (2006) 054507, hep-lat/0608013.

[42] F. Karsch, E. Laermann and Ch. Schmidt, Phys. Lett. B520 (2001) 41, hep-lat/0107020.

[43] Ch. Schmidt, F. Karsch and E. Laermann, Nucl. Phys. Proc. Suppl. 106 (2002) 423, hep-lat/0110039.

[44] F. Karsch, hep-lat/0601013.

[45] F. Karsch, J. Phys. Conf. Ser. 46 (2006) 122, hap-lat/0608003.

[46] M. Fukugita, Nucl. Phys. Proc. Suppl. **9** (1989) 291.

[47] F. Karsch, Nucl. Phys. A **590** (1995) 367c-382c.

[48] F. Karsch, Nucl. Phys. A **698** (2002) 199c-208c.

[49] F. Karsch et al., Nucl. Phys. (Proc. Suppl.) B **94** (2001) 411-414.

[50] F. Karsch et al., Nucl. Phys. B **605** (2001) 579-599.

[51] M. Fukugita, RIFP-703 (June 1987).

[52] M. Fukugita et al., Phys. Rev. Lett. **58** (1987) 2515; UTHEP-168 (August 1987).

[53] M. Fukugita et al.,Phys. Rev. Lett. **60** (1988) 178.

[54] M. Fukugita, Nucl. Phys. Proc. Suppl. **4** (1988) 105.

[55] M. Fukugita & A. Ukawa, Phys. Rev. D **38** (1988) 1971.

[56] R. V. Gavai et al., Phys. Lett. B **200** (1988) 137.

[57] F. R. Brown et al., Phys. Rev. Lett. **65** (1990) 2491.

[58] S. Aoki et al. (JLQCD Coll.), Nucl. Phys. B **63**A-C (1998) 403, **60**A (1998) 188.

[59] B. Lucini et al., Phys. Lett. B **545** (2002) 197.

[60] P. Cea et al., Nucl. Phys. (Proc. Suppl.) B **129, 130** (2004) 751.

[61] M. Cheng et al., Phys.Rev. D75 (2007) 034506; hep-lat/0612001.

[62] M. E. Fisher and M. N. Barber, Phys. Rev. Lett. 28 (1972) 1516.

[63] D. P. Landau, Phys. Rev. B vol. 14, N° 1 (1976) 255.

[64] M. E. Fisher and A. N. Berker, Phys. Rev. B **26** N° 5 (1982) 2507.

[65] M. N. Barber, in *Phase Transitions and Critical Phenomena*, Vol. 8, C. Domb and J. L. Lebowitz eds. (Academic Press, New York, 1983) 145.

[66] M. S. Challa, D. P. Landau and K. Binder, Phys. Rev. **B34** (1986) 1841.

[67] K. Binder and D. W. Heermann, *Monte Carlo Simulations in Statistical Physics*, (Springer-Verlag, 1988, 2nd edition 2002).

[68] K. Binder, Rep. Prog. Phys. **60** (1997) 487.

[69] P. Forcrand and O. Philipsen, hep-lat/ 0205016.

[70] H. Meyer-Ortmanns, Rev. Mod. Phys. **68** (1996) 473.

[71] V. Privman et M. E. Fischer, J. Stat. Phys. Vol 33, N° 2 (1983) 385; J. App. Phys. Vol 57, N° 1 (1985) 3327.

[72] A. Billoire, hep-lat/9208026.

[73] M. Fukugita et al., KEK-TH-233 (1989).

[74] M. Henkel, *Conformal Invariance and Critical Phenomena*, (Springer-Verlag, 1999).

[75] K. Binder, Phys. Rev. Lett. **47** (1981) 693; Z. Phys. **B43** (1981) 119.

[76] D. P. Landau & K. Binder, *A Guide to Monte Carlo Simulation in Statistical Physics, (*Cambridge University Press, 2000).

[77] Q.H. Zhang, hep-ph/0106242.

[78] J. Fingberg, U. Heller, and F. Karsch, Preprint HLRZ-92-39.

[79] G. S. Bali and K. Schilling, Phys. Rev. **D46** (1992) 2636.

[80] K. D. Born, et al., Phys. Lett. **B329** (1994) 325.

K. D. Born, et al., Phys. Lett. **B329** (1994) 332.

[81] C. Allton et al. (RBC and UKQCD Collaborations), hep-lat/0701013, BNL-HET-07/1, CU-TP-1175, Edinburgh 2007/1, KEK-TH-1132, RBRC-637, SHEP-0701, SWAT/07/502.

[82] A. Ukawa, preprint CERN-TH 5266/88.

[83] J. Engels, F. Karsch, H. Satz and I. Montvay, Nucl. Phys. **B205** [$FS5$] (1982) 545.

[84] A. Ait-El-Djoudi, M. Ladrem and G. Yezza, communication at the international conference *The Seventh Constantine High Energy Physics School on Theoretical Physics and Cosmology*, held in Constantine-Algeria from 03 to 08 April 2004.

[85] D. P. Landau and R. H. Swendsen, Phys. Rev. Lett. **46** (1981) 1437

[86] F. R. Brown et al., Phys. Rev. Lett. **61** (1988) 2058.

[87] P. Bacilieri et al., Phys. Rev. Lett. **61** (1988) 1545.

[88] J. F. McCarthy, Indiana University Preprint IUHET 164 (1989).

[89] M. Fukugita et al., Phys. Rev. Lett. **63** (1989) 1768.

[90] P. Bacilieri et al., Phys. Lett. **B220** (1989) 607.

[91] R. V. Gavai, F. Karsch and B. Petersson, Nucl. Phys. **B322** (1989) 738.

[92] M. Fukugita, Phys. Rev. Lett. **63** (1989) 13.

[93] M. Fukugita et al., Nucl. Phys. Proc. Suppl. **17** (1990) 204.

[94] S. Gupta et al., Nucl. Phys. **B329** (1990) 263.

[95] M. Fukugita et al., J. Phys. **A23** (1990) L561-L566.

[96] N. A. Alves et al., Phys. Rev. Lett. **64** (1990) 3107.

[97] A. Ait-El-Djoudi, Magister thesis in theoretical physics, Ecole Normale Supérieure-Kouba, Algiers (October 1999).

[98] C. Schmidt, Proceedings of Science (Lat2006) 021; hep-lat/0610116v2.

[99] J. Letessier and J. Rafelski, *Hadrons and Quark-Gluon Plasma*, (Cambridge University Press, 2002).

[100] S. A. Chin, Phys. Lett. **78B** (1978) 552.

[101] M. LeBellac, Lectures given at the XXX^{th} Schladming winter school, Austria, preprint INLN 1991/8.

[102] C. Barter, D. Blaschke and H. Voss, preprint CERN-TH. 6499/92.

[103] G. Auberson et al., J. Math. Phys. **27** (1986) 1658.

[104] F. Savatier, J. Math. Phys. **32** (1991) 2243.

[105] M. I. Gorenstein, O. A. Mogilevsky, V. K. Petrov, G. M. Zinovjev, Z. Phys. C **18** (1983) 13.

[106] Bo-Sture K. Skagerstam, Phys. Lett. **B133** (1983) 419.

[107] Bo-Sture K. Skagerstam, Z. Phys. **C24** (1984) 97.

[108] Ramesh Anishetty, J. Phys. **G10** (1984) 439.

[109] J. C. Anjos, J. Sá Borges, A. P. C. Malbouisson, F. R. A. Simão, Z. Phys. **C23** (1984) 243.

[110] S. I. Azakov, P. Salomonson and B. -S. Skagerstam, Phys. Rev. **D36** (1987) 2137.

[111] S. I. Azakov, Teor. Mat. Fiz, Vol. **76** N○ 3 (1988) 362.

[112] P. Von Brentano and Winfried Frank, Am. J. Phys. **64** (1996) 589.

[113] M. G. Mustafa and A. Ansari, Phys. Rev. **C55** (1997) 2005.

[114] L. Landau and E. M. Lifshitz, Hydrodynamics, (Pergamon Press, London, 1959).

[115] D. H. Rischke, Nucl. Phys. A610 (1996) 88c-101c; nucl-th/9608024

[116] D. H. Rischke and M. Gyulassy, Nucl. Phys. **A597** (1996) 701.

[117] D. H. Rischke, nucl-th/9809044.

[118] C. M. Hung and E. V. Shuryak, Phys. Rev. Lett. **75** (1995) 4003.

[119] M. Ladrem, A. Ait-El-Djoudi and G. Yezza, in the Proceedings of the international conference "Quark Confinement and the Hadron Spectrum" held in Gargnano-Italy from 10-14 September 2002.

[120] J. P. Blaizot and J. Y. Ollitraut, Phys. Rev. **D36** (1987) 916.

[121] M. Asakawa and T. Hatsuda, Phys.Rev. **D55** (1997) 4488.

[122] K. Binder, Phys. Rev. Lett. **47** (1981) 693; Zeit. Phys. **B43** (1981) 119.

[123] T. Çelik and Y. Gündüç, Preprint IC/85/296.

[124] R. Hagedorn, in Quark matter'84, Helsinki, 1984 (Springer, Berlin, 1985).

[125] S. Z. Belenky, Nucl. Phys. **2** (1956) 259.

[126] R. Hagedorn and J. Rafelski, Phys. Lett. **97B** (1980) 136.

[127] R. Hagedorn, I. Montvay and J. Rafelski, in Quark matter'84.

[128] K. Binder, Ferroelectrics 73 (1987) 43; in Computational Methods in Field Theory, H. Gausterer and C. B. Lang, (Eds. Springer, Berlin 1992) 59.

[129] W. Janke, Phys. Rev. B **47** (1993) 14757.

[130] K. Vollmayr, J.D. Reger, M. Scheucher, and K. Binder, Z. Phys. B **91** (1993) 113.

[131] J. G. Brankov, D. M. Danchev and N. S. Tonchev, *Theory of Critical Phenomena in Finite-Size Systems - Scaling and Quantum Effects*, (World Scientific, 2000).

[132] C. Borgs and R. Kotecky, J. Stat. Phys. **61** (1991) 79; C. Borgs, R. Kotecky and S. Miracle-Solé, J. Stat. Phys. **62** (1991) 529.

[133] B. Beinlich, F. Karsch, E. Laermann and A. Peikert, Eur. Phys. J. C **6** (1999) 133.

[134] K. Bitar et al., Nucl. Phys. B **337** (1990) 245.

[135] R. V. Gavai, Nucl. Phys. Proc. Suppl. **106** (2002) 480; Nucl. Phys. B **633** (2002) 127.

[136] M. Mathur et R. V. Gavai, Nucl. Phys. B **448** (1995) 399.

[137] D. Loison and K. D. Schotte, Eur. Phys. J. B **5** (1998) 735, B **14** (2000) 125.

[138] O. Dillmann, W. Janke and K. Binder, J. Stat. Phys. **92** 1/2 (1998) 57.

Eur. Phys. J. C (2005)
Digital Object Identifier (DOI) 10.1140/epjc/s2005-02357-y

THE EUROPEAN PHYSICAL JOURNAL C

Finite-size effects and scaling for the thermal QCD deconfinement phase transition within the exact color-singlet partition function

M. Ladrem[a], A. Ait-El-Djoudi[b]

Laboratoire de Physique des Particules et Physique Statistique, Ecole Normale Supérieure-Kouba, B.P. 92, 16050, Vieux-Kouba, Algiers, Algeria

Received: 11 January 2005 / Revised version: 7 July 2005 /
Published online: ♣ 2005 –

Abstract. We study the finite-size effects for the thermal quantum chromodynamics (QCD) deconfinement phase transition, and use a numerical finite-size scaling analysis to extract the scaling exponents characterizing its scaling behavior when approaching the thermodynamic limit ($V \longrightarrow \infty$). For this, we use a simple model of coexistence of hadronic gas and color-singlet quark gluon plasma (QGP) phases in a finite volume. The color-singlet partition function of the QGP cannot be exactly calculated and is usually derived within the saddle-point approximation. When we try to do calculations with such an approximate color-singlet partition function, a problem arises in the limit of small temperatures and/or volumes $\left(VT^3 << 1\right)$, requiring additional approximations if we want to carry out calculations. We propose in this work a method for an accurate calculation of any quantity of the finite system, without any approximation. By probing the behavior of some useful thermodynamic response functions on the whole range of temperature, it turns out that, in a finite-size system, all singularities in the thermodynamic limit are smeared out and the transition point is shifted away. A numerical finite-size scaling (FSS) analysis of the obtained data allows us to determine the scaling exponents of the QCD deconfinement phase transition. Our results expressing the equality between their values and the space dimensionality is a consequence of the singularity characterizing a first-order phase transition and agree very well with the predictions of other FSS theoretical approaches to a first-order phase transition and with the results of calculations using Monte Carlo methods in both lattice QCD and statistical physics models.

1 Introduction

It is generally believed that at sufficiently high temperatures and/or densities a new phase of matter called the quark gluon plasma (QGP) can be created. This is logically a consequence of the quark–parton level of the matter structure and of the dynamics of strong interactions described by the quantum chromodynamics (QCD) theory. Its existence, however, has been partly supported by lattice QCD calculations and cosmological standard model predictions. The only available and experimental way to study the QCD deconfinement phase transition is to try to create it in ultra-relativistic heavy-ion collision conditions similar to those in the early moments of the universe, right after the Big Bang. If ever the QGP is created in ultra-relativistic heavy-ion collisions, the volume within which the eventual formation would take place would certainly be finite. Also, in lattice QCD studies, the scale of the lattice space volume is finite. This motivates the study of finite-size effects on the expected deconfinement phase transition from a hadronic gas (HG) phase to a QGP phase. These effects are certainly important since statistical fluctuations in a finite volume may hinder a sharp transition between the two phases. Phase transitions are known to be infinitely sharp, signaled by some singularities, only in the thermodynamic limit [1]. In general, finite-size effects lead to a rounding of these singularities, as pointed out in [2, 3]. However, even in a such situation, it is possible to obtain information on the critical behavior. Large but finite systems show a *universal* behavior called "finite-size scaling" (FSS), allowing one to put all the physical systems undergoing a phase transition in a certain number of universality classes. The systems in a given universality class display the same critical behavior, meaning that certain dimensionless quantities have the same values for all these systems. *Critical exponents* are an example of these universal quantities.

In the present work, we study the finite-size behavior for the thermally driven deconfinement phase transition within a simple QCD model as used in [4]. The model is based on the standard MIT bag model with a mixed phase system having a finite total volume V [5]. The fraction of volume (defined by the parameter $\mathfrak{h}$) occupied by the HG phase is given by: $V_{HG} = \mathfrak{h}V$, and the remaining volume: $V_{QGP} = (1-\mathfrak{h})V$ then contains the QGP phase. Addition-

[a] e-mail: Ladrem@eepad.dz
[b] e-mail: Aitamel@eepad.dz

ally, we implement the color-charge confinement property by requiring that the QGP phase is a colorless object in the color space. Then, if we assume noninteracting phases (separability of the energy spectra of the two phases), the total partition function of the system can be written as the product:

$$Z(\mathfrak{h}) = Z_{\mathrm{QGP}}(\mathfrak{h}) Z_{\mathrm{HG}}(\mathfrak{h}) Z_{\mathrm{Vac}}(\mathfrak{h}), \tag{1}$$

where:

$$\begin{aligned} Z_{\mathrm{Vac}}(T,\mathfrak{h}) &= \exp(-BV_{\mathrm{QGP}}/T) \\ &= \exp(-BV(1-\mathfrak{h})/T), \end{aligned} \tag{2}$$

accounts for the confinement of quarks and gluons by the real vacuum pressure exerted on the perturbative vacuum (B) of the bag model. For the HG phase, the partition function is calculated just for a pionic gas and is simply given by:

$$Z_{\mathrm{HG}} = e^{\frac{\pi^2}{30} T^3 V_{HG}}. \tag{3}$$

The partition function $Z_{\mathrm{QGP}}(\mathfrak{h})$ of the QGP phase is calculated by considering a free gas of quarks and gluons with the exact color-singletness requirement. We can then perform calculation of the mean value of any thermodynamic quantity of the system $\langle \mathcal{A}(T,\mu,V) \rangle$, as defined in [4], by:

$$\langle \mathcal{A}(T,\mu,V) \rangle = \frac{\int_0^1 \mathcal{A}(\mathfrak{h},T,\mu,V)\, Z(\mathfrak{h})\, d\mathfrak{h}}{\int_0^1 Z(\mathfrak{h})\, d\mathfrak{h}}, \tag{4}$$

where $\mathcal{A}(\mathfrak{h},T,\mu,V)$ is the total thermodynamic quantity in the state $\mathfrak{h}$, given in the case of an extensive quantity by:

$$\begin{aligned} \mathcal{A}(\mathfrak{h},T,\mu,V) &= \mathcal{A}_{\mathrm{HG}}(T,\mu,\mathfrak{h}V) \\ &\quad + \mathcal{A}_{\mathrm{QGP}}(T,\mu,(1-\mathfrak{h})V), \end{aligned} \tag{5}$$

and in the case of an intensive quantity, by:

$$\begin{aligned} \mathcal{A}(\mathfrak{h},T,\mu,V) &= \mathfrak{h}\mathcal{A}_{\mathrm{HG}}(T,\mu,\mathfrak{h}V) \\ &\quad + (1-\mathfrak{h})\mathcal{A}_{\mathrm{QGP}}(T,\mu,(1-\mathfrak{h})V), \end{aligned} \tag{6}$$

with $\mathcal{A}_{\mathrm{QGP}}$ and $\mathcal{A}_{\mathrm{HG}}$ being the contributions relative to the individual QGP and HG phases, respectively.

Let us note that the coexistence of two phases in a finite system undergoing a phase transition taken alone seems not to be sufficient for anticipating the first-order nature of the phase transition when approaching the thermodynamic limit. A similar confusion can arise in the case of a correlation-length scaling with the volume and suggesting a second-order nature of the transition in the thermodynamic limit. This subtle situation has been noticed and clarified in several works [6–9]. Then, for a firm determination of the order of a phase transition in a finite system, a full and detailed finite-size scaling analysis of different response functions simultaneously, yielding various scaling critical exponents, seems to be necessary. This is not all in our case, since other basic parameters of QCD like the number of flavors and the current quark masses have a strong influence on how the phase transition occurs. A clear sensitivity of the order of the QCD deconfinement phase transition to these parameters has been revealed by several lattice QCD calculations (see, for example, [7,10,11]).

The color-singlet partition function of the QGP derived using the group-theoretical projection technique formulated by Turko and Redlich [12] cannot be exactly calculated and is usually calculated within the saddle-point approximation in the limit $V_{QGP}T^3 >> 1$ as in [13–16]. It turns out that the use of the obtained approximated partition function for the calculation of a mean value within the definition (4), has as a consequence the absence of the deconfinement phase transition [17]. This is due to the fact that the approximation used for the calculation of the color-singlet partition function breaks down at $V_{QGP}T^3 << 1$, and this limit is attained in our case. This has been emphasized in further works in which additional approximations have been used to carry out calculations, as in [4,14]. We propose in the following a method which allows us to calculate physical quantities accurately describing well the deconfinement phase transition at finite volumes within the QCD model chosen, thus avoiding then the problem arising at $V_{QGP}T^3 << 1$ without any approximation. We proceed by using the exact definition of the color-singlet partition function for Z_{QGP} in the definition (4) of the mean value of a physical quantity. A first analytical step in the calculation of the mean value is then achieved, and an expression with integral coefficients is obtained. The double integrals are then carried out with a suitable numerical method at each value of temperature and volume, and the behavior of the physical quantity of the finite system can so be obtained on the whole range of temperature, for various volumes, without any restriction. Afterwards, scaling critical exponents characterizing the scaling behavior of some quantities are determined using a numerical FSS analysis.

2 Exact color-singlet partition function of the QGP

The exact partition function for a color-singlet QGP contained in a volume V_{QGP}, at temperature T and quark chemical potential μ, is determined by [13]:

$$\begin{aligned} &Z_{\mathrm{QGP}}(T,V_{\mathrm{QGP}},\mu) \\ &= \frac{8}{3\pi^2} \int_{-\pi}^{+\pi}\int_{-\pi}^{+\pi} d\left(\tfrac{\varphi}{2}\right) d\left(\tfrac{\psi}{3}\right) M(\varphi,\psi) \widetilde{Z}(T,V_{\mathrm{QGP}},\mu;\varphi,\psi), \end{aligned} \tag{7}$$

$M(\varphi,\psi)$ is the weight function (Haar measure) given by:

$$M(\varphi,\psi) = \left(\sin\left(\tfrac{1}{2}(\psi+\tfrac{\varphi}{2})\right) \sin(\tfrac{\varphi}{2}) \sin\left(\tfrac{1}{2}(\psi-\tfrac{\varphi}{2})\right)\right)^2, \tag{8}$$

and $\widetilde{Z}$ the generating function defined by:

$$\widetilde{Z}(T,V_{\rm QGP},\mu;\varphi,\psi) \quad (9)$$
$$= Tr\left[\exp\left(-\beta\left(\widehat{H}_0-\mu\left(\widehat{N}_q-\widehat{N}_{\overline{q}}\right)\right)+i\varphi\widehat{I}_3+i\psi\widehat{Y}_8\right)\right],$$

where $\beta=\dfrac{1}{T}$ (with the units chosen as: $k_B=\hbar=c=1$), $\widehat{H}_0$ is the free quark–gluon Hamiltonian, $\widehat{N}_q\left(\widehat{N}_{\overline{q}}\right)$ denotes the (anti-) quark number operator, and $\widehat{I}_3$ and $\widehat{Y}_8$ are the color "isospin" and "hypercharge" operators respectively. Its final expression, in the massless limit, can be put in the form:

$$Z_{\rm QGP}(T,V_{\rm QGP},\mu) \quad (10)$$
$$=\frac{4}{9\pi^2}\int_{-\pi}^{+\pi}\int_{-\pi}^{+\pi}d\varphi d\psi M(\varphi,\psi)e^{V_{\rm QGP}T^3 g\left(\varphi,\psi,\frac{\mu}{T}\right)},$$

with:

$$g(\varphi,\psi,\frac{\mu}{T})$$
$$=\frac{\pi^2}{12}(\frac{21}{30}d_{\rm Q}+\frac{16}{15}d_{\rm G})$$
$$+\frac{\pi^2}{12}\frac{d_{\rm Q}}{2}\sum_{q=r,b,g}\left\{-1+\left(\frac{\left(\alpha_q-i(\frac{\mu}{T})\right)^2}{\pi^2}-1\right)^2\right\}$$
$$-\frac{\pi^2}{12}\frac{d_{\rm G}}{2}\sum_{g=1}^{4}\left(\frac{(\alpha_g-\pi)^2}{\pi^2}-1\right)^2, \quad (11)$$

$d_{\rm Q}=2N_f$ and $d_{\rm G}=2$ being the degeneracy factors of quarks and gluons respectively, α_q ($q=r,\,b,\,g$) the angles determined by the eigenvalues of the color charge operators in (9):

$$\alpha_r=\tfrac{\varphi}{2}+\tfrac{\psi}{3},\quad \alpha_g=-\tfrac{\varphi}{2}+\tfrac{\psi}{3},\quad \alpha_b=-\tfrac{2\psi}{3}, \quad (12)$$

and α_g ($g=1,\ldots,4$) being:

$$\alpha_1=\alpha_r-\alpha_g,\ \alpha_2=\alpha_g-\alpha_b,\ \alpha_3=\alpha_b-\alpha_r,\ \alpha_4=0. \quad (13)$$

3 Finite-size effects

To study the effects of volume finiteness on the thermal deconfinement phase transition within the QCD model chosen, we will examine in the following the behavior of some thermodynamic quantities of the system with temperature, at a vanishing chemical potential ($\mu=0$), considering the two lightest quarks u and d ($N_f=2$), and using the common value $B^{1/4}=145MeV$ for the bag constant.

The first quantity of interest for our study is the mean value of the hadronic volume fraction $<\mathfrak{h}(T,V)>$, which can be considered as representing the order parameter for the studied deconfinement phase transition. According to (4), $<\mathfrak{h}(T,V)>$ is expressed as:

$$<\mathfrak{h}(T,V)>=1-\frac{\int_{-\pi}^{+\pi}\int_{-\pi}^{+\pi}d\varphi d\psi M(\varphi,\psi)\int_0^1\mathfrak{q}e^{\mathfrak{q}\Re(\varphi,\psi;T,V)}d\mathfrak{q}}{\int_{-\pi}^{+\pi}\int_{-\pi}^{+\pi}d\varphi d\psi M(\varphi,\psi)\int_0^1 e^{\mathfrak{q}\Re(\varphi,\psi;T,V)}d\mathfrak{q}}, \quad (14)$$

with: $\Re\left(\varphi,\psi;T,V\right)=\left(g_{\mu=0}(\varphi,\psi)-\frac{\pi^2}{30}-\frac{B}{T^4}\right)VT^3$. After integration on the $\mathfrak{q}$ variable representing the QGP volume fraction, the order parameter can be written as:

$$<\mathfrak{h}(T,V)>=\frac{L_{01}+L_{02}-L_{12}}{L_{01}-L_{11}}, \quad (15)$$

where the general form of the integral terms appearing in this expression is:

$$L_{nm}=\int_{-\pi}^{+\pi}\int_{-\pi}^{+\pi}d\varphi d\psi M(\varphi,\psi)\frac{\left(e^{\Re(\varphi,\psi;T,V)}\right)^n}{\left(\Re\left(\varphi,\psi;T,V\right)\right)^m}. \quad (16)$$

These integrals are then carried out using a suitable numerical method at each fixed temperature and volume.

The second quantity of interest is the energy density $\varepsilon(T,V)$, whose mean value is related to $<\mathfrak{h}(T,V)>$ by:

$$<\varepsilon(T,V)>=\varepsilon_{HG}<\mathfrak{h}(T,V)>+B\left[1-<\mathfrak{h}(T,V)\right]$$
$$-3T^4\left[\frac{\widetilde{L}_{11}-\widetilde{L}_{12}+\widetilde{L}_{02}}{L_{01}-L_{11}}\right], \quad (17)$$

where the new integrals on φ and ψ , noted by $\widetilde{L}_{nm}$, are given by:

$$\widetilde{L}_{nm}=\int_{-\pi}^{+\pi}\int_{-\pi}^{+\pi}d\varphi d\psi M(\varphi,\psi)g_{\mu=0}(\varphi,\psi)$$
$$\times\frac{\left(e^{\Re(\varphi,\psi;T,V)}\right)^n}{\left(\Re\left(\varphi,\psi;T,V\right)\right)^m}, \quad (18)$$

and: $\varepsilon_{\rm HG}=\frac{\pi^2}{10}T^4$.

We can also examine the effects of volume finiteness by illustrating two more quantities representing the first derivatives of the two previous ones, that is, the susceptibility χ defined as:

$$\chi\left(T,V\right)=\frac{\partial\langle\mathfrak{h}\left(T,V\right)\rangle}{\partial T}, \quad (19)$$

and the specific heat density $c\left(T,V\right)$ defined as:

$$c\left(T,V\right)=\frac{\partial\langle\varepsilon\left(T,V\right)\rangle}{\partial T}. \quad (20)$$

Our results for the variations of these four response functions with temperature at different system sizes are presented in the plots on Figs. 1 and 2 and show a pronounced size dependence over almost the entire temperature range. The curves show that, in the limit of an infinite volume, both $\langle\mathfrak{h}\rangle$ and $\dfrac{<\varepsilon>}{T^4}$ exhibit a finite sharp

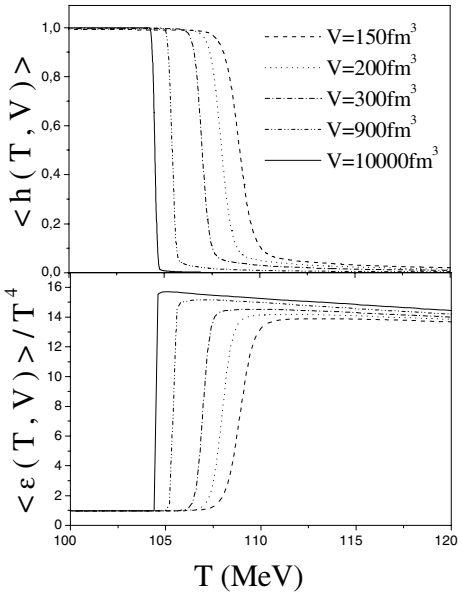

Fig. 1. Temperature variation of the order parameter (top) and the energy density normalized by T^4 (bottom) at $\mu = 0$, for different system volumes

discontinuity, which is related to the latent heat of the deconfinement phase transition, at a bulk transition temperature $T_c(\infty) \simeq 104.35\,\mathrm{MeV}$, reflecting the first-order character of the transition. The quantity $\frac{\langle\varepsilon\rangle}{T^4}$ is traditionally interpreted as a measure of the number of effective degrees of freedom; the temperature increase then causes a "melting" of the constituent degrees of freedom "frozen" in the hadronic state, making the energy density attain its plasma value. This finite discontinuity can be mathematically described by a step function, which transforms to a δ-function in χ and c. When the volume decreases, the four quantities vary continuously such that the finite sharp jump is rounded off and the δ-peaks are smeared out into finite peaks over a range of temperature $\delta T(V)$. This is due to the finite probability of the presence of the QGP phase below T_c and of the hadron phase above T_c, induced by the considerable thermodynamical fluctuations.

Another feature which can be noted is that the maxima of these rounded peaks occur at effective transition temperatures $T_c(V)$ shifted away from the bulk transition temperature for infinite volume $T_c(\infty)$. This shift is a consequence of the color-singletness requirement since the effective number of internal degrees of freedom for a color-singlet QGP is drastically reduced with decreasing volume, as can clearly be seen from the curves, and has been shown in [13]. Thus, the pressure of the QGP phase is lower at a given temperature, and the mechanical Gibbs equilibrium between the two phases would then be reached for $T_c(V) > T_c(\infty)$.

It can also be noted that, for decreasing volume, while the height of the peak decreases, its width gets larger. To see this in more detail, we illustrate in the following the second derivative of the order parameter $\langle \mathfrak{h}(T,V)\rangle'' = \frac{\partial^2\langle \mathfrak{h}(T,V)\rangle}{\partial T^2}$, which reaches its extrema at thetemperatures $T_1(V)$ and $T_2(V)$. The width of the transition region can simply be defined by the gap between these two temperatures, that is, $\delta T(V) = T_2(V) - T_1(V)$. The variations of $\langle \mathfrak{h}(T,V)\rangle''$ with temperature for various sizes are illustrated in Fig. 3, from which it can clearly be seen that the gap between the two extrema decreases with increasing volume.

Finally from the obtained results for the finite size response functions, four finite-size effects can be observed:

- the rounding effect of the discontinuities,
- the smearing effect of the singularities,
- the shifting effect of the transition point,
- the broadening effect of the transition region,

and to study quantitatively the volume dependence of these effects, a numerical scaling analysis is carried out, which will be presented in the next section.

4 Finite-size scaling analysis

4.1 Finite-size scaling

In statistical mechanics, it is known that only in the thermodynamic limit are phase transitions characterized by the appearance of singularities in some second derivatives of the thermodynamic potential, such as the susceptibility and the specific heat. For a first-order phase transition, the divergences are δ-function singularities, corresponding to the

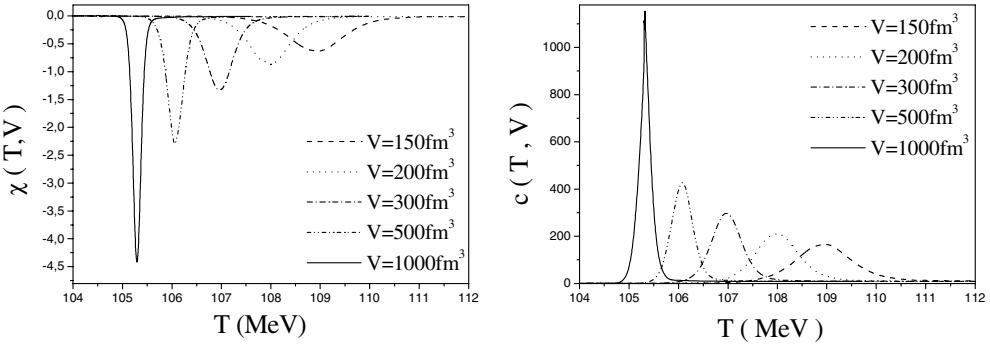

Fig. 2. Plot of (left) the susceptibility $\chi(T,V)$ and (right) the specific heat density $c(T,V)$, versus temperature for different system volumes

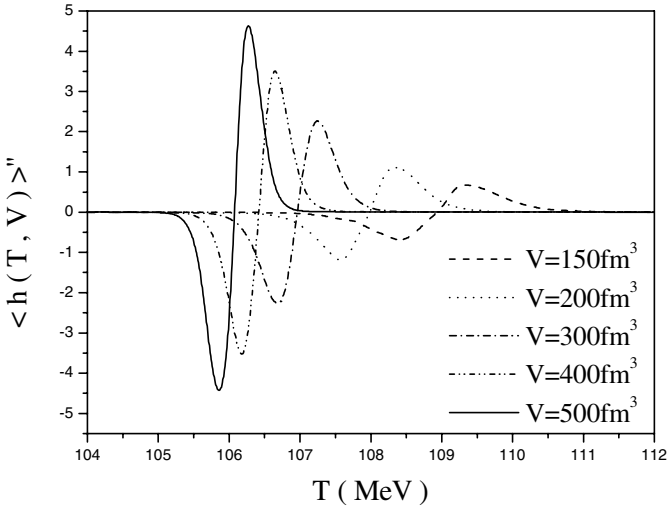

Fig. 3. Plot of the second derivative of the order parameter $\langle \mathfrak{h}(T,V)\rangle'' = \frac{\partial^2 \langle \mathfrak{h}(T,V)\rangle}{\partial T^2}$ versus temperature for different system volumes

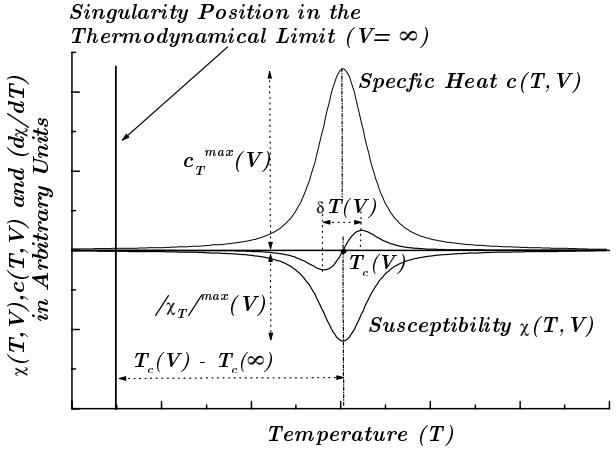

Fig. 4. Illustration of the finite-size behavior of the susceptibility $\chi\,(T,V)$, the specific-heat density $c\,(T,V)$ and the second derivative of the order parameter $\partial\chi/\partial\ T$

finite discontinuities in the first derivatives of the thermodynamic potential, while for a second-order phase transition the singularity has a power-law form. For the QCD model of the thermal deconfinement phase transition studied in this work, δ-singularities appear in the susceptibility χ and in the specific heat density c in the thermodynamic limit. In finite volumes, these δ-functions are found to be smeared out into finite peaks. To the finite-size effects, four useful characteristic quantities can be associated as illustrated on Fig. 4: the maxima of the peaks of the susceptibility $\chi_T^{\max}(V)$ and the specific heat density $c_T^{\max}(V)$, the shift of the transition temperature $\tau_T(V) = T_c\,(V) - T_c\,(\infty)$ and the width of the transition region $\delta T\,(V)$. Each of these quantities can be considered as a signature which may anticipate the behavior in the thermodynamic limit, and is expected to present a scaling behavior described by a power law of the volume $V = L^d$, where L is the linear extension of the volume and d the space dimensionality, characterized by a *scaling critical exponent*. For a first-order phase transition, the set of power laws is:

$$\begin{cases} \chi_T^{\max}(V) \sim V^{\gamma}\,, \\ c_T^{\max}(V) \sim V^{\alpha}\,, \\ \delta T\,(V) \sim V^{-\theta}\,, \\ \tau_T(V) = T_c\,(V) - T_c\,(\infty) \sim V^{-\lambda}\,, \end{cases} \tag{21}$$

and it has been shown in the FSS theory [18–21] that in this case, the scaling exponents θ, λ, α and γ are all equal to unity, and it is only the dimensionality which controls the finite-size effects.

At a second-order phase transition, the correlation length diverges as $\xi \propto |T - T_c|^{-\nu}$, and this we predict the same power-law behavior as for a first-order transition, but with different scaling critical exponents, usually given as:

$$\begin{cases} \chi_T^{\max}(V) \sim V^{\gamma/d\nu}\,, \\ c_T^{\max}(V) \sim V^{\alpha/d\nu}\,, \\ \delta T\,(V) \sim V^{-1/d\nu}\,, \\ \tau_T(V) = T_c\,(V) - T_c\,(\infty) \sim V^{-1/d\nu}\,. \end{cases} \tag{22}$$

The values of the scaling critical exponents may then give an indication on the order of a phase transition and are usually used as a criterion for the determination of this latter [9, 11, 22, 23].

4.2 Numerical determination of the scaling critical exponents for the thermal deconfinement phase transition

In the following, we use a FSS analysis to recover the scaling exponents θ, λ, α and γ for the thermally driven deconfinement phase transition. For this purpose, we proceed by studying the behavior of the response-function maxima, their rounding as well as the shift of the effective transition temperature with varying volume. Let us note that the determination of the location of the maxima of the finite-size peaks as well as their heights is done in a numerical way, and this yields a systematic error, which is estimated and given for the determined scaling exponents.

4.2.1 Susceptibility, specific heat and smearing scaling exponents

The data of the maxima of the rounded peaks of the susceptibility $\mid \chi_T \mid^{\max}(V)$ and the specific heat density $c_T^{\max}(V)$ are plotted versus volume in Fig. 5 (left) and Fig. 5 (right),respectively, and their linearity with V can clearly be noted. A numerical parameterization with the power-law forms: $\mid \chi_T \mid^{\max}(V) \sim V^{\gamma}$ and: $c_T^{\max}(V) \sim V^{\alpha}$, gives the values of the susceptibility scaling exponent: $\gamma = 1.01 \pm 0.03$, and the specific-heat scaling exponent: $\alpha = 1.007 \pm 0.031$, where the associated errors are systematic.

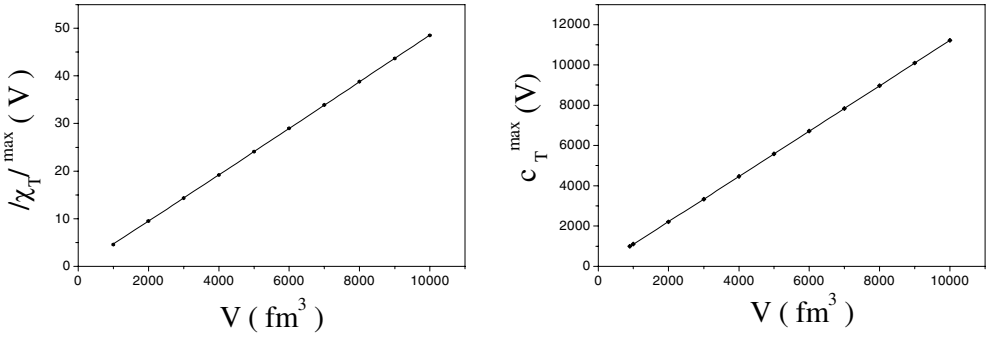

Fig. 5. Variation of (left) the susceptibility maxima $\mid \chi_T \mid^{\max}(V)$ and (right) the specific-heat density maxima ${c_T}^{\max}(V)$ with volume

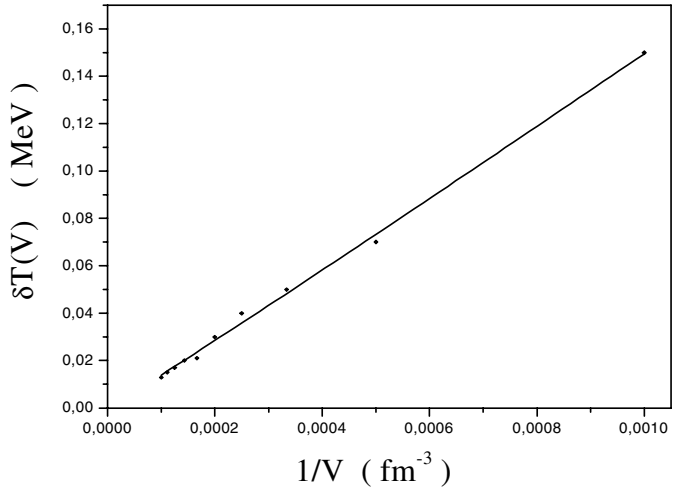

Fig. 6. Variation of the width of the temperature region over which the transition is smeared $\delta T(V)$ with inverse volume

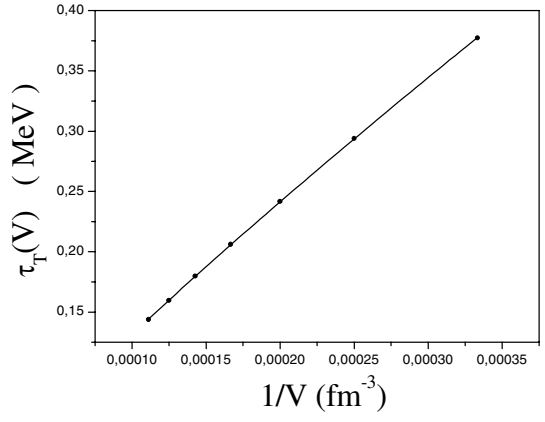

Fig. 7. Variation of the shift of the transition temperature $\tau_T(V)$ (from the maxima of $\chi(T,V)$ and $c(T,V)$) with inverse volume

Figure 6 illustrates the plot of the results of the width $\delta T(V)$ with the inverse of the volume, and their fit to the power-law form: $\delta T(V) \sim V^{-\theta}$. The obtained smearing scaling exponent is: $\theta = 1.03 \pm 0.03$.

4.2.2 The shift scaling exponent

For the study of the shift of the transition temperature $\tau_T(V) = T_c(V) - T_c(\infty)$, we need to locate the effective transition temperature in a finite volume $T_c(V)$. A way to define $T_c(V)$ is to locate the maxima of the rounded peaks of the susceptibility and the specific heat, shifted away from the true transition temperature $T_c(\infty)$. Results of the shift of the transition temperature obtained in this way are plotted in Fig. 7 versus inverse volume. The shift critical exponent obtained from a fit to the form: $\tau_T(V) \sim V^{-\lambda}$, is: $\lambda = 0.876 \pm 0.041$. Such a value $\neq 1$ suggests the contribution of non-leading terms in the expression of the volume variation of the shift. Different forms of the fit of $\tau_T(V)$, including additional terms with higher powers of V^{-1}, such as $A_1 V^{-\lambda} + A_2 V^{-2}$, and $A_1 V^{-\lambda} + A_2 V^{-2} + A_3 V^{-3}$, have been tested, and the obtained results show that effectively, the shift critical exponent λ increases from the value 0.876 and tends to 1, with a better χ^2. Other forms have been tested, where the value of the shift exponent has been fixed to 1, and finite-size correction terms have been included. In this case also, we note that we obtain a better χ^2 value with the presence of the non-leading terms.

4.2.3 The shift from the binder cumulant

Another way of locating $T_c(V)$ is to consider the fourth-order cumulant of the order parameter proposed in [3,19] and defined as:

$$B_4(T,V) = 1 - \frac{\langle \mathfrak{h}^4(T,V) \rangle}{3 \langle \mathfrak{h}^2(T,V) \rangle^2}, \tag{23}$$

which presents a minimum value at an effective transition temperature whose shift from the true transition temperature is of the order V^{-1} for a first-order transition. This cumulant is a finite-size scaling function [3,19,20,24,25], and has been proven to be a suitable indicator of the order of the transition in a finite volume.

The expression for $B_4(T,V)$ as function of the integral terms, for this case of the deconfinement transition, is after calculation:

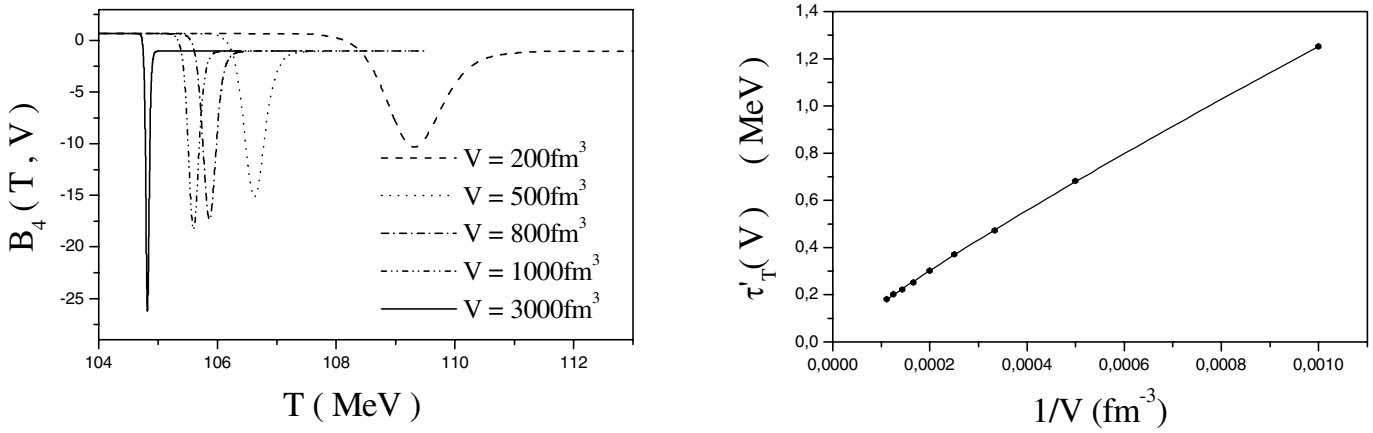

Fig. 8. Plot of the Binder cumulant $B_4(T,V)$ (left) versus temperature for different system volumes, and (right) variation of the shift of the transition temperature $\tau'_T(V)$ (from the minimum of $B_4(T,V)$) with inverse volume

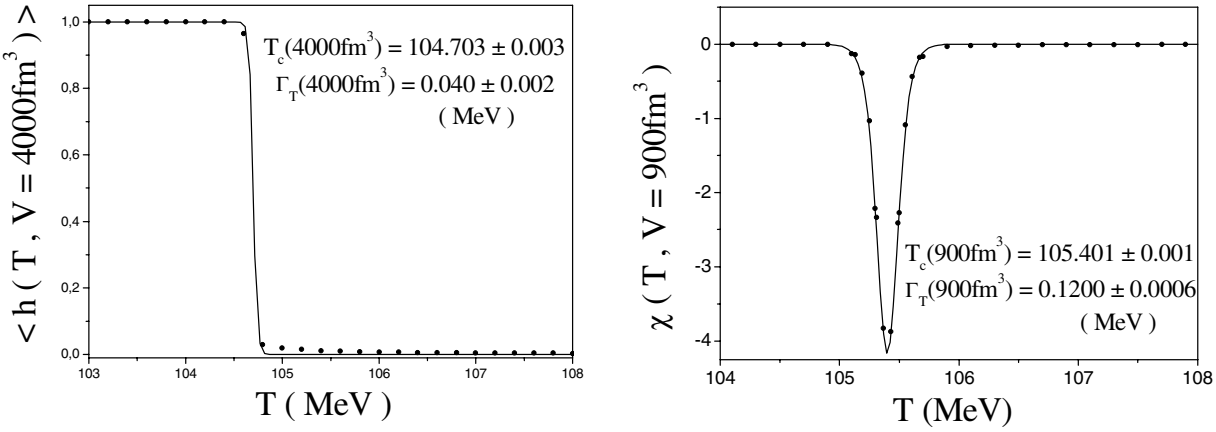

Fig. 9. Illustration of the fits of the order parameter to the form (26) at the volume $V = 4000 fm^3$, and of the susceptibility to the form (27) at the volume $V = 900\,\mathrm{fm}^3$

$$B_4(T,V) = 1 - \frac{(L_{11}-L_{01})(24(L_{15}-L_{05}-L_{04})-12L_{03}-4L_{02}-L_{01})}{3\,(2L_{13}-2L_{03}-2L_{02}-L_{01})^2}\,. \tag{24}$$

Figure 8 (left) illustrates the variations of the fourth cumulant of the order parameter with temperature for various volumes, and shows that the locations of the minima in finite sizes $T_{\min}(V)$ are shifted to higher values from $T_c(\infty)$. Data of the shift of the transition temperature obtained in this way are plotted in Fig. 8 (right) versus inverse volume, and the scaling shift critical exponent obtained from a fit to the form: $\tau'_T(V) = T_{\min}(V) - T_c(\infty) \sim V^{-\lambda'}$, is $\lambda' = 0.883 \pm 0.043$. In this case also, non-leading terms appear in the expression of $\tau'_T(V)$.

4.2.4 Parameterization of the order parameter and the susceptibility

Within the model used in this work, the order parameter in the limit of infinite volume being equal to 1 below the transition temperature and zero above, it can then be expressed in a simple way using the Heaviside step function as:

$$\langle \mathfrak{h}(T, V \longrightarrow \infty)\rangle = 1 - \Theta(T - T_c(\infty))\,. \tag{25}$$

Such a parameterization has been used in [26], for a similar case of a system of coexisting hadronic matter and QGP phases. Using one of the known mathematical representations of the smoothed step function $\Theta(T-T_c)$, the order parameter may then be expressed as:

$$\langle \mathfrak{h}(T,V)\rangle = \frac{1}{2}\left(1 - \tanh\left(\frac{T - T_c(V)}{\Gamma_T(V)}\right)\right), \tag{26}$$

where $T_c(V)$ is the effective transition temperature and $\Gamma_T(V)$ is the half-width of the rounded transition region, which leads to the susceptibility expression :

$$\chi(T,V) = \frac{-1}{2\Gamma_T(V)\ \cosh^2\left(\frac{T-T_c(V)}{\Gamma_T(V)}\right)}. \tag{27}$$

The parameterization choice (26) is the most accepted physically, and can be understood phenomenologically in the context of the double Gaussian peaks model where the obtained expressions of the order parameter and the susceptibility are very similar to (26) and (27) [3,9,27].

An illustration of such parameterizations of the order parameter at the volume $V = 4000\,\mathrm{fm}^3$, and the susceptibility at the volume $V = 900\,\mathrm{fm}^3$ are presented in Fig. 9

(left) and Fig. 9 (right), respectively, and the parameters $T_c(V)$ and $\Gamma_T(V)$ obtained from each fit are given.

The results for the width of the transition region and the shift of the transition temperature from the parameterizations of the order parameter and the susceptibility are fitted to power-law forms: ${\tau_T}^{\mathrm{fit}(1)}(V) \sim V^{-\lambda_1}$, ${\tau_T}^{\mathrm{fit}(2)}(V) \sim V^{-\lambda_2}$, $\delta T^{\mathrm{fit}(1)}(V) \sim V^{-\theta_1}$, and $\delta T^{\mathrm{fit}(2)}(V) \sim V^{-\theta_2}$ which give the scaling critical exponents: $\lambda_1 = 0.830 \pm 0.013$, $\lambda_2 = 0.857 \pm 0.006$, $\theta_1 = 0.990 \pm 0.015$, and $\theta_2 = 1.032 \pm 0.003$.

5 Conclusion

Our model has shown the influence of the finiteness of the system size on the behavior of some response functions in the vicinity of the transition point. The sharp transition observed in the thermodynamical limit, signaled by discontinuities in the order parameter and in the energy density at a transition temperature $T_c(\infty)$, is rounded off in finite volumes, and the variations of these thermodynamic quantities are perfectly smooth on the whole range of temperature. The delta function singularities appearing in the first derivatives of these discontinuous quantities, i.e., in the susceptibility and specific heat density, are then smeared out into finite peaks of widths $\delta T(V)$. The maxima of these peaks occur at effective transition temperatures $T_c(V)$ shifted away from the true transition temperature $T_c(\infty)$. An FSS analysis of the behavior of the maxima of the rounded peaks of the susceptibility $\chi_T^{\max}(V)$ and the specific heat density $c_T^{\max}(V)$, the width of the transition region $\delta T(V)$, and the shift of the effective transition temperature relative to the true one $\tau_T(V) = T_c(V) - T_c(\infty)$, shows their power-law variations with the volume characterized by the scaling critical exponents γ, α, θ, and λ, respectively. Numerical results for these scaling exponents are obtained and are in good agreement with our analytical results: $\gamma = \alpha = \theta = \lambda = 1$ obtained in [28], except for the shift critical exponent which slightly deflects from the analytical value 1. This may be due, on one hand, to the difficulty of locating accurately the peaks of χ, c and B_4, especially in the case of large volumes for which the peaks become very sharp and, on the other hand, to the non-leading terms which contribute to the expression of $\tau_T(V)$. However, a first estimate of the scaling critical exponents for the thermal deconfinement phase transition within this model has been obtained, and our result expressing the equality between all scaling exponents and the space dimensionality is a consequence of the singularity characterizing a first-order phase transition and agrees very well with the predictions of the standard FSS theoretical approaches to a first-order phase transition [19, 21, 29–33] and with those obtained in a rather different and rigorous way, generalizing the FSS description of a first-order phase transition [34]. Also, we note the good agreement with the results of calculations using Monte Carlo methods in both lattice QCD [8, 35–38] and other models in statistical physics [22, 39, 40].

References

1. C.N. Yang, T.D. Lee, Phys. Rev. **87**, 404 (1952); Phys. Rev. **87**, 410 (1952)
2. J. Imry, Phys. Rev. B **21**, 2042 (1980)
3. K. Binder, D.P. Landau, Phys. Rev. B **30**, 1477 (1984)
4. C. Spieles, H. Stöcker, C. Greiner, Phys. Rev. C **57**, 908 (1998)
5. A. Chodos et al., Phys. Rev. D **9**, 3471 (1974); J. Cleymans, R.V. Gavai, E. Suhonen, Phys. Rep. **130**, 217 (1986)
6. D.P. Landau, R.H. Swendsen, Phys. Rev. Lett. **46**, 1437 (1981); F.R. Brown et al., Phys. Rev. Lett. **61**, 2058 (1988); P. Bacilieri et al., Phys. Rev. Lett. **61**, 1545 (1988); J.F. McCarthy, Indiana University Preprint IUHET 164 (1989); M. Fukugita et al., Phys. Rev. Lett. **63**, 1768 (1989); P. Bacilieri et al., Phys. Lett. B **220**, 607 (1989); R.V. Gavai, F. Karsch, B. Petersson, Nucl. Phys. B **322** , 738 (1989); M. Fukugita, Phys. Rev. Lett. **63**, 13 (1989); M. Fukugita et al., Nucl. Phys. Proc. Suppl. **17**, 204 (1990); S. Gupta et al., Nucl. Phys. B **329**, 263 (1990); M. Fukugita et al., J. Phys. A **23**, L561–L566 (1990)
7. M. Fukugita, Nucl. Phys. Proc. Suppl. **9**, 291 (1989)
8. N.A. Alves et al., Phys. Rev. Lett. **64**, 3107 (1990)
9. H. Meyer-Ortmanns, Rev. Mod. Phys. **68**, 473 (1996)
10. F. Karsch, Nucl. Phys. A **590**, 367c–382c (1995); Nucl. Phys. A **698**, 199c–208c (2002); F. Karsch et al., Nucl. Phys. (Proc. Suppl.) B **94**, 411–414 (2001); Nucl. Phys. B **605**, 579–599 (2001)
11. M. Fukugita, RIFP-703 (June 1987); M. Fukugita et al., Phys. Rev. Lett. **58**, 2515 (1987); UTHEP-168 (August 1987); Phys. Rev. Lett. **60**, 178 (1988); M. Fukugita, Nucl. Phys. Proc. Suppl. **4**, 105 (1988), M. Fukugita, A. Ukawa, Phys. Rev. D **38**, 1971 (1988); R.V. Gavai et al., Phys. Lett. B **200**, 137 (1988); F.R. Brown et al., Phys. Rev. Lett. **65**, 2491 (1990); S. Aoki et al. (JLQCD Coll.), Nucl. Phys. B **63**A–C, 403 (1998), **60**A, 188 (1998); B. Lucini et al., Phys. Lett. B **545**, 197 (2002); P. Cea et al., Nucl. Phys. (Proc. Suppl.) B **129–130**, 751 (2004)
12. K. Redlich, L. Turko, Z. Phys. C **5**, 201 (1980); L.Turko, Phys. Lett. B **104**, 153 (1981)
13. H.-Th. Elze, W. Greiner, J. Rafelski, Phys. Lett. B **124**, 515 (1983); Z. Phys. C **24**, 361 (1984); H.-Th. Elze, W. Greiner, Phys. Lett. B **179**, 385 (1986)
14. A. Tounsi, J. Letessier, J. Rafelski, hep-ph/9811290
15. M.G. Mustafa, D.K. Srivastava, B. Sinha, Eur. Phys. J. C **5**, 711 (1998); nucl-th/9712014
16. J. Madsen, D.M. Jensen, M.B. Christiansen, Phys. Rev. C **53**, 1883 (1996)
17. G. Yezza, Magister thesis in theoretical physics, Ecole Normale Supérieure, Kouba, Algiers (March 2002)
18. M.E. Fisher, A.N. Berker, Phys. Rev. B **26**, 2507 (1982).
19. M.S. Challa, D.P. Landau, K. Binder, Phys. Rev. B **34**, 1841 (1986)
20. K. Binder, D.W. Heermann, Monte Carlo Simulations in Statistical Physics, (Springer-Verlag, 1988, 2nd ed. 2002)
21. V. Privman, M.E. Fischer, J. Stat. Phys. **33**(2), 385 (1983)
22. M. Fukugita et al., KEK-TH-233 (1989)
23. M. Henkel, Conformal Invariance and Critical Phenomena, (Springer-Verlag, 1999)
24. K. Binder, Rep. Prog. Phys. **60**, 487 (1997)
25. D.P. Landau, K. Binder, A Guide to Monte Carlo Simulation in Statistical Physics, (Cambridge University Press, 2000)

26. J.P. Blaizot, J.Y. Ollitraut, Phys. Rev. D **36**, 916 (1987)
27. K. Binder, Phys. Rev. Lett. **47**, 693 (1981); Z. Phys. B **43**, 119 (1981)
28. M. Ladrem, A. Ait-El-Djoudi, G. Yezza, communication at the international conference 'Quark Confinement and the Hadron spectrum', held in Gargnano, Italy, 10–14 September 2002
29. M.N. Barber, in Phase Transitions and Critical Phenomena, Vol. 8, edited by C.Domb, J.L. Lebowitz (Academic, New York, 1983) 145
30. K. Binder, Ferroelectrics **73**, 43 (1987); in Computational Methods in Field Theory, H. Gausterer, C.B. Lang, (Eds. Springer, Berlin 1992) 59
31. W. Janke, Phys. Rev. B **47**, 14757 (1993)
32. K. Vollmayr, J.D. Reger, M. Scheucher, K. Binder, Z. Phys. B **91**, 113 (1993)
33. J.G. Brankov, D.M. Danchev, N.S. Tonchev, Theory of Critical Phenomena in Finite-Size Systems – Scaling and Quantum Effects, (World Scientific, 2000)
34. C. Borgs, R. Kotecky, J. Stat. Phys. **61**, 79 (1991); C. Borgs, R. Kotecky, S. Miracle-Solé, J. Stat. Phys. **62**, 529 (1991)
35. B. Beinlich, F. Karsch, E. Laermann, A. Peikert, Eur. Phys. J. C **6**, 133 (1999)
36. K. Bitar et al., Nucl. Phys. B **337**, 245 (1990)
37. R.V. Gavai, Nucl. Phys. Proc. Suppl. **106**, 480 (2002); Nucl. Phys. B **633**, 127 (2002)
38. M. Mathur, R.V. Gavai, Nucl. Phys. B **448**, 399 (1995)
39. D. Loison, K.D. Schotte, Eur. Phys. J. B **5**, 735 (1998); B **14**, 125 (2000)
40. O. Dillmann, W. Janke, K. Binder, J. Stat. Phys. **92**, 1/2, 57 (1998)